Department of Chemistry

Functionalised Microporous Organic Polymers as Adsorbents

Thesis submitted in accordance with the requirements of the University of Liverpool for the degree of Doctor of Philosophy

By

Thanchanok Ratvijitvech

September 2015

Contents

List of Schemes 1

List of Figures 2

List of Tables 9

Abstract 11

Abbreviations 12

Acknowledgements 15

Publications 16

Chapter 1 Introduction 18

1.1 Microporous Organic Polymers 18

1.2 Synthesis 21

1.2.1 Synthesis of HCPs 21

1.2.2 Synthesis of CMPs 23

1.3 Characterisation 26

1.3.1 Structure and morphology 26

1.3.2 Porosity 27

1.4 Porosity Tuning 29

1.4.1 Structural tuning 29

1.4.2 Functionality tuning 31

1.5 MOPs as adsorbents 33

1.5.1 Gas storage and separations 33

1.5.2 Molecule Capture 37

1.6 Overview of the work in this thesis 39

1.7 References 39

Chapter 2 Methods 49

2.1 Experimental techniques 49

2.1.1 Gas sorption 49

2.1.1.1 Nitrogen isotherms 49

2.1.1.2 Surface area measurements 49

2.1.1.3 Pore size distribution 50

2.1.1.4 Nitrogen adsorption for selectivity calculation 50

2.1.1.5 Carbon dioxide adsorption 50

2.1.1.6 Calculation of CO_2/N_2 selectivity 50

2.1.2 Infrared spectroscopy (IR) 51

2.1.3 Solution nuclear magnetic resonance spectroscopy (NMR) 52

2.1.4 Solid state NMR (ssNMR) 52

2.1.5 Elemental analysis 52

2.1.6 Mass spectroscopy (MS) 52

2.1.7 Scanning electron microscopy (SEM) 53

2.1.8 Gel permeation chromatography (GPC) 53

2.1.9 Gas chromatography (GC) 53

2.1.10 High performance liquid chromatography (HPLC) 54

2.2 Synthesis for benzene-aniline copolymers 54

2.2.1 Materials 54

2.2.2 Synthesis of benzene-aniline copolymers 54

2.3 Synthesis for cross-linked polystyrenes 55

2.3.1 Materials 55

2.3.2 Synthesis of small molecules containing carboxylic acid 55

2.3.3 Synthesis of linear polystyrenes 56

2.3.4 Cross-linking of polystyrenes 59

2.4 Synthesis for post-synthetic modification 60
2.4.1 Materials 60
2.4.2 Synthesis of **CMP-1-NH_2** 60
2.4.3 Post-synthetic modification of **CMP-1-NH_2** to **CMP-1-AMDs** 61
2.4.3.1 Neat acid anhydrides at 30 °C 61
2.4.3.2 Neat acid anhydrides at room temperature 61
2.4.3.3 Acid anhydrides in $CHCl_3$ 61
2.5 Synthesis for molecular imprinting polymers 62
2.5.1 Materials 62
2.5.2 Monomer Synthesis 62
2.5.2.1 Esterification by using DCC/DMAP 62
2.5.2.2 Esterification by using triethylamine (NEt_3) 63
2.5.3 Polymer synthesis 64
2.5.4 Hydrolysis 65
2.5.5 Molecular uptakes 65
2.5.6 Calculation of menthol selectivity 65
2.6 References 65

Chapter 3 Benzene/aniline Co-polymers for CO_2 Capture 68
3.1 CO_2 Capture 68
3.2 Synthesis and Characterisation 69
3.3 Gas Sorption Properties 75
3.4 Conclusion 80
3.5 References 81

Chapter 4 Hypercross-linked Polystyrenes 86

4.1 Introduction 86

4.2 Cross-linking of carboxylic acid functionalised compounds 88

4.3 Styrene units variation 89

4.4 RAFT agent variation 99

4.5 Precipitation solvent variation 110

4.6 Conclusion 112

4.7 References 113

Chapter 5 Post-synthetic Modification (PSM) 118

5.1 Introduction 118

5.2 **CMP-1-NH_2** synthesis 120

5.3 PSM **CMP-1-NH_2** to **CMP-1-AMDs** 121

5.3.1 PSM 121

5.3.2 Gas sorption properties 125

5.4 Temperature Effect on PSM 130

5.5 Solvent Effect on PSM 131

5.6 Conclusion 135

5.7 References 136

Chapter 6 Molecular Imprinting Polymers (MIPs) 140

6.1 Introduction 140

6.2 Cholesterol 143

6.3 Menthol 150

6.3.1 Menthol-Non-functionalised copolymers (**MENT-Hs**) 154

6.3.2 Menthol adsorption in **MENT-Hs** 157

6.3.3 Menthol-Carboxylic acid functionalised copolymers (**MENT-COOHs**) 159

6.3.4 Different concentrations of menthol solution 162

6.3.5 Selectivity of menthol over terpinolene 165

6.3.6 Tetrahedral Monomers (**T-MENT-COOHs**) 167

6.4 Trimesic acid 174

6.4.1 **O-TRIM** 174

6.4.2 **N-TRIM** 189

6.5 Conclusion 198

6.6 References 200

Chapter 7 Conclusions 206

7.1 Conclusions 206

7.2 Future work 207

7.3 References 209

List of Schemes

Scheme 3.1 Synthetic scheme for benzene/aniline co-polymer networks 70

Scheme 4.1 Mechanism of RAFT polymerization. M refers to the monomer, R' and R refers to the propagating chains and the leaving group in RAFT agent, and Z refers to the modified group in RAFT agent which controls the addition and fragmentation rate. Z is generally alkyl, aryl, S-alkyl, O-alkyl or aryl, or N-alkyl or aryl.[35] 88

Scheme 4.2 Summary scheme of cross-linked polystyrenes synthesis 88

Scheme 5.1 Synthetic scheme for **CMP-1-AMDs** 119

Scheme 6.1 Synthetic scheme for **CHOL-CMP** 143

Scheme 6.2 Synthetic scheme for **CMP-1-COOH** 145

Scheme 6.3 Synthetic scheme for **CHOL-COOH** 147

Scheme 6.4 Synthetic scheme for **CHOL-OH** 149

Scheme 6.5 Synthetic scheme for **MENT-CMP** 151

Scheme 6.6 Synthetic scheme for **MENT-Hs** 154

Scheme 6.7 Synthetic scheme for **MENT-COOHs** 159

Scheme 6.8 Synthetic scheme for **T-MENT-COOHs** 168

Scheme 6.9 Synthetic scheme for **O-TRIM** 175

Scheme 6.10 Synthetic scheme for **O-TRIMs** 179

Scheme 6.11 Synthetic scheme for **N-TRIM** 189

Scheme 6.12 Synthetic scheme for **N-TRIMs** 193

List of Figures

Figure 1.1	The structure of microporous organic polymer	18
Figure 1.2	Example of each type of microporous organic polymers. Crystalline MOPs: (a) COFs, (b) CTFs. Amorphous MOPs: (c) PIMs, (d) HCPs (polycondensation), (e) HCPs (knitting), and (f) CMPs. Dashed lines show the connecting points.	20
Figure 1.3	Synthesis scheme of HCPs by post-cross-linking of polymer chains[65]	22
Figure 1.4	Examples of reactions for synthesis of CMPs	24
Figure 1.5	Types of nitrogen isotherms (left) and hysteresis loops (right)[90]	28
Figure 1.6	PSM of PPN-6 with amines and acids	32
Figure 1.7	Synthesis of azo-COPs[124]	35
Figure 1.8	Synthesis of CMPs with different functional groups	36
Figure 1.9	Phase-selective encapsulation of Py-PP. a) to c) The absorption of diesel upon addition of Py-PP to a beaker containing a diesel/water mixture. d) and e) The polymer and diesel, respectively, recovered by simple squeezing of the colleted material.[15]	38
Figure 3.1	Possible structures of aniline networks	70
Figure 3.2	Average yields of benzene/aniline co-polymer networks	72
Figure 3.3	Average nitrogen contents of benzene/aniline co-polymer networks (the dotted line shows the theoretical values)	73
Figure 3.4	IR spectra of benzene/aniline co-polymer networks	74
Figure 3.5	Solid state NMR spectra of benzene/aniline networks (data collected by Andrea Laybourn)[34]	74
Figure 3.6	Nitrogen adsorption (close symbols) and desorption (open symbols) isotherms of benzene/aniline co-polymer networks	75
Figure 3.7	Pore size distribution of benzene/aniline networks[34]	76

Figure 3.8 Surface areas of co-polymer networks (black), physical mixture of 100% benzene and 100% aniline (red), and expected surface areas of physical mixtures (dotted line) 77

Figure 3.9 Average BET surface areas from three experiments (black) and CO_2 uptakes at 300 K with no error bar (red) of benzene/aniline co-polymer networks 78

Figure 3.10 CO_2/N_2 IAST selectivity at 1 bar of benzene/aniline co-polymer networks 79

Figure 3.11 Plot of CO_2/N_2 selectivity against CO_2 uptakes of various kinds of polymers[34] including porous organic cages (black)[37-40], MOFs (blue)[41-43] and MOPs (green)[12], the aniline/benzene networks (red) 80

Figure 4.1 Structures of compounds used to try a directly prepare a cross-linked polymer containing a carboxylic acid or an ester. From left to right: benzoic acid, methyl benzoate, butyl benzoate and 3-phenylpropionic acid 89

Figure 4.2 **RAFT-1** (left) and ACVA (right) structure 90

Figure 4.3 ^{1}H-NMR spectrum and assignment of **PS-1-7**. The peaks marked with a * indicate the solvent peaks. 91

Figure 4.4 IR spectra of **PS-1-y** with different number of styrene units 92

Figure 4.5 IR spectrum of **CLPS-1-1**, compared to that of **PS-1-1** and **RAFT-1** 94

Figure 4.6 IR spectrum of **RAFT-1** after Friedel-Crafts reaction 95

Figure 4.7 IR spectrum of the product after Friedel-Crafts reaction of decanoic acid 96

Figure 4.8 Nitrogen adsorption (close symbols) and desorption (open symbols) isotherms of the **CLPS-1-y** 97

Figure 4.9 Surface areas of **CLPS-1-ys** synthesised from different DP of linear polystyrenes 98

Figure 4.10 CO_2 uptakes of the **CLPS-1-y** synthesised from different DP of linear polystyrenes 99

Figure 4.11 **RAFT-2** (left) and **RAFT-3** (right) structures 99

Figure 4.12 **RAFT-4** (left) and **RAFT-5** (right) 100

Figure 4.13 ^{1}H-NMR spectrum and assignment of **PS-2-2**. The peaks marked with a * indicate the solvent peaks. 102
Figure 4.14 ^{1}H-NMR spectrum and assignment of **PS-3-2**. The peaks marked with a * indicate the solvent peaks. 103
Figure 4.15 ^{1}H-NMR spectrum and assignment of **PS-4-2**. The peaks marked with a * indicate the solvent peaks. 103
Figure 4.16 ^{1}H-NMR spectrum and assignment of **PS-5-2**. The peaks marked with a * indicate the solvent peaks. 104
Figure 4.17 IR spectrum of **CLPS-2-1**, compared to that of **PS-2-1** and **RAFT-2** 105
Figure 4.18 IR spectrum of **CLPS-3-1**, compared to that of **PS-3-1** and **RAFT-3** 105
Figure 4.19 IR spectrum of **CLPS-4-1**, compared to that of **PS-4-1** and **RAFT-4** 106
Figure 4.20 IR spectrum of **CLPS-5-1**, compared to that of **PS-5-1** and **RAFT-5** 106
Figure 4.21 AIBN structure 107
Figure 4.22 IR spectrum of **CLPS-4-3**, compared to that of **PS-4-3** and **RAFT-4** 107
Figure 4.23 IR spectrum of **CLPS-5-3**, compared to that of **PS-5-3** and **RAFT-5** 108
Figure 4.24 Surface areas of **CLPS-1** to **5** 109
Figure 4.25 IR spectrum of the **PS-1-y** precipitated in different solvents 111

Figure 5.1 IR spectra of **CMP-1-NH$_2$** (black) compared to 1,3,5-triethynylbenzene (blue) and unfunctionalised **CMP-1** (green) 121
Figure 5.2 IR spectra of **CMP-1-NH$_2$** (black) and **CMP-1-AMD1** (red) 122
Figure 5.3 Solid state NMR spectra of **CMP-1-NH$_2$** (bottom) and **CMP-1-AMD1** (top) (data collected by Andrea Laybourn). * indicate spinning side bands. 123
Figure 5.4 SEM image of **CMP-1-NH$_2$** 123
Figure 5.5 SEM image of **CMP-1-AMD1** 124
Figure 5.6 IR spectra of **CMP-1-NH$_2$** (black) and **CMP-1-AMDs** 125

Figure 5.7 Nitrogen adsorption (close symbols) and desorption (open symbols) isotherms of **CMP-1-NH$_2$** and **CMP-1-AMDs** 126

Figure 5.8 NL-DFT pore size distributions of **CMP-1-NH$_2$** and **CMP-1-AMDs** 127

Figure 5.9 BET surface areas (columns), total pore volumes (red triangles), micropore volumes (blue triangles) and the proportion of micropore to total pore volumes (black circles) for **CMP-1-NH$_2$** and **CMP-1-AMDs** 128

Figure 5.10 CO_2 uptakes of **CMP-1-NH$_2$** and **CMP-1-AMDs** at 273 K and 298 K 129

Figure 5.11 CO_2 isosteric heat of adsorption of **CMP-1-NH$_2$** and **CMP-1-AMDs** 130

Figure 5.12 IR spectra of **CMP-1-AMD5s** modified by different conditions 133

Figure 5.13 Nitrogen contents of **CMP-1-AMDs** modified by different conditions 133

Figure 5.14 Surface areas of **CMP-1-AMDs** modified by different conditions 134

Figure 5.15 CO_2 uptakes of **CMP-1-AMDs** modified by different conditions 134

Figure 6.1 General procedure to synthesise MIPs 141

Figure 6.2 Templates used in this research: a) cholesterol, b) menthol, c) trimesic acid (TMA) 143

Figure 6.3 IR spectrum of cholesteryl 2,5-dibromobenzoate monomer (**cholesterol functionalised monomer**) (blue) compared to 2,5-dibromobenzoic acid (red) and cholesterol (black) 144

Figure 6.4 IR spectrum of **CHOL-CMP** compared to monomers 145

Figure 6.5 IR spectra of **CHOL-CMP** before (black) and after (purple) attempted hydrolysis with KOH/MeOH compared to **CMP-1-COOH** (red) 146

Figure 6.6 IR spectra of **CHOL-COOH** before (purple) and after (pink) attempted hydrolysis compared to **CHOL-CMP** (black) and **CMP-1-COOH** (red) 148

Figure 6.7 IR spectra of **CHOL-OH** before (blue) and after (green) attempted hydrolysis compared to **CHOL-CMP** (black) and **CMP-1-COOH** (red) 150

Figure 6.8 IR spectrum of menthyl 2,5-dibromobenzoate monomer (**menthol functionalised monomer**) (blue) compared to 2,5-dribromobenzoic acid (red) and menthol (black) 152
Figure 6.9 IR spectrum of **MENT-CMP** compared to monomers 152
Figure 6.10 IR spectra of **MENT-CMP** before (black) and after (purple) attempted hydrolysis with KOH/MeOH compared to **CMP-1-COOH** (red) 153
Figure 6.11 IR spectra of **MENT-Hs** before hydrolysis 155
Figure 6.12 IR spectra of **MENT-Hs** after hydrolysis (**MENT-H-Hs**) 156
Figure 6.13 GC chromatogram of menthol (left) and decanol (right) 157
Figure 6.14 Calibration curve of menthol in hexane calculated by GC using decanol as an internal standard 158
Figure 6.15 IR spectra of **MENT-COOHs** before hydrolysis 160
Figure 6.16 IR spectra of **MENT-COOHs** after hydrolysis (**MENT-COOH-Hs**) 161
Figure 6.17 Amount of menthol adsorbed in **MENT-H-Hs** when different concentrations of menthol solutions were used 163
Figure 6.18 Percentage of menthol adsorbed in **MENT-H-Hs** when different concentrations of menthol solutions were used 163
Figure 6.19 Amount of menthol adsorbed in **MENT-COOH-Hs** when different concentrations of menthol solutions were used 164
Figure 6.20 Percentage of menthol adsorbed in **MENT-COOH-Hs** when different concentrations of menthol solutions were used 164
Figure 6.21 Left axis: surface areas of **MENT-H-Hs** (blue). Right axis: their menthol (red) and terpinolene (green) adsorption and selectivity of menthol over terpinolene (purple). 166
Figure 6.22 Left axis: surface areas of **MENT-COOH-Hs** (blue). Right axis: their menthol (red) and terpinolene (green) adsorption and selectivity of menthol over terpinolene (purple). 167
Figure 6.23 IR spectra of **T-MENT-COOHs** before hydrolysis 169
Figure 6.24 IR spectra of **T-MENT-COOHs** after hydrolysis (**T-MENT-COOH-Hs**) 170

Figure 6.25 Left axis: surface areas of **T-MENT-COOH-Hs** (blue). Right axis: their menthol (red) and terpinolene (green) adsorption and selectivity of menthol over terpinolene (purple). 171

Figure 6.26 Comparison of menthol adsorption in **MENT-Hs**, **MENT-COOHs** and **T-MENT-COOHs** 172

Figure 6.27 Comparison of terpinolene adsorption in **MENT-Hs, MENT-COOHs** and **T-MENT-COOHs** 173

Figure 6.28 Comparison of selectivity of menthol over terpinolene in **MENT-Hs**, **MENT-COOHs** and **T-MENT-COOHs** 173

Figure 6.29 IR spectrum of tris(2,4-dibromophenyl) benzene-1,3,5-tricarboxylate (**Trimesate monomer**) (blue) compared to 2,5-dibromobenzoic acid (red) and trimesic acid (black) 176

Figure 6.30 IR spectrum of **O-TRIM-100** compared to monomers 177

Figure 6.31 IR spectrum of **O-TRIM** before (black) and after (purple) after attempted hydrolysis compared to **O-TRIM-0** (**CMP-OH**) (red) 178

Figure 6.32 IR spectra of **O-TRIMs** before hydrolysis 179

Figure 6.33 IR spectrum of **O-TRIMs** after hydrolysis 180

Figure 6.34 Graph shows HPLC chromatogram of trimesic acid 181

Figure 6.35 Calibration curve of trimesic acid in MeOH calculated by HPLC 182

Figure 6.36 Surface areas and amount of trimesic acid adsorbed in **O-TRIM-Hs** compared to **CMP-1** 183

Figure 6.37 HPLC chromatogram of the 5 compound mixture 184

Figure 6.38 Surface areas and amount of compounds adsorbed in **O-TRIMs** compared to **CMP-1** 185

Figure 6.39 IR spectra of **O-TRIMs** before hydrolysis 186

Figure 6.40 IR spectra of **O-TRIMs** after hydrolysis (**O-TRIM-Hs**) 186

Figure 6.41 Surface areas and amount of compounds adsorbed in **O-TRIMs** compared to **CMP-1** 188

Figure 6.42 IR spectrum of N^1,N^3,N^5-tris(2,4-dibromophenyl)benzene-1,3,5-tricarboxamide (**Trimesamide monomer**) (blue) compared to 2,5-dibromoaniline (red) and trimesic acid (black) 190

Figure 6.43 IR spectrum of **N-TRIM** compared to monomers 192

Figure 6.44 IR spectrum of **N-TRIM** before (black) and after (purple) after attempted hydrolysis compared to **N-TRIM-0** (**CMP-NH_2**) (red) 193

Figure 6.45 IR spectra of **N-TRIMs** before hydrolysis 194
Figure 6.46 IR spectra of **N-TRIMs** after hydrolysis (**N-TRIM-Hs**) 195
Figure 6.47 Surface areas and amount of compounds adsorbed in **N-TRIMs** compared to **CMP-1** 197
Figure 6.48 Surface areas and amount of compounds adsorbed in **N-TRIMs** compared to **CMP-1** 197
Figure 6.49 Possible model of the rigid imprinted cavity which might be too small for trimesic acid 199

List of Tables

Table 3.1 Yields and elemental analysis data for the benzene/aniline co-polymer networks 71

Table 3.2 Gas sorption data and CO_2/N_2 selectivity at 1 bar calculated from IAST method using 15% CO_2 and 85% N_2 of benzene/aniline co-polymer networks 76

Table 4.1 Yields, elemental analysis and GPC data of linear polystyrenes (**PS-1-ys**) 93

Table 4.2 Yields, elemental analysis and gas sorption data of the cross-linked linear polystyrenes (**CLPS-1-y**) 93

Table 4.3 Yields, elemental analysis and GPC data of the linear polystyrenes with different RAFT agents (**PS-x-ys**) 101

Table 4.4 Yields, elemental analysis and gas sorption data of the cross-linked polystyrenes with different RAFT agent (**CLPS-x-ys**) 109

Table 4.5 Yields, elemental analysis and GPC data for **PS-1-ys** precipitated in different solvents 111

Table 4.6 Yields, elemental analysis and gas sorption data of the **CLPS-1-ys** precipitated in different solvents 112

Table 5.1 Yields and elemental analysis data of **CMP-1-AMDs** 124

Table 5.2 Gas sorption data of **CMP-1-AMDs** 129

Table 5.3 Yields, elemental analysis and gas sorption data of **CMP-1-AMDs-RT** 130

Table 5.4 Yields, elemental analysis and gas sorption data of **CMP-1-AMDs-$CHCl_3$** 132

Table 6.1 Hydrolysis conditions of **CHOL-CMP** 147

Table 6.2 Hydrolysis conditions of **MENT-CMP** 153

Table 6.3 Yields, elemental analysis and gas sorption data of **MENT-Hs** 155

Table 6.4	Yields, elemental analysis and gas sorption data of **MENT-H-Hs**	157
Table 6.5	Surface areas and menthol adsorption of **MENT-H-Hs**	159
Table 6.6	Yields, elemental analysis and gas sorption data of **MENT-COOHs**	160
Table 6.7	Yields, elemental analysis and gas sorption data of **MENT-COOH-Hs**	162
Table 6.8	Surface areas and menthol adsorption of **MENT-COOH-Hs**	162
Table 6.9	Yields, elemental analysis and gas sorption data of **T-MENT-COOHs**	169
Table 6.10	Yields, elemental analysis and gas sorption data of **T-MENT-COOH-Hs**	170
Table 6.11	Surface areas, adsorption and selectivity data of **MENT-CMPs**	174
Table 6.12	Synthetic conditions for **Trimesate monomer**	177
Table 6.13	Yields, elemental analysis and gas sorption data of **O-TRIMs**	180
Table 6.14	Yields, elemental analysis and gas sorption data of **O-TRIM-Hs**	181
Table 6.15	Surface areas and adsorption data of **O-TRIMs**	184
Table 6.16	Yields, elemental analysis and gas sorption data of **O-TRIMs**	187
Table 6.17	Yields, elemental analysis and gas sorption data of **O-TRIM-Hs**	187
Table 6.18	Surface areas and adsorption data of **O-TRIMs**	188
Table 6.19	Synthetic conditions for **Trimesamide monomer**	191
Table 6.20	Yields, elemental analysis and gas sorption data of **N-TRIMs**	195
Table 6.21	Yields, elemental analysis and gas sorption data of **N-TRIM-Hs**	196
Table 6.22	Surface areas and adsorption data of **N-TRIMs**	198

Abstract

Microporous organic polymers (MOPs) are materials made from organic monomers that have a pore width smaller than 2 nm. Due to their high porosity and diversity of functional group, MOPs have potential in broad ranges of applications. As well as absolute surface area, the functional groups also play an important role in the design and synthesis of materials for desired utilisations. In this work, we demonstrate strategies to synthesise functionalised networks to be utilised as sorbents. The focus is on hypercross-linked polymers (HCPs) and conjugated microporous polymers (CMPs), which are amorphous networks and subclasses of MOPs. Different strategies including copolymerisation, post-cross-linking of functionalised linear polymer chains, and post-synthetic modification (PSM) were found able to incorporate different functional groups into the networks. The structures and properties of the networks could be fine tuned. The networks were investigated for applications in CO_2 capture and separations as well as molecular imprinting polymers (MIPs).

List of Abbreviations

ACVA	4,4′-azobis(4-cyanovaleric acid)
AIBN	azobisisobutyronitrile
ATR	attenuated total reflection
BA	benzyl alcohol
BCMCP	4,4’-bis(chloromethyl)-1,1’-biphenyl
BDM	1,4-benzenedimethanol
BEN	benzene
BET	Brunauer-Emmett-Teller
CDDPA	4-cyano-4-[(dodecylsulfanylthiocarbonyl)sulfanyl]pentanoic acid
CI	chemical ionisation
CLPS	crosslinked polystyrene
CMDP	1,4-bis(chloromethyl) diphenyl
CMM	tris(chloromethyl) mesitylene
CMP	conjugated microporous polymer
COF	covalent organic framework
COP	covalent organic polymer
CPBT	2-cyano-2-propyl benzodithioate
CPCPA	4-cyano-4-(phenylcarbonothioylthio)pentanoic acid
CPDT	2-cyano-2-propyl dodecyl trithiocarbonate
CP/MAS	cross-polarization magic angle spinning
CTF	covalent triazine framework
NL-DFT	nonlocal density functional theory
DCC	*N,N′*-dicyclohexylcarbodiimide
DCE	1,2-dichloroethane
DCM	dichloromethane
DCX	dichloroxylylene
DDMAT	2-(dodecylthiocarbonothioylthio)-2-methylpropionic acid
DFT	density functional theory
DMAP	4-dimethylaminopyridine
DMB	1,4-dimethoxybenzene

DMF	*N,N*-dimethylformamide
DNP	dynamic nuclear polarization
DP	degree of polymerisation
DPB	*p,p'*-bis(chloromethyl)-1,4-diphenylbutane
FDA	formaldehyde dimethyl acetal
FE-SEM	Field Emission Scanning Electron Microscope
FID	Flame Ionization Detector
FTIR	Fourier transformed infra-red spectroscopy
GC	gas chromatography
GPC	gel permeation chromatography
HCCMP	hypercrosslinked conjugated microporous polymer
HCP	hypercrosslinked polymer
HPLC	high performance liquid chromatography
IR	infrared
IUPAC	International Union of Pure and Applied Chemistry
M_n	number-average molecular weight
M_w	weight-average molecular weight
MCDE	monochlorodimethyl ether
MIP	molecular imprinting polymer
MO-CMP	metal-organic conjugated microporous organic polymer
MOF	metal-organic framework
MOP	microporous organic polymer
MS	mass spectroscopy
NAP	naphthalene
NMR	nuclear magnetic resonance
NTA	2-naphtholic acid
PAF	porous aromatic framework
PDI	polydispersity index
PIM	polymer of intrinsic microporosity
PPN	porous polymer network
PS	polystyrene
PSD	pore size distribution
PSM	post-synthetic modification
RAFT	reversible addition-fragmentation chain transfer

SA	surface area
SAM-HCP	sulfonic acid-modified hypercrosslinked polymer
SCMP	Scholl-coupling microporous polymers
SEM	scanning electron microscopy
ssNMR	solid state nuclear magnetic resonance
TBU	1-(tert-butyl)-3,5-dimethylbenzene
TCMP	triazine conjugated microporous polymer
TEM	transmission electron microscopy
TGA	thermogravimetric analysis
THF	tetrahydrofuran
TMA	trimesic acid
TMS	tetramethylsilane
TPPM	two-pulse phase modulation
$V_{0.1}$	micropore volume (pore volume at $p/p^0 = 0.1$)
V_{tot}	total pore volume
XPS	X-ray photoelectron spectroscopy
YBN	Yamamoto derived benzene network
YSN	Yamamoto derived spirobifluorene network

Acknowledgements

Firstly, I would like to express my sincere gratitude to my advisors Prof. Dave J. Adams and Prof. Andrew I. Cooper for the continuous support of my PhD study and related research, for their patience, motivation, and immense knowledge. Their guidance helped me in all the time of research and writing of this Thesis. I could not have imagined having better advisors and mentors for my PhD study.

Besides my advisors, I would like to thank Robert Dawson on his support and suggestions, as well as his help in measuring samples on gas sorption and other techniques at the early stage of my research. Special thanks also go to Rob Clowes, Sean Higgins, and other staffs in Centre of Materials Discovery (CMD) who trained and supported me to use various analysis instruments including gas sorption analysers, NMR spectrometer, and IR spectrometer in the CMD and also helped in samples measurements on gas sorption and GPC analysis.

I am grateful to Jean Ellis, George Miller, and Moya McCarron for their help in running instruments for elemental analysis and mass spectroscopy. I am also grateful to other departmental staff, especially Bonnie Cham, PA to Prof. Andrew I. Cooper, for their support during my study.

I would also thank past and present members of the Cooper and Adams groups as well as my friends in Liverpool for the stimulating discussions, support and help, and for all the fun we have had in the last four years. Special thanks go to Michael Briggs and Adam Kewley for HPLC and GC analysis.

My sincere thanks also go to Mahidol-Liverpool Stang Mongkolsuk PhD Scholarship supported by Mahidol University and University of Liverpool for my PhD financial funding and opportunity to conduct this research.

Last but not the least, I would like to thank my family especially my parents for supporting me spiritually throughout my study and my life in general. I would also like to specially thank my boyfriend, Natchapol Poonyayant, who was always supporting me in all means.

List of Publications

Parts of the work in this Thesis are published in the following Journals:

(1) Robert Dawson, Thanchanok Ratvijitvech, Matthew Corker, Andrea Laybourn, Yaroslav Z. Khimyak, Andrew I. Cooper and Dave J. Adams. ***Microporous copolymers for increased gas selectivity.*** *Polym. Chem.,* **2012**, *3,* 2034-2038.

(2) Thanchanok Ratvijitvech, Robert Dawson, Andrea Laybourn, Yaroslav Z. Khimyak, Andrew I. Cooper and Dave J. Adams. ***Post-synthetic modification of conjugated microporous polymers.*** *Polymer,* **2014**, *55*, 321-325.

(3) Thanchanok Ratvijitvech, Michael Barrow, Andrew I. Cooper, Dave J. Adams. ***The effect of molecular weight on the porosity of hypercrosslinked polystyrene.*** *Polym. Chem.,* **2015**, *6*, 7280-7285.

Chapter 1

Introduction

1. Introduction

1.1 Microporous Organic Polymers

Microporous organic polymers (MOPs) according to IUPAC classification are materials made from organic monomers that have a pore width smaller than 2 nm[1]. The focus in this thesis will be on the porosity formed by structure not by templating. Porous structures are generated by interconnecting networks that are not densely packed but form voids. In general, rigid building blocks are used to prevent collapsing of the network. Most rigid building blocks are aromatic compounds and their derivatives. For most MOPs, two components are necessary to form networks (**Figure 1.1**).[2] The first is the node or knot, which is the monomer that has two or more modes of connectivity. The second is the strut or linker, which is a monomer that has at least two functionalities. When these two components are connected, porous polymers are formed, unless they collapse and close the pore after removal of solvent.

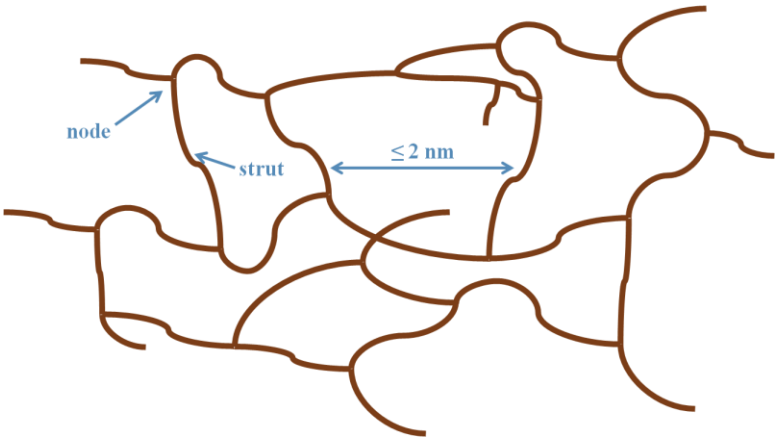

Figure 1.1 The structure of microporous organic polymer

There are many advantages of MOPs over other microporous materials. First of all, because MOPs generally only contain non-metallic, lighter elements like H, C, B, N and O, they can have low skeleton densities. In other words, they can be obtained in light mass, which can lead to high surface area materials. The most important benefit is the variety of functional groups that can be introduced as there

are a large number of methodologies to synthesise polymers.[2-5] It is also possible to post-synthetically modify the networks after formation, resulting in wider range of functional groups in the networks.[6-9] The structures and properties of the materials, therefore, can be tuned by design and synthesis. Moreover, many of the MOPs are thermally and chemically stable due to strong covalent bonding. Some MOPs can also be synthesised at a low cost with scalability.[3] MOPs are of interest due to their broad promising applications in areas such as gas storage and separations[10-14], molecules capture[15-17], catalysis[18, 19], light harvesting and emitting[20-22], sensors[23], and energy storage and conversion[24-26].

There are two main classes of MOPs: crystalline and amorphous. Crystalline MOPs are well-ordered networks. These polymers are usually synthesised by reversible bond-formation reactions to provide ordered, thermodynamically stable networks. Crystalline MOPs are divided into sub-groups due to their structures: for example, covalent organic frameworks (COFs)[27, 28] (**Figure 1.2a**) which are the analogues of metal organic frameworks (MOFs). The strong covalent bonds are formed by condensation reactions to provide B-O rings that can be compared to metal cluster in MOFs. Covalent triazine frameworks (CTFs)[29, 30] (**Figure 1.2b**) are other crystalline MOPs. The crystalline CTFs can be synthesised by using nitrile monomers which reversibly cyclotrimerise to form triazine networks.

Amorphous MOPs are often synthesised by high yielding, irreversible reactions to provide kinetic, disordered products. There are many sub-classes of these kinds of materials. One is polymers of intrinsic microporosity (PIMs)[31-33] (**Figure 1.2c**) which are inefficiently packed polymers in solid state. PIMs differ to other MOPs as they are linear polymers. The porosity in PIMs results from the rigid and contorted monomers which cannot efficiently fill the space leading to the free volume between linear polymer chains. They can be synthesised from irreversible condensation reactions of dihydroxy and dihalide monomers to form O-linkage aromatic rings. The second is hypercross-linked polymers (HCPs)[4, 34-36] (**Figure 1.2d**, **e**). Hypercross-linked polymers can be synthesised by extensive cross-linking reactions so that they cannot collapse. Conjugated microporous polymers (CMPs)[5, 37-39] (**Figure 1.2f**) are a kind of hypercross-linked polymers which are linked together in a conjugated manner e.g. by double or triple bonds or the linking of aromatics directly to one another.

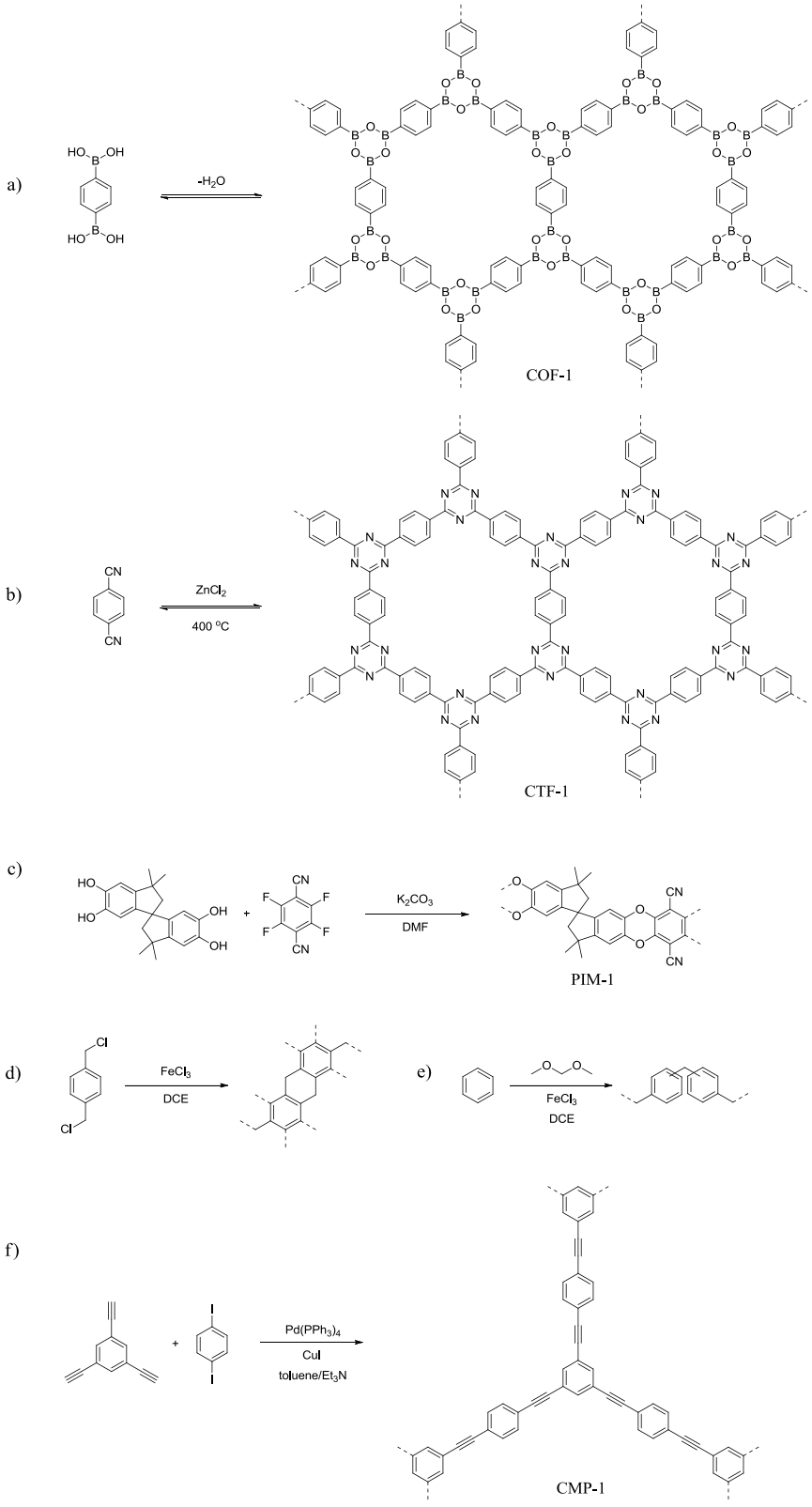

Figure 1.2 Example of each type of microporous organic polymers. Crystalline MOPs: (a) COFs, (b) CTFs. Amorphous MOPs: (c) PIMs, (d) HCPs (polycondensation), (e) HCPs (knitting), and (f) CMPs. Dashed lines show the connecting points.

Recently, many novel kinds of materials were created. For example, porous aromatic frameworks (PAFs), the network inspired by structure of diamond, was introduced in 2009 by Ben *et al*.[40] PAF-1 has an ultrahigh BET surface area of 5600 m^2/g which is useful for various applications.[41] In 2011, porous polymer networks (PPNs) were reported with exceptional high surface areas and gas uptakes.[42] PPN-4 exhibits the highest BET surface area, 6461 m^2/g, among reported porous organic materials.[43] Compared to other porous materials, it is lower than only the NU-109 and NU-110 MOFs,[44] which show BET surface areas of 7010 and 7140 m^2/g respectively.

1.2 Synthesis

Different organic reactions could be used in MOPs synthesis including condensation reaction[27, 45, 46], cyclotrimerisation[29, 47, 48], dibenzodioxane-forming reaction[31, 49, 50], Friedel-Crafts reaction[4, 34, 35, 51], Sonogashira-Hagihara coupling[38, 52-54], Suzuki cross-coupling[22, 25, 55], Yamamoto type Ullmann coupling[40, 43, 56], Heck reaction[57], Schiff base chemistry[58-60], Scholl coupling[61]. The focus will be mainly on the synthesis of HCPs and CMPs as they have been used in the work in this thesis.

1.2.1 Synthesis of HCPs

A Friedel-Crafts reaction is mainly used in the synthesis of HCPs. They can be produced by three different strategies: post-cross-linking of polymer chains, direct polycondensation or by using external cross-linker.[4]

Post-cross-linking of polymer chains is the extended cross-linking reaction of the preformed linear or lightly cross-linked polymer chains to obtain the rigid networks (**Figure 1.3**). The rigidity is aiming to preserve the porous structure after removal of solvent to obtain the networks with permanent porosity. The most well-known material synthesised by this strategy is Davankov resins or the hypercross-linked polystyrenes introduced by Davankov.[51, 62] Polystyrene chains were dissolved or swollen in solvent and cross-linked by the bi- or tri-functional cross-linkers including *p*-dichloroxylylene (DCX), 1,4-bis(chloromethyl) diphenyl (CMDP),

monochlorodimethyl ether (MCDE), formaldehyde dimethyl acetal (FDA), tris(chloromethyl) mesitylene (CMM), and p,p'-bis(chloromethyl)-1,4-diphenylbutane (DPB) using Friedel-Crafts reaction.[51] Such materials are widely studied and proven to have many applications such as gas storage, chromatography, and organic vapours adsorption.[63] Recently, Vinodh *et al.* suggested the new strategy to synthesise hypercross-linked polystyrene without a cross-linker with surface area of 224 m^2/g and CO_2 uptake of 4.2 wt% at 25 °C and 1 atm.[64]

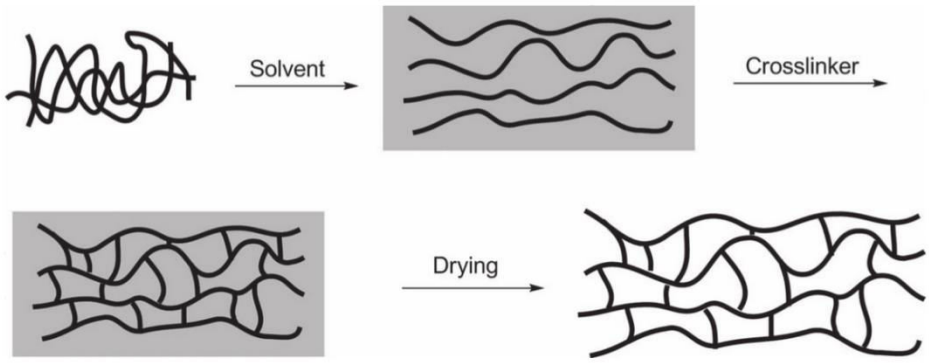

Figure 1.3 Synthesis scheme of HCPs by post-cross-linking of polymer chains[65]

HCPs can also synthesised by direct polycondensation of small molecules instead of prepared polymer chains. The networks are formed by self-condensation reaction of di- or tri- functionalised aromatic monomers. (**Figure 1.2d**) Tsyurupa and Davankov suggested the synthesis of HCPs by self-condensation of *p*-DCX using $SnCl_4$ as a Friedel-Carfts catalyst to obtain the networks with surface areas up to 1000 m^2/g.[62] The Cooper group also extended the study to different isomers of DCX and also other bis(chloromethyl) aromatic monomers like 4,4'-bis(chloromethyl)-1,1'-biphenyl (BCMCP) and 9,10-bis(chloromethyl)anthracene using $FeCl_3$ as a catalyst. The networks obtained have the surface areas up to 1904 m^2/g and exhibited H_2 uptakes up to 3.68 wt% at 77 K and 15 bar.[34] Copolymerisation of *p*-DCX and BCMCP for CO_2 capture was also investigated by the same group.[66] Porous networks were also obtained by acid catalysted polycondensation of fluorenone derivatives using methane sulfonic acid (CH_3SO_3H) as a catalyst.[67] In 2013, Luo *et al.* reported the use of hydroxymethyl monomers where the side product of the

Friedel-Crafts reaction is water instead of typical hydrochloric acid or methanol providing a more environmentally friendly method to construct HCPs. Bishydroxymethyl monomer (1,4-benzenedimethanol, BDM) generated the network with surface area of 847 m^2/g. Interestingly, the monohydroxymethyl monomer (benzyl alcohol, BA) could also constructed the network with surface area of 742 m^2/g which is the first time of using mono-functionalised compound as a self-condensing monomer.[68]

To overcome the limitation of self-condensation method which requires the functionalised monomers, the Tan group reported the preparation of HCPs by using external cross-linker or the so-called "knitting" method.[35] (**Figure 1.2e**) Aromatic building blocks such as benzene, biphenyl, 1,3,5-triphenylbenzene, methylbenzene, chlorobenzene, and phenol could be knitted by external cross-linker i.e. FDA using Friedel-Crafts reaction. Surface areas up to 1391 m^2/g by using benzene as a monomer could be obtained.[35] The Cooper group showed that using a tetrahedral monomer, tetraphenylmethane, could improve the surface area to 1470 m^2/g.[69] The knitting method is also compatible with heterocyclic aromatic building blocks like thiophene, pyrrole, and furan.[70] Chiral microporous materials could also easily obtained using such the strategy.[71] Copolymers, for example, benzene and aniline copolymer networks[72] were successfully synthesised for CO_2 capture utilisation as will be discussed in Chapter 3.

1.2.2 Synthesis of CMPs

Conjugated microporous polymers or CMPs were firstly introduced by the Cooper group in 2007.[38] Due to the conjugated systems containing in the networks, such materials have the potential in light harvesting and emitting applications apart from gas and molecules storage. Different methods could be used in the CMPs synthesis (**Figure 1.4**). The most common reactions are Sonogashira-Hagihara coupling[55, 73], Suzuki coupling[21, 55, 73, 74] and Yamamoto coupling[20, 21, 56]. Other reactions used in synthesis of CMPs include Friedel-Crafts reaction[74, 75], Schiff-base reaction[46, 58, 59], cyclotrimerisation[29, 47], and phenazine ring fusion reaction[26].

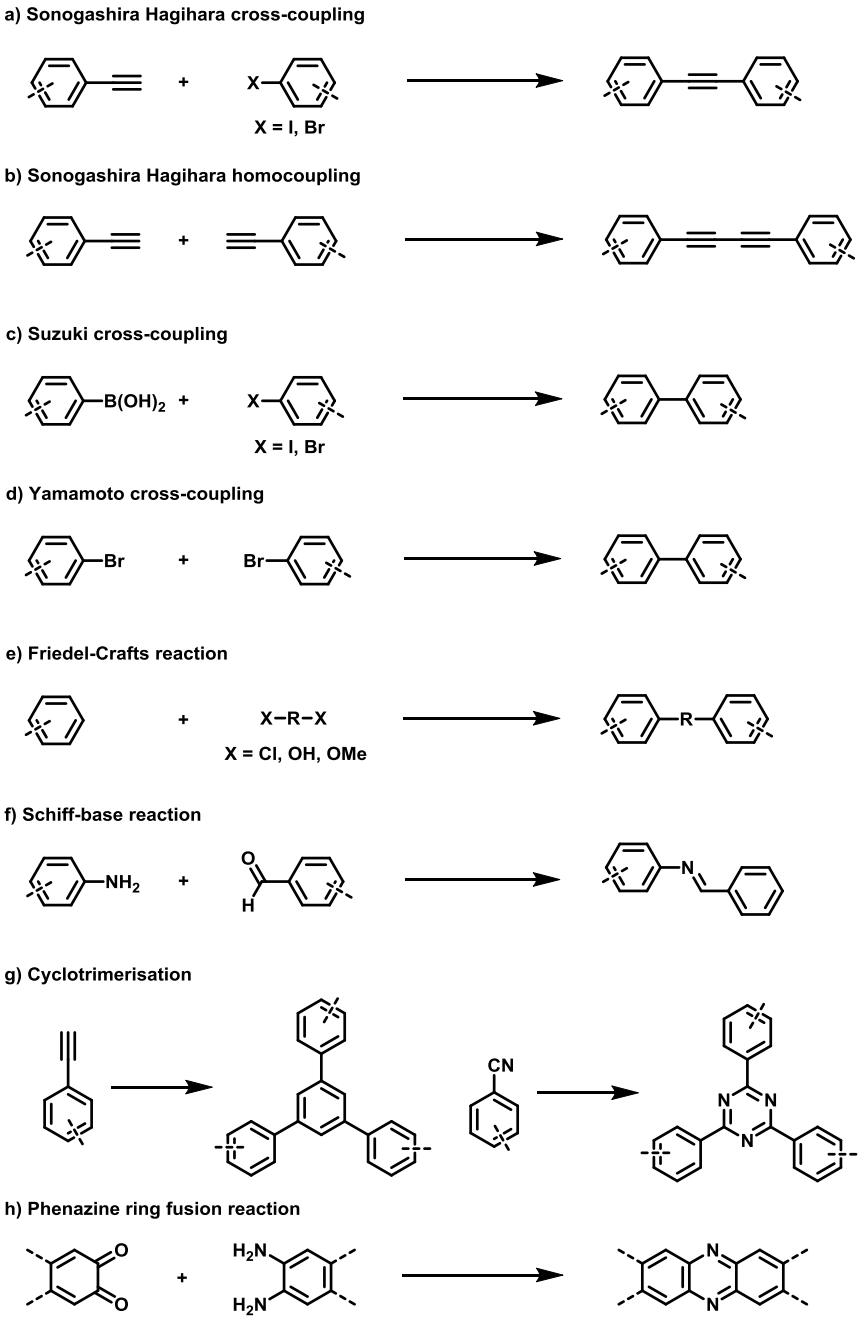

Figure 1.4 Examples of reactions for synthesis of CMPs

By using Pd/Cu-catalysed Sonogashira-Hagihara cross-coupling of aryl alkynes and aryl halides (**Figure 1.4a**), conjugated microporous networks with surface areas of 522-834 m^2/g could be obtained. Similar to crystalline networks, the porosity of CMPs could be tuned by tailoring the strut lengths[76], nodes[77] and solvent

choices[78] even though they are amorphous, suggesting that the crystallinity is not a requirement for fine tuning the properties of the networks.[38] The synthetic method could be used with different functional monomers providing diversity of functionalised networks.[79] Oxidative homocoupling reaction (**Figure 1.4b**) of poly(phenylene butadiynylene) was also used to form the CMPs with surface areas up to 842 m^2/g.[52] In fact, the homocoupling reaction was found to be involved even when cross-coupling reaction was used.[80]

CMPs could also be synthesised by Suzuki cross-coupling of aryl halides and boronic acid or boronic ester monomers (**Figure 1.4c**). The Suzuki reaction has advantages due to its mild reaction conditions and compatibility to wide range of functional groups. A greater diversity of monomers with different conformation and functionalities can then be used.[22, 25, 55, 73]

Schmidt *et al.* suggested the alternative way to produce CMPs by Yamamoto coupling of halogenated monomer using bis(1,5-cyclooctadiene)nickel(0) ($Ni(COD)_2$) as a catalyst (**Figure 1.4d**).[56] Yamamoto derived spirobifluorene network (YSN) and Yamamoto derived benzene network (YBN) were synthesised with surface areas of 1275 and 1255 m^2/g respectively. The advantage of Yamamoto reaction is that only single monomer with halogen-functional group is required. Other monomers such as 1,3,6,8-tetrabromopyrene[21], tetraphenylethene[20] and carbazole derivatives[23] could also be used. The reaction was also used in synthesis of PAF-1[40] and PPN-4, the highest surface areas MOPs.

CMPs were also prepared using Friedel-Crafts catalysts (**Figure 1.4e**), which are comparably cheap compared to the Pd or Ni catalysed reactions mentioned above. Li *et al.* demonstrated the synthesis of SCMPs (Scholl-coupling microporous polymers) by Scholl reaction using $AlCl_3$ as a catalyst. The method can be used with diversity of monomers providing the luminescent networks with good gas uptakes and catalytic properties.[61] Recently, CMPs could be synthesised by Friedel-Crafts reaction using external cross-linker similar to HCPs synthetic strategies. By using 1,4-dimethoxybenzene (DMB) as a cross-linker, hypercross-linked conjugated microporous polymers (HCCMPs) was obtained. The surface area of 800 m^2/g and other gas uptakes of the network is comparable to previously reported CMPs.[75]

1.3 Characterisation

1.3.1 Structure and morphology

To tune the polymers for the right properties, the structures of the networks should be understood. Nevertheless, characterisation of networks morphology is considered to be difficult. As most of them are insoluble, solution-phase techniques, such as solution nuclear magnetic resonance (NMR) spectroscopy, gel permeation chromatography (GPC) and mass spectroscopy (MS), cannot be used. Also, amorphous structures lead to the difficulty in characterisation by X-ray crystallographic techniques. Infrared spectroscopy (IR) is a useful technique to identify the functional groups in the polymers. If monomers or networks contain detectable functionalities, the reaction could be tracked by observing the reduction of starting material functional groups and presence of product functional groups. However, the limitation is IR spectra usually provide only qualitative data, quantitative information often cannot be obtained.

To measure the chemical compositions in the polymeric material, elemental analysis is a tool that can be used. Nevertheless, it still give an error due to porous properties of materials which can easily adsorb gases and water vapour as well as trap catalyst in their porous structures resulting in inaccurate information.[72, 81-83] Energy-dispersive X-ray spectroscopy (EDX or EDS)[53, 79, 83, 84] and X-ray photoelectron spectroscopy (XPS)[85-88] are another analytical methods which provide the elemental contents information used in confirming the amount of end groups and residual catalyst in the networks.

The most powerful method up to date may be the solid state NMR spectroscopy (ssNMR) to elucidate the quantitative information by different carbon environments. However, ssNMR normally takes a long experimental time, which can be hours or days. Recently, ssNMR was developed by using high-field dynamic nuclear polarization (DNP) to enhance the sensitivity of signal.[89] The time used to get a good signal-to-noise ratio was reduced to minutes compared to hours without the enhancement by DNP. The shortened time allows the high-throughput characterisation can be obtained although unfortunately there are very few suitable NMR spectrometers available for use.

Macroscopic morphology can be investigated by the images of the polymers using scanning electron microscopy (SEM) and transmission electron microscopy (TEM). The size and morphology of materials can be observed by SEM, while TEM can provide the porous texture information.

Physical stability of polymers is generally confirmed by thermogravimetric analysis (TGA). TGA is also used in some gas sorption experiment. The chemical stability of the network is normally studied by immersing materials in water, acids and bases.

1.3.2 Porosity

Porosity is the most important property of porous networks. In general, the porosity is measured by using nitrogen gas as a sorbent at 77 K providing nitrogen isotherms. Nitrogen is widely used because it has low cost and is highly abundant gas. However, other gases can be used in different purposes. For example, argon, hydrogen and carbon dioxide, which are smaller than nitrogen molecules, were used to probe the smaller pores in the network where nitrogen cannot access. While nitrogen and hydrogen adsorption measurements are normally performed at 77 K, carbon dioxide uptakes usually operate around room temperature. Ar isotherms are normally measured at 87 K.

The nitrogen isotherm is the plot between the amounts of nitrogen gas adsorbed against the equilibrium relative pressure (p/p^0) measured at the constant temperature, normally at 77 K. Much porous information can be obtained from nitrogen isotherms. The shape of nitrogen isotherms can be grouped into six types as shown in **Figure 1.5** (left). Type I isotherms (or Langmuir isotherms) demonstrated the microporous structure. Gas can be largely adsorbed at relative low pressure then saturated at the higher relative pressure where the micropores are filled. Type II isotherms are normally given by the non-porous or macroporous materials where unrestricted monolayer-multilayer adsorption occurred. Point B in **Figure 1.5** indicates the point where the monolayer coverage is complete and the multilayer adsorption begins. Type III isotherms are not generally observed. Such isotherms happen as the adsorbate-adsorbate interaction is greater than the adsorbent-adsorbate

interaction. Type IV isotherms are similar to Type II isotherms but possess the hysteresis loop attributed to capillary condensation in mesopores. Type IV isotherms are obtained by many mesoporous adsorbents. Type V isotherms are related to Type III isotherms but with hysteresis and also uncommonly found. Type VI isotherms represent the stepwise multilayer adsorption which each steps is responsible to each monolayer adsorption capacity.[90]

Hysteresis is observed when the adsorption and desorption curves do not coincide which is resulted from the capillary condensation. Hysteresis divided into four types as shown in **Figure 1.5** (right) according to its shape. Type H1 is the hysteresis which the adsorption curve is vertically parallel to the desorption one. For Type H4, the adsorption and desorption curves are horizontally parallel. Type H2 and H3 are the intermediate shape between Type H1 and H4. Type H1 hysteresis is often found in materials that have uniform spheres and narrow pore size distribution (PSD). Meanwhile, Type H2 hysteresis is observed in materials which the shape and size is not uniform. Type H3 and H4 are often obtained by slit-shaped pores with the narrow pores in Type H4.[90]

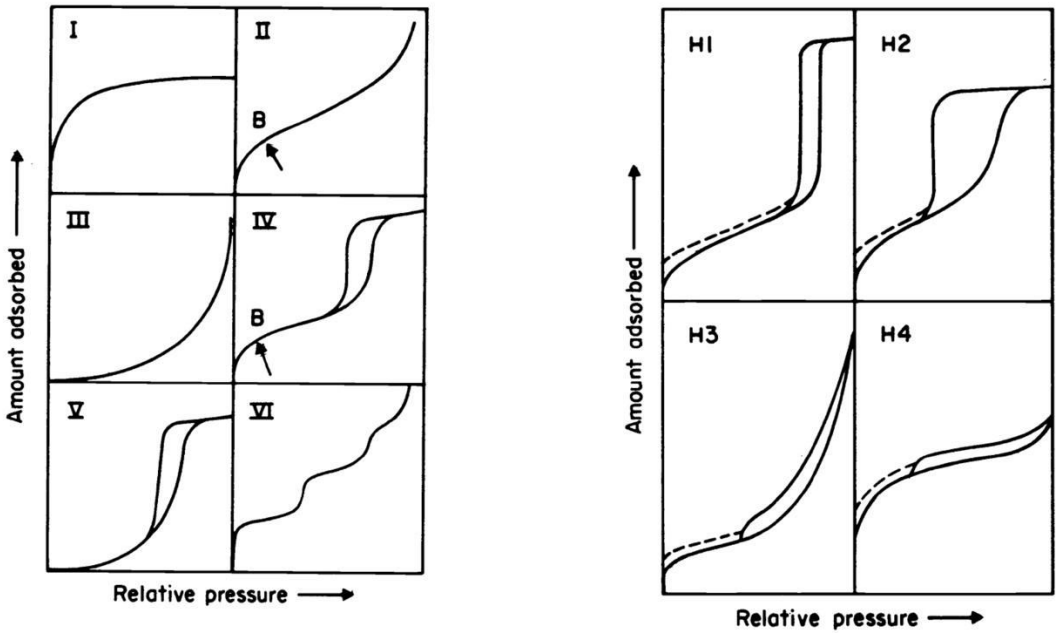

Figure 1.5 Types of nitrogen isotherms (left) and hysteresis loops (right)[90]

Gas sorption data can also be used to provide other useful porosity information such as surface areas, pore volumes and PSD. Surface areas can be calculated from either Langmuir[91] or Brunauer-Emmett-Teller (BET)[92] theories. Langmuir theory is based on the monolayer adsorption while BET theory is calculated from the multilayer adsorption assumption. Unfortunately, the accurate surface area is difficult to obtain as both theories are based on the assumption of rigid networks while MOPs could swell upon guest adsorption.[33, 93] Nevertheless, the calculated surface area provides the common way to compare between networks. PSD can also be calculated from gas sorption data. The use of different models results in different PSD. However, there is no universal model to date. For MOPs, density functional theory (DFT) and non-local DFT (NL-DFT) are generally used.

1.4 Porosity Tuning

Systematic design is essential to obtain materials with desired properties. Generally materials with high surface areas, simple synthesis, low production cost and low environmental impact are ideal. Two strategies of material design were suggested: bottom-up and top-down strategies.[94] Bottom-up is when the monomers were designed then the properties of the constructed networks were studied. On the other hand, a top-down strategy starts from the desired purposes of the networks then the monomers used in networks formation were modelled to meet the target properties. The important factors to obtain the MOPs with expected properties are monomer choice and polymerisation reactions. To date, there is a lot of literature that discusses factors regarding the tuning the properties of the polymers for practical applications.[5, 94] Different functionalities were also introduced into the network for specific utilisations.

1.4.1 Structural tuning

The most important property of porous materials is their porosity. Many researchers are focussing on the synthesis of ultrahigh surface area MOPs. For example, Lu *et al.* suggested that the high surface area network could be achieved by

optimising the size and geometry of monomers and also the polymerisation reactions.[95]

The choice of monomers is an important factor for networks design. Different monomers can provide different structure of networks obtained leading to changes in pore morphologies and surface areas of the materials. Monomers also define which polymerisation reactions are suitable for synthesis and also leading to different type of materials.

Different lengths of monomers could lead to materials with different surface areas.[34, 38] The pore size of the networks could also be tuned by using different size of monomers.[47] Different alkyl chain lengths could also be used to control the pore size as demonstrated in COFs[45], PIMs[96] and CMPs[6].

The geometry of the monomers also affects the porous structures. The Cooper group showed that the surface areas and H_2 adsorption of HCPs depended on the isomers of DCX used in synthesis.[34] The effect of the linkage geometry on porosity and photo properties of the networks was also studied by Xu and Jiang. Polyphenylene with *meta*-, *ortho*- and *para*-linked geometries showed different surface areas, CO_2 uptakes, particle sizes and also optical properties.[97] This can lead to a new strategy for material design.

Stockel *et al.* suggested that the tetrahedral monomers could enhance the surface area of the CMPs networks. By using monomers with a tetrahedral node[77], surface area increase to 1213 m^2/g compared to 744 m^2/g when using benzene node (CMP-4) [38] and also higher than when using the spiral node (P3, SA = 510 m^2/g)[73]. Hypercross-linked tetrahedral monomers also provided a network with a good surface area of 1314 m^2/g.[84] The tetrahedral monomer was later used to synthesise the diamond-like network, PAF-1, with an ultrahigh surface area and stablilty.[40]

Small changes in the molecular dimension by replacing C with Si node was also found to tailor the structure of CMPs, including surface areas, porosity and morphology.[77] Similarly, by simply changing of C in PAF-1 to Si, an exceptionally high surface area network, PPN-4, could be obtained.[43]

The effect of different reaction conditions such as synthetic methods[21, 54, 69], solvents[78, 98], temperature[26, 99], time[80], atmosphere[52], and catalysts[35, 100] on the material properties has also been investigated.

The morphology of materials is influenced by monomers and reaction conditions. Tan *et al.* studied the effect of structure of monomers on morphology of the networks. A polymer was synthesised using 1,3,5-triethynylbenzene and 1,4-dibromobenzene (CMP-F or CMP-1) and compared to the network obtained from 1,3,5-tribromobenzene and 1,4-diethynylbenzene (CMP-P or CMP-4). Similar chemical structures were demonstrated by IR and ssNMR, but different morphologies were found by SEM and TEM. The networks were formed in a film and nanotube-like morphology respectively.[101] Solvents used in the synthesis were also found affecting the morphology of networks. By using the toluene, *p*-xylene, and mesitylene solvents, sphere, tubular, and plate-like structures were observed. The storage capacity for organic solvents was also affected by the morphology of the networks.[98]

1.4.2 Functionality tuning

Functionality is another factor to tune the networks for a certain task.[102] Depending on the desired end use, different functional groups can be necessary. Introducing the functional groups in the networks can be mainly separated into two approaches: pre- and post-synthetic modification.

Pre-synthetic modification can be done by functionalisation or modification of the monomer prior to the polymerisation process. A variety of functional groups could be introduced into the networks by this method as there is significant diversity of monomers and polymerisation reactions that can be used in MOPs synthesis. This process is generally used in networks design and synthesis. The properties of the networks could be tuned.

Dawson *et al.* demonstrated the CMPs synthesised by monomers with different functional groups. The functionalised networks had different properties including isotherms, surface areas, and hydrophobicity.[79] CMPs with different

functional groups also showed the different surface areas and interaction with CO_2 molecules.[103]

However, such methods can suffer from complicated synthesis in monomer preparation. For examples, the desired functional groups might not be able to be tolerated by the polymerisation conditions. Incorporation of some functional groups can also be difficult and time consuming.

The post-synthetic modification (PSM) is the process of any modification after the networks are formed.[104] PSM provides the wider range of functionality incorporated into the networks. In many cases, the difficulty in monomer preparation might be overcome. MOPs are often compatible with PSM due to their chemical stability.

Guillerm *et al.* introduced the amine group into the PPNs by PSM from anchored aldehydes to prevent the free amine group from reacting while forming the networks.[9] PSM of PPN-6 with acid[7] and amines[8] (**Figure 1.6**) functional groups was achieved by Zhou group. PSM provided the easier approach to modify network than the pre-functionalised route[105].

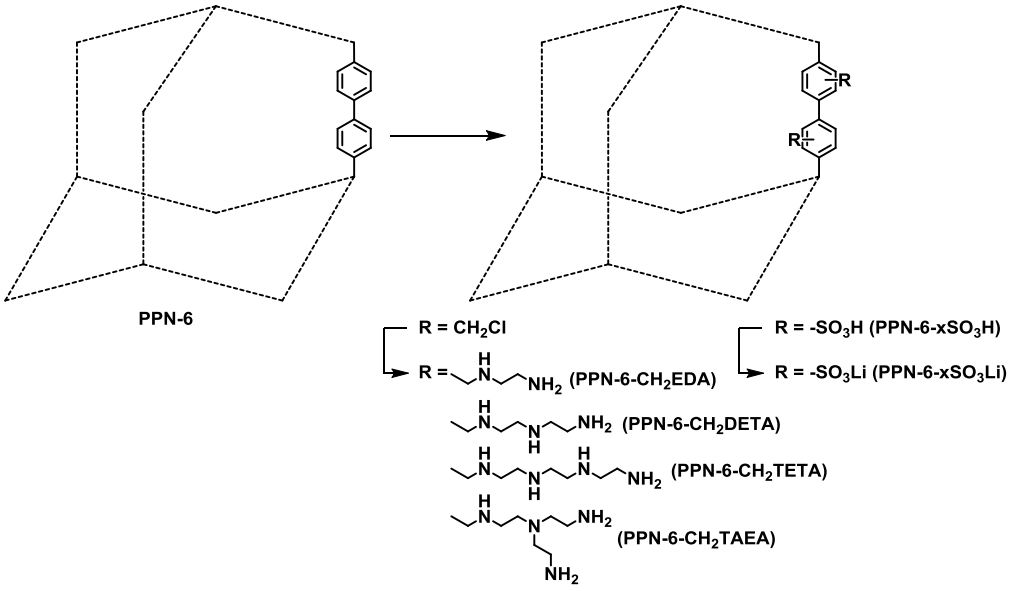

Figure 1.6 PSM of PPN-6 with amines and acids

Systematic control over the surface areas could also be achieved by PSM. We also showed the porosity properties of CMPs could be statistically controlled by PSM as will be discussed in Chapter 5.

1.5 MOPs as adsorbents

1.5.1 Gas storage and separations

Gas adsorption is the most obvious application that takes advantage of porous properties. The amount of gas adsorbed seems to depend on the surface area and pore size of the materials. Nevertheless, the adsorption effectiveness not only relies on physical properties but also on chemical ability to interact with guest molecules.[102]

Apart from hydrogen[34, 106-110] and methane[84, 111-113], which attract much research interest due to their use as novel alternative and clean energy resources, carbon dioxide (CO_2) capture is another target had been linked to materials.[13, 114, 115] CO_2 is a green house gas and is responsible for global warming.[116] There are three processes of carbon dioxide capture.[13] The first process is the pre-combustion capture dealing with contaminated carbon dioxide in natural gas. There is around 35.5 % CO_2 contained in the gas stream. It requires high temperature and pressure durable materials. The second process is the post-combustion capture coping with carbon dioxide in exhaust gas. This kind of gas consists of approximately 15 % CO_2 and contains a higher level of water compared to pre-combustion capture so selectivity for CO_2 and stability towards water is needed for any potential capture materials. The third process is the CO_2 capture from atmosphere to remove CO_2 directly from air. As the CO_2 is highly diluted, only about 0.04% or 400 ppm[117], materials should have CO_2 adsorption and selectivity at low CO_2 concentration.

At this time, the technologies used in CO_2 sorption are aqueous amine and amine solutions that can absorb CO_2 and form C-N bonds.[118] However, there are problems due to the high energy required for recycling and corrosion.[119] Moreover, energy needed for absorption is in principle more than for adsorption. Thus, materials used as adsorbents are expected to be a new technology for CO_2 capture, especially porous materials based on carbon, which generally have inert property,

low cost, and high surface area.[13] However, challenges still remain. Materials for CO_2 capture should have high capacity for CO_2 adsorption, low energy for the release of CO_2 from the materials, and low producing cost.[120] Therefore, materials have to be carefully designed to solve these problems. There are three strategies to optimise materials for CO_2 capture: (1) by changing the composition of the polymer frameworks, (2) by tailoring the surface areas and pore size, and (3) by pore surface modifications.[120]

Different kind of the frameworks of course affect the physical and chemical structures of the networks. Various materials and their CO_2 uptakes, selectivity and heat of adsorption were summarised by Dawson *et al.*[13, 69]

Surface area is an important constituent affecting the amount of CO_2 uptake and selectivity. The highest surface area MOP, PPN-4 which has surface area of 6460 m^2/g exhibited very high CO_2 uptake of 48.20 mmol/g at 50 bar and 295 K.[43] PAF-1 which is the second highest surface area MOPs also showed high CO_2 capacity of 29.55 mmol/g at 40 bar and 298 K.[40] Nevertheless, surface area is not the sole factor as high surface area materials did not always show impressive CO_2 uptakes, especially at low pressure.

There are other factors that influence the quantity of CO_2 sorption. As mentioned before, a pore size that is less than five times that of the gas molecule is considered to be the most effective.[121, 122] CO_2 molecular size is 0.209 nm so the appropriate pore size should be smaller than 1.0 nm to adsorb CO_2 at atmospheric pressure. For higher pressure, pore sizes could be 0.7 to 2.0 nm.[66]

Moreover, chemical modification of "CO_2-philic" on the surface of pores is believed to improve the interaction between CO_2 molecules and framework leading to higher CO_2 uptakes. Not only is high CO_2 capture adsorption important, selectivity over other gases is also needed to be considered. For an ideal CO_2 adsorbent, high CO_2 uptakes and selectivity required. Normally, the materials with high selectivity exhibit low adsorption. Many attempts have been tried to improve the networks with high the selectivity while CO_2 capacity still remain or increase.

Because CO_2 is slightly acidic, the basicity of adsorbents is predicted to play a significant part for CO_2 capture. Therefore, basic functional groups are introduced

in many materials especially amine functionality. Polyamine-tethered PPNs obtained by PSM of PPN-6 also showed significant increase in CO_2 uptakes even had much lower surface areas. PPN-6-CH_2DETA (SA = 555 m^2/g) had the CO_2 uptakes of 4.3 mmol/g, higher than PPN-6 (SA = 4023 m^2/g) which had CO_2 uptakes of 1.3 mmol/g.[8] The amine group introduced into the PPNs by PSM from anchored aldehydes was also found to have high carbon dioxide heat of adsorption up to 50 kJ/mol. Moreover, the selectivity of CO_2 over N_2 and CH_4 was also enhanced.[9]

N-containing materials were also investigated. By replacing the benzene node in a series of CMPs with N-containing, triazine node (TCMPs), the surface areas were comparable. However, the CO_2 uptakes increased.[123] Petal *et al.* also showed the catalyst-free synthesis of azo-bridged covalent organic polymers (azo-COPs, **Figure 1.7**) which provide high BET surface area materials up to 729 m^2/g as well as high selectivity of CO_2 over N_2 of 288 at 55 ^oC without lowering CO_2 capacity (CO_2 uptake of 151.3 mg/g).[124] This is resulting from the phobicity of N_2 to the azo group. Surprisingly, unlike most of other materials, the networks show higher selectivity when temperature was increased. More azo-COPs were further investigated. Increasing of π–surface area functional groups demonstrated more interaction with CO_2 which affect to CO_2 than N_2.[125] Combining azo N_2-phobic group with CO_2-philic group leads to improvement of CO_2/N_2 selectivity and CO_2 uptakes. This kind of material could have the very high CO_2 capacity up to 5.37 mmol/g at 273 K and 1 bar.[126]

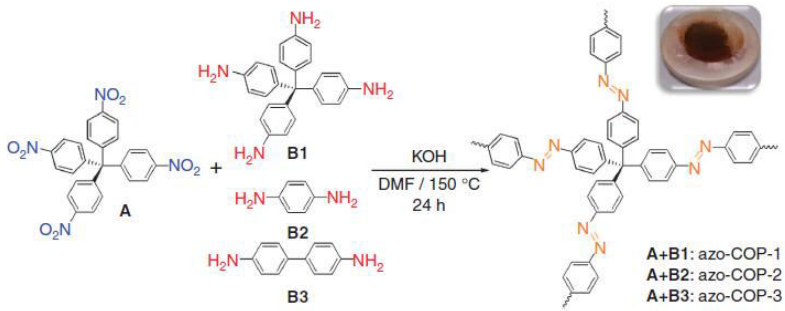

Figure 1.7 Synthesis of azo-COPs[124]

Apart from N-containing networks, other heteroatom-containing monomers such as S, O and P were also investigated. HCPs synthesised by heterocyclic monomers including thiophene, pyrrole and furan were investigated by Tan group.[70] All thiophene (Ty-1), pyrrole (Py-1) and furan (Fu-1) HCPs exhibited high CO_2 uptakes of 12.7, 11.9 and 9.7 wt% at 273 K and 1 bar. The capacities are higher than many MOPs reported earlier and also higher than 9.1 wt% in PAF-1[40] which has ultrahigh surface area under the similar conditions. The phosphorus node was also studied the effect on CO_2 sorption ability. Phosphine-containing MOPs were synthesised by Yang *et al.* The networks demonstrated good binding to CO_2 with isosteric heat of adsorption more than 25 kJ/mol as well as high CO_2/CH_4 selectivity.[127]

Acid functional groups were also found to influence the CO_2 uptakes. In fact, such the functional group exhibited higher CO_2 adsorption than basic group in many cases. Various functionalised CMPs were compared in terms of CO_2 uptakes and isosteric heats by the Cooper group. (**Figure 1.8**) Carboxylic acid functionalised CMP, CMP-1-COOH, showed higher heat of adsorption than other functional groups. This study supported that these factors depended on functionalities more than surface areas or pore volumes.[103] PPN-6 grafted with sulfonic acid (PPN-6-SO_3H) and its lithium salt (PPN-6-SO_3Li) also showed higher CO_2 uptake and selectivity than the parent networks even though they had lower surface areas.[7] The CO_2 capacity was also higher than the amine grafted analogue (PPN-6-CH_2DETA)[8].

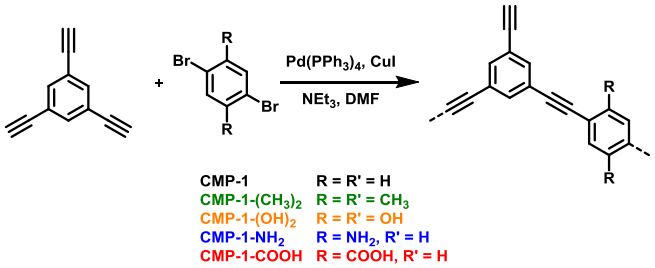

Figure 1.8 Synthesis of CMPs with different functional groups

1.5.2 Molecule Capture

In addition to gas adsorption, the porosity of MOPs also provides potential in molecules capture such as dyes, pollutants, and drugs offers potentials in water and air treatment and drugs delivery.

Dyes are used as the model for molecule capture in MOPs. Dawson *et al.* showed that methyl orange could be adsorbed by CMPs. Polarity of the networks was found influencing their wettability and amount of methyl orange uptakes in the networks. As methyl orange is water soluble, the networks with hydrophilic monomers could adsorb the dye better than the hydrophobic networks.[79]

Contaminates, such as oil, toxic metal, organic solvents, in water can cause a lot of environmental problems. Therefore, effective technologies are required. Rao *et al.* demonstrated the potential in using a hydrophobic CMP, Py-PP, as a phase-selective swelling and capturing organic solvents and oil from water mixtures at room temperature. The oil-adsorbed network could be easily scooped out leaving water without any trace of oil. Both oil and polymer could be recovered by simple mechanical squeezing. (**Figure 1.9**) The network also showed an efficient fullerene (C_{60}) adsorption where the fluorescent signal was quenched offering a potential for utilisation in sensors.[15] Wang *et al.* suggested the potential in using a porous porphyrin-based organic polymer, PCPF-1, for removing oil from water. PCPF-1 exhibited very high adsorption capacity and selectivity for both vapour and liquid saturated hydrocarbons in water.[128]

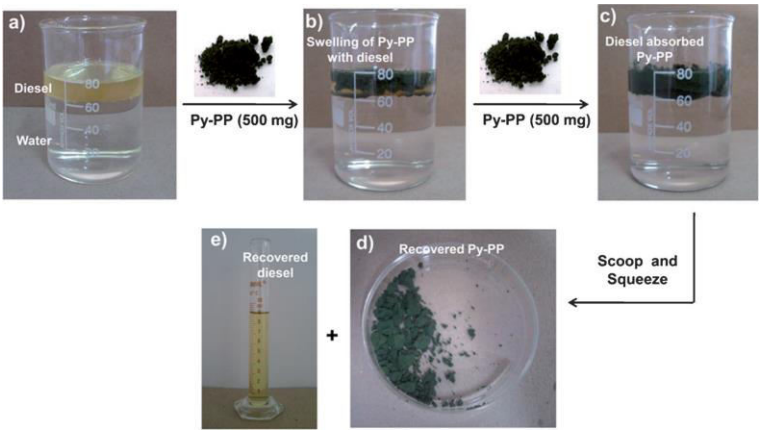

Figure 1.9 Phase-selective encapsulation of Py-PP. a) to c) The absorption of diesel upon addition of Py-PP to a beaker containing a diesel/water mixture. d) and e) The polymer and diesel, respectively, recovered by simple squeezing of the colleted material.[15]

The toxicity of heavy metals can affect human health and environment so the removal of such metal is necessary. Sulfonic acid-modified HCPs (SAM-HCPs) was synthesised by the Tan group. The hydrophilic improved networks could enhance the capacity of the toxic metal ion adsorption from water with recyclability leading to the potential in industrial applications.[17] Nickel ion-imprinted microporous polymer was also studied for the selective Ni^{2+} adsorption toward other metals.[129]

Liu *et al.* developed the super-sorbent porphyrin functionalised CMPs for amines, pollutant and hazardous compounds, adsorption. The combination of porphyrin that was responsible for uptake of amines with high surface area that open more interactive site and swelling ability that promote the capacity results in high amines adsorption efficiency.[130] The catechol-decorated MOPs was synthesised by Weston *et al.* for toxic industrial chemicals such as ammonia, cyanogen chloride, sulphur dioxide and octane trap.[131] In 2014, the Long group uses the concept of acid-base interaction of carboxylic and amine group, same as concept used in carbon dioxide capture but in reverse way, to make the materials for amine capture. The carboxylic functionalised in porous organic polymers was suggested to have interaction with amine hence enhance the NH_3 uptake.[16]

The incorporation of magnetic property to microporous polymer nanoparticles was reported by Yang to make the polymers being easily separated after used. The removal of toxic organic compounds ability was observed as well as the control release of ibuprofen for potential in drug delivery was studied.[132]

1.6 Overview of the work in this thesis

Due to the large number of applications of porous materials, these materials are gaining attention. However, there are still some limitations so it is necessary to delicately develop the materials to fulfil applicable requirements both for existing and further new applications.

In this thesis, the synthesis and structural development of functionalised MOPs will be described. The focus will be on HCPs and CMPs to be used as adsorbents.

In Chapter 3, a copolymerisation strategy is used in the synthesis of hypercross-linked benzene and aniline copolymers for application in CO_2 capture. The CO_2 capacity and selectivity of copolymer networks is investigated. Incorporation of carboxylic acid functional group into the HCPs by post-cross-linking of functionalised polypolystyrene chains will be described in Chapter 4. The influence of molecular weight of linear polystyrenes on the porosity properties is studied. The functionality of CMPs is tailored by PSM strategy. The effect of PSM on the properties of the networks (Chapter 5) and the attempt to apply for utilisation in molecular imprinting polymers (Chapter 6) will be discussed.

1.7 References

1. N. Z. Logar and V. Kaučič, *Acta Chim Slov*, 2006, **53**, 117-135.
2. R. Dawson, A. I. Cooper and D. J. Adams, *Progress in Polymer Science*, 2012, **37**, 530-563.
3. J. X. Jiang and A. Cooper, *Topics in current chemistry*, 2010, **293**, 1-33.
4. S. Xu, Y. Luo and B. Tan, *Macromolecular Rapid Communications*, 2013, **34**, 471-484.

5. Y. Xu, S. Jin, H. Xu, A. Nagai and D. Jiang, *Chemical Society Reviews*, 2013, **42**, 8012-8031.

6. T. Ratvijitvech, R. Dawson, A. Laybourn, Y. Z. Khimyak, D. J. Adams and A. I. Cooper, *Polymer*, 2014, **55**, 321-325.

7. W. Lu, D. Yuan, J. Sculley, D. Zhao, R. Krishna and H.-C. Zhou, *Journal of the American Chemical Society*, 2011, **133**, 18126-18129.

8. W. Lu, J. P. Sculley, D. Yuan, R. Krishna, Z. Wei and H.-C. Zhou, *Angewandte Chemie International Edition*, 2012, **51**, 7480-7484.

9. V. Guillerm, L. J. Weselinski, M. Alkordi, M. I. H. Mohideen, Y. Belmabkhout, A. J. Cairns and M. Eddaoudi, *Chemical Communications*, 2014, **50**, 1937-1940.

10. Z. Chang, D.-S. Zhang, Q. Chen and X.-H. Bu, *Physical Chemistry Chemical Physics*, 2013, **15**, 5430-5442.

11. H. Furukawa and O. M. Yaghi, *Journal of the American Chemical Society*, 2009, **131**, 8875-8883.

12. T. Ben, C. Pei, D. Zhang, J. Xu, F. Deng, X. Jing and S. Qiu, *Energy & Environmental Science*, 2011, **4**, 3991-3999.

13. R. Dawson, A. I. Cooper and D. J. Adams, *Polymer International*, 2013, **62**, 345-352.

14. P. Lindemann, M. Tsotsalas, S. Shishatskiy, V. Abetz, P. Krolla-Sidenstein, C. Azucena, L. Monnereau, A. Beyer, A. Gölzhäuser, V. Mugnaini, H. Gliemann, S. Bräse and C. Wöll, *Chemistry of Materials*, 2014, **26**, 7189-7193.

15. K. V. Rao, S. Mohapatra, T. K. Maji and S. J. George, *Chemistry – A European Journal*, 2012, **18**, 4505-4509.

16. J. F. Van Humbeck, T. M. McDonald, X. Jing, B. M. Wiers, G. Zhu and J. R. Long, *Journal of the American Chemical Society*, 2014.

17. B. Li, F. Su, H.-K. Luo, L. Liang and B. Tan, *Microporous and Mesoporous Materials*, 2011, **138**, 207-214.

18. P. Kaur, J. T. Hupp and S. T. Nguyen, *ACS Catalysis*, 2011, **1**, 819-835.

19. Y. Zhang and S. N. Riduan, *Chemical Society Reviews*, 2012, **41**, 2083-2094.

20. Y. Xu, L. Chen, Z. Guo, A. Nagai and D. Jiang, *Journal of the American Chemical Society*, 2011, **133**, 17622-17625.

21. J. X. Jiang, A. Trewin, D. J. Adams and A. I. Cooper, *Chemical Science*, 2011, **2**, 1777-1781.

22. L. Chen, Y. Honsho, S. Seki and D. Jiang, *Journal of the American Chemical Society*, 2010, **132**, 6742-6748.

23. X. Liu, Y. Xu and D. Jiang, *Journal of the American Chemical Society*, 2012, **134**, 8738-8741.

24. F. Vilela, K. Zhang and M. Antonietti, *Energy & Environmental Science*, 2012, **5**, 7819-7832.

25. R. S. Sprick, J.-X. Jiang, B. Bonillo, S. Ren, T. Ratvijitvech, P. Guiglion, M. A. Zwijnenburg, D. J. Adams and A. I. Cooper, *Journal of the American Chemical Society*, 2015, **137**, 3265-3270.

26. Y. Kou, Y. Xu, Z. Guo and D. Jiang, *Angewandte Chemie International Edition*, 2011, **50**, 8753-8757.

27. A. P. Côté, A. I. Benin, N. W. Ockwig, M. O'Keeffe, A. J. Matzger and O. M. Yaghi, *Science*, 2005, **310**, 1166-1170.

28. S.-Y. Ding and W. Wang, *Chemical Society Reviews*, 2013, **42**, 548-568.

29. P. Kuhn, M. Antonietti and A. Thomas, *Angewandte Chemie International Edition*, 2008, **47**, 3450-3453.

30. P. Katekomol, J. Roeser, M. Bojdys, J. Weber and A. Thomas, *Chemistry of Materials*, 2013, **25**, 1542-1548.

31. P. M. Budd, B. S. Ghanem, S. Makhseed, N. B. McKeown, K. J. Msayib and C. E. Tattershall, *Chemical Communications*, 2004, 230-231.

32. N. B. McKeown, *ISRN Materials Science*, 2012, **2012**, 16.

33. N. B. McKeown, P. M. Budd, K. J. Msayib, B. S. Ghanem, H. J. Kingston, C. E. Tattershall, S. Makhseed, K. J. Reynolds and D. Fritsch, *Chemistry – A European Journal*, 2005, **11**, 2610-2620.

34. C. D. Wood, B. Tan, A. Trewin, H. Niu, D. Bradshaw, M. J. Rosseinsky, Y. Z. Khimyak, N. L. Campbell, R. Kirk, E. Stöckel and A. I. Cooper, *Chemistry of Materials*, 2007, **19**, 2034-2048.

35. B. Li, R. Gong, W. Wang, X. Huang, W. Zhang, H. Li, C. Hu and B. Tan, *Macromolecules*, 2011, **44**, 2410-2414.

36. N. Fontanals, R. M. Marce, F. Borrull and P. A. G. Cormack, *Polymer Chemistry*, 2015.

37. Q. Liu, Z. Tang, M. Wu and Z. Zhou, *Polymer International*, 2014, **63**, 381-392.

38. J.-X. Jiang, F. Su, A. Trewin, C. D. Wood, N. L. Campbell, H. Niu, C. Dickinson, A. Y. Ganin, M. J. Rosseinsky, Y. Z. Khimyak and A. I. Cooper, *Angewandte Chemie*, 2007, **119**, 8728-8732.

39. A. I. Cooper, *Advanced Materials*, 2009, **21**, 1291-1295.

40. T. Ben, H. Ren, S. Ma, D. Cao, J. Lan, X. Jing, W. Wang, J. Xu, F. Deng, J. M. Simmons, S. Qiu and G. Zhu, *Angewandte Chemie International Edition*, 2009, **48**, 9457-9460.

41. C. Pei, T. Ben and S. Qiu, *Materials Horizons*, 2015, **2**, 11-21.

42. W. Lu, D. Yuan, D. Zhao, C. I. Schilling, O. Plietzsch, T. Muller, S. Bräse, J. Guenther, J. Blümel, R. Krishna, Z. Li and H.-C. Zhou, *Chemistry of Materials*, 2010, **22**, 5964-5972.

43. D. Yuan, W. Lu, D. Zhao and H.-C. Zhou, *Advanced Materials*, 2011, **23**, 3723-3725.

44. O. K. Farha, I. Eryazici, N. C. Jeong, B. G. Hauser, C. E. Wilmer, A. A. Sarjeant, R. Q. Snurr, S. T. Nguyen, A. Ö. Yazaydın and J. T. Hupp, *Journal of the American Chemical Society*, 2012, **134**, 15016-15021.

45. R. W. Tilford, S. J. Mugavero, P. J. Pellechia and J. J. Lavigne, *Advanced Materials*, 2008, **20**, 2741-2746.

46. M. G. Rabbani, A. K. Sekizkardes, O. M. El-Kadri, B. R. Kaafarani and H. M. El-Kaderi, *Journal of Materials Chemistry*, 2012, **22**, 25409-25417.

47. S. Yuan, B. Dorney, D. White, S. Kirklin, P. Zapol, L. Yu and D.-J. Liu, *Chemical Communications*, 2010, **46**, 4547-4549.

48. M. Rose, N. Klein, I. Senkovska, C. Schrage, P. Wollmann, W. Bohlmann, B. Bohringer, S. Fichtner and S. Kaskel, *Journal of Materials Chemistry*, 2011, **21**, 711-716.

49. T. O. McDonald, R. Akhtar, C. H. Lau, T. Ratvijitvech, G. Cheng, R. Clowes, D. J. Adams, T. Hasell and A. I. Cooper, *Journal of Materials Chemistry A*, 2015, **3**, 4855-4864.

50. J. Vile, M. Carta, C. G. Bezzu and N. B. McKeown, *Polymer Chemistry*, 2011, **2**, 2257-2260.

51. V. A. Davankov and M. P. Tsyurupa, *Reactive Polymers*, 1990, **13**, 27-42.

52. J.-X. Jiang, F. Su, H. Niu, C. D. Wood, N. L. Campbell, Y. Z. Khimyak and A. I. Cooper, *Chemical Communications*, 2008, 486-488.

53. J.-X. Jiang, A. Trewin, F. Su, C. D. Wood, H. Niu, J. T. A. Jones, Y. Z. Khimyak and A. I. Cooper, *Macromolecules*, 2009, **42**, 2658-2666.

54. Z. Wang, S. Yuan, A. Mason, B. Reprogle, D.-J. Liu and L. Yu, *Macromolecules*, 2012, **45**, 7413-7419.

55. Q. Chen, M. Luo, T. Wang, J.-X. Wang, D. Zhou, Y. Han, C.-S. Zhang, C.-G. Yan and B.-H. Han, *Macromolecules*, 2011, **44**, 5573-5577.

56. J. Schmidt, M. Werner and A. Thomas, *Macromolecules*, 2009, **42**, 4426-4429.

57. L. Sun, Z. Liang, J. Yu and R. Xu, *Polymer Chemistry*, 2013, **4**, 1932-1938.

58. C. Xu and N. Hedin, *Journal of Materials Chemistry A*, 2013, **1**, 3406-3414.

59. P. Pandey, A. P. Katsoulidis, I. Eryazici, Y. Wu, M. G. Kanatzidis and S. T. Nguyen, *Chemistry of Materials*, 2010, **22**, 4974-4979.

60. Y. Zhu, H. Long and W. Zhang, *Chemistry of Materials*, 2013, **25**, 1630-1635.

61. B. Li, Z. Guan, X. Yang, W. D. Wang, W. Wang, I. Hussain, K. Song, B. Tan and T. Li, *Journal of Materials Chemistry A*, 2014, **2**, 11930-11939.

62. M. P. Tsyurupa and V. A. Davankov, *Reactive and Functional Polymers*, 2002, **53**, 193-203.

63. M. P. Tsyurupa, Z. K. Blinnikova, N. A. Proskurina, A. V. Pastukhov, L. A. Pavlova and V. A. Davankov, *Nanotechnol Russia*, 2009, **4**, 665-675.

64. R. Vinodh, A. Abidov, M. Peng, C. Babu, M. Palanichamy, W. Cha and H.-T. Jang, *Fibers Polym*, 2015, **16**, 1458-1467.

65. J. Germain, J. M. J. Frechet and F. Svec, *Journal of Materials Chemistry*, 2007, **17**, 4989-4997.

66. C. F. Martin, E. Stockel, R. Clowes, D. J. Adams, A. I. Cooper, J. J. Pis, F. Rubiera and C. Pevida, *Journal of Materials Chemistry*, 2011, **21**, 5475-5483.

67. E. Preis, C. Widling, U. Scherf, S. Patil, G. Brunklaus, J. Schmidt and A. Thomas, *Polymer Chemistry*, 2011, **2**, 2186-2189.

68. Y. Luo, S. Zhang, Y. Ma, W. Wang and B. Tan, *Polymer Chemistry*, 2013, **4**, 1126-1131.

69. R. Dawson, E. Stockel, J. R. Holst, D. J. Adams and A. I. Cooper, *Energy & Environmental Science*, 2011, **4**, 4239-4245.

70. Y. Luo, B. Li, W. Wang, K. Wu and B. Tan, *Advanced Materials*, 2012, **24**, 5703-5707.

71. R. Dawson, L. A. Stevens, T. C. Drage, C. E. Snape, M. W. Smith, D. J. Adams and A. I. Cooper, *Journal of the American Chemical Society*, 2012, **134**, 10741-10744.

72. R. Dawson, T. Ratvijitvech, M. Corker, A. Laybourn, Y. Z. Khimyak, A. I. Cooper and D. J. Adams, *Polymer Chemistry*, 2012, **3**, 2034-2038.

73. J. Weber and A. Thomas, *Journal of the American Chemical Society*, 2008, **130**, 6334-6335.

74. Q. Chen, J.-X. Wang, F. Yang, D. Zhou, N. Bian, X.-J. Zhang, C.-G. Yan and B.-H. Han, *Journal of Materials Chemistry*, 2011, **21**, 13554-13560.

75. L. Tan, B. Li, X. Yang, W. Wang and B. Tan, *Polymer*, 2015, **70**, 336-342.

76. J.-X. Jiang, F. Su, A. Trewin, C. D. Wood, H. Niu, J. T. A. Jones, Y. Z. Khimyak and A. I. Cooper, *Journal of the American Chemical Society*, 2008, **130**, 7710-7720.

77. E. Stockel, X. Wu, A. Trewin, C. D. Wood, R. Clowes, N. L. Campbell, J. T. A. Jones, Y. Z. Khimyak, D. J. Adams and A. I. Cooper, *Chemical Communications*, 2009, 212-214.

78. R. Dawson, A. Laybourn, Y. Z. Khimyak, D. J. Adams and A. I. Cooper, *Macromolecules*, 2010, **43**, 8524-8530.

79. R. Dawson, A. Laybourn, R. Clowes, Y. Z. Khimyak, D. J. Adams and A. I. Cooper, *Macromolecules*, 2009, **42**, 8809-8816.

80. A. Laybourn, R. Dawson, R. Clowes, T. Hasell, A. I. Cooper, Y. Z. Khimyak and D. J. Adams, *Polymer Chemistry*, 2014, **5**, 6325-6333.

81. S. Ren, R. Dawson, D. J. Adams and A. I. Cooper, *Polymer Chemistry*, 2013, **4**, 5585-5590.

82. M. Yu, X. Wang, X. Yang, Y. Zhao and J.-X. Jiang, *Polymer Chemistry*, 2015, **6**, 3217-3223.

83. G. Liu, Y. Wang, C. Shen, Z. Ju and D. Yuan, *Journal of Materials Chemistry A*, 2015, **3**, 3051-3058.

84. M. Errahali, G. Gatti, L. Tei, G. Paul, G. A. Rolla, L. Canti, A. Fraccarollo, M. Cossi, A. Comotti, P. Sozzani and L. Marchese, *The Journal of Physical Chemistry C*, 2014, **118**, 28699-28710.

85. F. Y. Li, Y. Xiao, T.-S. Chung and S. Kawi, *Macromolecules*, 2012, **45**, 1427-1437.

86. Q. Zhang, Y. Yang and S. Zhang, *Chemistry – A European Journal*, 2013, **19**, 10024-10029.

87. S. Makhseed and J. Samuel, *Journal of Materials Chemistry A*, 2013, **1**, 13004-13010.

88. Z.-Z. Yang, Y. Zhao, H. Zhang, B. Yu, Z. Ma, G. Ji and Z. Liu, *Chemical Communications*, 2014, **50**, 13910-13913.

89. F. Blanc, S. Y. Chong, T. O. McDonald, D. J. Adams, S. Pawsey, M. A. Caporini and A. I. Cooper, *Journal of the American Chemical Society*, 2013, **135**, 15290-15293.

90. K. S. W. Sing, in *pac*, 1985, vol. 57, p. 603.

91. I. Langmuir, *Journal of the American Chemical Society*, 1918, **40**, 1361-1403.

92. S. Brunauer, P. H. Emmett and E. Teller, *Journal of the American Chemical Society*, 1938, **60**, 309-319.

93. R. T. Woodward, L. A. Stevens, R. Dawson, M. Vijayaraghavan, T. Hasell, I. P. Silverwood, A. V. Ewing, T. Ratvijitvech, J. D. Exley, S. Y. Chong, F. Blanc, D. J. Adams, S. G. Kazarian, C. E. Snape, T. C. Drage and A. I. Cooper, *Journal of the American Chemical Society*, 2014, **136**, 9028-9035.

94. G. Zhu and H. Ren, *Porous Organic Frameworks: Design, Synthesis and Their Advanced Applications*, 1 edn., Springer-Verlag Berlin Heidelberg, 2015.

95. W. Lu, Z. Wei, D. Yuan, J. Tian, S. Fordham and H.-C. Zhou, *Chemistry of Materials*, 2014, **26**, 4589-4597.

96. B. S. Ghanem, M. Hashem, K. D. M. Harris, K. J. Msayib, M. Xu, P. M. Budd, N. Chaukura, D. Book, S. Tedds, A. Walton and N. B. McKeown, *Macromolecules*, 2010, **43**, 5287-5294.

97. Y. Xu and D. Jiang, *Chemical Communications*, 2014.

98. D. Tan, W. Fan, W. Xiong, H. Sun, Y. Cheng, X. Liu, C. Meng, A. Li and W.-Q. Deng, *Macromolecular Chemistry and Physics*, 2012, **213**, 1435-1440.

99. P. Kuhn, A. Thomas and M. Antonietti, *Macromolecules*, 2009, **42**, 319-326.

100.M. Rose, N. Klein, W. Bohlmann, B. Bohringer, S. Fichtner and S. Kaskel, *Soft Matter*, 2010, **6**, 3918-3923.

101.D. Tan, W. Xiong, H. Sun, Z. Zhang, W. Ma, C. Meng, W. Fan and A. Li, *Microporous and Mesoporous Materials*, 2013, **176**, 25-30.

102.A. Thomas, *Angewandte Chemie International Edition*, 2010, **49**, 8328-8344.

103.R. Dawson, D. J. Adams and A. I. Cooper, *Chemical Science*, 2011, **2**, 1173-1177.

104.K. K. Tanabe and S. M. Cohen, *Chemical Society Reviews*, 2011, **40**, 498-519.

105.E. Verde-Sesto, M. Pintado-Sierra, A. Corma, E. M. Maya, J. G. de la Campa, M. Iglesias and F. Sánchez, *Chemistry – A European Journal*, 2014, **20**, 5111-5120.

106.J. Germain, J. M. J. Fréchet and F. Svec, *Small*, 2009, **5**, 1098-1111.

107.J. Y. Lee, C. D. Wood, D. Bradshaw, M. J. Rosseinsky and A. I. Cooper, *Chem Commun (Camb)*, 2006, 2670-2672.

108.B. Li, X. Huang, L. Liang and B. Tan, *Journal of Materials Chemistry*, 2010, **20**, 7444-7450.

109.A. Li, R.-F. Lu, Y. Wang, X. Wang, K.-L. Han and W.-Q. Deng, *Angewandte Chemie International Edition*, 2010, **49**, 3330-3333.

110.Z. Xiang, D. Cao, W. Wang, W. Yang, B. Han and J. Lu, *The Journal of Physical Chemistry C*, 2012, **116**, 5974-5980.

111.T. A. Makal, J.-R. Li, W. Lu and H.-C. Zhou, *Chemical Society Reviews*, 2012, **41**, 7761-7779.

112.C. D. Wood, B. Tan, A. Trewin, F. Su, M. J. Rosseinsky, D. Bradshaw, Y. Sun, L. Zhou and A. I. Cooper, *Advanced Materials*, 2008, **20**, 1916-1921.

113.M. Haranczyk, L.-C. Lin, K. Lee, R. L. Martin, J. B. Neaton and B. Smit, *Physical Chemistry Chemical Physics*, 2013, **15**, 20937-20942.

114.D. M. D'Alessandro, B. Smit and J. R. Long, *Angewandte Chemie International Edition*, 2010, **49**, 6058-6082.

115.N. Hedin, L. Chen and A. Laaksonen, *Nanoscale*, 2010, **2**, 1819-1841.

116.S. Solomon, G.-K. Plattner, R. Knutti and P. Friedlingstein, *Proceedings of the National Academy of Sciences*, 2009, **106**, 1704-1709.

117.http://scrippsco2.ucsd.edu/data/atmospheric_co2.

118.G. T. Rochelle, *Science*, 2009, **325**, 1652-1654.

119.C.-H. Yu, C.-H. Huang and C.-S. Tan, *Aerosol and Air Quality Research*, 2012, **12**, 745-769.

120.J. Wang, L. Huang, R. Yang, Z. Zhang, J. Wu, Y. Gao, Q. Wang, D. O'Hare and Z. Zhong, *Energy & Environmental Science*, 2014, **7**, 3478-3518.

121.J. M. Martín-Martínez, R. Torregrosa-Maciá and M. C. Mittelmeijer-Hazeleger, *Fuel*, 1995, **74**, 111-114.

122.A. Vishnyakov, P. I. Ravikovitch and A. V. Neimark, *Langmuir*, 1999, **15**, 8736-8742.

123.S. Ren, R. Dawson, A. Laybourn, J.-x. Jiang, Y. Khimyak, D. J. Adams and A. I. Cooper, *Polymer Chemistry*, 2012, **3**, 928-934.

124.H. A. Patel, S. Hyun Je, J. Park, D. P. Chen, Y. Jung, C. T. Yavuz and A. Coskun, *Nat Commun*, 2013, **4**, 1357.

125.H. A. Patel, S. H. Je, J. Park, Y. Jung, A. Coskun and C. T. Yavuz, *Chemistry – A European Journal*, 2014, **20**, 772-780.

126.P. Arab, M. G. Rabbani, A. K. Sekizkardes, T. İslamoğlu and H. M. El-Kaderi, *Chemistry of Materials*, 2014.

127.S. Qiao, Z. Du, C. Yang, Y. Zhou, D. Zhu, J. Wang, X. Chen and R. Yang, *Polymer*, 2014.

128.X.-S. Wang, J. Liu, J. M. Bonefont, D.-Q. Yuan, P. K. Thallapally and S. Ma, *Chemical Communications*, 2013, **49**, 1533-1535.

129.Y. Jiang and D. Kim, *Polymers for Advanced Technologies*, 2013, **24**, 747-751.

130.X. Liu, Y. Xu, Z. Guo, A. Nagai and D. Jiang, *Chem Commun*, 2013, **49**, 3233-3235.

131.M. H. Weston, G. W. Peterson, M. A. Browe, P. Jones, O. K. Farha, J. T. Hupp and S. T. Nguyen, *Chem Commun*, 2013, **49**, 2995-2997.

132.X. Yang, B. Li, I. Majeed, L. Liang, X. Long and B. Tan, *Polymer Chemistry*, 2013, **4**, 1425-1429.

Chapter 2

Methods

2. Methods

2.1 Experimental techniques

2.1.1 Gas sorption

Samples for gas sorption studies were weighed into gas sorption tubes in approximately 100 mg quantities and the exact masses were recorded to four decimal places. The samples were then degassed at 120 °C under vacuum for 900 minutes prior to the measurements. The exact masses after degassing were used as the weight of the materials.

2.1.1.1 Nitrogen isotherms

Nitrogen sorption isotherms were collected using Micromeritics ASAP 2420 or Micromeritics ASAP 2020 instruments at 77.3 K with equilibration interval of 30 seconds. Free spaces were collected automatically on ASAP2420 and manually for ASAP2020 after the sorption measurements without further degassing. The data were collected by either Dr. Robert Dawson or the author.

2.1.1.2 Surface area measurements

Surface areas were calculated using Brunauer-Emmett-Teller (BET) theory. For data collected on the Quantachrome instruments, the surface areas of networks were calculated by using nitrogen adsorptions collected on a Quantachrome NOVA® 4200e Surface Area Analyzer at 77 K using 5-point BET calculation. For Micromeritics instruments, surface areas were calculated by using nitrogen sorption collected on Micromeritics ASAP 2420 or Micromeritics ASAP 2020 instruments at 77.3 K over the relative pressure range of 0.05-0.15 p/p^0.

2.1.1.3 Pore size distribution

Pore size distributions were derived from nitrogen isotherm adsorption branches using the nonlocal density functional theory model (NL-DFT) for pillared clays with cylindrical pore geometries found within the Micromeritics ASAP software.

2.1.1.4 Nitrogen adsorption for selectivity calculation

Nitrogen adsorptions used for calculating gas selectivity were collected on the Micromeritics ASAP 2020 physisorption analyser up to 1 bar at 298 K using a chiller/circulator. The equilibration interval time was 35 seconds. Free spaces were collected automatically after the sorption measurements without further degassing.

2.1.1.5 Carbon dioxide adsorption

For the Quantachrome instruments, carbon dioxide uptakes were collected on the Quantachrome NOVA® 4200e Surface Area Analyzer at room temperature. For Micromeritics instruments, carbon dioxide uptakes were obtained from Micromeritics ASAP 2020 physisorption analyser up to 1 bar at 273 K, 298 K and 300 K using a chiller/circulator. The equilibration interval time was 35 seconds. Free spaces were collected automatically after the sorption measurements without further degassing.

2.1.1.6 Calculation of CO_2/N_2 selectivity

The selectivity of CO_2 over N_2 was calculated by using the Ideal Adsorbed Solution Theory (IAST) method.[1] The IAST theory provided the predicted selectivity of gases using only single component adsorption data collected at the same temperature on the same adsorbent. To calculate the selectivity, seven equations are involved:

$$\pi_1^0\ (P_1^0) = \frac{RT}{A}\int_{t=0}^{P_1^0} n_1^0(t)\ d\ ln\ t \quad (1)$$

$$\pi_2^0\ (P_2^0) = \frac{RT}{A}\int_{t=0}^{P_2^0} n_2^0(t)\ d\ ln\ t \quad (2)$$

$$Py_1 = P_1^0 x_1 \quad (3)$$

$$Py_2 = P_2^0 x_2 \quad (4)$$

$$\pi_1^0 = \pi_2^0 \quad (5)$$

$$x_1 + x_2 = 1 \quad (6)$$

$$y_1 + y_2 = 1 \quad (7)$$

In the equation (1) and (2), *n* is the amount of gas uptake as a function of pressure *t*. π^0 is the spreading pressure, and P^0 is the equilibrium pressure of the single-component gas corresponding to π^0. π^0 of each gas could be obtained from the experimental isotherms calculated from the area beneath the isotherm curve from pressure $t = 0$ to $t = P^0$. Mole fraction of gas phase *y* was set to be 0.15 for CO_2 and 0.85 for N_2. By using equation (5), P^0 of each component could be obtained by equation (1) and (2). After that, total pressure *P* and mole fraction of adsorbed gas phase *x* could be calculated. Then the selectivity could be determined by using equation (8).

$$S_{1,2} = \frac{x_1 y_2}{x_2 y_1} \quad (8)$$

2.1.2 Infrared spectroscopy (IR)

IR spectra were measured on a Bruker Tensor 27 using pressed KBr discs for the networks and Quest ATR (diamond crystal puck) attachment for monomer building blocks. The resolution of the measurement was 2 cm^{-1} with an air background subtracted.

2.1.3 Solution nuclear magnetic resonance spectroscopy (NMR)

^{1}H and ^{13}C NMR spectra were measured using a Bruker Avance 400 NMR spectrometer at 400.13 and 100.6 MHz, respectively. Deuterated solvents as specified were used and obtained from Sigma-Aldrich.

2.1.4 Solid state NMR (ssNMR)

Solid-state NMR spectra were measured by Andrea Laybourn (University of Liverpool) on a Bruker Avance 400 DSX spectrometer operating at 100.61 MHz for ^{13}C and 400.13 MHz for ^{1}H. ^{1}H-^{13}C cross-polarization magic angle spinning (CP/MAS) NMR experiments were carried out at an MAS rate of 10.0 kHz using zirconia rotors 4 mm in diameter. The ^{1}H $\pi/2$ pulse was 3.0 μs, and two-pulse phase modulation (TPPM) decoupling was used during the acquisition. The Hartmann-Hahn condition was set using hexamethylbenzene. The spectra were measured using a contact time of 2.0 ms and a relaxation delay of 8.0 s. Typically, 2048 scans were accumulated. The values of the chemical shifts are referred to that of TMS. The analysis of the spectra (deconvolution and integration) was carried out using Bruker TOPSPIN software.

2.1.5 Elemental analysis

Elemental contents in the samples were analysed by CHN analysis using a Thermo FlashEA 1112 Elemental Analyser. Samples were analysed as dry powders. All CHN data was collected and processed by either Jean Ellis or George Miller (University of Liverpool).

2.1.6 Mass spectroscopy (MS)

Accurate molecular weights of samples were determined by chemical ionisation (CI) mass spectroscopy using Agilent Q-TOF 7201 mass spectrometer. All data was collected by Moya McCarron (University of Liverpool).

2.1.7 Scanning electron microscopy (SEM)

Images showing the morphology of the polymers were collected using a Hitachi S-4800 cold Field Emission Scanning Electron Microscope (FE-SEM). The dry samples were spread on 15 mm Hitachi M4 aluminium stubs using an adhesive high purity carbon tab. The samples were then coated with a 2 nm layer of gold using an Emitech K550X automated sputter coater. The FE-SEM measurement scale bar was calibrated using certified SIRA calibration standards. Imaging was conducted at a working distance of 8 mm and a working voltage of 3 kV using a mix of upper and lower secondary electron detectors. The data were collected by Dr. Robert Dawson (University of Liverpool).

2.1.8 Gel permeation chromatography (GPC)

GPC data were collected by Dr. Sean Higgins (University of Liverpool) on a Viscotek system, which was comprised of a GPCmax solvent/sample module, and a TDA302 detector module housing a refractive index, viscometer and light-scattering detectors. The system was fitted with 2x ViscoGel HHR-H columns housed in an oven at 40 °C, and THF was used as the eluent. The system was calibrated with low molecular weight polystyrene standards, and the OmniSEC Universal calibration method was used.

2.1.9 Gas chromatography (GC)

Gas Chromatography was performed on a TRACE 1310 gas chromatrograph with a TriScore PLUS RSH Autosampler (Thermo Scientific corporation) using Flame Ionization Detector (FID) as a detector. Supleco B-DEX 325 (30 m x 0.25 um x 0.25 um film thickness) column was used. A 10 µL liquid injection syringe was used for injections. Injections had the following conditions: injection temperature 300 °C and detection temperature 300 °C with hydrogen, air, and make-up flow-rates of 35, 350, and 20 mL/min respectively. Helium (99.999 %) was used as the carrier gas. Oven program was set as 100 °C for 20 min, then 150 °C at 10 °C/min with 0 min hold. Integration and chromatographic calculations of the resulting peaks was

performed using the supplied Chromeleon 7.1.2.1478 (Thermo Scientific) software. The optimisation of the measurement conditions was done by Adam Kewley (University of Liverpool).

2.1.10 High performance liquid chromatography (HPLC)

HPLC chromatogram was obtained using the Dionex Ultimate 3000 HPLC system. A Phenomenex Synergi 4u Hydro-RP, polar endcapped C18, 150 × 2.0 mm, 4 µm (P/N is 00F-4375-B0, S/N 615339-12) column was used. The mobile phase was methanol with 0.1% formic acid at a flow rate of 0.5 mL/min. The injection volume was 5 µL with dilution factor of 1. The sample concentration was about 1 mg/mL in methanol. The column oven temperature was set to 30 °C. Detection for HPLC analysis was conducted at 254 nm. The data were collected by Dr. Michael Briggs (University of Liverpool).

2.2 Synthesis for benzene-aniline copolymers

2.2.1 Materials

All chemicals and solvents were purchased from Sigma-Aldrich and used as received except aniline and iron(III) chloride, which were purchased from VWR.

2.2.2 Synthesis of benzene-aniline copolymers

General procedure

The polymers were synthesised followed the method introduced by Li *et al.*[2] To the solution of monomer(s) (10 mmol) in 1,2-dichloroethane (DCE) (20 mL), was added formaldehyde dimethyl acetal (FDA) (20 mmol, 1.77 mL), following by iron (III) chloride ($FeCl_3$) (20 mmol, 3.24 g). Then the reaction was heated up to 80 °C with stirring overnight. After that, the reaction was quenched by using methanol (MeOH) (10 mL), filtrated, and washed with MeOH until the filtrate is colourless.

The product was then purified by Soxhlet extraction overnight using MeOH and dried *in vacuo* at 70 °C overnight to obtain knitting network.

50% benzene-aniline copolymer. Benzene (5 mmol, 0.447 mL) and aniline (5 mmol, 0.456 mL) were used as monomers. 50% benzene-aniline copolymer was obtained as dark brown solid. **Yield:** 0.95 g, 87%. **Elemental analysis:** calculated (%) for $C_{16}H_{13}N$: C 87.64, H 5.98, N 6.39; found: C 74.43, H 5.61, N 5.54.

2.3 Synthesis for cross-linked polystyrenes

2.3.1 Materials

All reagents were purchased from Sigma Aldrich. Styrene was passed through the alumina to remove the inhibitor before use. All other chemicals were used as received.

2.3.2 Synthesis of small molecules containing carboxylic acid

General procedure

See **Section 2.2.2**.

Benzoic acid. Benzoic acid (10 mmol, 1.22 g) was used. No solid was observed.

Methyl benzoate. Methyl benzoate (10 mmol, 1.25 mL) was used. No solid was observed.

Butyl benzoate. Butyl benzoate (10 mmol, 1.77 mL) was used. No solid was observed.

3-Phenylpropionic acid. 3-Phenylpropionic acid (10 mmol, 1.50 g) was used. Knitted 3-phenylpropionic acid was obtained as black solid. **Yield:** 1.89 g, 107%. **Elemental analysis:** calculated (%) for $C_{11}H_{12}O_2$: C 74.98, H 6.86, O 18.16; found: C 72.66, H 5.83.

2.3.3 Synthesis of linear polystyrenes

General procedure

Linear polystyrene was synthesised by RAFT polymerisation. To the solution of a RAFT agent (1 eq.) in dioxane (7.5 mL) was added styrene (eq. = DP, 18 mmol) and an initiator (0.5 eq.). The solution was deoxygenated by nitrogen purging for 30 minutes. The reaction was then heated to 60 °C and stirred under nitrogen. The conversion was monitored by ^{1}H NMR. After 90 hours, the reaction was cooled to room temperature and the product precipitated. After drying in *vacuo* at 40 °C overnight, **PS-x-y** was obtained. The molecular weight of **PS-x-y** was varied by changing the ratio of RAFT agent and initiator to styrene monomer. By changing the RAFT agents, **PS-x-y** with different RAFT end groups could be synthesised.

*Synthesis of **PS-1-y***

4-cyano-4-[(dodecylsulfanylthiocarbonyl) sulfanyl]pentanoic acid (CDDPA; **RAFT-1**) was used as a RAFT agent and 4,4′-azobis(4-cyanovaleric acid) (ACVA) was used as an initiator. The products were precipitated into water for **PS-1-1** and **PS-1-2**, in MeOH for **PS-1-3** and **PS-1-4**, and in EtOH for **PS-1-5** to **PS-1-10**. All **PS-1s** provided yellow solid.

PS-1-7. **RAFT-1** (1 eq., 0.72 mmol, 0.29 g), ACVA (0.5 eq., 0.36 mmol, 0.10 g) and styrene (25 eq., 18 mmol, 2.1 mL) were used. **PS-1-7** was obtained as yellow solid. **Yield:** 0.75 g, 40%. **^{1}H NMR** ($CDCl_3$, 400 MHz) δ = 0.88 (m, 3H), 0.90–2.50 (m, 89H), 3.25 (m, 2H), 4.62–5.07 (m, 1H), 6.25–7.35 (m, 105 H) ppm. **GPC:** M_n = 2609, M_w = 2783, PDI = 1.07. **Elemental analysis:** calculated (%) for $C_{187}H_{201}NO_2S_3$: C 86.69, H 7.82, N 0.54, S 3.71, O 1.24; found: C 86.86, H 7.74, N 0.57, S 3.17.

*Synthesis of **PS-2-y***

4-Cyano-4-(phenylcarbonothioylthio)pentanoic acid (CPCPA; **RAFT-2**) was used as a RAFT agent and ACVA was used as an initiator. The products were

precipitated into water for **PS-2-1** and in EtOH for **PS-2-2**. Both **PS-2-1** and **PS-2-2** provided pink solid.

PS-2-2. **RAFT-2** (1 eq., 0.36 mmol, 0.10 g), ACVA (0.5 eq., 0.18 mmol, 0.05 g) and styrene (50 eq., 18 mmol, 2.1 mL) were used. **PS-2-2** was obtained as pale pink solid. **Yield:** 0.19 g, 23%. **^{1}H NMR** ($CDCl_3$, 400 MHz) δ = 0.70–2.60 (m, 84H), 4.72–4.97 (m, 1H), 6.25–7.35 (m, 130 H) ppm, 7.31 (m, 2 H), 7.46 (m, 1H), 7.84 (m, 2H). **GPC:** M_n = 2941, M_w = 3278, PDI = 1.11. **Elemental analysis:** calculated (%) for $C_{221}H_{221}NO_2S_2$: C 88.86, H 7.46, N 0.47, S 2.15, O 1.07; found: C 88.66, H 7.45, N 0.55, S 1.77.

Synthesis of ***PS-3-y***

2-(Dodecylthiocarbonothioylthio)-2-methylpropionic (DDMAT; **RAFT-3**) was used as a RAFT agent and ACVA was used as an initiator. The products were precipitated into water for **PS-3-1** and in EtOH for **PS-3-2**. Both **PS-3-1** and **PS-3-2** provided yellow solid.

PS-3-2. **RAFT-3** (1 eq, 0.72 mmol, 0.26 g), ACVA (0.5 eq, 0.36 mmol, 0.10 g) and styrene (25 eq, 18 mmol, 2.1 mL) were used. **PS-3-2** was obtained as yellow solid. **Yield:** 0.91 g, 48%. **^{1}H NMR** ($CDCl_3$, 400 MHz) δ = 0.65–2.50 (m, 91H), 3.24 (m, 2H), 4.62–5.00 (m, 1H), 6.25–7.35 (m, 105 H) ppm. **GPC:** M_n = 2504, M_w = 2791, PDI = 1.11. **Elemental analysis:** calculated (%) for $C_{185}H_{200}O_2S_3$: C 87.08, H 7.90, N 0.00, S 3.77, O 1.25; found: C 86.88, H 7.88, N 0.20, S 3.21.

Synthesis of ***PS-4-y***

2-Cyano-2-propyl dodecyl trithiocarbonate (CPDT; **RAFT-4**) was used as a RAFT agent. ACVA was used as an initiator for **PS-4-1** and **PS-4-2**. Azobisisobutyronitrile (AIBN) was used as an initiator for **PS-4-3**. The products were precipitated into water for **PS-4-1** and **PS-4-3**, and in EtOH for **PS-4-2**. All **PS-4s** provided yellow solid.

PS-4-2. **RAFT-4** (1 eq, 0.72 mmol, 0.25 g), ACVA (0.5 eq, 0.36 mmol, 0.10 g) and styrene (25 eq, 18 mmol, 2.1 mL) were used. **PS-4-2** was obtained as pale yellow solid. **Yield:** 1.07 g, 59%. **^{1}H NMR** ($CDCl_3$, 400 MHz) δ = 0.60–2.70 (m, 82H), 3.26 (m, 2H), 4.61–5.02 (m, 1H), 6.15–7.45 (m, 90 H) ppm. **GPC:** M_n = 2173, M_w = 2353, PDI = 1.08. **Elemental analysis:** calculated (%) for $C_{161}H_{175}NS_3$: C 87.09, H 7.94, N 0.63, S 4.33; found: C 86.51, H 7.90, N 0.72, S 4.01.

PS-4-3. **RAFT-4** (1 eq, 0.90 mmol, 0.31 g), AIBN (0.5 eq, 0.45 mmol, 0.07 g) and styrene (10 eq, 9 mmol, 1.0 mL) were used. **PS-4-3** was obtained as yellow oil. **Yield:** 0.37 g, 32%. **^{1}H NMR** ($CDCl_3$, 400 MHz) δ = 0.65–2.70 (m, 49H), 3.24 (m, 2H), 4.66–5.02 (m, 1H), 6.40–7.65 (m, 35 H) ppm. **GPC:** M_n = 976, M_w = 1167, PDI = 1.20. **Elemental analysis:** calculated (%) for $C_{73}H_{87}NS_3$: C 81.59, H 8.16, N 1.30, S 8.95; found: C 81.81, H 8.32, N 1.60, S 9.46.

Synthesis of ***PS-5-y***

2-Cyano-2-propyl benzodithioate (CPBT; **RAFT-5**) was used as a RAFT agent. ACVA was used as an initiator for **PS-5-1** and **PS-5-2**. AIBN was used as an initiator for **PS-5-3**. The products were precipitated into water for **PS-5-1** and in EtOH for **PS-5-2** and **PS-5-3**. All **PS-5s** provided pink solid.

PS-5-2. **RAFT-5** (1 eq., 0.36 mmol, 0.08 g), ACVA (0.5 eq., 0.18 mmol, 0.05 g) and styrene (50 eq., 18 mmol, 2.1 mL) were used. **PS-5-2** was obtained as pale pink solid. **Yield:** 0.28 g, 33%. **^{1}H NMR** ($CDCl_3$, 400 MHz) δ = 0.75–2.70 (m, 62H), 4.57–4.97 (m, 1H), 6.20–7.40 (m, 95 H), 7.32 (m, 2H), 7.47 (m, 1H), 7.84 (m, 2H) ppm. **GPC:** M_n = 2207, M_w = 2436, PDI = 1.10. **Elemental analysis:** calculated (%) for $C_{163}H_{163}NS_2$: C 88.98, H 7.47, N 0.64, S 2.91; found: C 88.89, H 7.50, N 0.67, S 2.60.

PS-5-3. **RAFT-5** (1 eq., 0.36 mmol, 0.08 g), AIBN (0.5 eq., 0.18 mmol, 0.03 g) and styrene (50 eq., 18 mmol, 2.1 mL) were used. **PS-5-3** was obtained as pink solid. **Yield:** 0.30 g, 37%. **^{1}H NMR** ($CDCl_3$, 400 MHz) δ = 0.75–2.70 (m, 68H), 4.52–5.06 (m, 1H), 6.20–7.40 (m, 105 H), 7.31 (m, 2H), 7.46 (m, 1H), 7.85 (m, 2H) ppm. **GPC:** M_n = 2495, M_w = 2689, PDI = 1.08. **Elemental analysis:** calculated (%) for

$C_{179}H_{179}NS_2$: C 89.26, H 7.49, N 0.58, S 2.66; found: C 89.12, H 7.41, N 0.62, S 2.49.

2.3.4 Cross-linking of polystyrenes

General procedure

Cross-linking of polystyrene was performed followed the method of Li *et al*.[2] To a solution of linear polystyrene (**PS-x-y**) in 1,2-dichloroethane (DCE) (*n* mL) was added formaldehyde dimthyl acetal (FDA) (*n* mmol) and iron (III) chloride ($FeCl_3$) (*n* mmol). The amount of FDA, $FeCl_3$ and solvent were used in the proportion to the number of aromatic rings in the **PS-x-y** where *n* is equal to twice of the number of styrene units in the **PS-x-y**. The reaction was heated to 80 °C overnight under nitrogen. The reaction was quenched by using methanol (MeOH), filtered and washed with MeOH. The product was further purified by Soxhlet extraction using MeOH for three days and dried in *vacuo* at 70 °C overnight. Cross-linked polystyrenes (**CLPS-x-y**) were obtained as brown solid networks.

CLPS-1-7. **PS-1-7** (0.04 mmol, 0.10 g), FDA (1.7 mmol, 0.15 mL), $FeCl_3$ (1.7 mmol, 0.27 g) and DCE (1.7 mL) were used. **CLPS-1-7** was obtained as brown solid. **Yield:** 0.12 g, 99%. **Elemental analysis:** calculated (%) for $C_{229}H_{243}NO_2S_3$: C 87.66, H 7.81, N 0.45, S 3.07, O 1.02; found: C 81.82, H 6.94, N 0.46, S 1.50.

CLPS-2-2. **PS-2-2** (0.03 mmol, 0.09 g), FDA (1.6 mmol, 0.14 mL), $FeCl_3$ (1.6 mmol, 0.26 g) and DCE (1.6 mL) were used. **CLPS-2-2** was obtained as light brown solid. **Yield:** 0.11 g, 98%. **Elemental analysis:** calculated (%) for $C_{273}H_{273}NO_2S_2$: C 89.48, H 7.51, N 0.38, S 1.75, O 0.87; found: C 78.95, H 6.31, N 0.37, S 1.25.

CLPS-3-2. **PS-3-2** (0.05 mmol, 0.13 g), FDA (2.1 mmol, 0.19 mL), $FeCl_3$ (2.1 mmol, 0.34 g) and DCE (2.1 mL) were used. **CLPS-3-2** was obtained as brown solid. **Yield:** 0.16 g, 91%. **Elemental analysis:** calculated (%) for $C_{227}H_{242}O_2S_3$: C 87.99, H 7.87, N 0.00, S 3.10, O 1.03; found: C 79.48, H 6.84, N 0.16, S 1.50.

CLPS-4-2. **PS-4-2** (0.05 mmol, 0.12 g), FDA (1.8 mmol, 0.16 mL), $FeCl_3$ (1.8 mmol, 0.29 g) and DCE (1.8 mL) were used. **CLPS-4-2** was obtained as light brown

solid. **Yield:** 0.14 g, 92%. **Elemental analysis:** calculated (%) for $C_{197}H_{211}NS_3$: C 87.99, H 7.91, N 0.52, S 3.58; found: C 80.69, H 7.10, N 0.53, S 2.17.

CLPS-4-3. **PS-4-3** (0.10 mmol, 0.10 g), FDA (1.4 mmol, 0.12 mL), $FeCl_3$ (1.4 mmol, 0.22 g) and DCE (1.4 mL) were used. **CLPS-4-3** was obtained as brown solid. **Yield:** 0.10 g, 89%. **Elemental analysis:** calculated (%) for $C_{87}H_{101}NS_3$: C 83.13, H 8.10, N 1.11, S 7.65; found: C 80.14, H 7.15, N 1.48, S 4.41.

CLPS-5-2. **PS-5-2** (0.05 mmol, 0.11 g), FDA (1.9 mmol, 0.17 mL), $FeCl_3$ (1.9 mmol, 0.31 g) and DCE (1.9 mL) were used. **CLPS-5-2** was obtained as light brown solid. **Yield:** 0.13 g, 94%. **Elemental analysis:** calculated (%) for $C_{201}H_{201}NS_2$: C 89.58, H 7.52, N 0.52, S 2.38; found: C 80.94, H 6.34, N 0.50, S 1.36.

CLPS-5-3. **PS-5-3** (0.05 mmol, 0.13 g), FDA (2.1 mmol, 0.19 mL), $FeCl_3$ (2.1 mmol, 0.34 g) and DCE (2.1 mL) were used. **CLPS-5-3** was obtained as brown solid. **Yield:** 0.15 g, 100%. **Elemental analysis:** calculated (%) for $C_{221}H_{221}NS_2$: C 89.82, H 7.54, N 0.47, S 2.17; found: C 81.06, H 6.53, N 0.47, S 1.33.

2.4 Synthesis for post-synthetic modification

2.4.1 Materials

1,3,5-Triethynylbenzene and tetrakis(triphenylphosphine) palladium(0) were purchased from Alfa-Aesar. All other chemicals were purchased from Sigma-Aldrich with a purity of 97% or greater.

2.4.2 Synthesis of CMP-1-NH_2

The polymers were synthesised followed the procedure suggested by Dawson *et al.*[3] 1,3,5-Triethynylbenzene (600 mg, 4 mmol) and 2,5-dibromoaniline (1003 mg, 4 mmol) were added to a 100 mL Radleys reaction flask fitted with a condenser and magnetic stirrer. The flask was evacuated and backfilled with nitrogen three times before anhydrous *N,N'*-dimethylformamide (6 mL) and anhydrous triethylamine (6 mL) were added via a syringe. The solution was then heated to 100 °C. Tetrakis(triphenylphosphine)palladium(0) (200 mg) and CuI (60 mg) were then

added as a slurry in *N,N'*-dimethylformamide (2 mL). The reaction was stirred at 100 °C under nitrogen for 24 h after which the solid precipitate was washed with hot *N,N'*-dimethylformamide and purified by Soxhlet extraction with methanol for 18 h. The insoluble brown powder was dried under vacuum at 70 °C for at least 12 h. **Yield:** 0.86 g, 90%. **Elemental analysis:** calculated (%) for $C_{18}H_8N$: C 90.74, H 3.38, N 5.88; found: C 78.18, H 3.59, N 2.62.

2.4.3 Post-synthetic modification of CMP-1-NH_2 to CMP-1-AMDs

2.4.3.1 Neat acid anhydrides at 30 °C

CMP-1-NH_2 (119 mg, 0.5 mmol) was stirred in the neat anhydride (2 mL) for 24 h at 30 °C, after which the solid was filtered off and washed with $CHCl_3$ to obtain brown powder. The product was then dried in vacuo at 70 °C for at least 12 h. **Yield:** 0.11-0.13 g, 67-84%.

2.4.3.2 Neat acid anhydrides at room temperature

CMP-1-NH_2 (80 mg, 0.34 mmol) was stirred in the neat anhydride (2 mL) for 24 h at room temperature, after which the solid was filtered off and washed with $CHCl_3$ to obtain brown powder. The product was then dried in vacuo at 70 °C for at least 12 h. **Yield:** 0.53-0.61 g, 49-56 %.

2.4.3.3 Acid anhydrides in $CHCl_3$

CMP-1-NH_2 (119 mg, 0.5 mmol) in $CHCl_3$ was added acid anhydride (2 mL). The reaction was stirred for 24 h at room temperature, after which the solid was filtered off and washed with $CHCl_3$ to obtain brown powder. The product was then dried in vacuo at 70 °C for at least 12 h. **Yield:** 0.11-0.12 mg, 57-75%.

2.5 Synthesis for molecular imprinting polymers

2.5.1 Materials

1,3,5-Triethynylbenzene and tetrakis(triphenylphosphine) palladium(0) were purchased from Alfa-Aesar. All other chemicals were purchased from Sigma-Aldrich.

2.5.2 Monomer Synthesis

2.5.2.1 Esterification by using DCC/DMAP

General procedure

2,5-Dibromobenzoate compounds were synthesised using *N,N'*-dicyclohexylcarbodiimide (DCC) and 4-dimethylaminopyridine (DMAP) following the method of Stackhouse *et al.*[4] To the solution of 2,5-dibromobenzoic acid (1 eq.), monomer template (1 eq.) and DMAP (0.04 eq.) in dichloromethane (DCM) at 0 °C was added 1 M DCC in DCM solution (1 eq.) drop wisely. The reaction was allowed to stir at room temperature overnight. After that, the reaction was filtered and the solvent was removed using a rotary evaporator. The crude product was purified by column chromatography using DCM to obtain the 2,5-dibromobenzoate.[5]

Cholesteryl 2,5-dibromobenzoate. Cholesterol was used as the monomer template. Cholesterol (4.77 mmol, 1.84 g), 2,5-dibromobenzoic acid (4.77 mmol, 1.33 g), 1 M DCC in DCM (4.77 mmol, 4.77 mL), DMAP (0.21 mmol, 0.025 g) and DCM (40 mL) were used. **Cholesterol functionalised monomer** (cholesteryl 2,5-dibromobenzoate) was obtained as white solid. **Yield:** 2.51 g, 81%. **^{1}H NMR** ($CDCl_3$, 400 MHz) δ = 1.96-0.61 (m, 41H), 2.41(d, 2H, J = 8 Hz), 4.80 (m, 1H), 5.35 (d, 1H, J = 4 Hz), 7.33 (dd, 1H, J = 3, 8 Hz), 7.41 (d, 1H, J = 8 Hz), 7.79 (d, 1H, J = 3 Hz) ppm. **^{13}C NMR** ($CDCl_3$, 400 MHz) δ = 14.8, 21.7, 22.3, 24.0, 25.5, 25.8, 26.8, 27.2, 30.7, 30.9, 31.2, 34.7, 34.8, 38.7, 39.1, 39.5, 39.9, 40.9, 42.4, 42.6, 45.2, 52.9, 59.1, 59.6, 79.0, 123.1, 123.9, 126.0, 136.8, 137.3, 138.1, 138.5, 142.2, 167.2 ppm. **Elemental analysis:** calculated (%) for $C_{34}H_{48}Br_2O_2$: C 62.97, H 7.46; found: C 62.72, H 7.47. **MS:** $[M+Na]^+$ m/z 669.

Menthyl 2,5-dibromobenzoate. Menthol was used as the monomer template. Menthol (14.30 mmol, 2.23 g), 2,5-dibromobenzoic acid (14.30 mmol, 4.00 g), 1 M DCC in DCM (14.30 mmol, 14.30 mL), DMAP (0.62 mmol, 0.075 g) and DCM (125 mL) were used. **Menthol functionalised monomer** (menthyl 2,5-dibromobenzoate) was obtained as pale yellow oil. **Yield:** 4.92 g, 82%. **^{1}H NMR** ($CDCl_3$, 400 MHz) δ = 0.82 (d, 3H, J = 7 Hz), 0.94 (m, 7H), 1.15 (m, 2H), 1.54 (m, 2H), 1.73 (m, 2H), 1.97 (m, 1H), 2.15 (m, 1H), 4.97 (dt, 1H, J = 4, 11 Hz), 7.42 (dd, 1H, J = 2, 8 Hz), 7.50 (d, 1H, J = 8 Hz), 7.82 (d, 1H, J = 2 Hz) ppm. **^{13}C NMR** ($CDCl_3$, 400 MHz) δ = 16.2, 20.8, 22.0, 23.3, 26.3, 31.5, 34.2, 40.8, 47.0, 76.4, 120.1, 121.0, 133.6, 134.8, 135.1, 135.6, 164.6 ppm. **Elemental analysis:** calculated (%) for $C_{17}H_{22}Br_2O_2$: C 48.83, H 5.30; found: C 49.38, H 5.38. **MS:** $[M+Na]^+$ m/z 439.

2.5.2.2 Esterification by using triethylamine (NEt_3)

General procedure

Following the method of Audorff *et al.* or Lewis *et.al.*, dibromo-monomer was dissolved in dry either toluene[6] or DCM[7]. Then dry triethylamine (NEt_3) was added to the solution following by trimesic acid trichloride dropwise. The reaction was stirred and then filtered. Various reaction conditions were attempted to improve the yield of the products as discussed in the result chapter. The product was purified by precipitation or recrystallisation as specified below.

Trimesate monomer. 2,4-Dibromophenol (6.6 mmol, 1.66 g), trimesic acid trichloride (2 mmol, 0.36 mL), NEt_3 (10 mL) and toluene or DCM (150 mL) were mixed. The reaction was stirred at either 110 °C (for toluene) or room temperature (for DCM) for 24 hours. After filtration, solvent was removed using a rotary evaporator. The crude product was dissolved in THF and precipitated in ethanol. Tris(2,4-dibromophenyl) benzene-1,3,5-tricarboxylate was obtained as white solid. **Yield:** 0.58 g, 32% (toluene), 1.29 g, 71% (DCM). **^{1}H NMR** ($CDCl_3$, 400 MHz) δ = 7.22 (d, 3H, J = 8 Hz), 7.55 (dd, 3H, J = 2, 8 Hz), 7.84 (d, 3H, J = 2 Hz), 9.31 (s, 3H) ppm. **^{13}C NMR** ($CDCl_3$, 400 MHz) δ = 117.1, 120.2, 124.8, 130.7, 131.8, 136.0,

136.7, 147.2, 162.0 ppm. **Elemental analysis:** calculated (%) for $C_{27}H_{12}Br_6O_6$: C 35.57, H 1.33; found: C 35.96, H 1.34.

Trimesamide monomer. 2,4-Dibromoaniline (20 mmol, 5.02 g), trimesic acid trichloride (2 mmol, 0.36 mL), NEt_3 (1.5 mL) and toluene or DCM (150 mL) were used. The reaction was stirred at either 110 °C (for toluene) or room temperature (for DCM) for 24 hours. After filtration, filtrant was recrystallised in DMF and water. N^1,N^3,N^5-tris(2,4-dibromophenyl)benzene-1,3,5-tricarboxamide was obtained as white solid. **Yield:** 0.82 g, 45% (toluene), 0.83 g, 46% (DCM). **^{1}H NMR** (DMSO-d_6, 400 MHz) δ = 7.54 (d, 3H, J = 8 Hz), 7.69 (dd, 3H, J = 2, 8 Hz), 8.02(d, 3H, J = 2 Hz), 8.78 (s, 3H), 10.53 (s, 3H) ppm. **^{13}C NMR** (DMSO-d_6, 400 MHz) δ = 119.5, 121.7, 130.2, 130.4, 131.2, 134.6, 134.7, 135.9, 164.4 ppm. **Elemental analysis:** calculated (%) for $C_{27}H_{15}Br_3N_3O_3$: C 35.68, H 1.66, N 4.62; found: C 35.59, H 1.70, N 4.61.

2.5.3 Polymer synthesis

General procedure

1,3,5-Triethynylbenzene (1 mmol, 0.15 g) and the functionalised monomer (1 mmol for **CHOL-CMPs** and **MENT-CMPs** or 0.33 mmol for **O-TRIMs** and **N-TRIMs**) as prepared above were placed in a Radleys reaction flask. This was evacuated and back filled with nitrogen three times. Pre-nitrogen bubbling, anhydrous dimethylformamide (DMF) (1.5 mL) and anhydrous triethylamine (NEt_3) (1.5 mL) were added. The solution was then heated to 100 °C. A slurry of tetrakis(triphenylphosphine) palladium (0) ($Pd(PPh_3)_4$) (50 mg) and copper (I) iodide (CuI) (15 mg) in DMF (0.5 mL) was quickly added to the reaction. After stirring at 100 °C overnight, the solid product was filtered, and washed with MeOH. The product was then purified by Soxhlet extraction overnight using MeOH and dried in *vacuo* at 60 °C overnight to obtain the CMPs.

2.5.4 Hydrolysis

To the vial of CMP (0.15 g) in MeOH (4.50 mL) was added KOH (0.45 g). The reaction was heated up to either 35 °C (for **CHOL-CMPs** and **MENT-CMPs**) or 60 °C (for **O-TRIMs** and **N-TRIMs**) for 24 hours. The polymer was then collected by filtration, purified by Soxhlet extraction with MeOH overnight and dried in *vacuo* at 60 °C overnight to obtain the **CMP-Hs**.

2.5.5 Molecular uptakes

To the vial of polymer (25 mg) was added solvent (1 mL). After 24 hours, the polymer was collected by filtration. The solution was further analysed by GC or HPLC.

2.5.6 Calculation of menthol selectivity

The selectivity of menthol over terpinolene was calculated as

$$Selectivity = \frac{M - T}{M + T} \times 100$$

where M and T are the amount of menthol and terpinolene adsorbed in the networks.

2.6 References

1. A. L. Myers and J. M. Prausnitz, *AIChE Journal*, 1965, **11**, 121-127.

2. B. Li, R. Gong, W. Wang, X. Huang, W. Zhang, H. Li, C. Hu and B. Tan, *Macromolecules*, 2011, **44**, 2410-2414.

3. R. Dawson, D. J. Adams and A. I. Cooper, *Chemical Science*, 2011, **2**, 1173-1177.

4. P. J. Stackhouse, A. Wilson, D. Lacey and M. Hird, *Liquid Crystals*, 2010, **37**, 1191-1203.

5. G. Castruita, V. Garcia, E. Arias, I. Moggio, R. Ziolo, A. Ponce, V. Gonzalez, J. E. Haley, J. L. Flikkema and T. Cooper, *Journal of Materials Chemistry*, 2012, **22**, 3770-3780.

6. H. Audorff, R. Walker, L. Kador and H.-W. Schmidt, *Chemistry – A European Journal*, 2011, **17**, 12722-12728.

7. F. D. Lewis, T. M. Long, C. L. Stern and W. Liu, *The Journal of Physical Chemistry A*, 2003, **107**, 3254-3262.

Chapter 3

Benzene/aniline Co-polymers for CO_2 Capture

3. Benzene/aniline Co-polymers for CO_2 Capture

3.1 CO_2 Capture

CO_2 is considered to be one of the causes of global warming.[1] Therefore, many research groups are interested in making materials for CO_2 capture and utilisation.[2] Generally, CO_2 either in natural sources or from industrial exhaustion is mixed with other gases as well as water.[3] Materials for CO_2 capture should be able to adsorb high amounts of CO_2, as well as being selective to CO_2 over other gases. The materials should also be stable to humidity, high temperature and pressure.[4] Cost and scalability should also be considered.[5] Therefore, materials have to be carefully designed. Aqueous amine and ammonia solutions are the normal methods used nowadays to capture CO_2 from industrial sites.[6] Such methods have a drawback on the high energy needed to recycle the solutions, as well as corrosion problems.[7] Solid adsorbents are then an expected new technology for CO_2 capture, especially porous materials based on carbon, which generally have inert properties, low cost, and high surface area.[8]

Surface area is of course an important factor for high adsorption ability.[9] However, other factors like pore size[10, 11] or functionalities[12] could also improve the CO_2 sorption and selectivity. Amine functionality is often introduced to the networks for CO_2 capture.[13] Because of the basicity of amine group, it is expected to have a good interaction with acidic CO_2.[14] Much research has found that amine functionalised materials can improve the CO_2 sorption and selectivity. For example, the amine-anchored mesoporous silica (MCM-41-NH_2) exhibited higher CO_2 uptake than the non-functionalised one.[15] The Long group showed that incorporation of *N,N'*-dimethylethylenediamine into Cu-MOF could enhance the CO_2 uptake and the CO_2 heat of adsorption.[16] The work done by Lu *et al.* demonstrated that higher uptakes and selectivity of CO_2 in porous polymer networks (PPNs) could be obtained when the network was modified with polyamine groups.[13]

Considering the expected production costs for the large amounts of material that would be needed to absorb the necessary amount of CO_2 to solve the greenhouse gas problem, cheap approaches to synthesise the adsorbents are required.[4] In 2011, a

new synthetic method for making polymers called the 'knitting method' was introduced by Li *et al.*[17] With this method, monomers were linked together by Friedel-Crafts alkylation using iron (III) chloride ($FeCl_3$) as a catalyst and formaldehyde dimethyl acetal (FDA) as a cross-linker. Comparing to other common methods, this method seems to be relatively simple and inexpensive. The common reactions, such as Sonogashira-Hagihara reaction[18], Suzuki cross-coupling[19], and Yamamoto coupling[20, 21], used to synthesise porous materials are normally Pd or Ni catalysed reactions. Such catalysts are much more expensive compared to $FeCl_3$.

In this Chapter, our target is to synthesise amine-containing networks by the inexpensive Friedel-Crafts alkylation (knitting method) for CO_2 capture. By using the Friedel-Crafts reaction, an aromatic ring is required.[22] Considering the aromatic compound which contains an amine functionality, the simplest is perhaps aniline. Therefore hypercross-linked aniline was synthesised and characterised. However, Friedel-Crafts alkylation of aniline could have an issue on catalyst deactivation by coordination to the aniline.[22] Oxidative polymerisation reaction of aniline with $FeCl_3$ forming polyaniline (**Figure 3.1b**) could also occur as a side reaction.[23, 24] Porosity properties like the surface area as well as CO_2 uptakes and selectivity of the networks obtained were also investigated.

3.2 Synthesis and Characterisation

Aniline was hypercross-linked by Friedel-Crafts reaction using FDA as a cross-linker. However, aniline alone generated comparable low yielding network (72 % yield) with low surface area (7 m^2/g) and carbon dioxide uptake (0.35 mmol/g). Aniline monomer could be cross-linked together by methylene group from the FDA cross-linker forming the network as shown in **Figure 3.1a**. The oxidative polymerisation side reaction of aniline could also possibly occur, which would form the polymer shown in **Figure 3.1b**.[25] However, as the polymer obtained was insoluble and amorphous, it is difficult to characterise the exact structure of the network.[26]

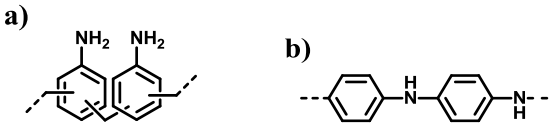

Figure 3.1 Possible structures of aniline networks

Co-polymerisation was found to be able to improve the surface area of materials as reported by Jiang *et al*.[27] Therefore, co-polymerisation with benzene, which provided a high surface area of over 1,200 m^2/g when polymerised alone,[17] was attempted to modify the network properties (**Scheme 3.1**).

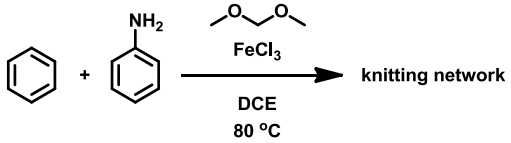

Scheme 3.1 Synthetic scheme for benzene/aniline co-polymer networks

Again, benzene/aniline co-polymers were synthesised by Friedel-Crafts reaction following the method from the literature.[17] FDA was used as a cross-linker in the ratio of two equivalents for each aromatic ring. $FeCl_3$ and DCE were used as a catalyst and solvent, respectively. Different ratios of aniline and benzene, i.e. 0%, 10%, 20%, 30%, 40%, 50%, 60%, 70%, 80%, 90%, and 100%, were used to study the effect on the properties of the networks. After leaving the reactions overnight, the co-polymers were washed with methanol using Soxhlet extraction to remove monomer and catalyst residues. Three repeat experiments were performed to confirm the reproducibility of the co-polymers.

All networks were obtained as brown-black insoluble solids. As shown in **Table 3.1**, the networks were formed in high yields (72-104 %) and the nitrogen contents from elemental analysis increased as more aniline monomer was used. Both these observations could be preliminarily used to confirm the inclusion of both monomers in networks. Yields higher than 100% and a deviation from the theoretical

values in elemental analysis were generally observed in this kind of materials.[11, 28-32] This could be caused by trapped catalyst, solvent, water or air within the pores.[8, 31, 33]

Table 3.1 Yields and elemental analysis data for the benzene/aniline co-polymer networks

%Aniline	Yields (%)	Theory			Analysis		
		C	H	N	C	H	N
0	104	94.08	5.92	0.00	83.66	5.34	0.00
10	101	92.72	5.93	1.35	83.12	5.36	1.11
20	99	91.39	5.94	2.66	80.51	5.26	1.96
30	90	90.10	5.95	3.94	77.59	5.18	2.81
40	88	88.85	5.97	5.18	74.97	5.11	3.90
50	85	87.64	5.98	6.39	74.43	5.61	5.54
60	82	86.45	5.99	7.56	70.28	5.45	6.56
70	87	85.30	6.00	8.70	65.59	5.30	7.41
80	83	84.18	6.00	9.82	64.23	5.14	7.88
90	79	83.09	6.01	10.90	64.18	5.11	9.40
100	72	82.02	6.02	11.96	62.90	5.06	9.40

The yields (**Figure 3.2**) dropped systematically as the aniline content increased. The lower the yield when more aniline was used could due to the inefficiency of aniline monomer towards Friedel-Crafts reaction.[22] As aniline could form the complex with $FeCl_3$ and precipitate, it could reduce the amount of aniline monomer left to form the networks. Oxidative polymerisation of aniline could also occur[25] leading to the lower molecular weight of the networks obtained as the methylene groups were excluded.

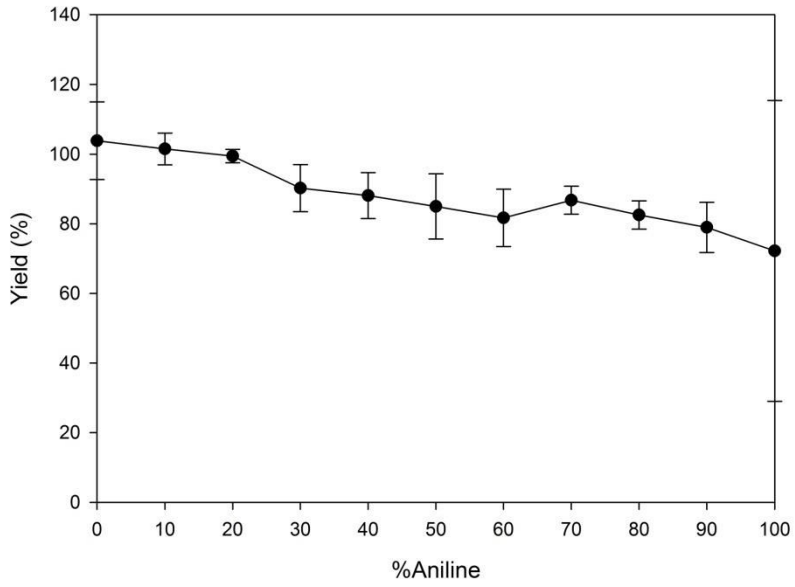

Figure 3.2 Average yields of benzene/aniline co-polymer networks

Despite the yields decreasing, the nitrogen contents (**Figure 3.3**) in the networks increased as the aniline ratio was increased. In fact, the nitrogen contents became close to the expected, theoretical value. This might imply the high content of aniline in the networks. However, the total amount of C, H and N in the networks decreased as the higher ratio of aniline was used (**Table 3.1**). It is possible that $FeCl_3$ was trapped in the networks by forming the complex with amino groups[22] leading to lower total percentage of C, H and N in the networks. At the higher amount of aniline, the more $FeCl_3$ might be expected to be trapped. Forming of polyaniline from oxidative polymerisation side reaction[25] could also be responsible for the higher content of nitrogen. Considering the hypercross-linked aniline with FDA cross-linker (**Figure 3.1a**), the theoretical C, H and N contents were calculated as 80.63, 7.61 and 11.75 % respectively. Meanwhile, the theoretical C, H and N contents of the polyaniline (**Figure 3.1b**) were respective 79.10, 5.53, and 15.37 %. Therefore, if the oxidative polymerisation side reaction occurred, it could also raise the nitrogen content in the networks.

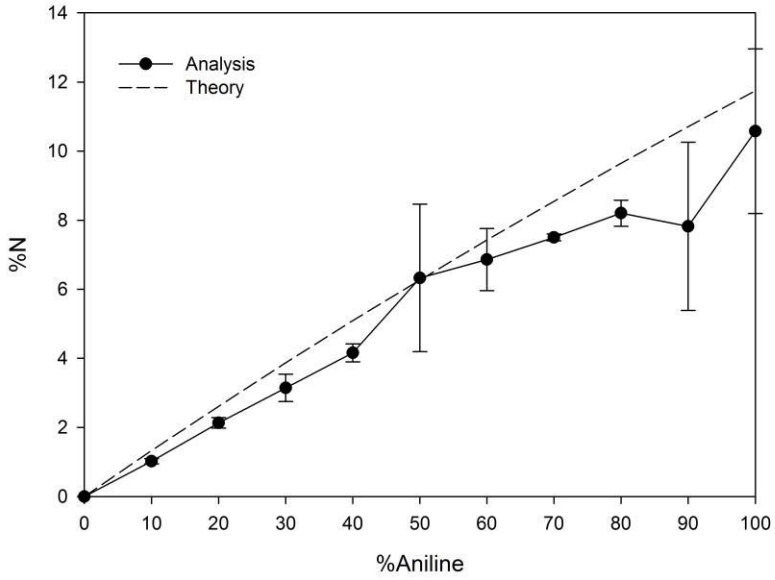

Figure 3.3 Average nitrogen contents of benzene/aniline co-polymer networks (the dotted line shows the theoretical values)

Figure 3.4 shows the IR spectra that were measured by the KBr method. The spectra presented the existence of aromatic ring (C=C stretching peaks around 1500-1680 cm^{-1} and C-H stretching peaks about 3000 cm^{-1}). C-H stretching peaks of alkyl group of the cross-linker appeared at 2900 cm^{-1}. Meanwhile, the amine functional group was difficult to identify because N-H stretching bands, normally observed around 3500 cm^{-1}, could overlap with O-H stretching of water which was easily adsorbed into both KBr discs and networks during the measurements. It is also possible that the primary amine was converted to secondary or tertiary amine as oxidative reaction occurred[25] or co-ordinated with $FeCl_3$[22] leading to disappearance of N-H peaks.

Solid state NMR spectra of 100% benzene, 50% aniline/benzene and 100% aniline networks measured by Andrea Laybourn (University of Liverpool) are shown in **Figure 3.5**. Three significant signals at 36-40, 129-132, and 137-140 ppm were observed. The peaks at 129-132 and 137-140 ppm indicated the non-substituted and substituted aromatic carbons respectively. The co-polymer showed unique aromatic carbons peaks from the homopolymers, implying that the network was not just the admixture of the two homopolymers. The peak at 36-40 ppm represented the

methylene carbon from the cross-linker. The signal decreased as the increasing of aniline contents which could due to the formation of polyaniline (**Figure 3.1b**) from oxidation side reaction[25] resulting in less methylene groups in the networks.

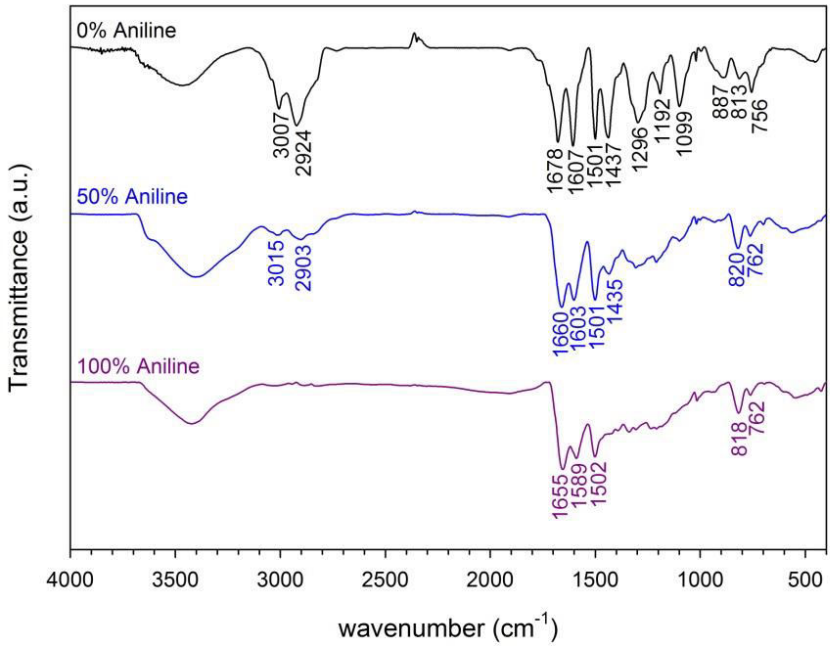

Figure 3.4 IR spectra of benzene/aniline co-polymer networks

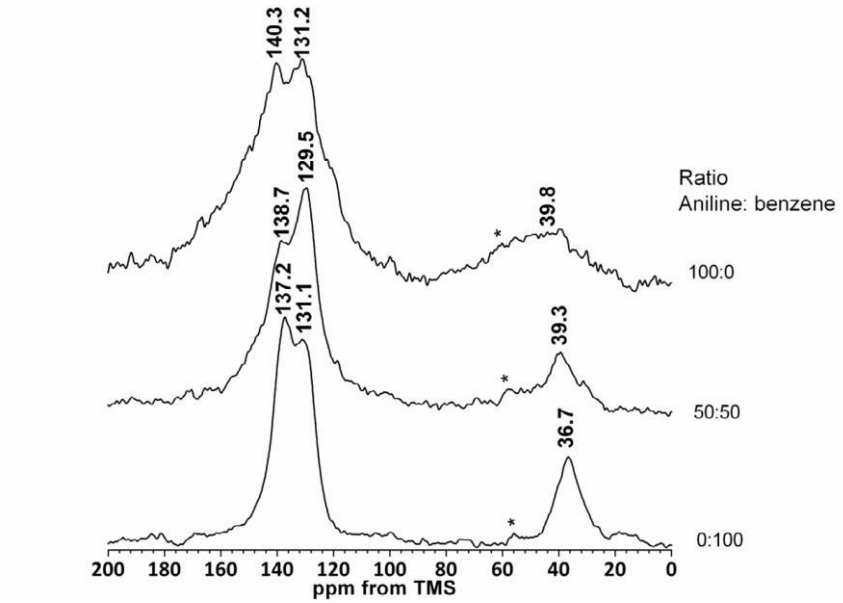

Figure 3.5 Solid state NMR spectra of benzene/aniline networks (data collected by Andrea Laybourn)[34]

3.3 Gas Sorption Properties

The porosity properties of the networks were measured by using nitrogen and carbon dioxide gases. Nitrogen isotherms of each co-polymer were measured at 77 K using Micromeritics ASAP 2420 by Dr. Robert Dawson (University of Liverpool). Type IV isotherms with hysteresis were observed as illustrated in **Figure 3.6**.

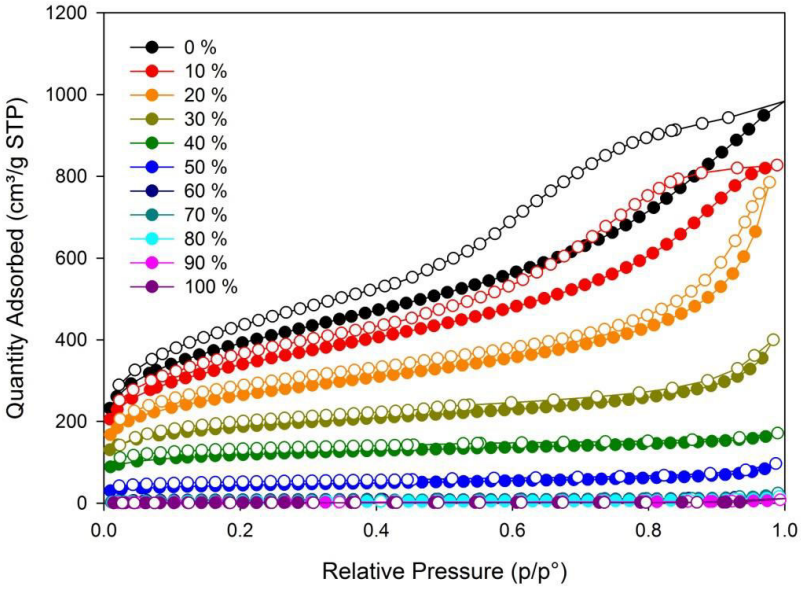

Figure 3.6 Nitrogen adsorption (close symbols) and desorption (open symbols) isotherms of benzene/aniline co-polymer networks

Figure 3.7 shows the pore size distributions of 0% to 50% aniline/benzene co-polymers calculated using the NL-DFT method. The pores were predominantly below 2 nm, indicating the polymers are microporous. The pore volume decreased as the ratio of aniline increased.

Surface areas were calculated using BET method and are summarised in **Table 3.2**. The surface area of hypercross-linked benzene (0 % aniline) was comparable to that reported in the literature.[17] Similar to CMP co-polymer networks reported by Jiang *et al.* where the surface area of a network with low porosity was improved by co-polymerisation with higher porous networks,[27] the BET surface areas declined as the ratio of aniline increased.

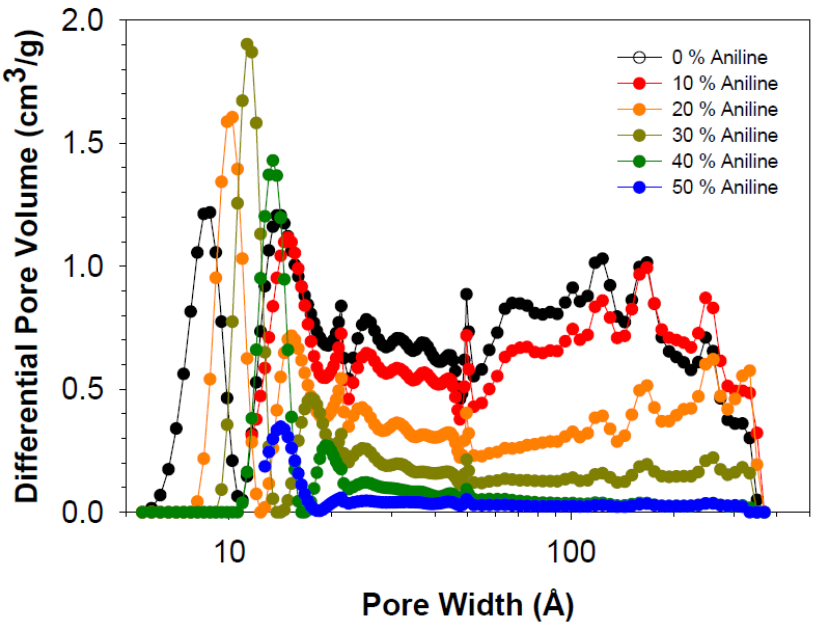

Figure 3.7 Pore size distribution of benzene/aniline networks[34]

Table 3.2 Gas sorption data and CO_2/N_2 selectivity at 1 bar calculated from IAST method using 15% CO_2 and 85% N_2 of benzene/aniline co-polymer networks

%Aniline	SA_{BET} (m^2/g)	CO_2 uptakes at 300 K(mmol/g)	CO_2/N_2 selectivity
0	1289	1.61	15.9 : 1
10	1097	1.51	16.5 : 1
20	757	1.37	18.7 : 1
30	481	1.33	21.6 : 1
40	238	1.18	24.9 : 1
50	152	0.85	26.0 : 1
60	48	0.59	26.7 : 1
70	24	0.44	32.2 : 1
80	10	0.46	34.7 : 1
90	22	0.41	45.0 : 1
100	7	0.35	49.2 : 1

From **Figure 3.8**, a non-linear decrease of the surface areas of co-polymer networks was observed (black data). The surface areas of physical mixtures of 100 % hypercross-linked benzene (0 % aniline) and 100 % hypercross-linked aniline in the same ratio were measured for comparison (red data). The physical mixtures provided a linear decrease in the surface areas as the amount of the aniline-based network was included. This implies that the co-polymerisation of benzene and aniline in the networks did not result in a simple mixture of benzene and aniline polymers.

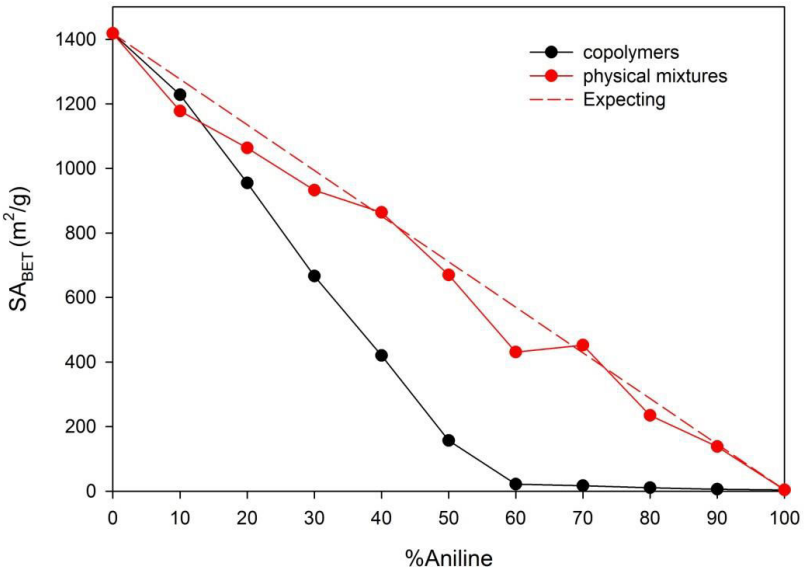

Figure 3.8 Surface areas of co-polymer networks (black), physical mixture of 100% benzene and 100% aniline (red), and expected surface areas of physical mixtures (dotted line)

CO_2 adsorption of the co-polymer networks was measured using Micromeritics ASAP 2020 at 300 K. The hypercross-linked benzene (0 % aniline) adsorbed 1.61 mmol/g of CO_2 compared to 2.78 mmol/g at 273 K reported previously.[17] Similar to the surface areas, which were calculated from nitrogen uptakes, the CO_2 uptakes declined as the percentage of the aniline monomer increased. Interestingly, the BET surface areas dropped more significantly than CO_2 uptakes, showing a possibility of CO_2/N_2 selectivity. (**Figure 3.9**)

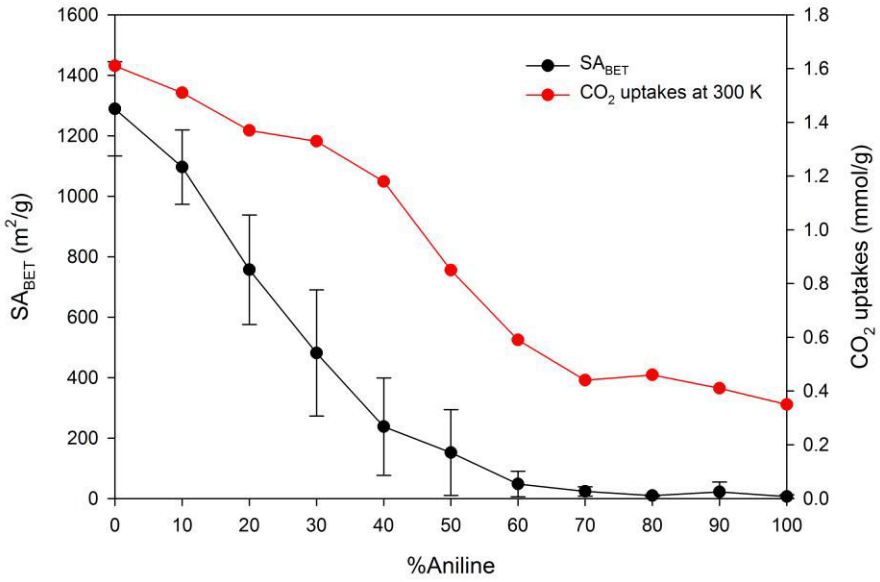

Figure 3.9 Average BET surface areas from three experiments (black) and CO_2 uptakes at 300 K with no error bar (red) of benzene/aniline co-polymer networks

The calculation of CO_2 over N_2 selectivity of the co-polymers was carried out by Dr. Robert Dawson (University of Liverpool) by using the Ideal Adsorbed Solution Theory (IAST) method,[35] with a gas composition of 15% carbon dioxide and 85% nitrogen at 1 bar. It can be seen that increasing of aniline in networks enhances the selectivity of CO_2/N_2 as presented in **Figure 3.10**.

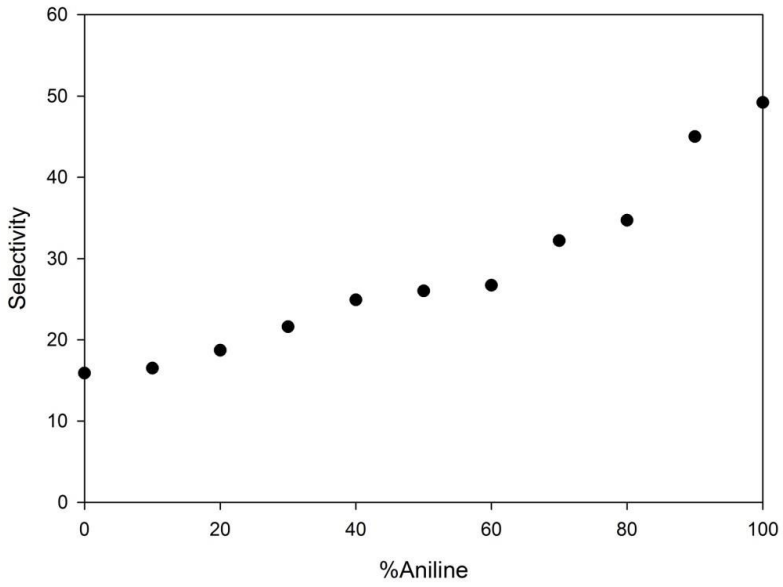

Figure 3.10 CO_2/N_2 IAST selectivity at 1 bar of benzene/aniline co-polymer networks

As CO_2 is generally mixed with other gases either in natural sources or from industrial exhaustion, many kinds of materials have been developed for CO_2/N_2 selectivity.[36] The ideal materials for carbon dioxide capture and separation should adsorb high amount of carbon dioxide as well as have high selectivity over other gases.[4, 5] However, typically materials with high selectivity showed low adsorption. For example, an organic molecular cage synthesised by the Zhang group demonstrated a high selectivity of CO_2/N_2 of 73:1, but could adsorb only 0.2 mmol/g of CO_2.[37] The same group also reported the imine cages with a selectivity of CO_2/N_2 as high as 138:1. However, the CO_2 uptake was still low (0.33 mmol/g).[38] Even though materials showed high selectivity of CO_2 over N_2, the absolute CO_2 uptakes were lower than the networks synthesised here. An imine-based cage was also synthesised by the Cooper group, which showed higher CO_2 uptake (0.9 mmol/g) than the networks formed by the Zhang group, but a lower selectivity of only 11:1 was observed.[39] Comparing to our benzene/aniline networks with similar uptake, this cage showed a lower selectivity.

Compared to other similar types of materials measured the gas sorption and selectivity with the comparable conditions as our networks, data collected at the time when the project was done, such as porous organic cages (black)[37-40], MOFs (blue)[41-43] and MOPs (green)[12], the aniline/benzene networks (red) showed higher CO_2 uptake amongst materials that have high selectivity and higher selectivity among highly CO_2 uptake materials. (**Figure 3.11**)

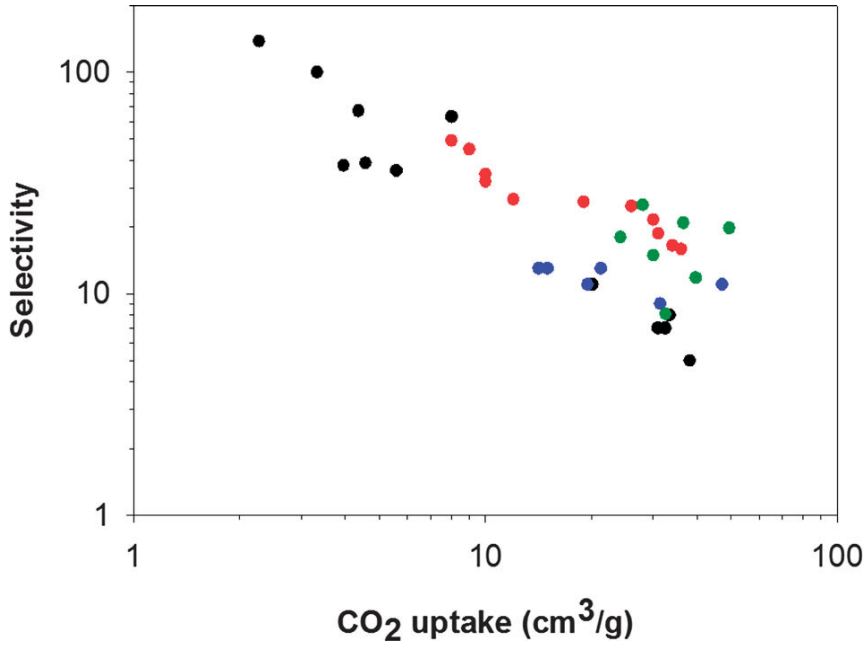

Figure 3.11 Plot of CO_2/N_2 selectivity against CO_2 uptakes of various kinds of polymers[34] including porous organic cages (black)[37-40], MOFs (blue)[41-43] and MOPs (green)[12], the aniline/benzene networks (red)

3.4 Conclusion

A series of benzene and aniline co-polymer networks were synthesised by using Friedel-Crafts reactions. The method was considered to be inexpensive compared to other approaches that use expensive Pd or Ni catalysts to synthesise such materials. The amorphous co-polymers demonstrated unique structures compared to their parent homopolymers indicating that the co-polymers formed were not only the admixture of the domains of two monomers.

The low surface area of the aniline network could be successfully improved by incorporation of benzene into the network using the co-polymerisation strategy. The surface areas increased with increasing of benzene component but in non-linear manner. This could also confirm the incorporation of two monomers in the networks, not only the admixture. The networks showed the highest CO_2 uptake up to 1.61 mmol/g at 300 K and 1 bar. With increasing of aniline ratio, the surface areas of the networks dropped more significantly than CO_2 uptakes leading to enhancing of CO_2/N_2 selectivity. The more aniline ratio in the networks, the higher selectivity was observed. The 100% aniline network was found to have highest CO_2/N_2 selectivity of 49.2:1. Comparing to similar materials, these co-polymers showed a trade-off between CO_2 uptakes and CO_2/N_2 selectivity.

Thus, this work demonstrated that the materials could be varied continuously by co-polymerisation. The structures and properties of the networks could be tuned. The benzene/aniline co-polymers could be tailored to improve the carbon dioxide capture and separation application.

3.5 References

1. S. Solomon, G.-K. Plattner, R. Knutti and P. Friedlingstein, *Proceedings of the National Academy of Sciences*, 2009, 106, 1704-1709.

2. D. M. D'Alessandro, B. Smit and J. R. Long, *Angewandte Chemie International Edition*, 2010, 49, 6058-6082.

3. R. Dawson, D. J. Adams and A. I. Cooper, *Chemical Science*, 2011, 2, 1173-1177.

4. T. C. Drage, C. E. Snape, L. A. Stevens, J. Wood, J. Wang, A. I. Cooper, R. Dawson, X. Guo, C. Satterley and R. Irons, *Journal of Materials Chemistry*, 2012, 22, 2815-2823.

5. G. Ferey, C. Serre, T. Devic, G. Maurin, H. Jobic, P. L. Llewellyn, G. De Weireld, A. Vimont, M. Daturi and J.-S. Chang, *Chemical Society Reviews*, 2011, 40, 550-562.

6. G. T. Rochelle, *Science*, 2009, 325, 1652-1654.

7. C.-H. Yu, C.-H. Huang and C.-S. Tan, *Aerosol and Air Quality Research*, 2012, 12, 745-769.

8. R. Dawson, A. I. Cooper and D. J. Adams, *Progress in Polymer Science*, 2012, 37, 530-563.

9. D. Yuan, W. Lu, D. Zhao and H.-C. Zhou, *Advanced Materials*, 2011, 23, 3723-3725.

10. J. M. Martín-Martínez, R. Torregrosa-Maciá and M. C. Mittelmeijer-Hazeleger, *Fuel*, 1995, 74, 111-114.

11. C. F. Martin, E. Stockel, R. Clowes, D. J. Adams, A. I. Cooper, J. J. Pis, F. Rubiera and C. Pevida, *Journal of Materials Chemistry*, 2011, 21, 5475-5483.

12. R. Dawson, E. Stockel, J. R. Holst, D. J. Adams and A. I. Cooper, *Energy & Environmental Science*, 2011, 4, 4239-4245.

13. W. Lu, J. P. Sculley, D. Yuan, R. Krishna, Z. Wei and H.-C. Zhou, *Angewandte Chemie International Edition*, 2012, 51, 7480-7484.

14. D. Y. Kim, H. M. Lee, S. K. Min, Y. Cho, I.-C. Hwang, K. Han, J. Y. Kim and K. S. Kim, *The Journal of Physical Chemistry Letters*, 2011, 2, 689-694.

15. M. R. Mello, D. Phanon, G. Q. Silveira, P. L. Llewellyn and C. M. Ronconi, *Microporous and Mesoporous Materials*, 2011, 143, 174-179.

16. T. M. McDonald, D. M. D'Alessandro, R. Krishna and J. R. Long, *Chemical Science*, 2011, 2, 2022-2028.

17. B. Li, R. Gong, W. Wang, X. Huang, W. Zhang, H. Li, C. Hu and B. Tan, *Macromolecules*, 2011, 44, 2410-2414.

18. J.-X. Jiang, F. Su, A. Trewin, C. D. Wood, N. L. Campbell, H. Niu, C. Dickinson, A. Y. Ganin, M. J. Rosseinsky, Y. Z. Khimyak and A. I. Cooper, *Angewandte Chemie*, 2007, 119, 8728-8732.

19. Y. Yuan, F. Sun, H. Ren, X. Jing, W. Wang, H. Ma, H. Zhao and G. Zhu, *Journal of Materials Chemistry*, 2011, 21, 13498-13502.

20. J. Schmidt, M. Werner and A. Thomas, *Macromolecules*, 2009, 42, 4426-4429.

21. T. Ben, H. Ren, S. Ma, D. Cao, J. Lan, X. Jing, W. Wang, J. Xu, F. Deng, J. M. Simmons, S. Qiu and G. Zhu, *Angewandte Chemie International Edition*, 2009, 48, 9457-9460.

22. M. Rueping and B. J. Nachtsheim, *Beilstein Journal of Organic Chemistry*, 2010, 6, 6.

23. Y. Cao, A. Andreatta, A. J. Heeger and P. Smith, *Polymer*, 1989, 30, 2305-2311.

24. A. Yasuda and T. Shimidzu, *Synthetic Metals*, 1993, 61, 239-245.

25. I. Y. Sapurina and M. A. Shishov, *Oxidative Polymerization of Aniline: Molecular Synthesis of Polyaniline and the Formation of Supramolecular Structures*, 2012.

26. A. Trewin, D. J. Willock and A. I. Cooper, *The Journal of Physical Chemistry C*, 2008, 112, 20549-20559.

27. J.-X. Jiang, F. Su, A. Trewin, C. D. Wood, H. Niu, J. T. A. Jones, Y. Z. Khimyak and A. I. Cooper, *Journal of the American Chemical Society*, 2008, 130, 7710-7720.

28. C. D. Wood, B. Tan, A. Trewin, H. Niu, D. Bradshaw, M. J. Rosseinsky, Y. Z. Khimyak, N. L. Campbell, R. Kirk, E. Stöckel and A. I. Cooper, *Chemistry of Materials*, 2007, 19, 2034-2048.

29. R. Dawson, L. A. Stevens, T. C. Drage, C. E. Snape, M. W. Smith, D. J. Adams and A. I. Cooper, *Journal of the American Chemical Society*, 2012, 134, 10741-10744.

30. Y. Luo, S. Zhang, Y. Ma, W. Wang and B. Tan, *Polymer Chemistry*, 2013, 4, 1126-1131.

31. M. Errahali, G. Gatti, L. Tei, G. Paul, G. A. Rolla, L. Canti, A. Fraccarollo, M. Cossi, A. Comotti, P. Sozzani and L. Marchese, *The Journal of Physical Chemistry C*, 2014, 118, 28699-28710.

32. G. Liu, Y. Wang, C. Shen, Z. Ju and D. Yuan, *Journal of Materials Chemistry A*, 2015, 3, 3051-3058.

33. V. Davankov and M. Tsyurupa, in *Comprehensive Analytical Chemistry*, eds. A. D. Vadim and P. T. Maria, Elsevier, 2011, vol. Volume 56, pp. 166-193.

34. R. Dawson, T. Ratvijitvech, M. Corker, A. Laybourn, Y. Z. Khimyak, A. I. Cooper and D. J. Adams, *Polymer Chemistry*, 2012, 3, 2034-2038.

35. A. L. Myers and J. M. Prausnitz, *AIChE Journal*, 1965, 11, 121-127.

36. A.-H. Lu and G.-P. Hao, *Annual Reports Section "A" (Inorganic Chemistry)*, 2013, 109, 484-503.

37. Y. Jin, B. A. Voss, R. D. Noble and W. Zhang, *Angewandte Chemie International Edition*, 2010, 49, 6348-6351.

38. Y. Jin, B. A. Voss, A. Jin, H. Long, R. D. Noble and W. Zhang, *Journal of the American Chemical Society*, 2011, 133, 6650-6658.

39. S. Jiang, J. Bacsa, X. Wu, J. T. A. Jones, R. Dawson, A. Trewin, D. J. Adams and A. I. Cooper, *Chemical Communications*, 2011, 47, 8919-8921.

40. T. Tozawa, J. T. A. Jones, S. I. Swamy, S. Jiang, D. J. Adams, S. Shakespeare, R. Clowes, D. Bradshaw, T. Hasell, S. Y. Chong, C. Tang, S. Thompson, J. Parker, A. Trewin, J. Bacsa, A. M. Z. Slawin, A. Steiner and A. I. Cooper, *Nat Mater*, 2009, 8, 973-978.

41. B. Wang, A. P. Cote, H. Furukawa, M. O/'Keeffe and O. M. Yaghi, *Nature*, 2008, 453, 207-211.

42. S. Surblé, F. Millange, C. Serre, T. Düren, M. Latroche, S. Bourrelly, P. L. Llewellyn and G. Férey, *Journal of the American Chemical Society*, 2006, 128, 14889-14896.

43. Y.-S. Bae, O. K. Farha, J. T. Hupp and R. Q. Snurr, *Journal of Materials Chemistry*, 2009, 19, 2131-2134.

Chapter 4

Hypercross-linked Polystyrenes

4. Hypercross-linked Polystyrenes

4.1 Introduction

The so-called "knitting method" is an effective and efficient method to construct porous networks.[1] A Friedel-Crafts reaction is used to cross-link rigid aromatic building blocks to form hypercross-linked polymers (HCPs). A number of aromatic monomers have been used, including benzene[1], toluene[1], carbazole[2], indoles[3] and thiophenes[4]. Tuning of the porosity and chemical properties of the networks is important for the design of these polymers for specific uses.[5-7] However, the limitation of the Friedel-Crafts reaction is generally unsuccessful if there is an electron-withdrawing group such as a carboxylic acid on the benzene ring.[8, 9] Carboxylic acid functional groups are useful in many applications, for example, to adjust the polarity of the networks for selective extractions.[10-12] As one example, a carboxylic acid functionalised CMP was shown to have a strong interaction with carbon dioxide as compared to polymer networks containing other functional groups.[13] It is also possible to transform carboxylic acids into esters, amides, etc. Hence, the incorporation of carboxylic acids into HCP networks, while retaining porosity, would be interesting and useful.

Generally, the Friedel-Crafts cross-linking of a phenyl ring substituted with a carboxylic acid or an ester was not successful even when an external cross-linker was used as described in **Section 4.2**. Jiang *et al.* used the hydroxyl group to help in Friedel-Crafts reaction of a carboxylic acid functionalised building block, but a low surface area polymer, with a BET surface area of only 20 m^2/g, was obtained.[9] Using the benzene-based monomer with a carboxylic acid further away from the ring (3-phenylpropionic acid) was also found to help the network formation but again a low surface area polymer was formed (**Section 4.2**). Thus, we hypothesised that the extension of aromatic rings might improve the surface areas of carboxylic acid functionalised network. However, the balance between the proportion of functional groups in the networks has to be considered. Cross-linked carboxylic acid functionalised oligostyrenes and polystyrenes with different number of styrene units were therefore investigated.

Hypercross-linking of polystyrene was pioneered by Davankov *et al.*[14] The hypercross-linked polystyrenes were prepared by cross-linking the polystyrene chains with the large amount of rigid bridging spacers. These networks were modified and used in many applications, including separation[15-17] as well as gas storage[18, 19] and catalysis.[20] It is also possible to hypercross-link polystyrene films (M_w *ca.* 15,900 Da) to form porous membranes.[21] Many researchers have focused on varying synthetic conditions, such as the degree of cross-linking, and the resulting effect on the surface areas of the polymers.[22-27] Recently, Vinodh *et al.* demonstrated the synthesis and detailed characterisation of hypercross-linked polystyrene without the use of an external cross-linker, leading to networks with surface area of 224 m^2/g.[28] Previously, surface areas were found to be independent of the linear polystyrene molecular weight for polymers ranging from 8.8×10^3 to 3×10^6 Da.[29] However, to the best of our knowledge, hypercross-linking of low molecular weight linear polystyrene has not been examined. Recently, Zhang *et al.* have showed the influence of molecular weight of linear poly-*p*-phenylenes on the porosity properties of the networks after cross-linking.[30] The surface areas and pore volumes were found to first rise and then fall again as the molecular weight was increased.

To prepare the linear polystyrene with carboxylic functional groups, reversible addition-fragmentation chain transfer (RAFT) polymerisation was used. RAFT polymerisation is one of the most effective ways to synthesise polymers with well-defined functional structures and molecular weights.[31] RAFT polymerisation is a versatile technique because of the compatibility to wide range vinyl monomers and synthetic conditions such as temperature and solvents.[32] Controlled molecular weight and low polydispersity polymers can be obtained using living polymerisation concept.[33] By using additives that could reversibly react with chain carriers, chains are kept in an inert (dormant) form, which is inactive to propagation or termination. Only a small amount of active species would be released for chain growth at any one time. Therefore, as long as the conversion rate between the active and dormant forms is rapid, chains are able to continuously grow in the same rate without termination. RAFT polymerisation used certain chain transfer agents, i.e. RAFT agents, as additives through the reversible chain transfer mechanism where the propagation species is in equilibrium with dormant species as shown in **Scheme 4.1**.[34]

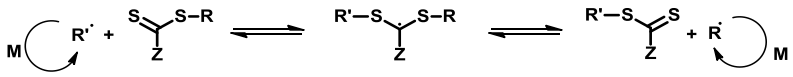

Scheme 4.1 Mechanism of RAFT polymerization. M refers to the monomer, R' and R refers to the propagating chains and the leaving group in RAFT agent, and Z refers to the modified group in RAFT agent which controls the addition and fragmentation rate. Z is generally alkyl, aryl, S-alkyl, O-alkyl or aryl, or N-alkyl or aryl.[35]

In this chapter, we firstly investigated the cross-linking reactions of a phenyl ring substituted with a carboxylic acid or esters. Then we examined the "knitting" of a series of linear polystyrenes, synthesised by RAFT polymerisation.[32] By using carboxylic acid containing RAFT agents, linear polystyrenes with pendant carboxylic acids were obtained. After cross-linking by the Friedel-Crafts reaction (**Scheme 4.2**), we investigated the effect of the presence of the carboxylic acid and the degree of polymerisation (DP) of the polymer on the porosity properties of resulting networks.

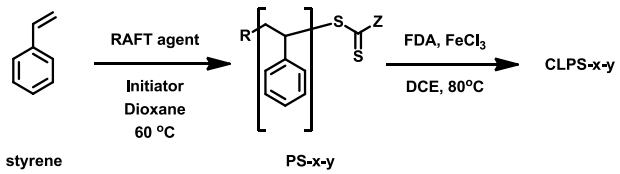

Scheme 4.2 Summary scheme of cross-linked polystyrenes synthesis

4.2 Cross-linking of carboxylic acid functionalised compounds

Cross-linking of benzoic acid (**Figure 4.1a**) using FDA in the present of $FeCl_3$ in DCE was carried out. No solid was formed after stirring the reaction at 80 ^{o}C overnight. We interpret this as there being no cross-linking, as we would expect to form an insoluble solid. We also tried to cross-link benzoic acid ester derivatives, methyl (**Figure 4.1b**) and butyl benzoate (**Figure 4.1c**), but again no

solid was obtained. This showed that the carboxylic acid and esters on the benzene rings inhibited the Friedel-Crafts alkylation reaction with the cross-linker, FDA.[8, 9]

3-Phenylpropionic acid (**Figure 4.1d**), where the carboxylic acid was further away from the benzene ring, was found to be able to undergo Friedel-Crafts reaction using FDA as external cross-linker to form the black solid in a good yield (107 %). Yields higher than 100%, which were generally observed in this kind of materials[36-41], could be due to trapped catalyst, solvent, water or air within the pores[40, 42]. However, the network was found to have a very low porosity (SA_{BET} 15 m^2/g).

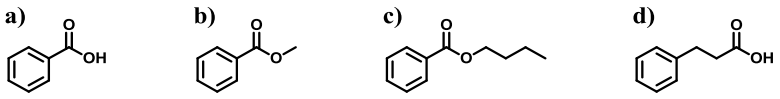

Figure 4.1 Structures of compounds used to try a directly prepare a cross-linked polymer containing a carboxylic acid or an ester. From left to right: benzoic acid, methyl benzoate, butyl benzoate and 3-phenylpropionic acid

The increase of the ratio of the benzene rings to the carboxylic acid group was expected to help in surface area improvement of carboxylic acid functionalised network. As the balance proportions of functional groups to non-functionalised aromatic part had to be considered, cross-linked carboxylic acid functionalised polystyrenes with different number of styrene units were studied.

4.3 Styrene units variation

A series of linear polystyrenes with different molecular weights containing carboxylic acid functional groups (**PS-1-ys**) were synthesised by RAFT polymerisation[43], using the RAFT agent containing a carboxylic acid, 4-cyano-4-[(dodecylsulfanylthiocarbonyl)sulfanyl]pentanoic acid (CDDPA; **RAFT-1**) shown in **Figure 4.2** with styrene and 4,4′-azobis(4-cyanovaleric acid) (ACVA) as initiator in dioxane at 60 ^oC. The linear polystyrenes in this chapter were named **PS-x-y**, with x

referring to the RAFT agent used, and y referring to the sample number. As **RAFT-1** was used in this Section, thus, the samples are called **PS-1-y**. (**Scheme 4.2**)

Figure 4.2 RAFT-1 (left) and ACVA (right) structure

The reaction was monitored by ^{1}H NMR. The reactions were stopped when around 80-95 % conversions were observed. The reactions were cooled down, concentrated and precipitated in water for **PS-1-1** and **PS-1-2**, in MeOH for **PS-1-3** and **PS-1-4**, and in EtOH for **PS-1-5** to **PS-1-10**. The **PS-1-ys** were obtained as pale yellow to yellow solids in 40-85 % yields. The colour of **PS-1-ys** was found to have a stronger yellow colour at lower molecular weights.

The ^{1}H NMR spectrum (**Figure 4.3**) showed the presence of the aromatic peaks at 6.30-7.30 ppm corresponding to the repeating styrene units (k). The peaks for RAFT agent part was observed at 0.80-3.50 ppm. There were the peaks of methylene next to thiocarbonate group at 3.25 ppm (c), methyl peak at 0.88 ppm (a) and at 2.17 ppm (d) corresponding to the RAFT agent. The broad peaks at 0.9-2.4 ppm were assigned as the proton of styrene backbone (h, i, j) and RAFT agent (b, e, f). The proton of the styrene backbone next to the thiocarbonate group (g) appeared at 4.62-5.07 ppm. The ratio of aromatic to RAFT agent peaks increased with increasing of the molecular weight. No styrene monomer was detected after the polymers were purified by precipitation as indicated by the disappearance of the vinyl proton peaks at 5.27 and 5.83 ppm.

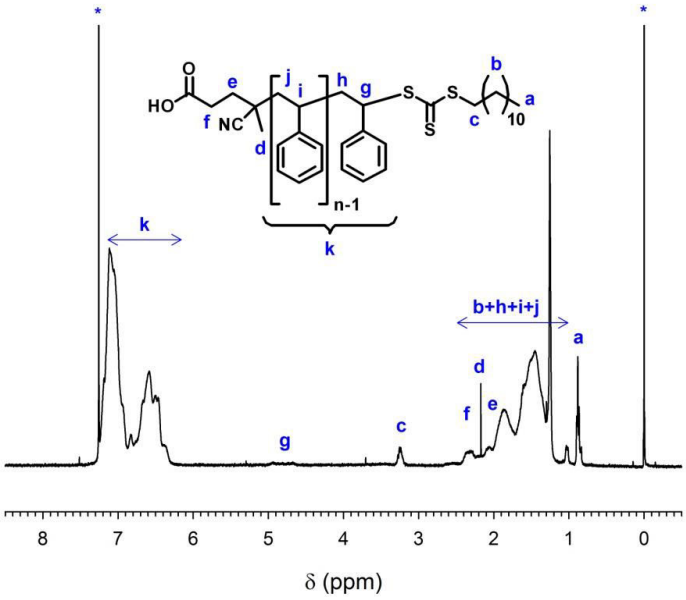

Figure 4.3 ^{1}H-NMR spectrum and assignment of **PS-1-7**. The peaks marked with a * indicate the solvent peaks.

As expected, elemental analysis illustrated the reduction of sulphur (S) and nitrogen (N) contents as the number of styrene units increased. (**Table 4.1**) The presence of C≡N peak at 2233 cm^{-1} and C=O peak at 1709 cm^{-1} in IR spectrum showed the presence of the expected RAFT agent end group. The peaks of aromatic C=C at 1601, 1493 and 1453 cm^{-1} indicated the incorporation of styrene units as well as the monosubstituted benzene peaks at 759 and 697 cm^{-1}. As the higher molecular weight of linear polystyrene, the intensity of C≡N (2233 cm^{-1}) and C=O (1709 cm^{-1}) peaks were suppressed while intensity of aromatic peaks (1400-1600 cm^{-1}) were enhanced. (**Figure 4.4**)

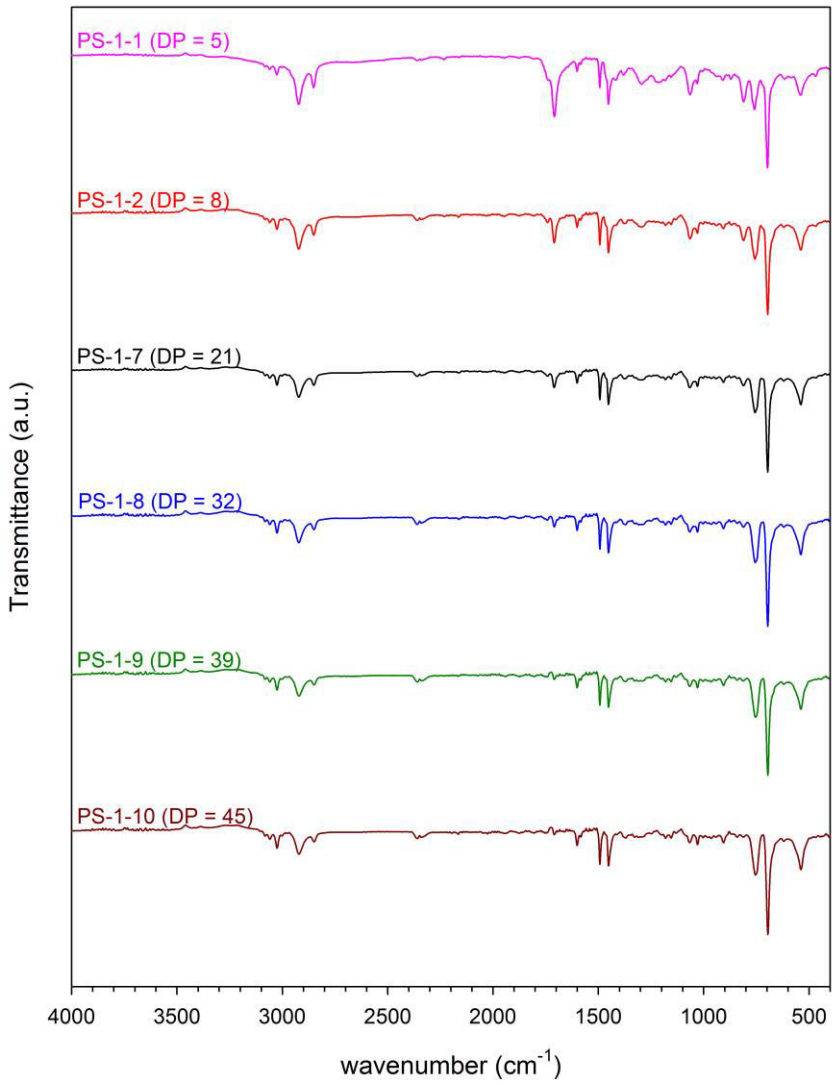

Figure 4.4 IR spectra of **PS-1-y** with different number of styrene units

The DP was measured by gel permeation chromatography (GPC), which is widely used to estimate the molecular weight of polymers. GPC data showed that all polymers had narrow molecular weight distributions, with a polydispersity index (PDI) of less than 1.2. The DP, i.e. numbers of the styrene repeating units in the polymers, could be calculated from the molecular weight (M_n). (**Table 4.1**)

Table 4.1 Yields, elemental analysis and GPC data of linear polystyrenes (**PS-1-ys**)

Sample	%Yield	%N	%S	M_w	M_n	PDI	Styrene units (DP)
PS-1-1	78	2.81	9.42	1060	950	1.12	5
PS-1-2	74	1.18	7.23	1,350	1,220	1.11	8
PS-1-3	84	1.16	5.82	1,670	1,490	1.12	10
PS-1-4	57	0.84	5.30	1,790	1,680	1.07	12
PS-1-5	64	0.84	4.81	2,200	2,060	1.07	16
PS-1-6	87	0.79	3.58	2,320	1,960	1.18	15
PS-1-7	40	0.57	3.17	2,780	2,610	1.07	21
PS-1-8	73	0.37	1.82	4,140	3,740	1.11	32
PS-1-9	69	0.30	1.51	5,090	4,520	1.13	39
PS-1-10	67	0.27	1.21	5,700	5,040	1.13	45

The **PS-1-y** were cross-linked with FDA using a Friedel-Crafts catalysed reaction using $FeCl_3$ at 80 ^oC overnight (**Scheme 4.2**).[1] The product was purified by Soxhlet extraction to remove the monomer and catalyst residues providing a series of **CLPS-1-y** as brown solids in yields of 81-107 % (**Table 4.2**).

Table 4.2 Yields, elemental analysis and gas sorption data of the cross-linked linear polystyrenes (**CLPS-1-y**)

Sample	%Yield	%N	%S	SA_{BET} (m^2/g)	CO_2 uptakes (mmol/g)	
					273 K	298 K
CLPS-1-1	81	2.25	4.51	9	0.73	0.45
CLPS-1-2	90	0.90	2.88	27	1.21	0.78
CLPS-1-3	92	0.83	2.48	222	1.51	0.92
CLPS-1-4	97	0.66	2.53	366	1.29	0.81
CLPS-1-5	90	0.70	2.29	502	1.60	0.91
CLPS-1-6	102	0.53	1.27	658	1.77	1.05
CLPS-1-7	99	0.46	1.50	767	1.87	1.13
CLPS-1-8	107	0.25	0.62	862	2.04	1.20
CLPS-1-9	104	0.21	0.57	898	2.06	1.22
CLPS-1-10	100	0.17	0.44	974	2.17	1.30

Elemental analysis (**Table 4.2**) of cross-linked polymers showed the decrease of both S and N content as the number of styrene units in the **PS-1-y** increased as expected. This decrease corresponded to that for the **PS-1-y**. The discrepancy between theory and analysis of elemental contents is typical for this kind of materials.[7, 40, 41, 44] Again, common explanations include trapped catalyst in the networks, the unreacted end of cross-linkers, or the adsorption of gases and water in the porous structures.[45]

IR spectra (**Figure 4.5**) illustrated the decrease in the intensity of the peaks due to the monosubstituted benzene at about 760 and 700 cm^{-1} after polymerisation, indicating the successful of cross-linking. The peak at 1734 cm^{-1} showed that the carbonyl group could survive the polymerisation process. Davankov quoted that identification of carbonyl group in hypercross-linked polymers could be a problem as it could overlap with benzene-ring peak which showed the absorbance around 1700 cm^{-1} as shown in many hypercross-linked polystyrenes.[45] Comparing to the cross-linked polystyrene without carboxylic acid group (**Figure 4.22**), the peak at 1734 cm^{-1} was not present in such a network. However, the wavenumber seemed to be relatively high for carboxylic acid carbonyl peak.

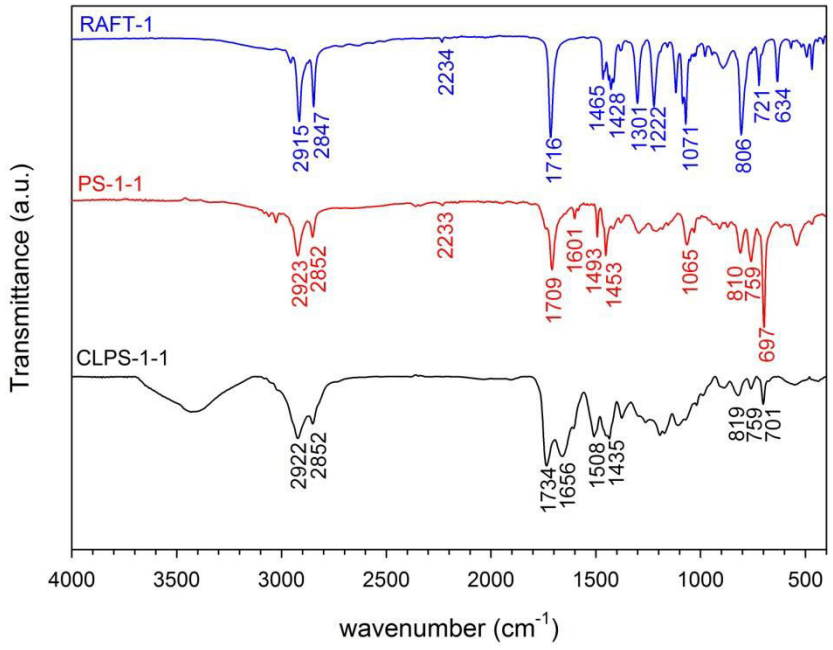

Figure 4.5 IR spectrum of **CLPS-1-1**, compared to that of **PS-1-1** and **RAFT-1**

The reaction of the RAFT agent alone with FDA and $FeCl_3$ in DCE was also investigated. The carbon peak in ^{13}C NMR at 172 ppm comparing to 176 ppm of carboxylic acid in RAFT agent as well as the presence of the methoxy peak at 52 ppm in ^{13}C NMR and at 3.70 ppm in ^{1}H NMR suggested the ester could be formed during the reaction.[46] The IR spectrum of the product after the reaction was shown in **Figure 4.6**. The C=O peak at 1735 and 1667 cm^{-1} was also observed comparing to carboxylic acid C=O band of the **RAFT-1** before reaction at 1716 cm^{-1} (**Figure 4.5**) indicating the formation of ester and carboxylate.

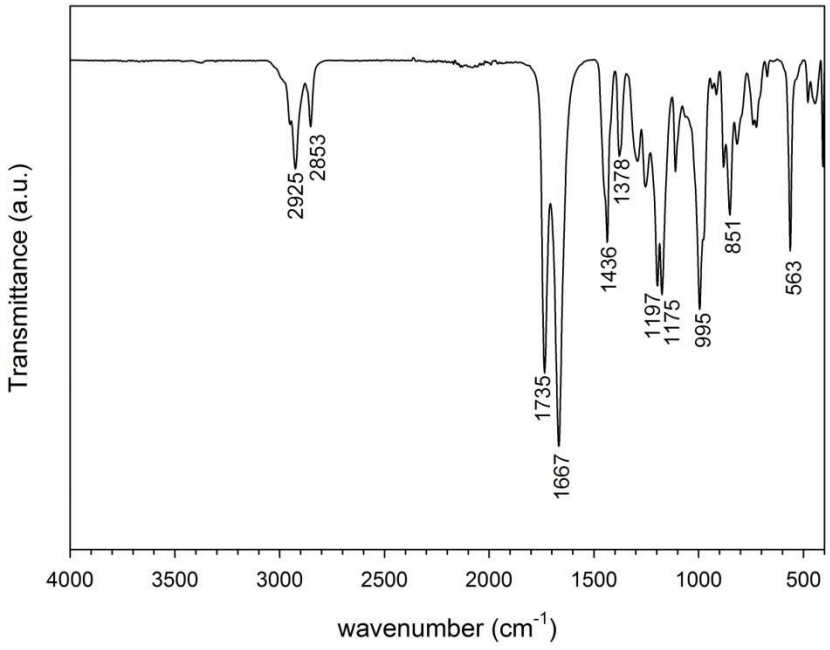

Figure 4.6 IR spectrum of **RAFT-1** after Friedel-Crafts reaction

For simplicity, the reaction of decanoic acid with FDA and $FeCl_3$ in DCE was also investigated. The product obtained after the reaction was the methyl ester product. ^{1}H NMR exhibited the methoxy proton at 3.66 ppm. ^{13}C NMR also showed the methoxy carbon at 51 ppm as well as the carbonyl peak at 174 ppm. IR spectrum (**Figure 4.7**) illustrated the carbonyl ester peak at 1740 cm^{-1}. Therefore, it unfortunately appeared that the carboxylic acid might not survive the knitting process.

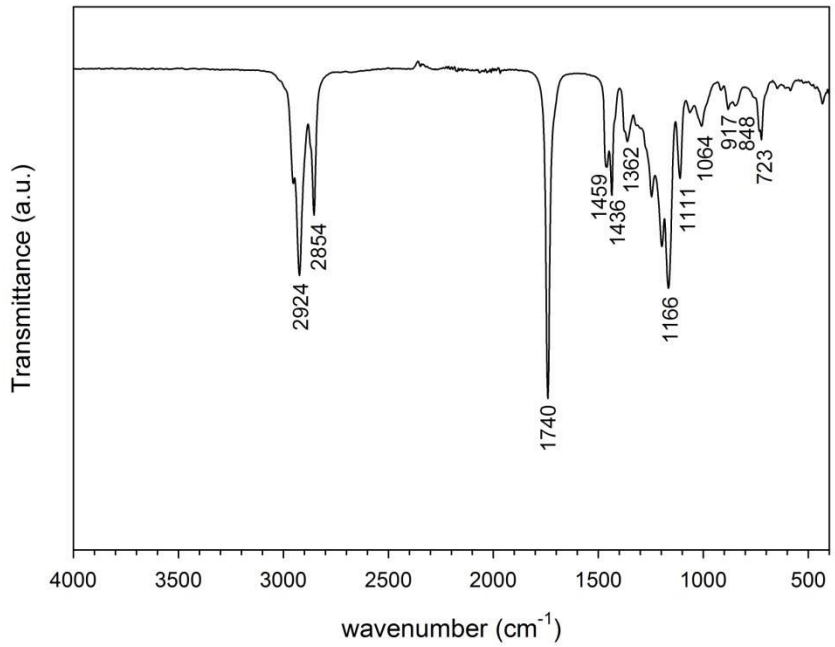

Figure 4.7 IR spectrum of the product after Friedel-Crafts reaction of decanoic acid

The effect of the number of styrene units in the **CLPS-1-y** on the surface areas of the final polymers was studied. The porosity properties were measured by nitrogen sorption at 77 K using Micromeritrics ASAP 2420. Nitrogen isotherms of the **CLPS-1-y** are shown in **Figure 4.8**. The networks could adsorb more nitrogen when higher DP polystyrene (**PS-1-y**) was used.

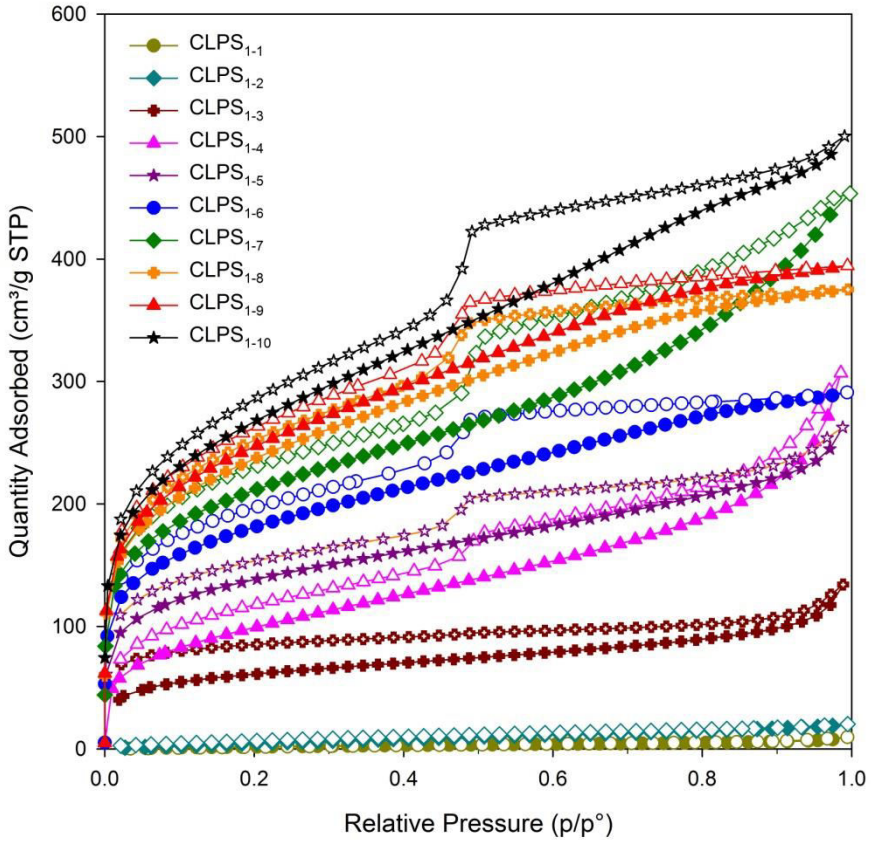

Figure 4.8 Nitrogen adsorption (close symbols) and desorption (open symbols) isotherms of the **CLPS-1-y**

Surface areas were calculated using BET theory. As the number of styrene units of the **PS-1-y** increased, the surface areas increased (**Table 4.2**). Linear polystyrenes with a DP of 5 and 8 provided essentially non-porous networks when cross-linked. The surface areas increased readily from 222 m^2/g to 767 m^2/g when cross-linking linear polystyrenes with DPs from 10 to 21 were used. A slight increase of surface areas was observed for higher molecular weight polystyrenes above DP of 32. Further investigation on hypercross-linked commercial polystyrenes with molecular weight of 35K, 100K, and 230K (approximate DP of 336, 960 and 2208), provided networks with surface areas of 865, 1035 and 856 m^2/g, respectively, exhibited no significant change from that of **CLPS-1-10**. (**Figure 4.9**) This could imply that the surface areas of cross-linked polystyrenes did not depend

on the molecular weight of the linear polymers for the networks with DP higher than around 30 which is in agreement with the work of Davankov *et al*.[29]

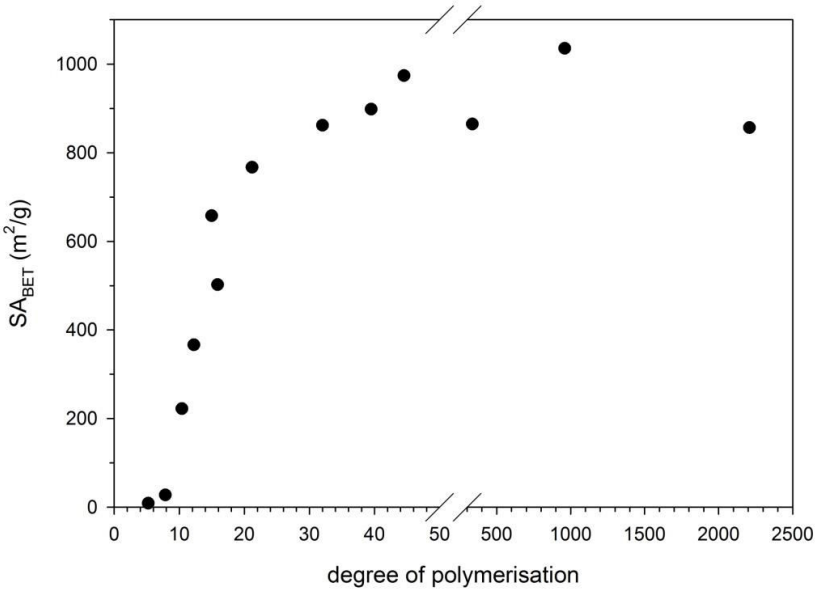

Figure 4.9 Surface areas of **CLPS-1-ys** synthesised from different DP of linear polystyrenes

Vinodh *et al.* claimed that the hypercross-linked polystyrene might be a good candidate for a CO_2 adsorbent because of its cheap synthesis and good CO_2 uptakes.[28] Similar to nitrogen adsorption, CO_2 uptakes increased when the higher molecular weights of linear polystyrenes were used. (**Figure 4.10**) Interestingly, the hypercross-linked commercial polystyrenes with molecular weight of 35K, 100K, and 230K, which showed higher surface areas, exhibited lower CO_2 adsorption of 0.15, 0.97 and 0.86 mmol/g at room temperature. This could be due to the RAFT agent end group in the networks which help in improving the CO_2 uptakes. Heteroatoms such as S or N and carboxylic acid functional group were calculated to have interaction with CO_2 leading to better adsorption than non-functionalised benzene.[47] CMP networks functionalised with carboxylic acids showed the highest CO_2 heat of adsorption compared to other functional groups as reported by Dawson *et al*.[13] Heterocyclic HCPs also showed higher CO_2 adsorption than many of porous networks with the similar surface areas and are also comparable with ultrahigh surface area network like PAF-1.[3]

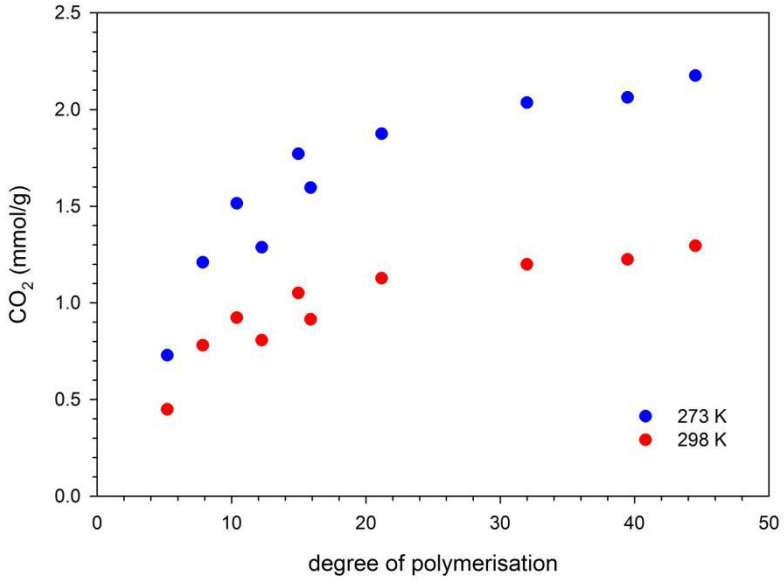

Figure 4.10 CO_2 uptakes of the **CLPS-1-y** synthesised from different DP of linear polystyrenes

4.4 RAFT agent variation

The effect of RAFT agent end group to the properties of the networks was studied. Two different RAFT agents containing a carboxylic acid, i.e. 4-cyano-4-(phenylcarbonothioylthio)pentanoic acid (CPCPA; **RAFT-2**) which had phenyl ring instead of long carbon chain and 2-(dodecylthiocarbonothioylthio)-2-methylpropionic acid (DDMAT; **RAFT-3**) which had shorter carbon chain between thioester and carboxylic acid group as well as methyl group instead of nitrile group, were used in polystyrene synthesis to compare with **RAFT-1**. The structures are shown in **Figure 4.11**.

Figure 4.11 RAFT-2 (left) and **RAFT-3** (right) structures

Another two RAFT agents without a carboxylic acid were also used to study the effect of carboxylic acid group. 2-Cyano-2-propyl dodecyl trithiocarbonate (CPDT; **RAFT-4**) and 2-cyano-2-propyl benzodithioate (CPBT; **RAFT-5**) were analogues of respective **RAFT-1** and **RAFT-2,** where the carboxylic acid was replaced by a methyl group. The structures are shown in **Figure 4.12**.

Figure 4.12 RAFT-4 (left) and **RAFT-5** (right)

Polystyrenes were synthesised using all the RAFT agents to obtain **PS-2-y** to **PS-5-y** respectively with two different target degrees of polymerisations ca. 10 and 20 styrene units.[43] These DP were used as these results in a significant difference in the final surface areas in the **CLPS-1-y** after cross-linking as shown in previous section. Again, the linear polystyrenes were named **PS-x-y**, with x referring to the RAFT agent used, and y referring to the sample number. For **RAFT-2** to **5**, y is 1 for the linear polystyrene with DP c.a. 10, 2 for the polystyrene with DP c.a. 20 and 3 for the networks synthesised by using azobisisobutyronitrile (AIBN) as an initiator instead of ACVA. AIBN was used here because it contains no carboxylic acid so it could be used to synthesise control materials without this functional group. This will be explained in detail later in this chapter.

PS-2 to **5** were successfully synthesised with approximated target styrene units. The **PS-3-y** and **PS-4-y** were yellow solids formed in 80-90 % conversion. However, **PS-2** and **PS-5** were polymerised at a slower rate. The radical fragmentation rate of **RAFT-2** and **RAFT-5** is known to be lower than **RAFT-1**, **RAFT-3**, and **RAFT-4**.[34, 35] After 90 hours, only up to 50 % conversion could be obtained. Therefore, higher amount of styrene monomer was used in polymerisation reactions to provide the linear polystyrenes with the target styrene units. The **PS-2-y** and **PS-5-y** were pink followed the colour of the reddish RAFT agents used with 50-60 % conversion. The colour of the polymers was paler at a higher DP. Again, the molecular weights and number of styrene units were estimated from GPC data

shown in **Table 4.3**. Narrow PDI of less than 1.2 were obtained for all of the polymers.

Table 4.3 Yields, elemental analysis and GPC data of the linear polystyrenes with different RAFT agents (**PS-x-ys**)

Sample	%Yield	%N	%S	M_w	M_n	PDI	Styrene units (DP)
PS-2-1	75	1.50	4.76	1,460	1,180	1.24	9
PS-2-2	23	0.55	1.77	3,280	2,940	1.11	26
PS-3-1	76	0.61	7.07	1,350	1,140	1.18	7
PS-3-2	48	0.20	3.21	2,790	2,500	1.11	21
PS-4-1	41	1.63	8.32	1,200	1,000	1.20	6
PS-4-2	59	0.72	4.01	2,350	2,170	1.08	18
PS-4-3	32	1.60	9.46	1,170	980	1.20	7
PS-5-1	61	1.50	5.40	1,200	1,030	1.16	8
PS-5-2	33	0.67	2.60	2,440	2,210	1.10	19
PS-5-3	37	0.62	2.49	2,690	2,500	1.08	21

The linear polystyrenes were characterised by ^{1}H NMR and IR spectroscopy. Elemental contents were indicated by elemental analysis. N and S contents were shown in **Table 4.3**. The polystyrenes with higher DP showed lower N and S contents. Unexpected N contents in the **PS-3-y** could be attributed to the incorporation of an initiator (ACVA) containing -CN functional group (**Figure 4.2**). The amount of ACVA end group incorporated in the polymers was calculated by using N and S content in elemental analysis as 60 % for **PS-3-1** and 43 % for **PS-3-2**.

^{1}H NMR spectra showed the presence of the aromatic peaks at 6.30-7.30 ppm corresponding to the repeating styrene units (k). For the **PS-3-y** (**Figure 4.14**) and the **PS-4-y** (**Figure 4.15**), the peaks for RAFT agent part were observed at 0.80-3.50 ppm. The methylene next to thiocarbonate group showed the peaks at about 3.25 ppm (c). For the **PS-2-y** (**Figure 4.13**) and the **PS-5-y** (**Figure 4.16**), the peaks for RAFT agents were appeared at around 7.31 (b), 7.47 (a) and 7.83 (c) ppm represented the aromatic ring in RAFT agents. The broad peaks at 0.9-2.4 ppm could be assigned as the proton of styrene backbone (h, i, j) and carbon linear chain in

RAFT agents. The proton of the styrene backbone next to the thiocarbonate group (g) appeared at 4.62-5.07 ppm. The ratio of aromatic to RAFT agent peaks increased with increasing of the molecular weight. No styrene monomer was detected after the polymers were purified by precipitation as indicated by the disappearance of the vinyl proton peaks at 5.27 and 5.83 ppm.

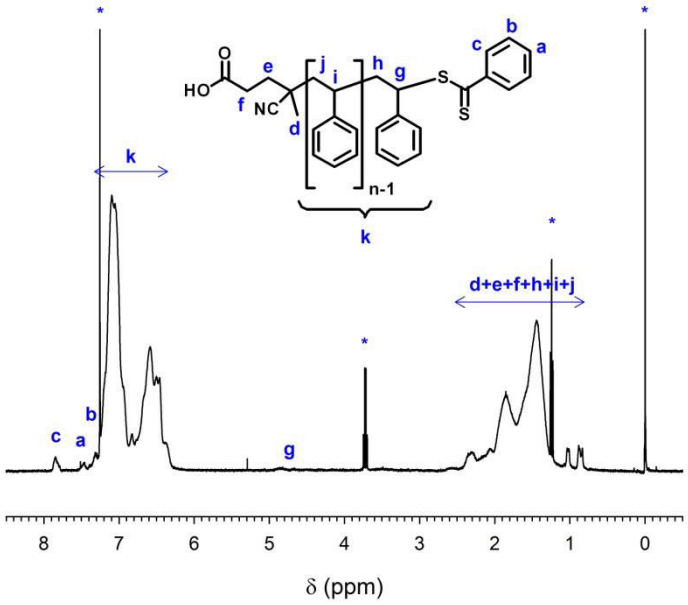

Figure 4.13 ^{1}H-NMR spectrum and assignment of **PS-2-2**. The peaks marked with a * indicate the solvent peaks.

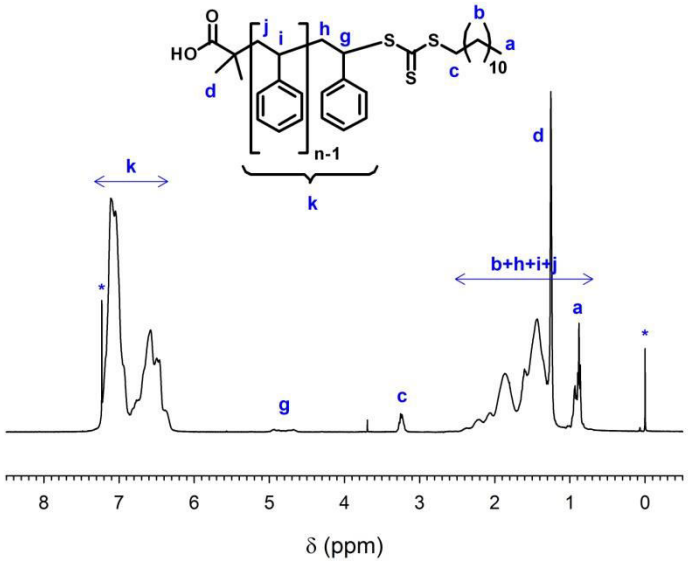

Figure 4.14 ^{1}H-NMR spectrum and assignment of **PS-3-2**. The peaks marked with a * indicate the solvent peaks.

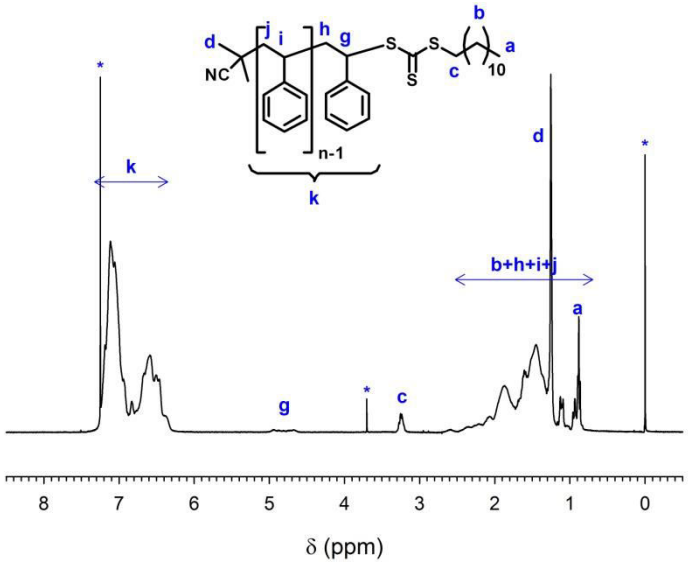

Figure 4.15 ^{1}H-NMR spectrum and assignment of **PS-4-2**. The peaks marked with a * indicate the solvent peaks.

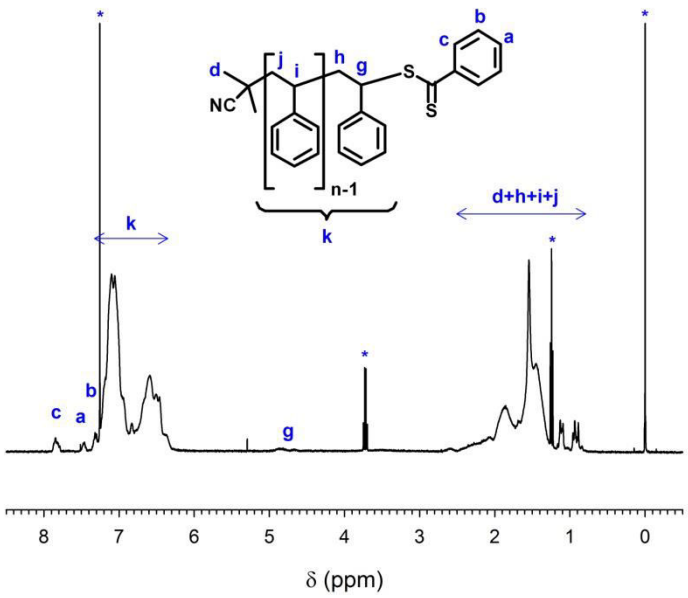

Figure 4.16 ^{1}H-NMR spectrum and assignment of **PS-5-2**. The peaks marked with a * indicate the solvent peaks.

IR spectra of the **PS-2-y** (**Figure 4.17**), the **PS-3-y** (**Figure 4.18**), the **PS-4-y** (**Figure 4.19**), and the **PS-5-y** (**Figure 4.20**) demonstrated the peaks of aromatic C=C at around 1600, 1490 and 1450 cm^{-1} as well as the monosubstituted benzene peaks at around 760 and 700 cm^{-1} indicated the incorporation of styrene units. The presence of C≡N peak at about 2230 cm^{-1} in the spectra of the **PS-2-y**, the **PS-4-y**, and the **PS-5-y** spectra as well as C=O peak at about 1700 cm^{-1} in the spectra of the **PS-2-y** and the **PS-3-y** confirmed the presence of the expected RAFT agent end groups. Similar to the **PS-1-y**, the higher the molecular weight of linear polystyrene, the higher intensity of aromatic peaks (1400-1600 cm^{-1}) was observed.

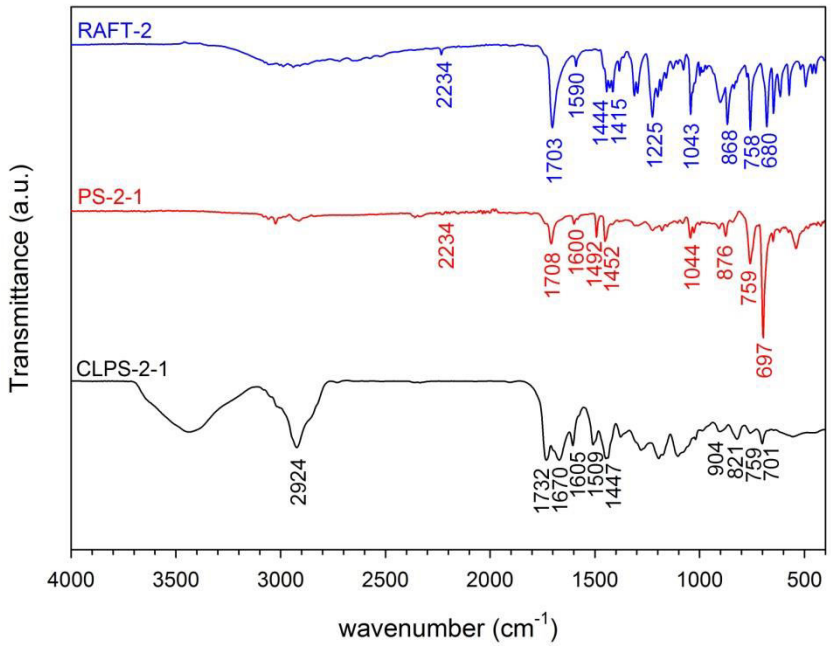

Figure 4.17 IR spectrum of **CLPS-2-1**, compared to that of **PS-2-1** and **RAFT-2**

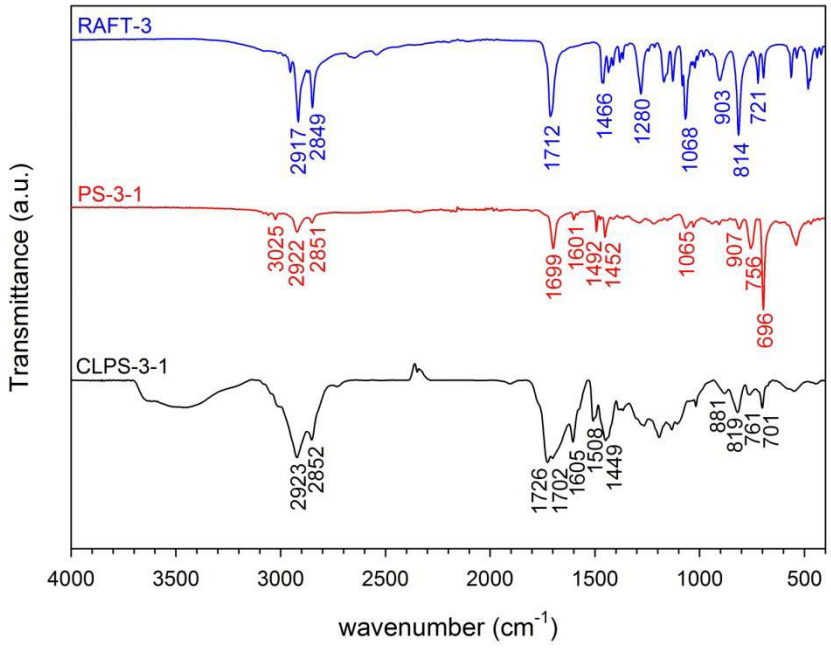

Figure 4.18 IR spectrum of **CLPS-3-1**, compared to that of **PS-3-1** and **RAFT-3**

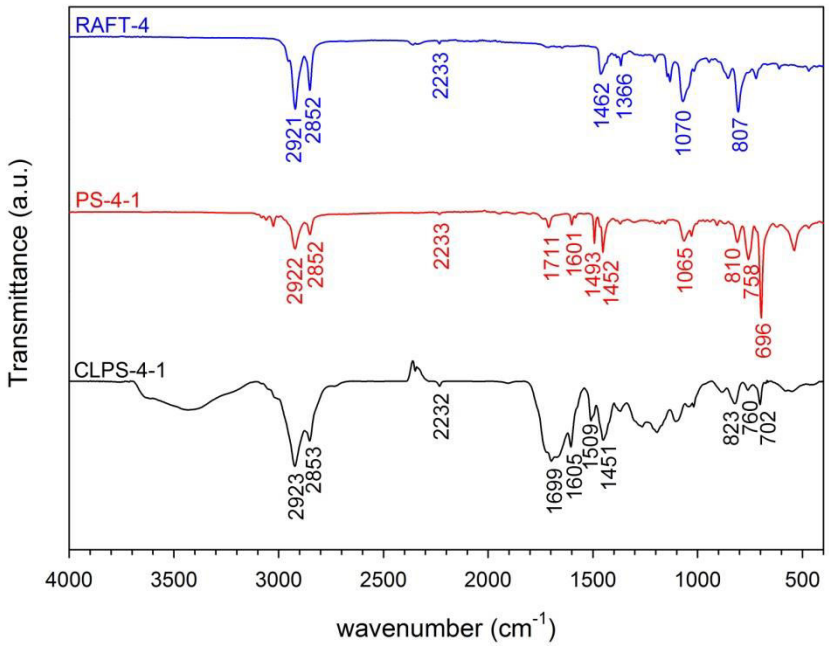

Figure 4.19 IR spectrum of **CLPS-4-1**, compared to that of **PS-4-1** and **RAFT-4**

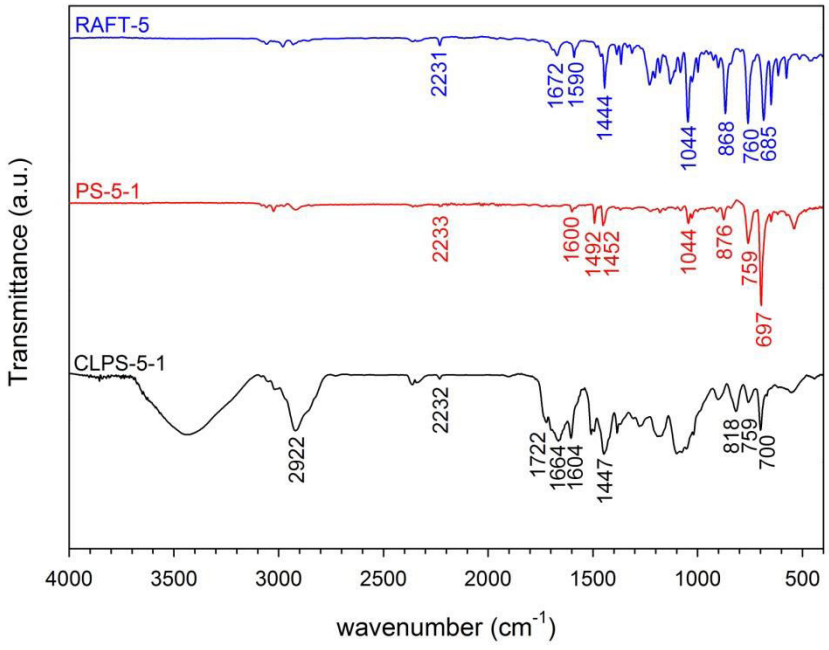

Figure 4.20 IR spectrum of **CLPS-5-1**, compared to that of **PS-5-1** and **RAFT-5**

However, a C=O band was also present in **PS-4** (**Figure 4.19**) even though **RAFT-4** does not formally contain a C=O group and no such peak was present in the IR spectrum of **RAFT-4**. This could result from carboxylic acid containing initiator ACVA which was used as an initiator in the RAFT polymerisation. Therefore, AIBN was used as an initiator since it contains no carboxylic acid group instead of ACVA providing **PS-4-3**. (**Scheme 4.2**) The structure of AIBN was shown in **Figure 4.21**.

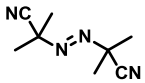

Figure 4.21 AIBN structure

The IR spectrum of **PS-4-3** (**Figure 4.22**) did not show the C=O peak. Therefore, the polymer without a carboxylic acid could be prepared to study the effect of carboxylic acid on the properties of the networks after cross-linking. AIBN was also used with **RAFT-5** to obtain **PS-5-3**, with the IR spectrum shown in **Figure 4.23**.

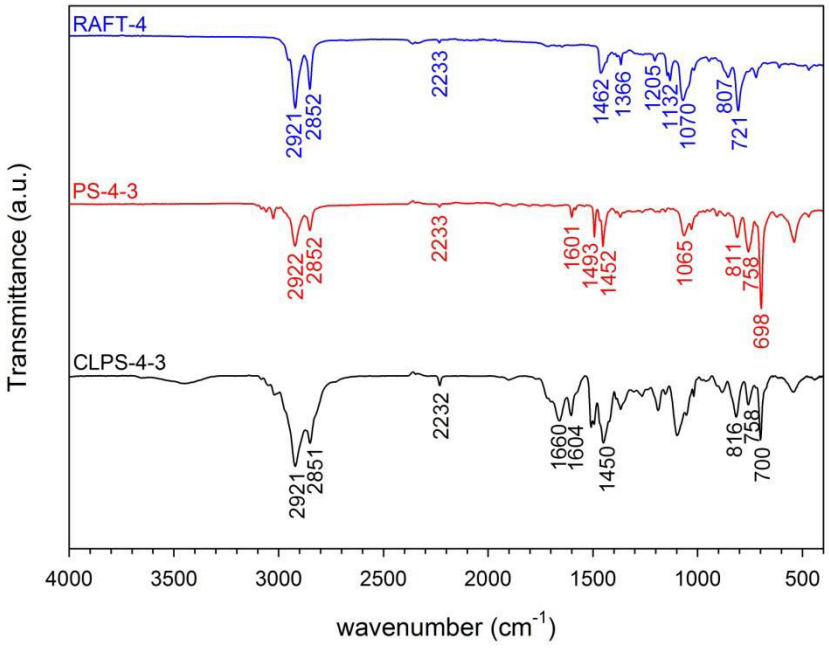

Figure 4.22 IR spectrum of **CLPS-4-3**, compared to that of **PS-4-3** and **RAFT-4**

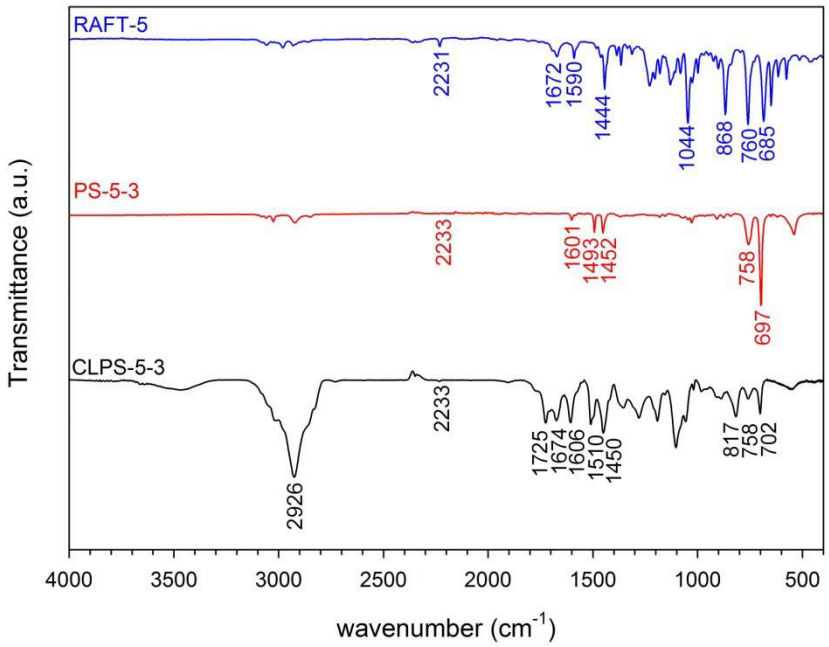

Figure 4.23 IR spectrum of **CLPS-5-3**, compared to that of **PS-5-3** and **RAFT-5**

Cross-linking **PS-x-y** with FDA by Friedel-Crafts reaction formed the corresponding **CLPS-x-y** as brown solids with high yields (70 - 100 % yield).[1] The summary data of the networks was shown in **Table 4.4**.

The surface areas were measured. No significant differences in surface areas were obtained when polymers with similar degrees of polymerisation were used. Networks with a DP of around 10 were found to be non-porous, whilst MOPs with surface areas of over 600 m^2/g were obtained by cross-linking polystyrene with DP of around 20. (**Figure 4.24**)

Table 4.4 Yields, elemental analysis and gas sorption data of the cross-linked polystyrenes with different RAFT agent (**CLPS-x-ys**)

Sample	%Yield	%N	%S	SA_{BET} (m^2/g)	CO_2 uptakes (mmol/g)	
					273 K	298 K
CLPS-2-1	90	1.08	3.20	59	1.44	0.90
CLPS-2-2	98	0.37	1.25	869	2.10	1.28
CLPS-3-1	93	0.40	3.72	9	1.13	0.70
CLPS-3-2	91	0.16	1.50	774	1.78	1.06
CLPS-4-1	94	1.32	4.23	12	1.05	0.66
CLPS-4-2	92	0.53	2.17	643	1.67	0.99
CLPS-4-3	89	1.48	4.41	44	0.91	0.59
CLPS-5-1	70	1.19	3.61	8	1.65	1.02
CLPS-5-2	94	0.50	1.36	879	2.18	1.29
CLPS-5-3	100	0.47	1.33	886	2.14	1.27

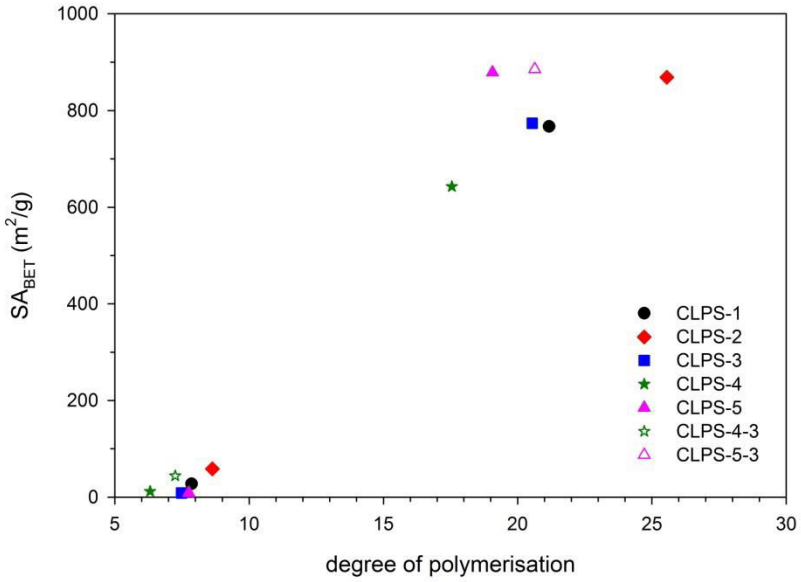

Figure 4.24 Surface areas of **CLPS-1** to **5**

It can be concluded that surface areas of the networks did not depend on the nature of the type of RAFT agents used, but mainly on number of styrene units in the primary polymer chain as discussed in the previous section.

4.5 Precipitation solvent variation

Different solvents used for precipitation were used to study the effect on the calculation of styrene units and surface areas after cross-linking. **PS-1** was synthesised following the general procedure with the target DP of 20. The reaction were separated into 5 parts and each part was precipitated into a different solvent i.e. EtOH, MeOH, water, acetone, and hexane. The polystyrene was dissolved in acetone and hexane. The yellow precipitates were obtained by using EtOH (**PS-1-EtOH**), MeOH (**PS-1-MeOH**), and water (**PS-1-water**).

EtOH and MeOH provided the paler solid than water. Yields were found higher when water was used. This could due to the presence of residual RAFT agent and intiator which were insoluble or partially soluble in water. This was confirmed by high N content in **PS-1-water**. It is possible that some lower molecular weight polymers were washed out more effectively by MeOH than by EtOH during precipitation. As MeOH has a higher polarity than EtOH[48], MeOH is expected to be a better solvent for shorter polystyrenes, which has a higher polarity due to higher ratio of the polar RAFT end groups to non-polar styrene backbones. Hence, the sample precipitated from MeOH had higher yield and also N and S contents than that from EtOH. However, the polymers showed similar IR spectra (**Figure 4.25**) as well as the calculated molecular weights and styrene units from GPC (**Table 4.5**). The **PS-1-MeOH** exhibited the slightly lower molecular weight than **PS-1-EtOH** and **PS-1-water**.

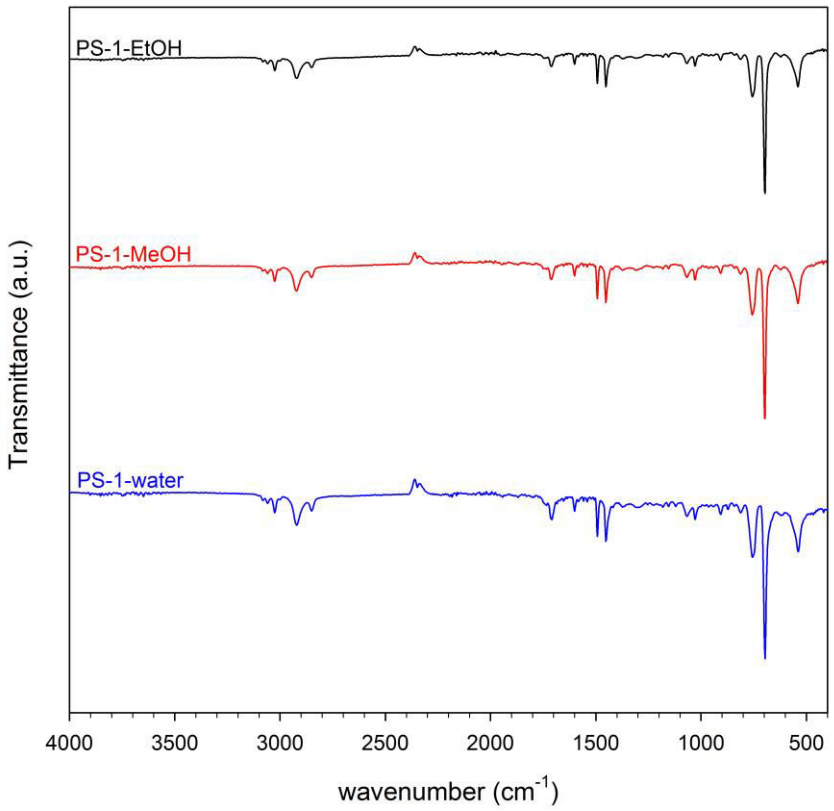

Figure 4.25 IR spectrum of the **PS-1-y** precipitated in different solvents

Table 4.5 Yields, elemental analysis and GPC data for **PS-1-ys** precipitated in different solvents

Sample	%Yield	%N	%S	M_w	M_n	PDI	Styrene units
PS-1-EtOH	40	0.57	3.17	2,780	2,610	1.07	21
PS-1-MeOH	68	0.66	3.53	2,640	2,450	1.08	20
PS-1-water	91	0.94	3.19	2,750	2,510	1.09	20

After cross-linking with FDA using Friedel-Crafts reaction as described above, insoluble brown solids were obtained in high yield. N and S contents as well as the IR spectra were similar. The surface areas and CO_2 uptakes were also comparable. (**Table 4.6**) Therefore, it is likely that solvents using for precipitation showed little effect on the properties of the networks.

Table 4.6 Yields, elemental analysis and gas sorption data of the **CLPS-1-ys** precipitated in different solvents

Sample	%Yield	%N	%S	SA_{BET} (m^2/g)	CO_2 uptakes (mmol/g)	
					273 K	298 K
CLPS-1-EtOH	99	0.46	1.50	767	1.87	1.13
CLPS-1-MeOH	101	0.49	1.59	738	1.86	1.11
CLPS-1-water	94	0.58	1.74	643	1.74	1.04

4.6 Conclusion

We have shown that benzoic acid and its ester derivatives would not undergo Friedel-Crafts reaction with FDA. A network could be formed when carboxylic acid functional group was further away from the benzene ring, but low surface area polymer was obtained. The extension of aromatic rings by cross-linking of the carboxylic acid functionalised polystyrenes synthesised by RAFT polymerisation could improve the surface areas of the networks but also decrease the proportion of functional groups. Cross-linking of polystyrenes with different DP were then prepared to study the balance ratio between functionalities to aromatic rings.

The surface areas of a series of networks were found depending on the DP of the linear polystyrenes. The nature of the RAFT agent and solvent used to precipitate the linear polystyrenes did not seem to affect the porosity of the final networks. At low DP, networks with low porosity are obtained. This is surprising considering that hypercross-linking of either benzene or biphenyl leads to networks with high porosity. There is a gradual increase in porosity as the DP of the parent polystyrene increases up to around a DP of 20. Beyond this point, there is little further increase, even when very high DP polymers are used. These data agree with those of Davankov, where the DP was found not to be an important parameter for the high molecular weight polystyrenes used in their study.[29]

The concept of hypercross-linking polystyrene with a low DP could be used, conceptually, to generate porous networks with a relatively high percentage of functional groups. Unfortunately, we show here that carboxylic acids do not survive the cross-linking process. Nonetheless, benefit of polymers synthesised by RAFT

polymerisation was that the RAFT end group itself could be modified to different functionalities.[49, 50] Therefore, further modification of RAFT end group might be done after networks formation to incorporate carboxylic acid or other functionalities into the networks. The need for a DP of greater than approximately 10 to achieve good levels of porosity, however, puts an upper limit on the maximum concentration of functional group that could be incorporated by this method.

4.7 References

1. B. Li, R. Gong, W. Wang, X. Huang, W. Zhang, H. Li, C. Hu and B. Tan, *Macromolecules*, 2011, **44**, 2410-2414.
2. X. Zhu, S. M. Mahurin, S.-H. An, C.-L. Do-Thanh, C. Tian, Y. Li, L. W. Gill, E. W. Hagaman, Z. Bian, J.-H. Zhou, J. Hu, H. Liu and S. Dai, *Chemical Communications*, 2014, **50**, 7933-7936.
3. M. Saleh, H. M. Lee, K. C. Kemp and K. S. Kim, *ACS Applied Materials & Interfaces*, 2014, **6**, 7325-7333.
4. Y. Luo, B. Li, W. Wang, K. Wu and B. Tan, *Advanced Materials*, 2012, **24**, 5703-5707.
5. R. Dawson, A. I. Cooper and D. J. Adams, *Polymer International*, 2013, **62**, 345-352.
6. Y. Zhang and S. N. Riduan, *Chemical Society Reviews*, 2012, **41**, 2083-2094.
7. N. Fontanals, J. Cortés, M. Galià, R. Maria Marcé, P. A. G. Cormack, F. Borrull and D. C. Sherrington, *Journal of Polymer Science Part A: Polymer Chemistry*, 2005, **43**, 1718-1728.
8. N. O. Calloway, *Chemical Reviews*, 1935, **17**, 327-392.
9. K. Jiang, D. Kuang, T. Fei and T. Zhang, *Sensors and Actuators B: Chemical*, 2014, **203**, 752-758.
10. C. F. Poole, *TrAC Trends in Analytical Chemistry*, 2003, **22**, 362-373.
11. D. Bratkowska, R. M. Marcé, P. A. G. Cormack, D. C. Sherrington, F. Borrull and N. Fontanals, *Journal of Chromatography A*, 2010, **1217**, 1575-1582.

12. D. Bratkowska, A. Davies, N. Fontanals, P. A. G. Cormack, F. Borrull, D. C. Sherrington and R. M. Marcé, *Journal of Separation Science*, 2012, **35**, 2621-2628.

13. R. Dawson, D. J. Adams and A. I. Cooper, *Chemical Science*, 2011, **2**, 1173-1177.

14. V. A. Davankov and M. P. Tsyurupa, *Reactive Polymers*, 1990, **13**, 27-42.

15. V. Davankov, M. Tsyurupa, M. Ilyin and L. Pavlova, *Journal of Chromatography A*, 2002, **965**, 65-73.

16. N. Fontanals, R. M. Marcé, P. A. G. Cormack, D. C. Sherrington and F. Borrull, *Journal of Chromatography A*, 2008, **1191**, 118-124.

17. N. Fontanals, P. A. G. Cormack, D. C. Sherrington, R. M. Marcé and F. Borrull, *Journal of Chromatography A*, 2010, **1217**, 2855-2861.

18. J. Y. Lee, C. D. Wood, D. Bradshaw, M. J. Rosseinsky and A. I. Cooper, *Chem Commun (Camb)*, 2006, 2670-2672.

19. C. Long, Q. Li, Y. Li, Y. Liu, A. Li and Q. Zhang, *Chemical Engineering Journal*, 2010, **160**, 723-728.

20. D. C. Sherrington, D. J. Craig, J. Dagleish, G. Domin, J. Taylor and G. V. Meehan, *European Polymer Journal*, 1977, **13**, 73-76.

21. Z.-A. Qiao, S.-H. Chai, K. Nelson, Z. Bi, J. Chen, S. M. Mahurin, X. Zhu and S. Dai, *Nat Commun*, 2014, **5**.

22. H. Binglin, Z. Quanxing, L. Xiaobai, S. Rongfu, S. Zuoqing, G. Xianquan, Z. Xiaolun and W. Jianying, *Chinese Journal of Polymer Science (CJPS)*, 1986, **4**, 220-228.

23. M. P. Tsyurupa and V. A. Davankov, *Reactive and Functional Polymers*, 2002, **53**, 193-203.

24. M. P. Tsyurupa and V. A. Davankov, *Reactive and Functional Polymers*, 2006, **66**, 768-779.

25. J.-H. Ahn, J.-E. Jang, C.-G. Oh, S.-K. Ihm, J. Cortez and D. C. Sherrington, *Macromolecules*, 2006, **39**, 627-632.

26. D. C. Sherrington, *Chemical Communications*, 1998, 2275-2286.

27. B. Li, R. Gong, Y. Luo and B. Tan, *Soft Matter*, 2011, **7**, 10910-10916.

28. R. Vinodh, A. Abidov, M. Peng, C. Babu, M. Palanichamy, W. Cha and H.-T. Jang, *Fibers Polym*, 2015, **16**, 1458-1467.

29. V. Davankov and M. Tsyurupa, in *Comprehensive Analytical Chemistry*, eds. A. D. Vadim and P. T. Maria, Elsevier, 2011, vol. Volume 56, pp. 195-295.

30. D. Zhang, L. Tao, J. Ju, Y. Wang, Q. Wang and T. Wang, *Polymer*, 2015, **60**, 234-240.

31. G. Moad, E. Rizzardo and S. H. Thang, *Chemistry – An Asian Journal*, 2013, **8**, 1634-1644.

32. J. Chiefari, Y. K. Chong, F. Ercole, J. Krstina, J. Jeffery, T. P. T. Le, R. T. A. Mayadunne, G. F. Meijs, C. L. Moad, G. Moad, E. Rizzardo and S. H. Thang, *Macromolecules*, 1998, **31**, 5559-5562.

33. A. D. Jenkins, R. G. Jones and G. Moad, *pac*, 2009, **82**, 483-491.

34. D. J. Keddie, *Chemical Society Reviews*, 2014, **43**, 496-505.

35. D. J. Keddie, G. Moad, E. Rizzardo and S. H. Thang, *Macromolecules*, 2012, **45**, 5321-5342.

36. C. D. Wood, B. Tan, A. Trewin, H. Niu, D. Bradshaw, M. J. Rosseinsky, Y. Z. Khimyak, N. L. Campbell, R. Kirk, E. Stöckel and A. I. Cooper, *Chemistry of Materials*, 2007, **19**, 2034-2048.

37. C. F. Martin, E. Stockel, R. Clowes, D. J. Adams, A. I. Cooper, J. J. Pis, F. Rubiera and C. Pevida, *Journal of Materials Chemistry*, 2011, **21**, 5475-5483.

38. R. Dawson, L. A. Stevens, T. C. Drage, C. E. Snape, M. W. Smith, D. J. Adams and A. I. Cooper, *Journal of the American Chemical Society*, 2012, **134**, 10741-10744.

39. Y. Luo, S. Zhang, Y. Ma, W. Wang and B. Tan, *Polymer Chemistry*, 2013, **4**, 1126-1131.

40. M. Errahali, G. Gatti, L. Tei, G. Paul, G. A. Rolla, L. Canti, A. Fraccarollo, M. Cossi, A. Comotti, P. Sozzani and L. Marchese, *The Journal of Physical Chemistry C*, 2014, **118**, 28699-28710.

41. G. Liu, Y. Wang, C. Shen, Z. Ju and D. Yuan, *Journal of Materials Chemistry A*, 2015, **3**, 3051-3058.

42. R. Dawson, A. I. Cooper and D. J. Adams, *Progress in Polymer Science*, 2012, **37**, 530-563.

43. J.-P. Gao, W. Wu, L. Rong, G.-L. Mao, Y.-N. Ning, Q.-L. Zhao, J. Huang and Z. Ma, *European Polymer Journal*, 2014, **59**, 171-179.

44. R. Dawson, T. Ratvijitvech, M. Corker, A. Laybourn, Y. Z. Khimyak, A. I. Cooper and D. J. Adams, *Polymer Chemistry*, 2012, **3**, 2034-2038.

45. V. Davankov and M. Tsyurupa, in *Comprehensive Analytical Chemistry*, eds. A. D. Vadim and P. T. Maria, Elsevier, 2011, vol. Volume 56, pp. 166-193.

46. *Japan Pat.*, JP 63066152, 1988.

47. H. M. Lee, I. S. Youn, M. Saleh, J. W. Lee and K. S. Kim, *Phys Chem Chem Phys*, 2015, **17**, 10925-10933.

48. C. Reichardt, *Chemical Reviews*, 1994, **94**, 2319-2358.

49. G. Moad, Y. K. Chong, A. Postma, E. Rizzardo and S. H. Thang, *Polymer*, 2005, **46**, 8458-8468.

50. H. Willcock and R. K. O'Reilly, *Polymer Chemistry*, 2010, **1**, 149-157.

Chapter 5

Post-synthetic Modification (PSM)

5. Post-synthetic Modification (PSM)

5.1 Introduction

One key advantage of microporous organic polymers (MOPs) is that diverse chemical functionalities can be introduced into the network providing controllable pore sizes and various chemical interactions toward guest molecules.[1] The introduction of desired functional groups can be carried out by modifying the monomers before network formation. The pre-functionalisation of monomer precursors can be time-consuming and/or require many synthetic steps. Also, some functional groups might be incompatible with the reaction conditions used for network formation. An alternative approach is the modification after networks are formed or post-synthetic modification (PSM) which refers to any changes to polymers after polymerisation.[2]

PSM would be of benefit to the polymers that require harsh condition to be polymerised, as some functionality may not be able to tolerate or can interfere with the polymerisation conditions. Moreover, the purification and isolation of the networks might be easier after the network formation. The networks with identical topologies but containing different functional groups could also obtained by PSM. PSM also conceptually allows the synthesis of networks with multiple functionalities in a combinatorial manner. Thus, PSM is an alternative strategy to tailor the prepared pore to introduce more functional groups to the polymers giving potential for extended applications.[3]

Generally, PSM needs pendant functional groups that do not react when networks are formed but can then be modified in subsequent reactions. PSM of metal-organic frameworks (MOFs) has been widely studied.[2-4] Various reactions, such as amide coupling[5-9], imine condensation[9-13], urea formation[14], *N*-alkylation[15], bromination[8], reduction[12], or click chemistry[16, 17], can be carried out by PSM. The concept of PSM was introduced by Hoskins and Robson.[18] The early research focused on the non-covalent interactions until covalent modification was published by Kim group in 2000.[15] The transformation of amines to amides is one of the most reported for MOFs PSM.[4] The pioneering research was reported in 2007 by Cohen

and Wang using acid anhydrides to modify amines to amides providing the membrane with carbon dioxide selectivity over n-propane.[5] However, MOFs with some functional groups can have a difficulty in surviving the solvothermal synthesis conditions and some functional group can also interfere in the formation of MOFs.[19]

Conjugated microporous polymers (CMPs), a class of microporous polymer, were recently shown to form a wide range of functionalised polymers with high surface areas.[20, 21] Their stabilities are also good. However, limited literature had been reported on the PSM of CMPs at the time when this work was carried on. Post-synthetic addition of metals to bipiridine-CMPs was achieved by the Cooper group providing catalytic active metal-organic CMPs (MO-CMPs).[22] Kiskan *et al.*[23] and Urakami *et al.*[24] also demonstrated the successful PSM of CMPs using thio-ene reaction. There are also some studies on similar kinds of materials such as COFs[25-27], PIMs[28, 29], and PAFs[30, 31].

In this work, amine functionalised conjugated microporous polymer (**CMP-1-NH_2**) was post-synthetically modified by reacting various chain lengths of acid anhydrides to form the amide CMPs (**CMP-1-AMDs**). We demonstrate that the porosity properties such as surface areas and pore size distributions as well as carbon dioxide captures can be tuned using PSM.

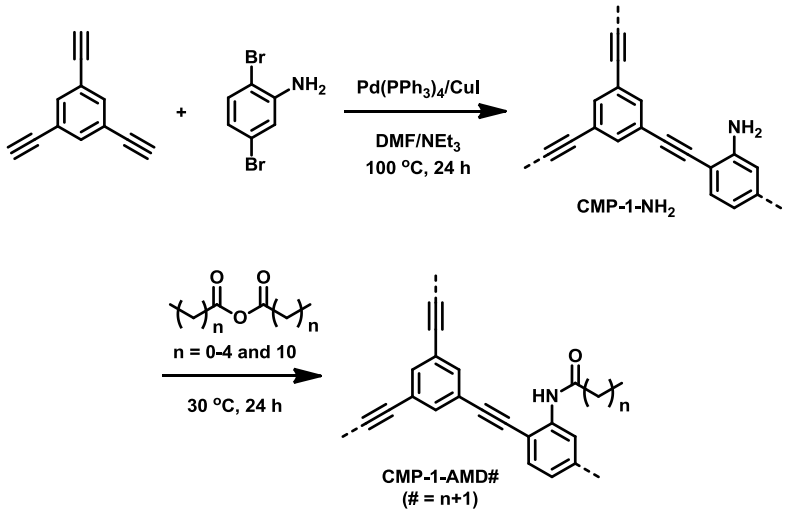

Scheme 5.1 Synthetic scheme for **CMP-1-AMDs**

5.2 CMP-1-NH_2 synthesis

An amine functionalised CMP, **CMP-1-NH_2**, was synthesised by Sonogashira-Hagihara cross-coupling reaction using 1,3,5-triethynylbenzene and 2,5-dibromoaniline as shown in **Scheme 5.1** followed the literature procedure.[20] The reaction gave a brown powder in a 90% yield. The measured Brunauer-Emmett-Teller (BET) surface area of 656 m^2/g was comparable to the previously reported 710 m^2/g even at this higher synthetic scale. The total pore volume (V_{tot}), micropore volume ($V_{0.1}$) and the micropore volume to total pore volume ratio ($V_{0.1/tot}$) were calculated to be 0.41, 0.25 and 0.61 respectively. These were also comparable to the values stated in the literature which are $V_{tot} = 0.39$, $V_{0.1} = 0.24$ and $V_{0.1/tot} = 0.62$.[20]

The incorporation of the amine group was confirmed by elemental analysis and IR spectroscopy. A discrepancy between the theory and analysis for the elemental analysis results (**Table 5.1**) was found as in many MOPs reported previously.[21, 32-34] This could be because of the amorphous nature of the networks and porosity properties which means that water, solvent, catalyst or gas could be trapped in the networks.[34, 35] However, a reasonable amount of nitrogen content of 2.62% could be used to confirm the amine group in the network.

The IR spectrum of the polymer illustrated the N-H stretching peaks of amine at 3381 and 3466 cm^{-1} and N-H bending peak at 1610 cm^{-1}. Two bands of N-H stretching indicated the primary amine functional group in the network. Aromatic C-H stretching peak was observed at 3296 cm^{-1} and C=C peaks were presented around 1400-1600 cm^{-1}. The respective terminal and internal alkyne peaks at around 2100 and 2200 cm^{-1} demonstrated the incorporation of the triethynylbenzene part in the network. The increase of internal alkyne and decrease of terminal alkyne confirmed network formation. (**Figure 5.1**)

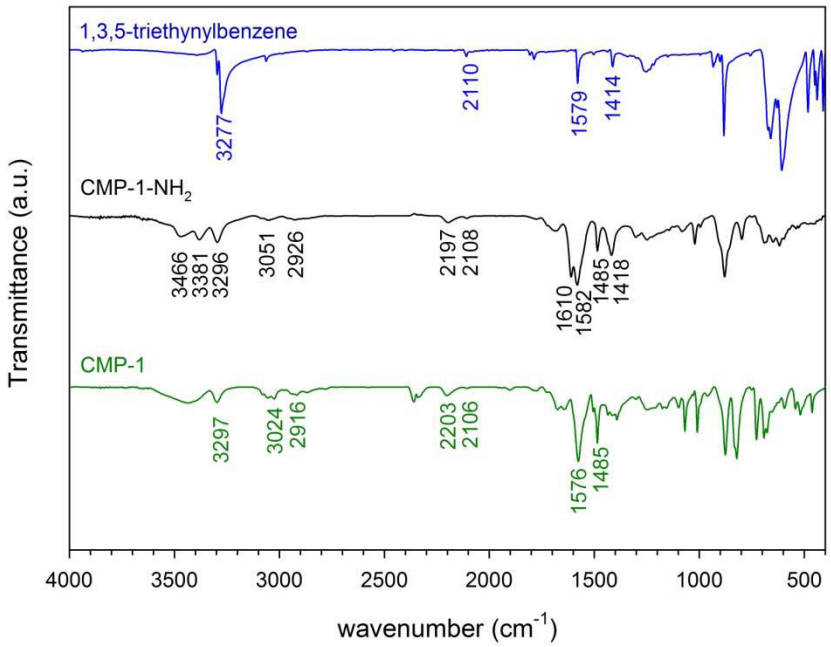

Figure 5.1 IR spectra of **CMP-1-NH$_2$** (black) compared to 1,3,5-triethynylbenzene (blue) and unfunctionalised **CMP-1** (green)

5.3 PSM CMP-1-NH$_2$ to CMP-1-AMDs

5.3.1 PSM

The network was post-synthetically modified by stirring with neat acetic anhydride for 24 hours at 30 ^{o}C to provide acetyl amide CMP (**CMP-1-AMD1**) in an 84 % yield after washing with $CHCl_3$. The conversion of amine to amides was confirmed by IR spectroscopy and elemental analysis. The presence of C=O stretching peak around 1693 cm^{-1} in IR spectra (**Figure 5.2**) showed the incorporation of carbonyl group in the network. Moreover, only one N-H stretching peak at 3400 cm^{-1} was present instead of two peaks, meaning that the primary amines were substituted by secondary amines. C-H and C=C stretching peaks of aromatic rings were found at 3294 cm^{-1} and around 1400-1600 cm^{-1}. The terminal and internal alkynes could survive the reaction as confirmed by the peaks at around 2100 and 2200 cm^{-1}, respectively. The decrease of nitrogen content in elemental analysis from 2.62% in **CMP-1-NH$_2$** to 2.27% in **CMP-1-AMD1**, due to the increase of carbon in the amide chain, supported the conversion of amine to amide.

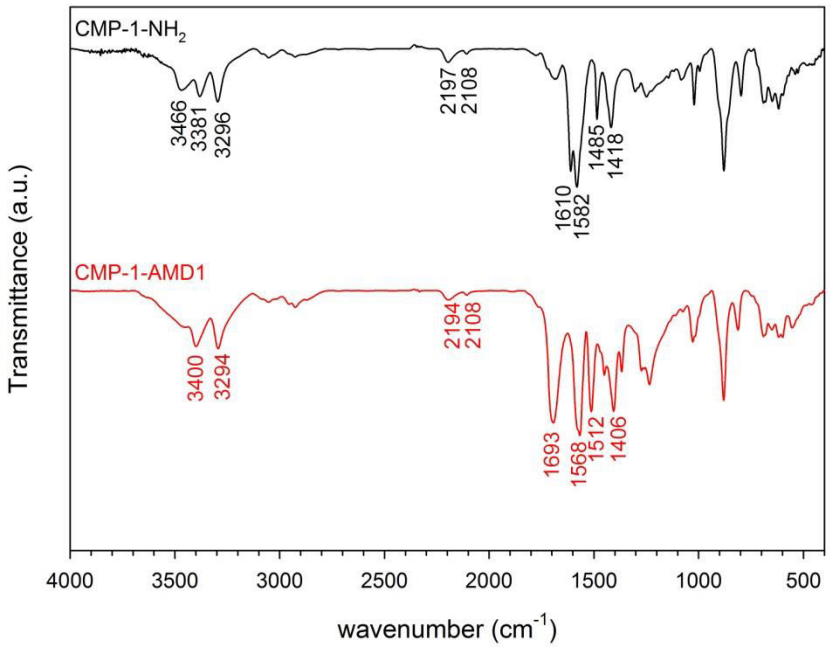

Figure 5.2 IR spectra of **CMP-1-NH$_2$** (black) and **CMP-1-AMD1** (red)

Solid state NMR spectra of **CMP-1-NH$_2$** and **CMP-1-AMD1** collected by Andrea Laybourn (University of Liverpool) confirmed the conversion of amine to amide. The peak of an aromatic carbon next to the amine group at 144.0 ppm disappeared after PSM. At the same time, a methyl peak at 23.9 ppm and a carbonyl peak at 169.2 ppm for the amide chain were observed after PSM. (**Figure 5.3**)

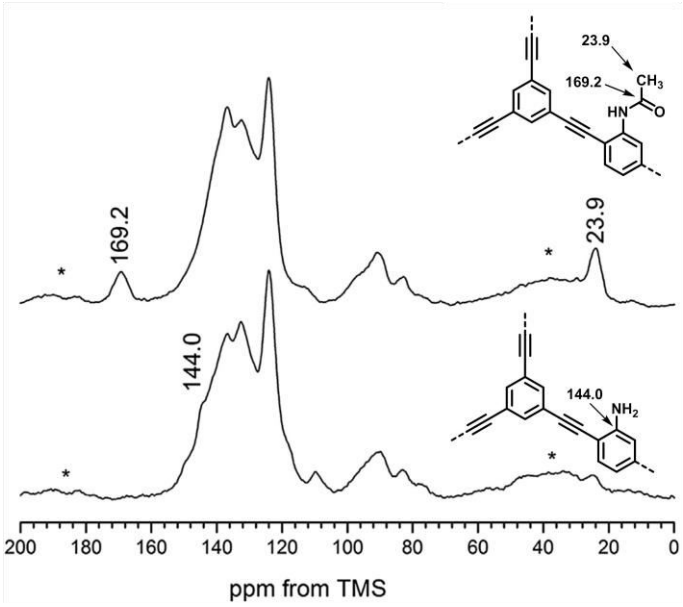

Figure 5.3 Solid state NMR spectra of **CMP-1-NH$_2$** (bottom) and **CMP-1-AMD1** (top) (data collected by Andrea Laybourn). * indicate spinning side bands.

SEM images of **CMP-1-NH$_2$** (**Figure 5.4**) collected by Dr. Robert Dawson (University of Liverpool) illustrated the rough-textured morphology, which is comparable with previous literature.[20] After PSM, SEM images of **CMP-1-AMD1** (**Figure 5.5**) showed a similar texture as **CMP-1-NH$_2$** (**Figure 5.4**), implying the PSM did not change the morphology significantly.

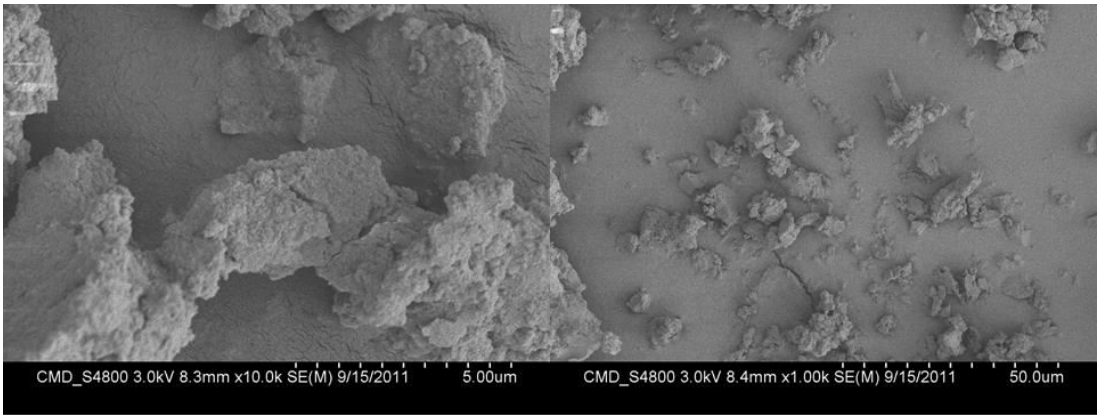

Figure 5.4 SEM image of **CMP-1-NH$_2$**

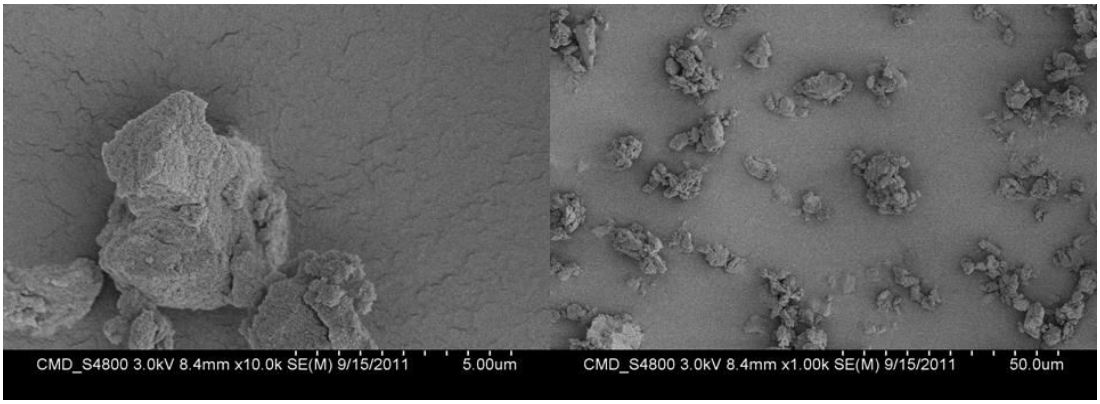

Figure 5.5 SEM image of **CMP-1-AMD1**

Further investigation was conducted by using longer chain lengths of anhydrides to provide CMPs with different chain length of amides (**CMP-1-AMDs**) in 65 – 85 % yields. The number after **CMP-1-AMD** indicates the number of carbon in the chain (**Scheme 5.1**). The transformation of amine to amides was again confirmed by the reduction in an orderly way of the nitrogen content to be 1.65% in **CMP-1-AMD9**. (**Table 5.1**)

Table 5.1 Yields and elemental analysis data of **CMP-1-AMDs**

CMP-1-	Yield (%)	Theory (%)			Analysis (%)		
		C	H	N	C	H	N
NH_2	90	90.74	3.38	5.88	78.18	3.59	2.62
AMD1	84	85.70	3.60	5.00	74.27	3.73	2.27
AMD2	72	85.70	4.11	4.76	72.81	4.01	2.13
AMD3	82	85.69	4.58	4.54	73.94	4.27	2.13
AMD4	79	85.69	5.00	4.34	74.64	4.53	2.07
AMD5	78	85.69	5.39	4.16	74.16	4.81	2.03
AMD9	67	85.68	6.68	3.57	74.71	6.27	1.65

From **Figure 5.6**, infrared spectra also showed the carbonyl and one N-H stretching peaks at around 1700 and 3400 cm^{-1} similar to the **CMP-1-AMD1**. The intensity of C-H stretching of amide carbon chains around 2800-2900 cm^{-1} increased

as the longer chain of acid anhydrides were used. The terminal and internal alkynes were observed at around 2100 and 2200 cm^{-1}, respectively.

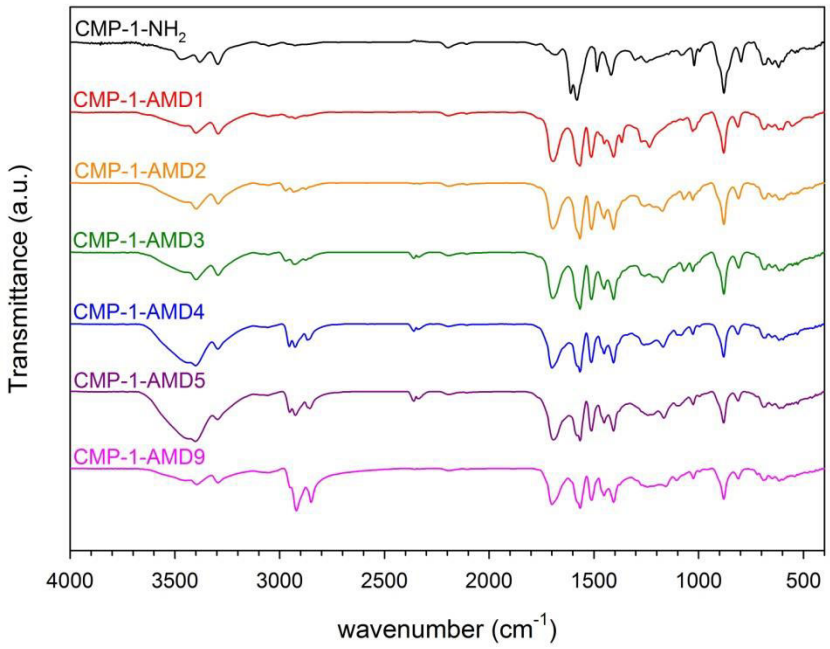

Figure 5.6 IR spectra of **CMP-1-NH_2** (black) and **CMP-1-AMDs**

5.3.2 Gas sorption properties

Nitrogen isotherms were collected from Micromeritics ASAP 2020 at 77.3 K. (**Figure 5.7**) **CMP-1-NH_2** and **CMP-1-AMDs** exhibited the Type 1 isotherms with a step in the desorption isotherms. A lower amount of nitrogen was adsorbed in the networks modified with the longer chain of amides. Total pore volumes, which could be determined by amount of nitrogen adsorbed at a p/p^0 of about 1, reduced with the longer chain length of amides. Micropores, which could be indicated by the amount of nitrogen adsorbed at a p/p^0 of less than 0.1, also decreased as the chain length of amides increase from **CMP-1-AMD1** to **CMP-1-AMD5** and nearly no micropores were observed in **CMP-1-AMD9**.

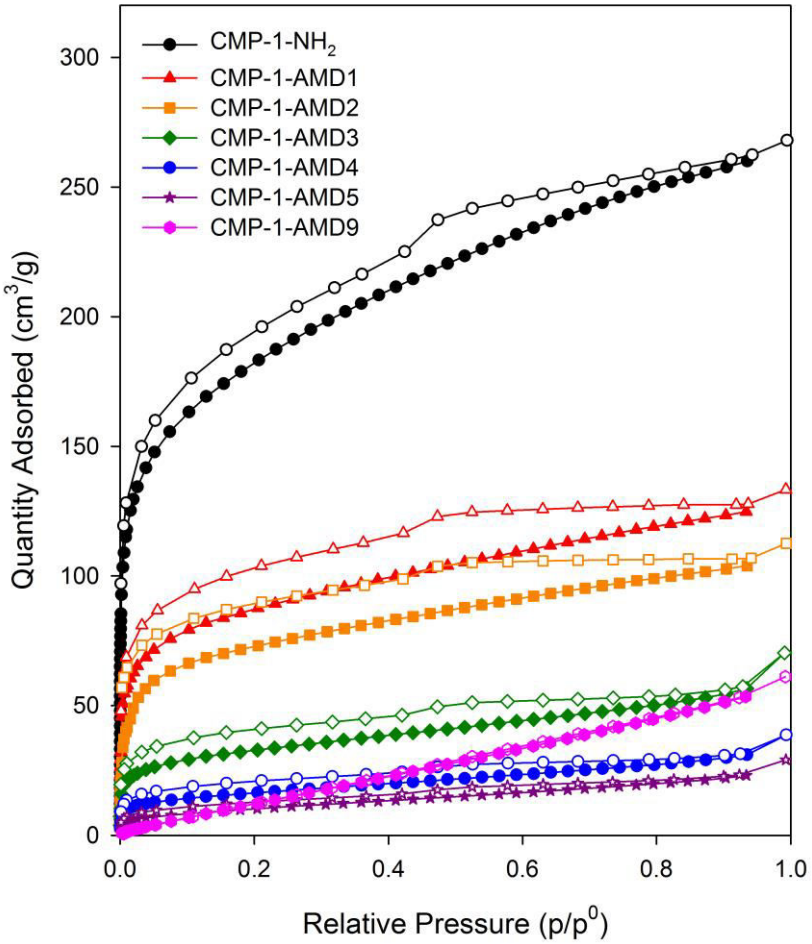

Figure 5.7 Nitrogen adsorption (close symbols) and desorption (open symbols) isotherms of **CMP-1-NH$_2$** and **CMP-1-AMDs**

The calculated pore size distribution (**Figure 5.8**) also shows the reduction of the pore volume from **CMP-1-NH$_2$** to **CMP-1-AMD1** and further decrease when longer chain of amides were used until the micropores (pores smaller than 2 nm) almost disappeared in **CMP-1-AMD9**.

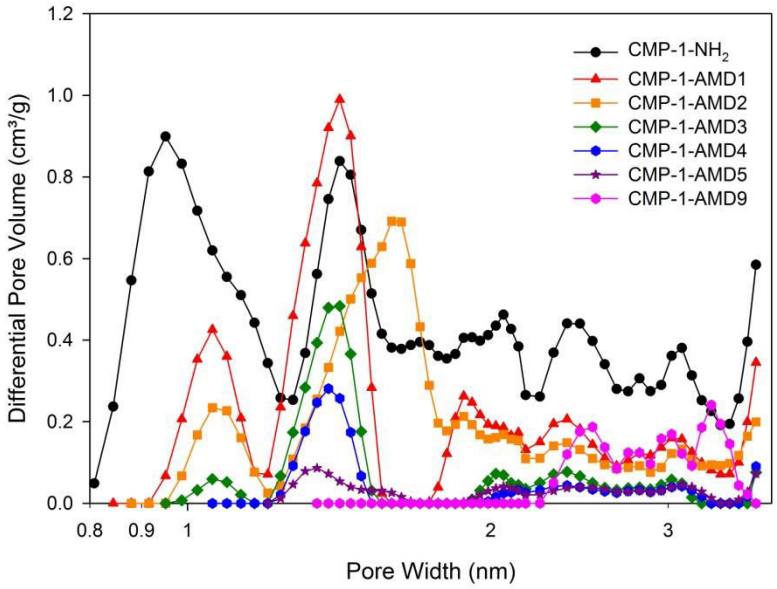

Figure 5.8 NL-DFT pore size distributions of **CMP-1-NH$_2$** and **CMP-1-AMD**s

After PSM, the BET surface areas of **CMP-1-AMDs** were lower than surface area of **CMP-1-NH$_2$** indicating the success of PSM. The apparent BET surface areas, as well as the total pore volumes and micropore volumes, systematically declined with the growing of amides chain length. (**Figure 5.9**) The ratio of the micropore volume to total pore volume stayed stable for one and two carbon chain lengths (**CMP-1-AMD1** and **CMP-1-AMD2**), before falling with increasing length of the amide chains.

The BET surface area dropped dramatically from 656 m^2/g in the case of **CMP-1-NH$_2$** to 316 m^2/g for **CMP-1-AMD1**, and then slowly decreased when the chain length was expanded to the lowest surface area in the series of 37 m^2/g for **CMP-1-AMD5**. (**Figure 5.9**) This may be either because the pores were filled by alkyl chains, or the paths for gas accessibility to the pores were blocked by the chains. Similar results were also found in functionalised MOFs[6], COFs[36], and PIMs[37] with alkyl chains. The BET surface area slightly increases again for **CMP-1-AMD9**, possibly due to the bulkiness of decanoic anhydride making the reaction with the amine groups more difficult.

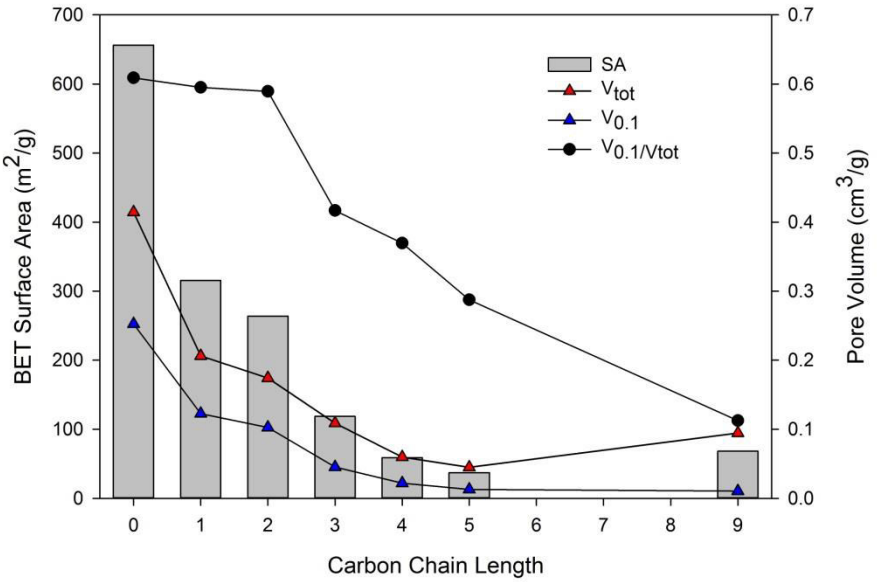

Figure 5.9 BET surface areas (columns), total pore volumes (red triangles), micropore volumes (blue triangles) and the proportion of micropore to total pore volumes (black circles) for **CMP-1-NH$_2$** and **CMP-1-AMD**s

The PSM can also be used to tune the carbon dioxide adsorption properties of the materials. With increasing of the length of amide chains, carbon dioxide uptakes (**Figure 5.10**) and carbon dioxide heat of adsorption (**Figure 5.11**) decreased systematically. Carbon dioxide uptakes (**Table 5.2**), measured at 1 bar by using Micromerimetric ASAP 2020, dropped from 1.65 and 0.96 mmol/g of **CMP-1-NH$_2$** to 1.51 and 0.96 mmol/g of **CMP-1-AMD1** at 273 K and 298 K respectively and further decrease was observed when chain length of amides are longer to be 0.87 mmol/g at 273 K and 0.54 mmol/g at 298 K in **CMP-1-AMD9**.

Table 5.2 Gas sorption data of **CMP-1-AMDs**

CMP-1-	SA_{BET} (m^2/g)	Pore Volume (cm^3/g)			CO_2 uptakes (mmol/g)	
		V_{tot}	$V_{0.1}$	$V_{0.1/tot}$	273 K	298 K
NH_2	656	0.41	0.25	0.61	1.65	0.96
AMD1	316	0.21	0.12	0.59	1.51	0.96
AMD2	264	0.17	0.10	0.59	1.46	0.92
AMD3	119	0.11	0.05	0.42	1.31	0.83
AMD4	59	0.06	0.02	0.37	1.13	0.71
AMD5	37	0.04	0.01	0.29	1.10	0.64
AMD9	68	0.09	0.01	0.11	0.87	0.54

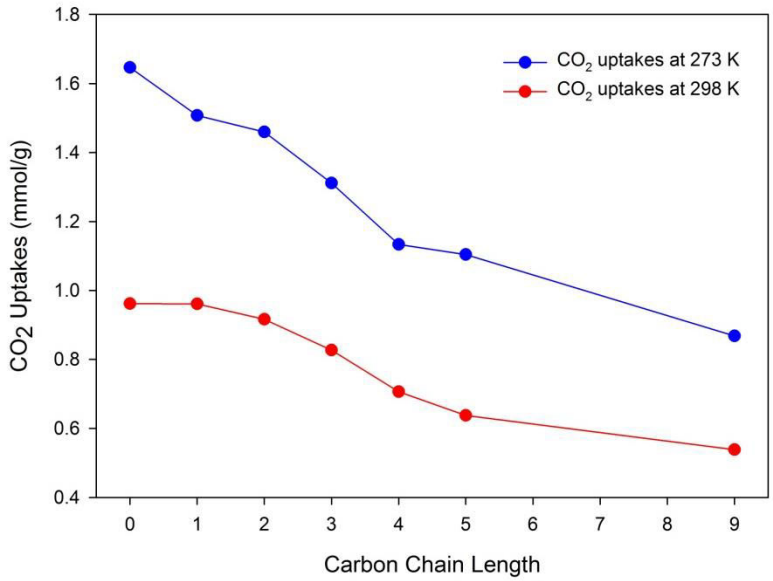

Figure 5.10 CO_2 uptakes of **CMP-1-NH_2** and **CMP-1-AMDs** at 273 K and 298 K

The isosteric heats of adsorption (**Figure 5.11**) were calculated from the carbon dioxide isotherms collected at the two different temperatures. All networks showed decrease isosteric heats as a function of increasing CO_2 coverage. The isosteric heats decreased when going from the amine network to the corresponding amides and decreased gradually with the length of amides. Similar to the nitrogen adsorption, the lower amount of CO_2 adsorbed might due to the reduction of surface area and pore volumes. It is also possible that this is a result of the coverage of the active amine group by the carbon chains when modified to be amides.

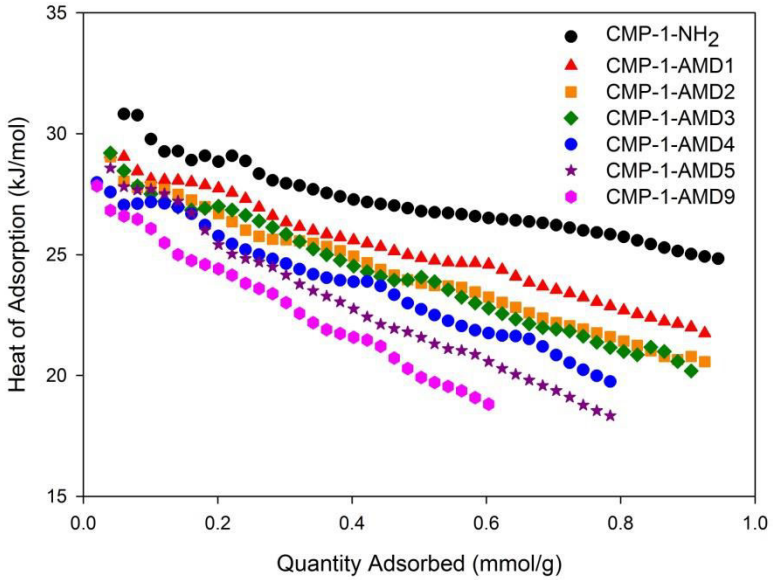

Figure 5.11 CO_2 isosteric heat of adsorption of **CMP-1-NH$_2$** and **CMP-1-AMDs**

5.4 Temperature Effect on PSM

The temperature used for PSM reaction was studied. **CMP-1-NH$_2$** was synthesised and post-synthetic modified followed the same procedure as the reaction at 30 ^oC but reaction was stirred at room temperature instead to provide **CMP-1-AMDs-RT**. The properties of **CMP-1-AMDs-RT** were summarised in **Table 5.3**.

Table 5.3 Yields, elemental analysis and gas sorption data of **CMP-1-AMDs-RT**

CMP-1-	Yield (%)	Theory (%)			Analysis (%)			SA_{BET} (m^2/g)	CO_2 uptakes at r.t. (mmol/g)
		C	H	N	C	H	N		
NH$_2$	140	90.74	3.38	5.88	73.10	3.45	2.83	517	0.87
AMD1	56	85.70	3.60	5.00	70.64	3.61	2.72	441	0.87
AMD2	54	85.70	4.11	4.76	72.03	3.70	2.72	396	0.88
AMD3	54	85.69	4.58	4.54	72.94	4.01	2.70	311	0.71
AMD4	49	85.69	5.00	4.34	73.83	4.19	2.67	294	0.63
AMD5	54	85.69	5.39	4.16	73.89	4.30	2.62	216	0.57

Again, the success of PSM of amine to amides was validated by infrared spectroscopy (IR) and elemental analysis. IR spectra (**Figure 5.12**) showed the carbonyl C=O stretching peak around 1690 cm^{-1} and the one N-H stretching peak at 3395 cm^{-1} indicating secondary amine. The small peak around 3468 cm^{-1} might indicate unreacted primary amine in the networks. The trend in the IR spectra was also similar to that of the networks modified at 30 ^{o}C. The intensity of C-H stretching peaks 2800-2900 cm^{-1} increased as the longer chain of acid anhydrides were used.

The nitrogen content also slightly dropped from 2.83 % in **CMP-1-NH$_2$** to 2.72 % in **CMP-1-AMD1-RT** after PSM. The nitrogen content further reduced as the carbon chain of amide was longer to 2.62 % in **CMP-1-AMD5-RT**. Comparing to the networks post-synthetic modified at 30 ^{o}C, the reduction of the nitrogen content was less in **CMP-1-AMDs-RT**, indicating that less reaction occurred when the PSM was operated at lower temperature. (**Figure 5.13**)

Similar to **CMP-1-AMDs** modified at 30 ^{o}C, systematic reduction of surface areas (**Figure 5.14**) and CO_2 uptakes (**Figure 5.15**) were also observed. The surface areas dropped from 517 m^2/g in **CMP-1-NH$_2$** to 441 m^2/g in **CMP-1-AMD1-RT** and further decrease when longer chain acid anhydrides were used until 216 m^2/g in **CMP-1-AMD5-RT**. CO_2 uptakes also decreased from 0.87 mmol/g in **CMP-1-NH$_2$** to 0.57 m^2/g in **CMP-1-AMD5-RT**. However, comparing between materials PSM at different temperature, less of a reduction in the surface areas were observed at lower reaction temperature. This could imply that the PSM was more effective at higher temperature.

5.5 Solvent Effect on PSM

The solvent effect was studied by using chloroform ($CHCl_3$) as a solvent at room temperature in modification step instead of neat anhydrides to obtain **CMP-1-AMDs-CHCl$_3$**. We chose $CHCl_3$, as it is commonly used as a solvent for PSM of MOFs by amide coupling.[5-8, 14] The summary data of **CMP-1-AMDs-CHCl$_3$** was shown in **Table 5.4**.

Table 5.4 Yields, elemental analysis and gas sorption data of **CMP-1-AMDs-$CHCl_3$**

CMP-1-	Yield (%)	Theory (%)			Analysis (%)			SA_{BET} (m^2/g)	CO_2 uptakes at r.t. (mmol/g)
		C	H	N	C	H	N		
NH_2	103	90.74	3.38	5.88	71.74	3.39	2.94	596	1.02
AMD1	75	85.70	3.60	5.00	73.29	3.61	2.82	549	0.96
AMD2	73	85.70	4.11	4.76	73.55	3.75	2.84	544	0.83
AMD3	74	85.69	4.58	4.54	73.97	3.88	2.82	521	0.79
AMD4	72	85.69	5.00	4.34	74.50	3.98	2.79	515	0.75
AMD5	70	85.69	5.39	4.16	73.12	4.00	2.71	449	0.73
AMD11	57	85.68	7.19	3.33	75.40	4.57	2.69	181	0.57

The trend in IR spectra was similar to those of the reactions carried out in neat anhydride. The C=O and N-H stretching peaks were observed around 1693 and 3391 cm^{-1} respectively. The intensity of C-H stretching peaks 2800-2900 cm^{-1} increased as the longer chain of acid anhydrides were used. (**Figure 5.12**) However, only slight reduction of nitrogen content was observed when $CHCl_3$ was used as a solvent i.e. from 2.82 % for **CMP-1-AMD1-$CHCl_3$** to 2.71 % for **CMP-1-AMD5-$CHCl_3$**. (**Table 5.4**) The lower decrease of the nitrogen content for **CMP-1- AMDs-$CHCl_3$** series compared to the reactions carried out in neat anhydride indicates less successful PSM in the networks. (**Figure 5.13**)

The surface areas (**Figure 5.14**) and CO_2 uptakes (**Figure 5.15**) of **CMP-1-AMDs-$CHCl_3$** also systematically dropped when the longer chain length of acid anhydrides was used. The surface areas decreased less than when neat anhydrides were used. (**Figure 5.14**) This might be due to the swelling which affects the porosity properties of the networks when solvents were used. As the networks could swell in solvent,[38] it could be possible that the networks shrank in different manner after the solvent was removed to jam into a network that was different to before swelling leading to different porous structures.[39] However, as the nitrogen content (**Figure 5.13**) also reduced less when solvent was used, it could also be that less PSM occurred. This might be because of the dilution of the anhydrides so the reactions could not proceed well.

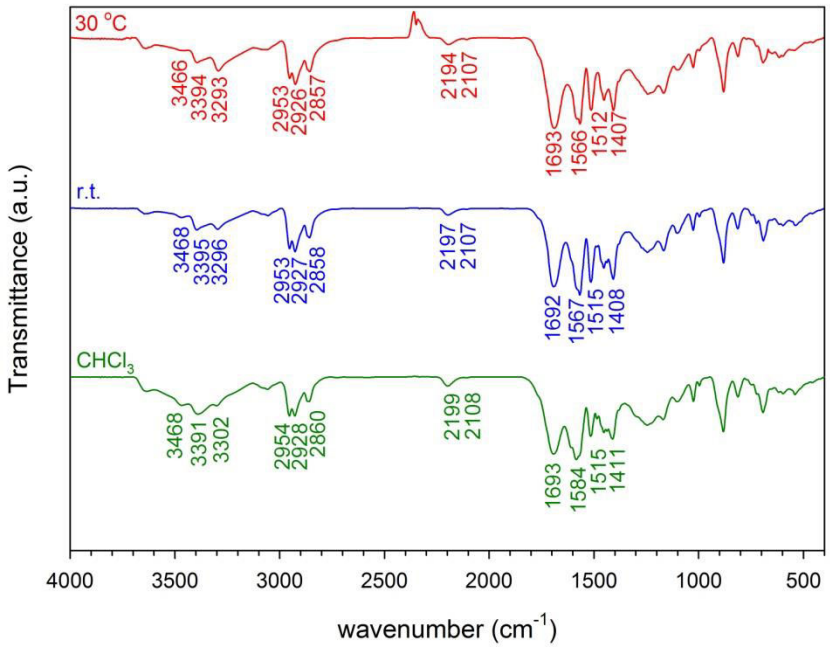

Figure 5.12 IR spectra of **CMP-1-AMD5s** modified by different conditions

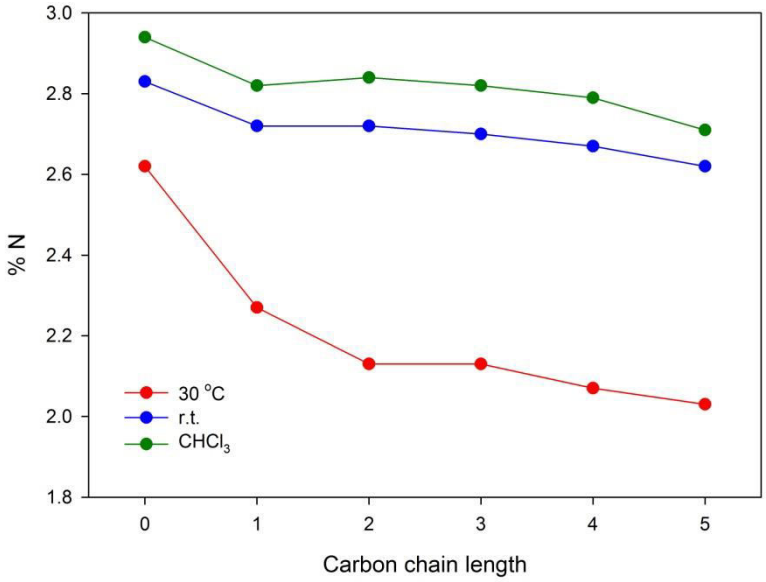

Figure 5.13 Nitrogen contents of **CMP-1-AMDs** modified by different conditions

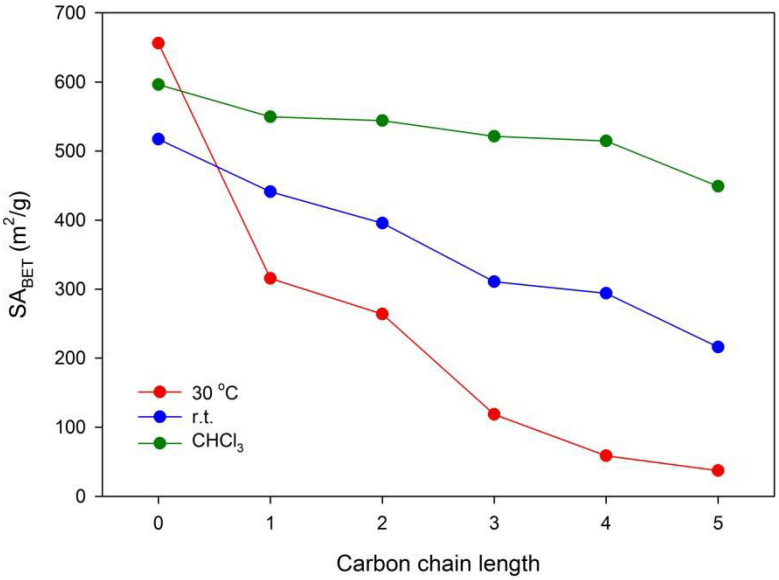

Figure 5.14 Surface areas of **CMP-1-AMDs** modified by different conditions

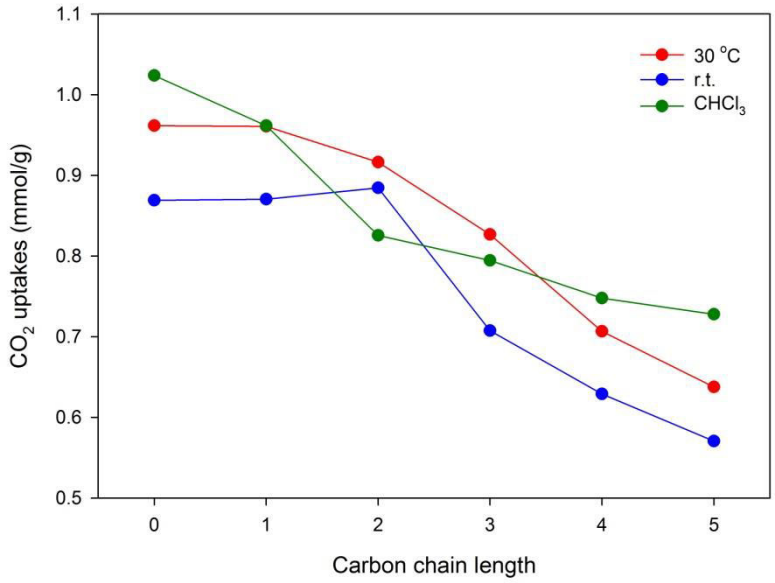

Figure 5.15 CO_2 uptakes of **CMP-1-AMDs** modified by different conditions

5.6 Conclusion

The introduction of functional groups is one of the key methods to tune materials for specific applications. However, some functional groups may not be able to be tolerated in the polymer synthetic conditions. Thus, PSM provides the opportunity to introduce more functional groups to the polymer providing the potential to extend wider range of functionalities to the polymers.

The PSM of amine-CMPs into amides with different alkyl chains has been achieved in this study. Primary amine functionalised conjugated microporous polymer (**CMP-1-NH_2**) could be prepared by Sonogashira-Hagihara cross-coupling reaction using 1,3,5-triethynylbenzene and 2,5-dibromoaniline giving the similar yield and porous properties comparable to the previous report even be scaled-up.[20] The incorporation of amine group was confirmed by nitrogen content in elemental analysis and IR spectroscopy. The **CMP-1-NH_2** was post-synthetic modified by stirring with different chain length of anhydrides providing CMPs with amides (**CMP-1-AMDs**). Again, the conversion of amine to amides was confirmed by elemental analysis and IR spectroscopy. The modified polymers shows the systematical drop of surface areas and pore volumes as well as the CO_2 uptakes and CO_2 heat of adsorptions with increasing the length of amide chains. We also showed that the synthetic conditions such as temperature and solvent also affected the PSM process. This demonstrated that the new functional groups can be introduced into the CMPs and the properties of the networks can be tailored systematically by PSM strategy.

We have shown that various functionalities could be introduced into CMPs.[20, 21] Many pendant functional groups such as carboxylic acid, alcohol, and amine are possibly further modified to different functionalities. For example, the carboxylic acid group might be able to be modified to an ester or an amide. This will provide wider range of functionalities in the networks. Thus, the PSM strategy offers the potential to extend the diversity of functionalised networks leading to more applications can be applied.

5.7 References

1. R. Dawson, A. I. Cooper and D. J. Adams, *Polymer International*, 2013, **62**, 345-352.
2. K. K. Tanabe and S. M. Cohen, *Chemical Society Reviews*, 2011, **40**, 498-519.
3. Z. Wang and S. M. Cohen, *Chemical Society Reviews*, 2009, **38**, 1315-1329.
4. A. D. Burrows, in *Metal Organic Frameworks as Heterogeneous Catalysts*, The Royal Society of Chemistry, 2013, pp. 31-75.
5. Z. Wang and S. M. Cohen, *Journal of the American Chemical Society*, 2007, **129**, 12368-12369.
6. K. K. Tanabe, Z. Wang and S. M. Cohen, *Journal of the American Chemical Society*, 2008, **130**, 8508-8517.
7. Z. Wang, K. K. Tanabe and S. M. Cohen, *Inorganic Chemistry*, 2009, **48**, 296-306.
8. Z. Wang and S. M. Cohen, *Angewandte Chemie International Edition*, 2008, **47**, 4699-4702.
9. T. Kawamichi, T. Kodama, M. Kawano and M. Fujita, *Angewandte Chemie International Edition*, 2008, **47**, 8030-8032.
10. T. Haneda, M. Kawano, T. Kawamichi and M. Fujita, *Journal of the American Chemical Society*, 2008, **130**, 1578-1579.
11. M. J. Ingleson, J. Perez Barrio, J.-B. Guilbaud, Y. Z. Khimyak and M. J. Rosseinsky, *Chemical Communications*, 2008, 2680-2682.
12. W. Morris, C. J. Doonan, H. Furukawa, R. Banerjee and O. M. Yaghi, *Journal of the American Chemical Society*, 2008, **130**, 12626-12627.
13. A. D. Burrows, C. G. Frost, M. F. Mahon and C. Richardson, *Angewandte Chemie International Edition*, 2008, **47**, 8482-8486.
14. E. Dugan, Z. Wang, M. Okamura, A. Medina and S. M. Cohen, *Chemical Communications*, 2008, 3366-3368.
15. J. S. Seo, D. Whang, H. Lee, S. I. Jun, J. Oh, Y. J. Jeon and K. Kim, *Nature*, 2000, **404**, 982-986.
16. T. Gadzikwa, G. Lu, C. L. Stern, S. R. Wilson, J. T. Hupp and S. T. Nguyen, *Chemical Communications*, 2008, 5493-5495.

17. Y. Goto, H. Sato, S. Shinkai and K. Sada, *Journal of the American Chemical Society*, 2008, **130**, 14354-14355.

18. B. F. Hoskins and R. Robson, *Journal of the American Chemical Society*, 1990, **112**, 1546-1554.

19. S. J. Garibay, Z. Wang, K. K. Tanabe and S. M. Cohen, *Inorganic Chemistry*, 2009, **48**, 7341-7349.

20. R. Dawson, D. J. Adams and A. I. Cooper, *Chemical Science*, 2011, **2**, 1173-1177.

21. R. Dawson, A. Laybourn, R. Clowes, Y. Z. Khimyak, D. J. Adams and A. I. Cooper, *Macromolecules*, 2009, **42**, 8809-8816.

22. J.-X. Jiang, C. Wang, A. Laybourn, T. Hasell, R. Clowes, Y. Z. Khimyak, J. Xiao, S. J. Higgins, D. J. Adams and A. I. Cooper, *Angewandte Chemie International Edition*, 2011, **50**, 1072-1075.

23. B. Kiskan and J. Weber, *ACS Macro Letters*, 2012, **1**, 37-40.

24. H. Urakami, K. Zhang and F. Vilela, *Chemical Communications*, 2013, **49**, 2353-2355.

25. P. A. Kerneghan, S. D. Halperin, D. L. Bryce and K. E. Maly, *Canadian Journal of Chemistry*, 2011, **89**, 577-582.

26. Z. Xiang, D. Cao, W. Wang, W. Yang, B. Han and J. Lu, *The Journal of Physical Chemistry C*, 2012, **116**, 5974-5980.

27. D. N. Bunck and W. R. Dichtel, *Chemical Communications*, 2013, **49**, 2457-2459.

28. N. Du, G. P. Robertson, J. Song, I. Pinnau and M. D. Guiver, *Macromolecules*, 2009, **42**, 6038-6043.

29. N. Du, H. B. Park, G. P. Robertson, M. M. Dal-Cin, T. Visser, L. Scoles and M. D. Guiver, *Nat Mater*, 2011, **10**, 372-375.

30. W. Lu, D. Yuan, J. Sculley, D. Zhao, R. Krishna and H.-C. Zhou, *Journal of the American Chemical Society*, 2011, **133**, 18126-18129.

31. W. Lu, J. P. Sculley, D. Yuan, R. Krishna, Z. Wei and H.-C. Zhou, *Angewandte Chemie International Edition*, 2012, **51**, 7480-7484.

32. J.-X. Jiang, A. Trewin, F. Su, C. D. Wood, H. Niu, J. T. A. Jones, Y. Z. Khimyak and A. I. Cooper, *Macromolecules*, 2009, **42**, 2658-2666.

33. J.-X. Jiang, A. Laybourn, R. Clowes, Y. Z. Khimyak, J. Bacsa, S. J. Higgins, D. J. Adams and A. I. Cooper, *Macromolecules*, 2010, **43**, 7577-7582.

34. S. Ren, R. Dawson, D. J. Adams and A. I. Cooper, *Polymer Chemistry*, 2013, **4**, 5585-5590.

35. M. Yu, X. Wang, X. Yang, Y. Zhao and J.-X. Jiang, *Polymer Chemistry*, 2015, **6**, 3217-3223.

36. R. W. Tilford, S. J. Mugavero, P. J. Pellechia and J. J. Lavigne, *Advanced Materials*, 2008, **20**, 2741-2746.

37. B. S. Ghanem, M. Hashem, K. D. M. Harris, K. J. Msayib, M. Xu, P. M. Budd, N. Chaukura, D. Book, S. Tedds, A. Walton and N. B. McKeown, *Macromolecules*, 2010, **43**, 5287-5294.

38. D. Tan, W. Fan, W. Xiong, H. Sun, Y. Cheng, X. Liu, C. Meng, A. Li and W.-Q. Deng, *Macromolecular Chemistry and Physics*, 2012, **213**, 1435-1440.

39. R. K. Totten, L. L. Olenick, Y.-S. Kim, S. Chakraborty, M. H. Weston, O. K. Farha, J. T. Hupp and S. T. Nguyen, *Chemical Science*, 2014, **5**, 782-787.

Chapter 6

Molecular Imprinting Polymers (MIPs)

6. Molecular Imprinting Polymers (MIPs)

6.1 Introduction

Molecular imprinting polymers (MIPs) are polymers that have specific cavities, in terms of size, shape and electron density, resulting in selectivity towards template molecules[1-3]. Templates ranging from organic small molecules[4], macromolecules[5, 6], cells[7] , viruses[8] to bacteria[9, 10] can be used. Specific recognition endows MIPs as selective adsorbents, with potential applications in separation[11-13], sensors[14-16], structure elucidation[17], catalysis[18] and artificial natural recognition systems[19, 20].

The concept of molecular imprinting began from the finding of materials for use in chromatography by Polyakov in 1931[21]. Sodium silicate was found to capture more of the compounds that were used in gel preparation than their analogues. Further detailed investigation lead to the conclusion that the recognition came from the change in structure of the silica following the nature of additives which acted as templates [22, 23]. The study of silica-based materials has been extended, especially in 1950s.

In the same period, the theory of the human antibody mechanism was of interest to many research groups[24-26]. Pauling suggested in 1942 that the structure of antibody was induced by antigen[27] which was later proven to be wrong[28]. However, his later work attempting to prove the hypothesis by mimicking the mechanism of an antibody[29] inspired the bio-imprinting field[30]. After that, he initiated the research on non-biotic imprinting materials using silica by the lead of Dickey, which was the pioneering method for preparing the imprinting materials[31, 32]. However, due to the limitation of silica systems, the research in the field declined in the decade afterwards.

In 1972, the molecular imprinting in polymers was firstly investigated by two independent research groups, Wulff[17, 33] and Klotz[34]. Wulff and Sarhan described a new method to make polymers with fixed configuration by using the concept of enzyme arrangement[35]. The polymers showed the ability to resolve a racemic

solution[17]. Tagagishi and Klotz found that the cross-linking of the polymers in the presence of Methyl Orange resulted in higher adsorption of the dye in the MIPs than in reference polymers[34].

MIPs can be prepared by using a monomer that can interact with the target template to form the monomer-template complexes. After polymerisation and removal of the template, a specific cavity in the polymers that fits the template is expected to be formed. The templates would be theoretically selectively adsorbed into the polymer by interaction with active sites and shape recognition. The polymers can be reused by removing of the template to provide the cavity again (**Figure 6.1**).

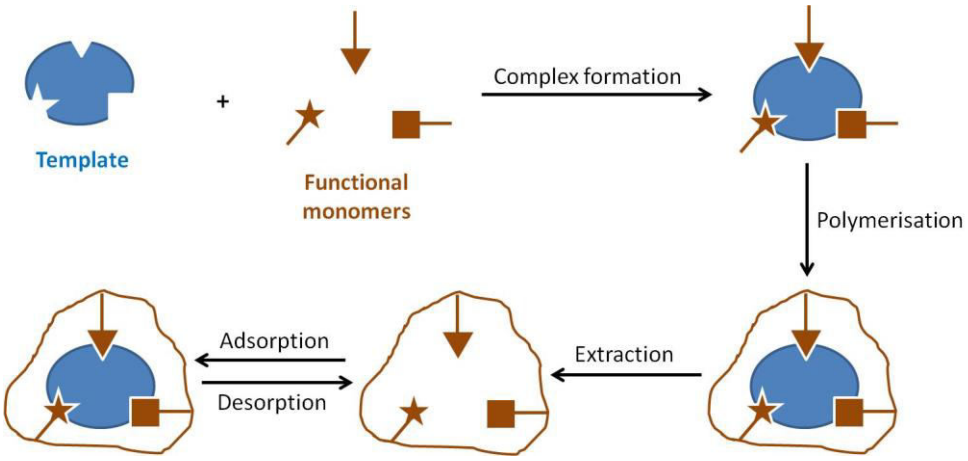

Figure 6.1 General procedure to synthesise MIPs

The interaction between templates and monomers can either be covalent[36] or non-covalent[37] interaction. Covalent bonds have been used in MIPs including boronate esters[17, 38], Schiff bases[39, 40], acetals and ketals[41-43], and esters[44-48]. The covalent bond between templates and monomers is useful only if the templates can be reversibly removed from the polymers. This method has the advantages of utilising strong bonds so harsh conditions can be used for the polymerisation and the fixed configuration of polymers could be obtained leading to more specific cavities. However, the template is normally difficult to remove and also with a slow rate. This leads to the limited range of templates that can be effectively used.

Non-covalent imprinting has been carried out by Mosbach in 1984 to widen the range of templates that could be used in MIPs[49]. Compared to the covalent bond approach, non-covalent bonds such as hydrogen bonding (H-bonding), electrostatic, hydrophobic, and π-π interactions between monomer and template are weaker, which helps in forming the complexes by self-association and means that the templates are easier to extract. More templates can then be applied to form MIPs, even though the structure of the cavity formed may not be as rigid as one prepared by covalent imprinting.[50]

In 1995, Whitcombe utilised the benefits of both methods in the so-called "semi-covalent imprinting"[51]. MIPs were formed using covalently bound template-monomer complexes but non-covalent interactions were used in the rebinding step. This procedure, in theory, allowed the MIPs to align in the predetermined configuration and also rapidly adsorb the templates. However, diffusion still remained the limiting factor. Therefore, porous materials could possibly help to overcome the problem.

In the previous chapter, the post-synthetic modification (PSM) of CMPs was demonstrated. The functional groups in the networks could be modified after polymerisation allowing the properties of the networks to be tuned[52]. Because of the adaptability as well as the rigidity of these polymers, CMPs may have the potential for use in a molecular imprinting application. The porous property of the CMPs might improve the diffusion of analytes to the active site. Another potential advantage of CMPs is that the vinyl group necessary in the conventional polymerisation process used to form MIPs[53] is not required in CMPs synthesis.

Semi-covalent imprinting was used in this research. As CMP synthesis requires harsh condition, covalent interaction, i.e. esters or amides, of templates and functional monomers was selected in polymerisation step. The templates were then removed by hydrolysis. The rebinding of the templates with polymers carried out using non-covalent interactions, where H-bonds between carboxylic acid and hydroxyl (in ester case) or amino (in amide case) was expected to be main interaction. The target templates used in this research were cholesterol, menthol and trimesic acid. The structures of the templates are illustrated in **Figure 6.2**.

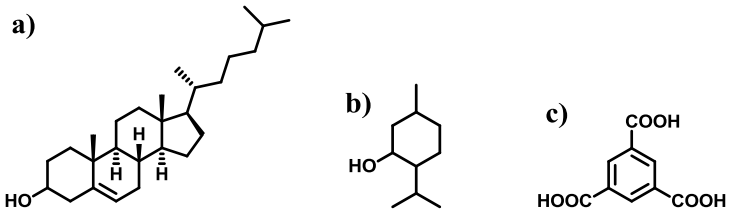

Figure 6.2 Templates used in this research: a) cholesterol, b) menthol, c) trimesic acid (TMA)

6.2 Cholesterol

Cholesterol (**Figure 6.2a**) was considered to be a good target template as it contains a hydroxyl functional group which can interact with a carboxylic acid functional monomer. Cholesterol also has a specific shape, which could lead to a specific cavity being formed.

To begin with, the cholesteryl 2,5-dibromobenzoate monomer (**cholesterol functionalised monomer**) was synthesised from 2,5-dibromobenzoic acid and cholesterol by coupling using DCC and DMAP followed a literature procedure[54] (**Scheme 6.1**).

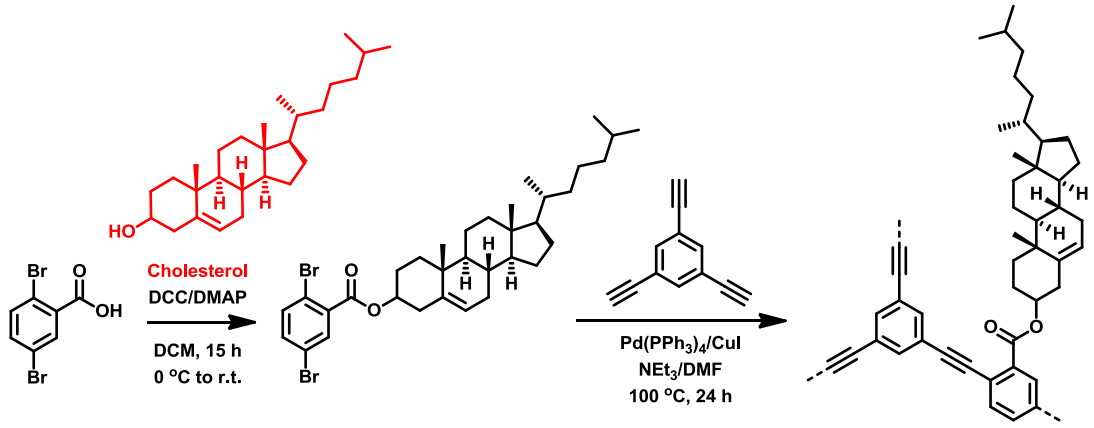

Scheme 6.1 Synthetic scheme for **CHOL-CMP**

The esterification was confirmed by ^{1}H NMR, ^{13}C NMR, IR spectroscopy, elemental analysis and mass spectroscopy. ^{1}H NMR spectra illustrated the shift of the position of the peak of the proton on the same carbon as the hydroxyl group from

3.5 ppm in cholesterol to 4.8 ppm in the cholesteryl 2,5-dibromobenzoate. In the ^{13}C NMR spectra of the starting materials and the product, a shift of the hydroxyl carbon peak from 75 to 79 ppm and of the carbonyl peak from 169 to 167 ppm indicated the success of the esterification. The IR spectrum of the monomer showed the presence of the ester C=O peak at around 1730 cm^{-1} which differed from the carboxylic acid C=O peak at 1705 cm^{-1}. The O-H peak at 3430 cm^{-1} was also not present in the monomer. (**Figure 6.3**) Elemental analysis and mass spectroscopy were in agreement with the theoretical value.

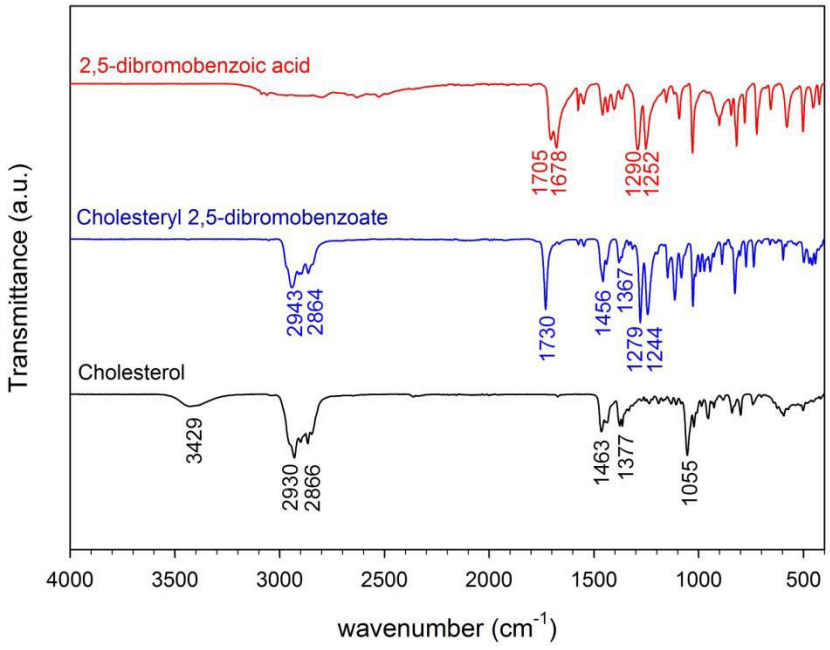

Figure 6.3 IR spectrum of cholesteryl 2,5-dibromobenzoate monomer (**cholesterol functionalised monomer**) (blue) compared to 2,5-dibromobenzoic acid (red) and cholesterol (black)

The cholesteryl 2,5-dibromobenzoate was used to prepare a polymer by reaction with 1,3,5-triethynylbenzene using a Sonogashira-Hagihara reaction to provide **CHOL-CMP** (**Scheme 6.1**). Infrared spectroscopy (IR) was used to confirm the incorporation of both monomers into the network. The spectrum showed the C-H stretching peak of cholesteryl group, C=O stretching of ester and aromatic C=C bending peak around 2900, 1715, and 1400-1600 cm^{-1} respectively. The decrease

intensity of terminal alkyne peak at 2110 cm^{-1} and increase in intensity of the internal alkyne peak at 2206 cm^{-1} compared to the monomers also validated the network formation (**Figure 6.4**).[55, 56]

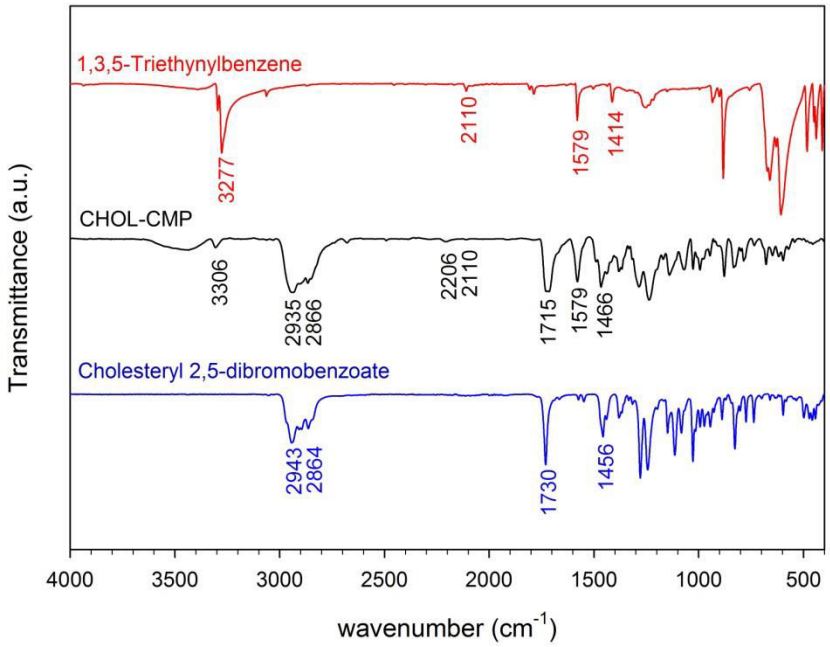

Figure 6.4 IR spectrum of **CHOL-CMP** compared to monomers

We attempted to remove the template using base hydrolysis as shown in **Table 6.1**. IR spectroscopy was again used to determine the success of the template extraction (**Figure 6.5**). For comparison here, the spectrum of **CMP-1-COOH** (**Scheme 6.2**) is shown, which should contain the expected structure of the polymer after hydrolysis.

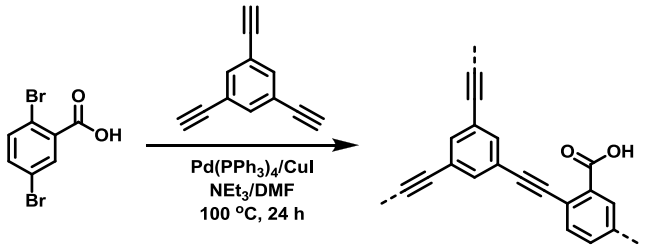

Scheme 6.2 Synthetic scheme for **CMP-1-COOH**

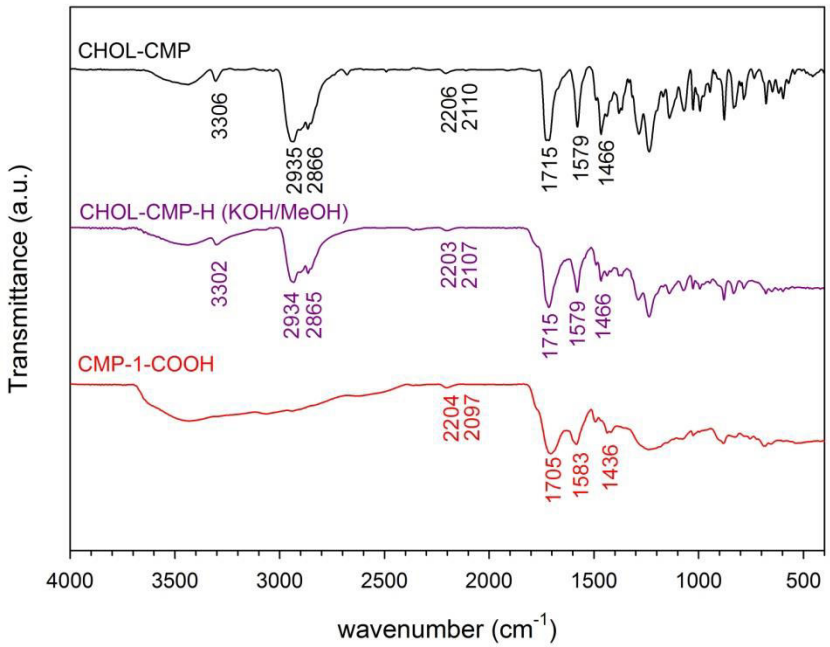

Figure 6.5 IR spectra of **CHOL-CMP** before (black) and after (purple) attempted hydrolysis with KOH/MeOH compared to **CMP-1-COOH** (red)

A common method to hydrolyse the ester bond is the use of base in water. However, after mixing the polymer with NaOH in water ($NaOH/H_2O$), there was no change in the IR spectrum even when the product was re-exposed to the hydrolysis conditions twice. This lack of hydrolysis might due to the hydrophobicity of the polymer. THF was then used as a co-solvent ($NaOH/H_2O/THF$) but hydrolysis was again not found to occur. Lithium hydroxide ($LiOH/H_2O/THF$) was also tried but again without success. The hydrolysis was also unsuccessful using a base in MeOH (LiOH, NaOH or KOH/MeOH). The surface areas of polymers did not significantly change after the attempted reaction (**Table 6.1**).

Table 6.1 Hydrolysis conditions of **CHOL-CMP**

Condition	SA_{BET} before (m^2/g)	SA_{BET} after (m^2/g)	hydrolysed? (by IR)
$NaOH/H_2O$	20	10	No
$NaOH/H_2O$ twice	20	9	No
$NaOH/H_2O$/THF	20	27	No
$LiOH/H_2O$/THF	20	12	No
LiOH/MeOH	4	18	No
NaOH/MeOH	4	9	No
KOH/MeOH	4	41	No

The unsuccessful hydrolysis could be due to the low polarity of the polymer. More polar polymers were then investigated. The cholesteryl benzoate monomer was co-polymerised with a carboxylic acid monomer in a 1:1 ratio to form **CHOL-COOH** (**Scheme 6.3**).

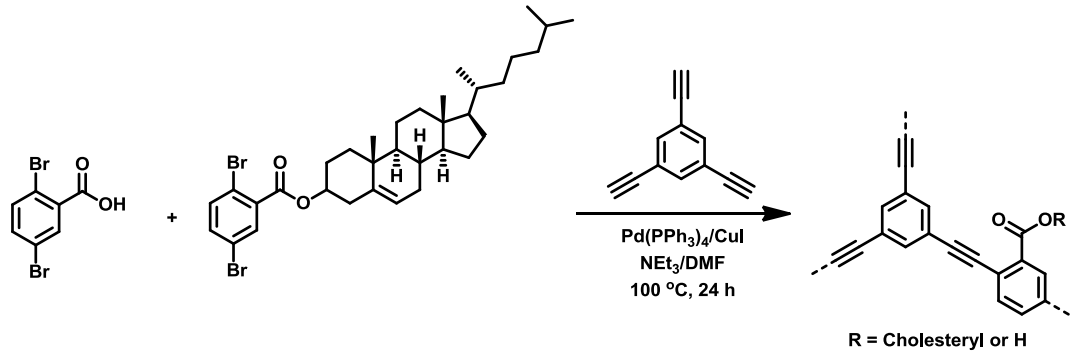

Scheme 6.3 Synthetic scheme for **CHOL-COOH**

The incorporation of the carboxylic acid was difficult to prove because of the similarity of the functional groups. Elemental analysis showed the decrease of H content from 7.64 % in **CHOL-CMP** to 6.50 % in **CHOL-COOH** as expected. The surface area was also improved from non-porous in **CHOL-CMP** to about 133 m^2/g in **CHOL-COOH**. From IR spectra, the shift of C=O stretching of carbonyl peak from 1715 cm^{-1} in **CHOL-CMP** to 1722 cm^{-1} in **CHOL-COOH** as well as the presence of the small peak at 1790 cm^{-1} which might indicate the formation of an

anhydride due to the condensation of carboxylic acid during the polymerisation process. This peak was not found in the **CHOL-CMP**. However, the C-H stretching peaks around 2900 cm^{-1} demonstrated the incorporation of the cholesteryl group in the network. The internal alkyne peak was present at 2206 cm^{-1}. (**Figure 6.6**)

Unfortunately, hydrolysis was again not be achieved according to IR spectra, as illustrated in **Figure 6.6**. A change in the IR spectrum was not observed. The surface area of the polymer after hydrolysis (100 m^2/g) was also unchanged compared to that before hydrolysis (133 m^2/g). This shows that the use of the carboxylic acid monomer did not improve degree of template removal.

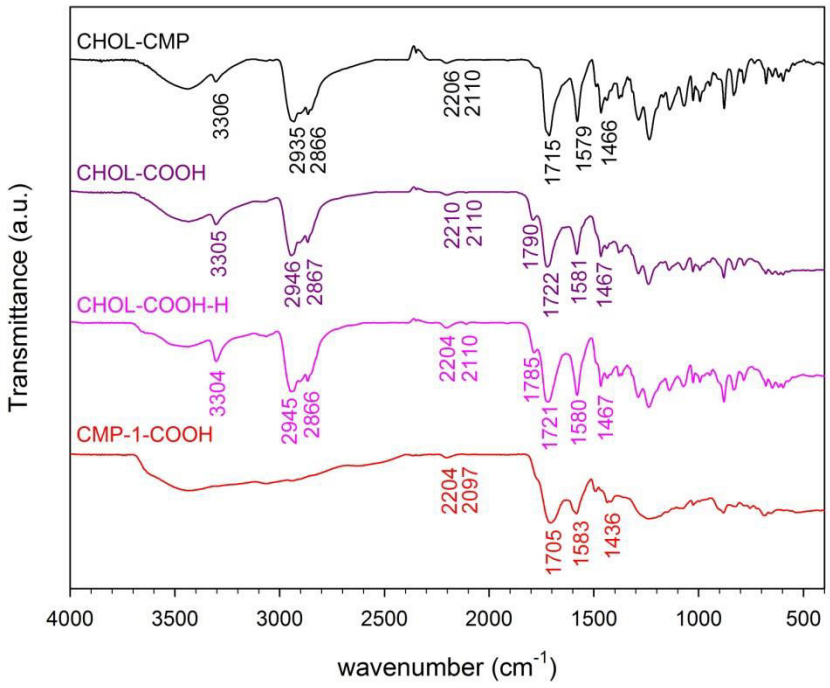

Figure 6.6 IR spectra of **CHOL-COOH** before (purple) and after (pink) attempted hydrolysis compared to **CHOL-CMP** (black) and **CMP-1-COOH** (red)

A 1:1 mixture of the cholesteryl benzoate and a hydroxylated monomer was also used to synthesise **CHOL-OH**. (**Scheme 6.4**)

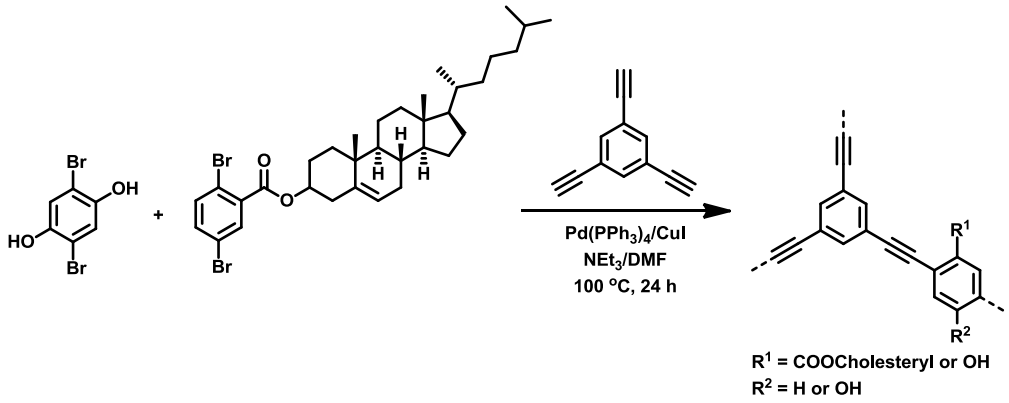

Scheme 6.4 Synthetic scheme for **CHOL-OH**

Again, the incorporation of hydroxyl monomer was difficult to prove because the significant peaks for the monomer in IR spectrum were found in the same region as ester and carboxylic acid groups. The IR spectrum of **CHOL-OH** was, therefore, found similar to that of **CHOL-CMP**. The presence of C-H stretching peaks around 2900 cm^{-1} and internal alkyne at 2202 cm^{-1} showed the incorporation of cholesteryl and alkyne groups. (**Figure 6.7**) The H content analysed from elemental analysis in **CHOL-OH** (6.94 %) was lower than **CHOL-CMP** (7.64 %) and higher than **CHOL-COOH** (6.50 %) as expected.

After attempted hydrolysis, the slight decrease of C-H stretching peak in the 2900 cm^{-1} region suggested some template was removed. However, no significant shift of the carbonyl peak around 1700 cm^{-1} was observed. Elemental analysis showed a slight change in H content from 6.94 % to 5.26 %. There was also a small increase in the surface area from 35 m^2/g of **CHOL-OH** to 51 m^2/g in **CHOL-OH-H**. Therefore, the degree of hydrolysis was still considered to be low.

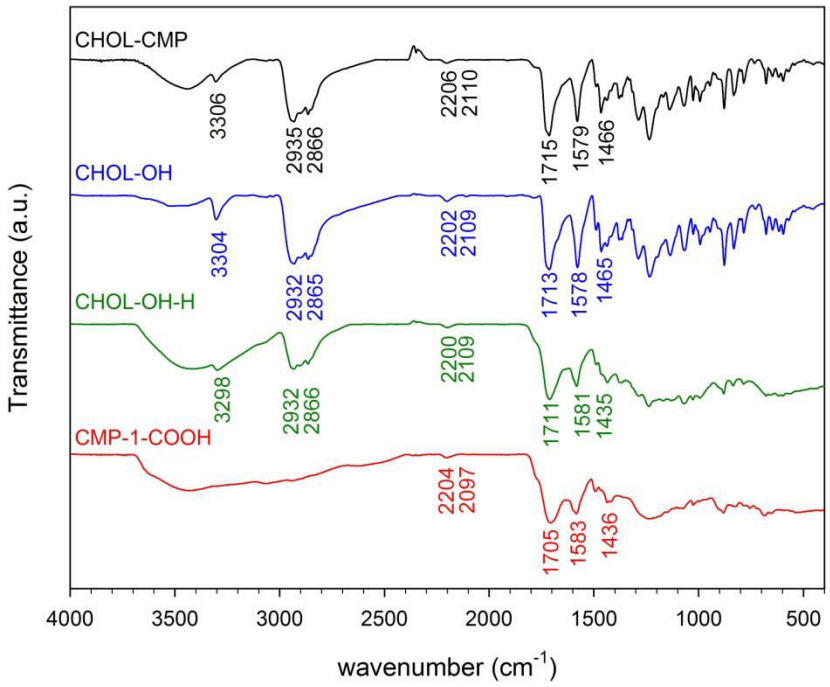

Figure 6.7 IR spectra of **CHOL-OH** before (blue) and after (green) attempted hydrolysis compared to **CHOL-CMP** (black) and **CMP-1-COOH** (red)

The removal of cholesterol from the template might be difficult because cholesterol is quite a large molecule and also has low polarity. Increasing the polarity in **CHOL-COOH** and **CHOL-OH** does not seem to overcome this issue. Thus, a smaller template, menthol, was considered.

6.3 Menthol

Menthol (**Figure 6.2b**) is another molecule containing an alcohol functional group. The smaller size as well as the higher polarity of menthol compared to cholesterol was expected to mean that it would be easier to remove from the networks.

The menthyl 2,5-dibromobenzoate monomer (**menthol functionalised monomer**) and menthyl functionalised polymer were synthesised following the same procedure as **CHOL-CMP** to provide **MENT-CMP** (**Scheme 6.5**).

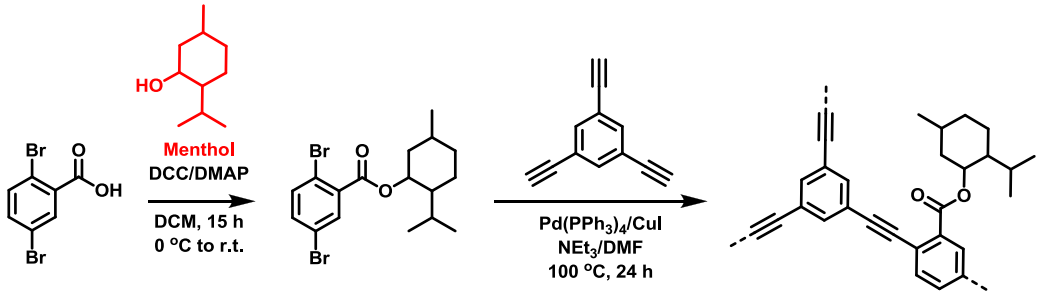

Scheme 6.5 Synthetic scheme for **MENT-CMP**

^{1}H NMR, ^{13}C NMR, IR spectroscopy, elemental analysis and mass spectroscopy were used to characterise the monomer. The peak of the proton on the same carbon as hydroxyl group at 3.4 ppm of menthol in ^{1}H NMR spectra shifted to 5.0 ppm in menthyl 2,5-dibromobenzoate monomer. ^{13}C NMR spectra also exhibited shifts of peaks from the carbons functionalised with the hydroxyl and carbonyl groups from 72 to 76 and 169 to 165 ppm, respectively. IR spectra showed the presence of an ester C=O peak at 1720 cm^{-1} which differs from a peak at about 1705 cm^{-1} for the carboxylic acid peak in the benzoic acid. Additionally, C-H stretching peaks around 2900 cm^{-1} were present and the O-H peak at 3260 cm^{-1} disappeared. (**Figure 6.8**) The agreement of the elemental analysis and mass spectroscopy with the theoretical values also confirmed the success of esterification.

Similarly to **CHOL-CMP**, the C-H stretching around 2900 cm^{-1} and carbonyl C=O stretching at 1713 cm^{-1} in IR spectra were used to confirm the incorporation of the menthyl ester group in the polymer, as well as alkyne peaks around 2100-2200 cm^{-1} validating the incorporation of triethynylbenzene in the network. The intensity of the terminal alkyne peak at 2110 cm^{-1} decreased and intensity of the internal alkyne peak at 2206 cm^{-1} increased compared to the monomer, supporting the evidence of network forming. (**Figure 6.9**)

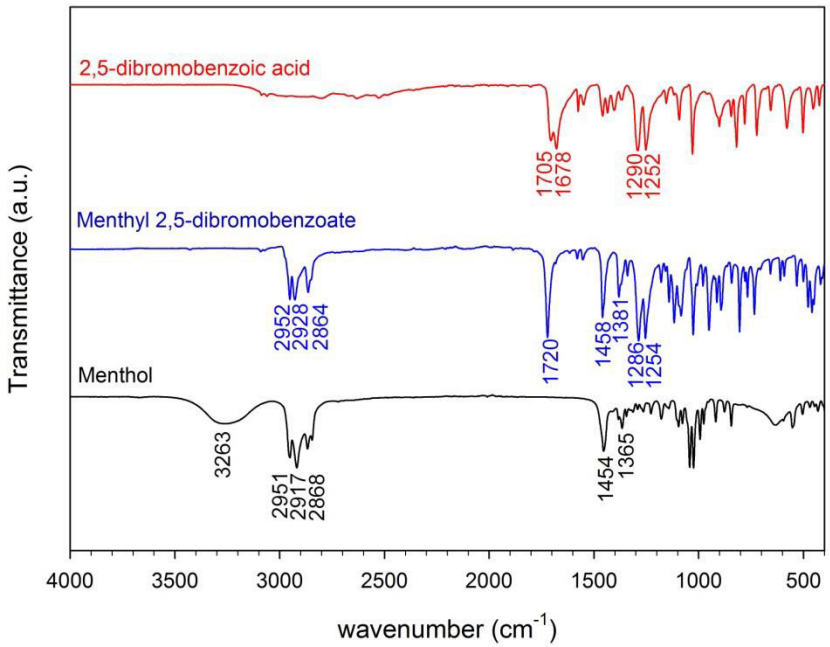

Figure 6.8 IR spectrum of menthyl 2,5-dibromobenzoate monomer (**menthol functionalised monomer**) (blue) compared to 2,5-dribromobenzoic acid (red) and menthol (black)

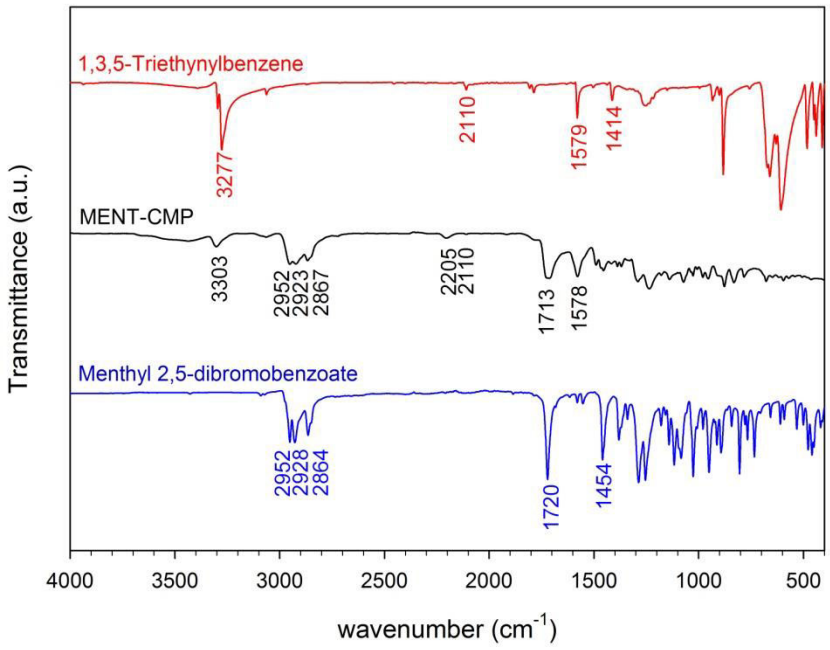

Figure 6.9 IR spectrum of **MENT-CMP** compared to monomers

We tried to remove the template by hydrolysis using the different conditions mentioned in **Table 6.2**, similar to those used for **CHOL-CMP**. According to the IR spectra (**Figure 6.10**), the decrease of the intensity of the C-H stretching peak around 2900 cm^{-1} and shifting of the C=O stretching peak to around 1700 cm^{-1} indicated that KOH in MeOH (KOH/MeOH) performed the most effective method for menthol removal. Again, **CMP-1-COOH** was used as a comparison.

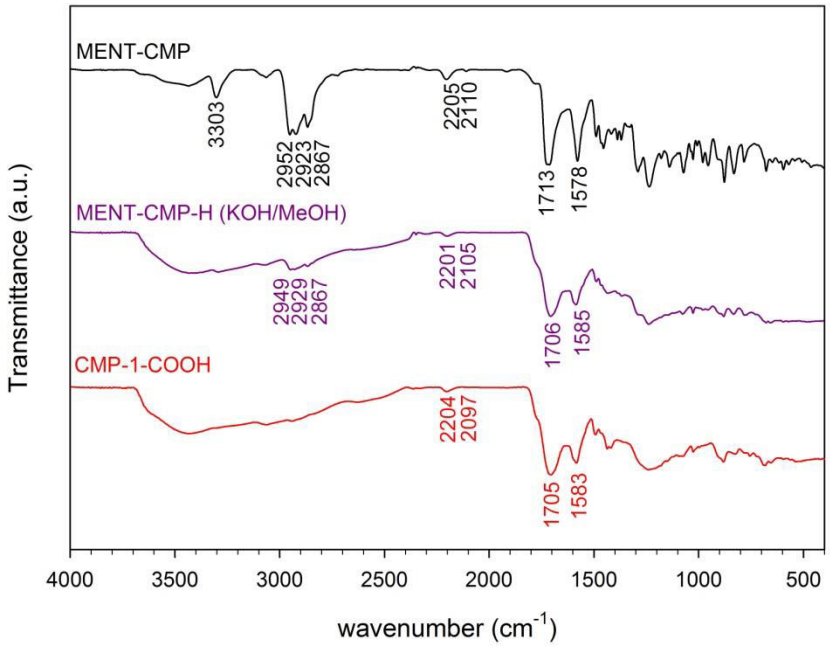

Figure 6.10 IR spectra of **MENT-CMP** before (black) and after (purple) attempted hydrolysis with KOH/MeOH compared to **CMP-1-COOH** (red)

Table 6.2 Hydrolysis conditions of **MENT-CMP**

Condition	SA_{BET} before (m^2/g)	SA_{BET} after (m^2/g)	hydrolysed (by IR)
$NaOH/H_2O$	53	65	No
$LiOH/H_2O/THF$	53	32	No
$NaOH/H_2O/THF$	53	15	No
$KOH/H_2O/THF$	53	14	No
KOH/MeOH	53	22	Yes

However, after hydrolysis the **MENT-CMP** had a low surface area. The copolymerisation was found to be a way to improve the surface areas of the networks. The work carried out by Jiang *et al.* showed that the porosity of the networks could be tuned by copolymerisation.[57] As **non-functionalised monomer** provided high surface area network, CMP-1[55], the copolymerisation of **menthol functionalised monomer** with a **non-functionalised monomer** was then expected to improve the surface area.

6.3.1 Menthol-Non-functionalised copolymers (MENT-Hs)

Menthyl 2,5-dibromobenzoate (**menthol functionalised monomer**) was used to prepare the copolymers with 2,5-dibromobenzene (**non-functionalised monomer**) in five different ratios, i.e. 0%, 25%, 50%, 75% and 100%, by Sonogashira-Hagihara couplings, following the general procedure to obtain **MENT-Hs**. The networks were named as **MENT-H-x** where x referred to percentage of **menthol functionalised monomer**. (**Scheme 6.6**)

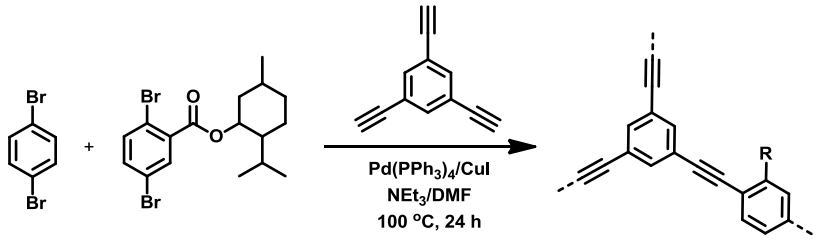

Scheme 6.6 Synthetic scheme for **MENT-Hs**

The IR spectra in **Figure 6.11** demonstrated the increase of the C-H stretching intensity of the menthyl group at around 2900 cm^{-1} and the C=O stretching peak at around 1726 cm^{-1} as a higher percentage of **menthol fuctionalised monomers** was included in the reaction mixture. The peaks in both regions indicated the incorporation of the menthyl ester group in the polymers. Alkyne peaks at around 2100-2200 cm^{-1} also confirmed the presence of 1,3,5-triethynylbenzene in the networks. Elemental analysis, as expected, also showed the decrease of C content

and increase of H content when higher ratio of **menthol functionalised monomer** was used. The N content in the network could be from residual DMF, NEt_3 or nitrogen adsorbed in the networks. The surface areas of the polymers were improved on increasing the ratio of the **non-functionalised monomer**. (**Table 6.3**)

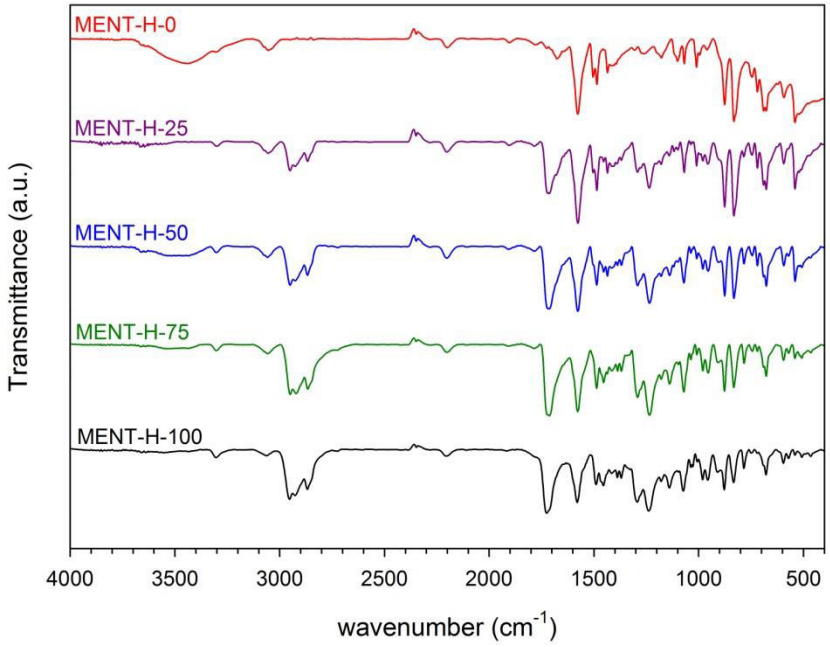

Figure 6.11 IR spectra of **MENT-Hs** before hydrolysis

Table 6.3 Yields, elemental analysis and gas sorption data of **MENT-Hs**

Sample	Yield (%)	Theory (%)			Analysis (%)			SA_{BET} (m^2/g)
		C	H	N	C	H	N	
MENT-H-0	121	96.84	3.16	0.00	84.02	3.75	0.25	860
MENT-H-25	97	92.71	4.31	0.00	83.08	4.48	0.26	445
MENT-H-50	92	89.78	5.13	0.00	83.29	5.01	0.00	393
MENT-H-75	103	87.59	5.74	0.00	82.01	5.71	0.20	326
MENT-H-100	99	85.89	6.21	0.00	81.21	6.10	0.33	99

After that, the menthol template was removed by hydrolysis using KOH/MeOH at 35 ^{o}C for 24 hours providing **MENT-Hs**. The polymers were called **MENT-H-xH** where x was the percentage of **menthol functionalised monomer**. From **Figure 6.12**, the IR results showed the decrease of C-H stretching intensity around 2900 cm^{-1} of the menthyl group and the shift of carbonyl peak from 1726 to 1718 cm^{-1} indicating the removal of template. The peaks at 2204 and 2107 cm^{-1} demonstrated the presence the alkyne group in the networks. The increase in intensity of the carbonyl peaks when a higher ratio of **menthol functionalised monomers** was used was also observed.

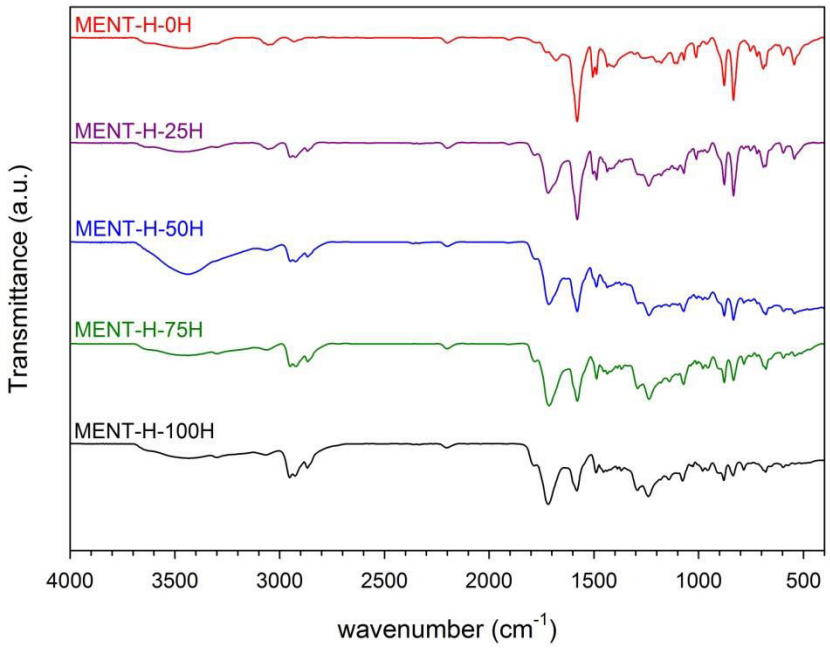

Figure 6.12 IR spectra of **MENT-Hs** after hydrolysis (**MENT-H-Hs**)

The increase of surface areas after hydrolysis implied the success of the template extraction. The elemental analysis also showed the reduction of H content in the networks as expected after networks were hydrolysed. However, when a higher amount of **menthol functionalised monomer** was used, it seems that the hydrolysis was less successful as can be seen in less H content decrease. (**Table 6.4**)

Table 6.4 Yields, elemental analysis and gas sorption data of **MENT-H-Hs**

Sample	Yield (%)	Theory (%)			Analysis (%)			SA_{BET} (m^2/g)
		C	H	N	C	H	N	
MENT-H-0H	73	96.84	3.16	0.00	83.43	3.78	0.00	1035
MENT-H-25H	88	93.57	3.01	0.00	82.73	4.15	0.00	832
MENT-H-50H	98	90.60	2.88	0.00	80.75	4.41	0.00	654
MENT-H-75H	110	87.88	2.75	0.00	79.41	4.63	0.00	328
MENT-H-100H	121	85.39	2.64	0.00	78.27	4.78	0.26	540

6.3.2 Menthol adsorption in MENT-Hs

A menthol adsorption measurement was performed by soaking 25 mg of the polymer into 1 mL menthol solution. The menthol solution was prepared by dissolving 1 mg of menthol into 1 mL of hexane. The concentration of menthol in the solution was measured by gas chromatography (GC) using decanol as an internal standard. **Figure 6.13** shows an example chromatogram obtained from the GC. The GC results showed a good separation of the menthol and decanol peaks, as well as the separation of the menthol enantiomers.

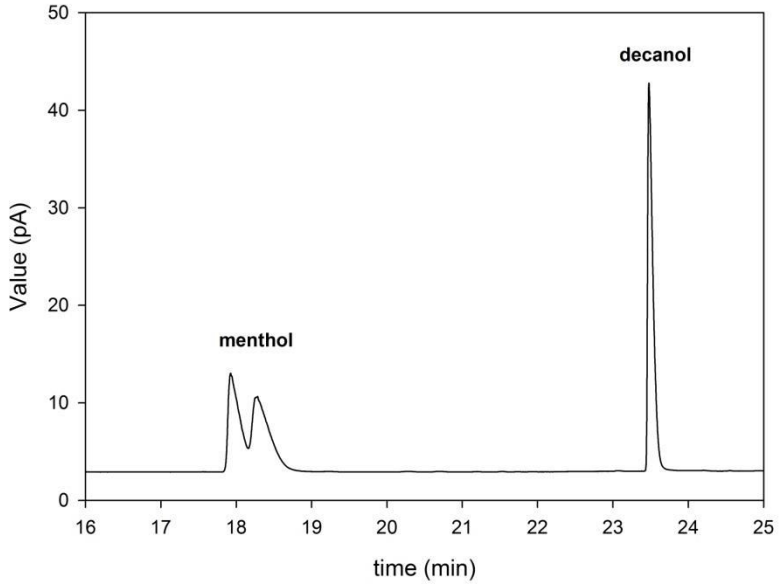

Figure 6.13 GC chromatogram of menthol (left) and decanol (right)

A calibration curve (**Figure 6.14**) was obtained by measuring the peak areas at different concentrations of menthol solutions comparing to decanol. The amount of menthol adsorbed inside the polymers could be calculated by the difference of initial concentration of menthol solution (1 mg/mL) and the concentration of menthol left in the solution after binding experiment.

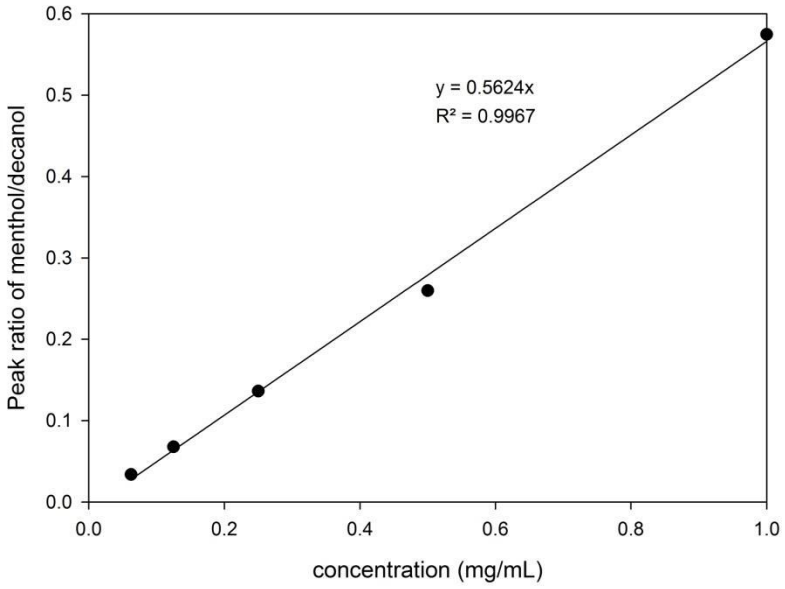

Figure 6.14 Calibration curve of menthol in hexane calculated by GC using decanol as an internal standard

The surface areas and the amount of menthol adsorbed in the polymers of **MENT-Hs** is summarised in **Table 6.5**. Menthol was assumed to rebind with the polymer by the non-covalent interaction i.e. H-bonding between hydroxyl group in menthol and carboxylic acid group in the network. Although the surface areas increased with higher ratio of non-functionalised monomer, the menthol uptakes decreased. This could be because when more non-functionalised monomer was used, there were fewer carboxylic acid binding sites leading to fewer interactions with menthol. This suggests that the carboxylic acid group plays an important role in the interaction with menthol.

Table 6.5 Surface areas and menthol adsorption of **MENT-H-Hs**

Sample	SA_{BET} (m^2/g)	Amount of menthol adsorbed (%)
MENT-H-0H	1035	64
MENT-H-25H	832	64
MENT-H-50H	654	67
MENT-H-75H	328	75
MENT-H-100H	540	79

6.3.3 Menthol-Carboxylic acid functionalised copolymers (MENT-COOHs)

To control the number of active binding sites, i.e. carboxylic acid group, the carboxylic acid functionalised monomer was copolymerised with the menthol functionalised monomer using 1,3,5-triethnylbenzene as a node. The menthyl 2,5-dibromobenzoate (**menthol functionalised monomer**) was used to prepare the copolymers with 2,5-dibromobenzoic acid (**carboxylic acid functionalised monomer**) in five different ratio: 0%, 25%, 50%, 75% and 100% using the same conditions as described above for the non-functionalised monomer to obtain **MENT-COOHs**. The networks were labelled as **MENT-COOH-x** where x indicated the percentage of **menthol functionalised monomer**. (**Scheme 6.7**)

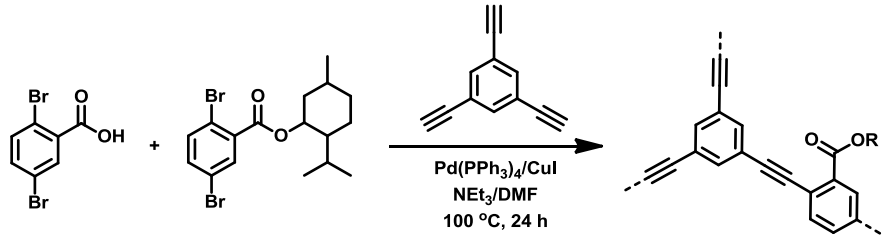

Scheme 6.7 Synthetic scheme for **MENT-COOHs**

The IR spectra shown in **Figure 6.15** demonstrated the increase of the C-H stretching intensity of menthyl group around 2900 cm^{-1} with increase ratio of

menthol functionalised monomers and the small shift of C=O stretching around 1720 cm^{-1}. Alkyne peaks around 2100-2200 cm^{-1} indicated the incorporation of 1,3,5-triethynylbenzene in the networks.[55] Elemental analysis showed the increase of C and H content when higher ratio of **menthol functionalised monomer** was used as expected. N content in the network could be from the residue of DMF, NEt_3 or nitrogen adsorbed in the networks. The surface areas of the polymers decreased as more benzoic acid monomer was used. (**Table 6.6**)

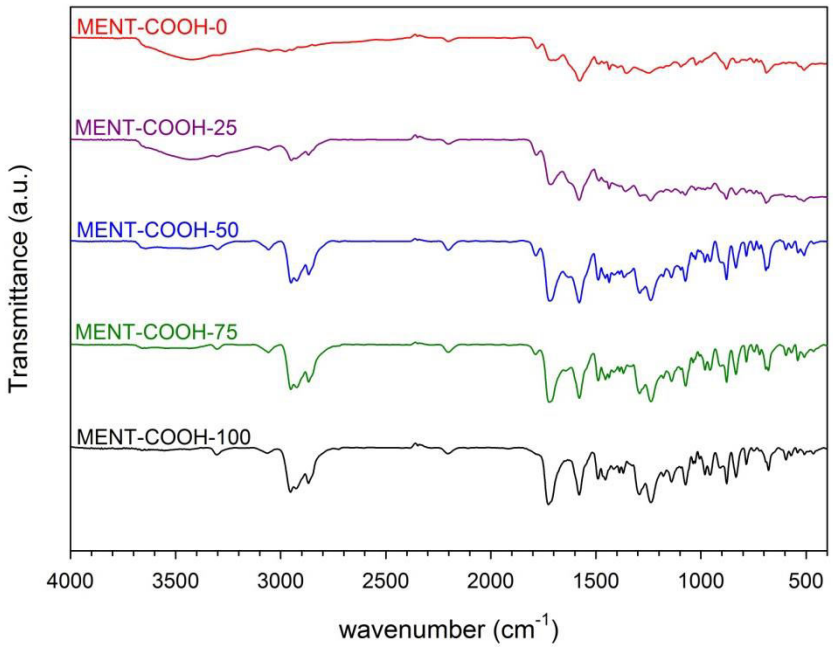

Figure 6.15 IR spectra of **MENT-COOHs** before hydrolysis

Table 6.6 Yields, elemental analysis and gas sorption data of **MENT-COOHs**

Sample	Yield (%)	Theory (%)			Analysis (%)			SA_{BET} (m^2/g)
		C	H	N	C	H	N	
MENT-COOH-0	110	85.39	2.64	0.00	72.91	4.38	1.15	53
MENT-COOH-25	115	85.56	3.84	0.00	75.85	4.83	0.91	212
MENT-COOH-50	112	85.69	4.79	0.00	79.20	5.30	0.51	295
MENT-COOH-75	105	85.80	5.57	0.00	80.69	5.67	0.31	492
MENT-COOH-100	97	85.89	6.21	0.00	81.21	6.10	0.33	512

After that, the menthol templates were removed by hydrolysis using KOH/MeOH at 35 ^{o}C to obtain **MENT-COOH-Hs**. The polymers were called **MENT-COOH-xH** where x specified the percentage of **menthol functionalised monomer** used to synthesise the networks. In **Figure 6.16**, the IR results illustrated the shift of the C=O peaks to 1718 cm^{-1} and the decrease of C-H stretching intensity around 2900 cm^{-1} of menthyl group indicating the achievement of menthol extraction from the polymers. Again, the degree of hydrolysis seemed to be less when the higher ratio of **menthol functionalised monomer** was used.

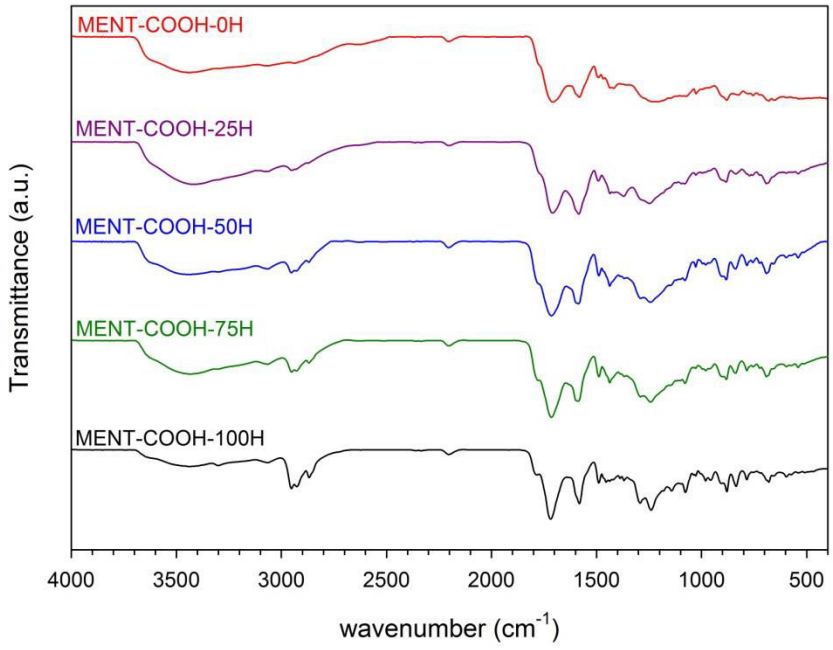

Figure 6.16 IR spectra of **MENT-COOHs** after hydrolysis (**MENT-COOH-Hs**)

Elemental analysis showed the reduction of C and H content in the networks after hydrolysis. When a higher percentage of the **menthol functionalised monomer** was used, a greater C and H content was found in the networks which was in agreement with the IR results. The increase of surface areas after hydrolysis also confirmed the achievement of template extraction. The surface areas decreased as the ratio of **carboxylic acid functionalised monomer** increased. (**Table 6.7**)

Table 6.7 Yields, elemental analysis and gas sorption data of **MENT-COOH-Hs**

Sample	Yield (%)	Theory (%)			Analysis (%)			SA_{BET} (m^2/g)
		C	H	N	C	H	N	
MENT-COOH-0H	68	85.39	2.64	0.00	72.17	3.43	0.00	116
MENT-COOH-25H	65	85.39	2.64	0.00	70.10	3.77	0.25	343
MENT-COOH-50H	75	85.39	2.64	0.00	74.20	3.81	0.00	443
MENT-COOH-75H	81	85.39	2.64	0.00	74.49	3.98	0.00	509
MENT-COOH-100H	91	85.39	2.64	0.00	78.27	4.78	0.26	540

The menthol adsorption measurement was performed following the same procedure as **MENT-Hs**. For the **MENT-COOH** networks, the menthol adsorptions were high as around 90 %. Similar menthol capacities could due to the similar number of binding sites in the polymers. The surface areas showed little effect on the menthol capture. (**Table 6.8**)

Table 6.8 Surface areas and menthol adsorption of **MENT-COOH-Hs**

Sample	SA_{BET} (m^2/g)	Amount of menthol adsorbed (%)
MENT-COOH-0H	116	95
MENT-COOH-25H	343	94
MENT-COOH-50H	443	96
MENT-COOH-75H	509	92
MENT-COOH-100H	540	78

6.3.4 Different concentrations of menthol solution

The effect of the solution concentration on the amount of menthol adsorbed in the networks was also studied. Menthol in hexane solutions were prepared in different concentrations i.e. 1, 2.5, 5, and 10 mg/mL. Polymers were added to the menthol solutions and left overnight. Similar to previous experiment, the amount of

menthol adsorption was calculated from the GC data. No repeat measurement was carried out as only rough idea is needed for further experiment.

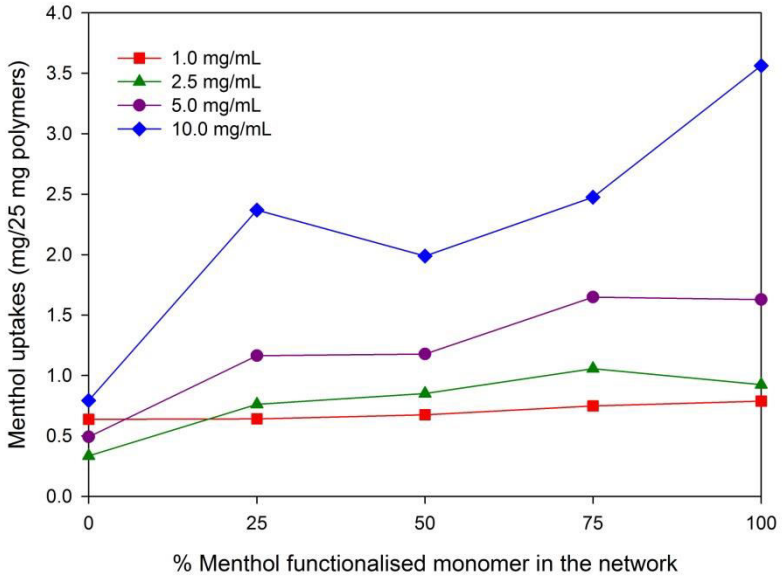

Figure 6.17 Amount of menthol adsorbed in **MENT-H-Hs** when different concentrations of menthol solutions were used

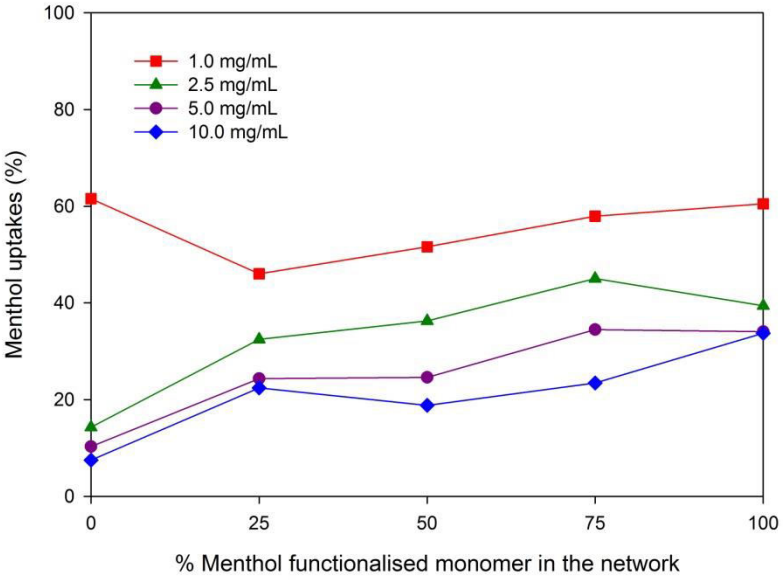

Figure 6.18 Percentage of menthol adsorbed in **MENT-H-Hs** when different concentrations of menthol solutions were used

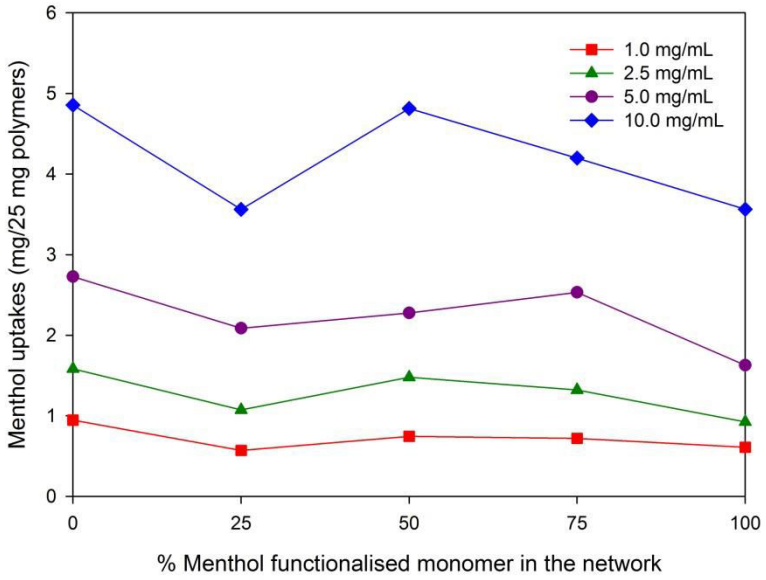

Figure 6.19 Amount of menthol adsorbed in **MENT-COOH-Hs** when different concentrations of menthol solutions were used

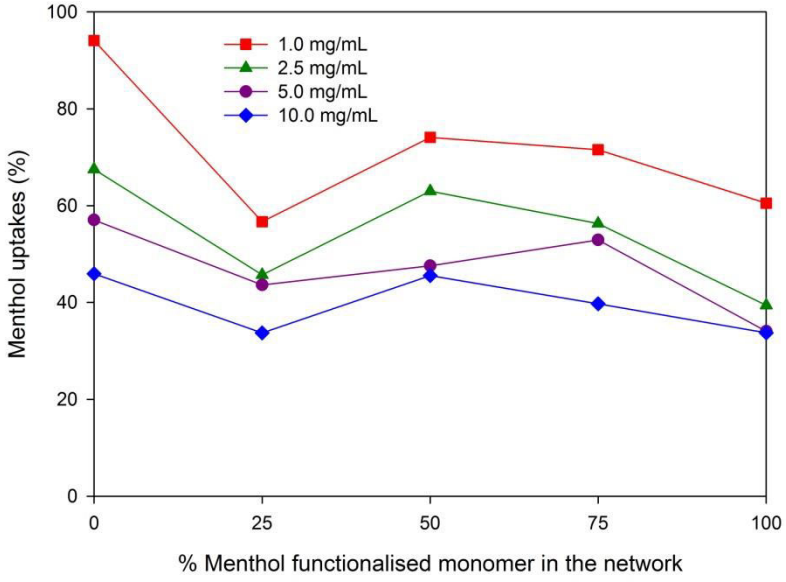

Figure 6.20 Percentage of menthol adsorbed in **MENT-COOH-Hs** when different concentrations of menthol solutions were used

For both **MENT-H-Hs** and **MENT-COOH-Hs**, more menthol was adsorbed when the higher concentration solutions were used. However, if comparing to the starting concentration as a percentage, the lower concentration of solution showed a higher overall percentage adsorption. Therefore, 1 mg/mL of menthol solution was used throughout the experiments.

6.3.5 Selectivity of menthol over terpinolene

The selectivity of materials to menthol was investigated by using terpinolene as a comparison. Terpinolene has a similar chemical structure to menthol but contains no hydroxyl group. This made terpinolene a good candidate to measure the selectivity of MIPs towards menthol. A menthol solution in hexane (2 mg/mL) was mixed with a terpinolene solution in hexane (2 mg/mL) in 1:1 ratio. The solution (1 mL) was then added to the polymers (25 mg). GC was used to measure the concentration of menthol and terpinolene left in the solution using decanol as an internal standard. Then, the amount of menthol and terpinolene adsorbed in networks and the selectivity of menthol over terpinolene could be calculated.

For **MENT-Hs**, the terpinolene uptakes increased with the increase in the content of the **menthol functionalised monomer**. This could possibly be resulting from the shape recognition of the network to the terpinolene as it had similar structure as menthol. When a higher ratio of the **menthol functionalised monomer** was used to form the network, the number of pockets that are specific to the shape of such a compound was expected to increase. However, the terpinolene adsorption was observed to be lower than for menthol. Unfortunately, the selectivity of the networks with a high proportion of the **menthol functionalised monomer** was lower than the control (**MENT-H-0H; CMP-1**). This could imply that shape recognition also plays an important role in imprinting network as less menthol and terpinolene could be adsorbed in the **MENT-H-0H** comparing to the imprinting ones. (**Figure 6.21**)

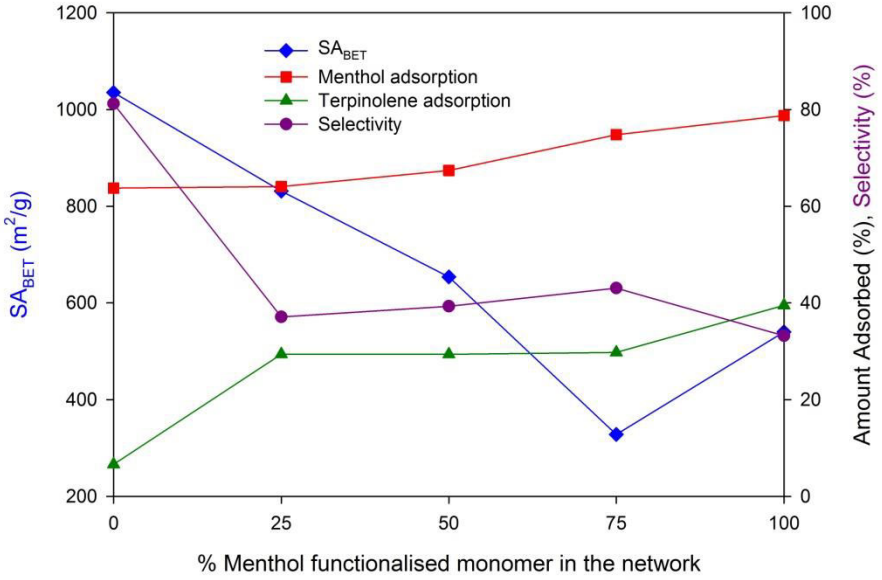

Figure 6.21 Left axis: surface areas of **MENT-H-Hs** (blue). Right axis: their menthol (red) and terpinolene (green) adsorption and selectivity of menthol over terpinolene (purple).

Similarly, the copolymers of **menthol functionalised** and **carboxylic functionalised monomers** (**MENT-COOHs**) showed a selectivity of menthol over terpinolene. However, the selectivity was less than for that of the control network (**MENT-COOH-0H; CMP-1-COOH**). The menthol capacities in **MENT-COOHs** were similar. However, the amount of terpinolene adsorption increased when a higher percentage of the **menthol functionalised monomer** were used to form the networks. Therefore, the selectivity was less than that of the carboxylic acid networks (**MENT-COOH-0H**). (**Figure 6.22**)

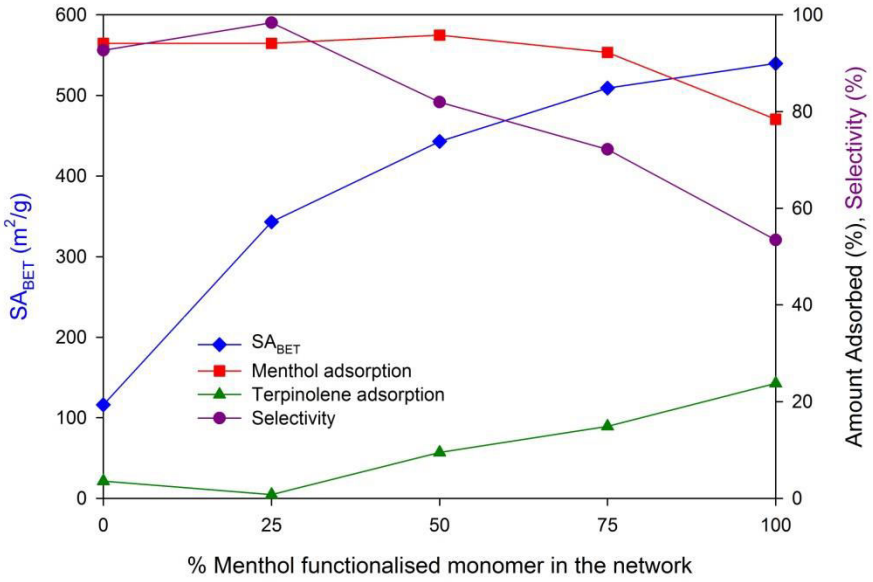

Figure 6.22 Left axis: surface areas of **MENT-COOH-Hs** (blue). Right axis: their menthol (red) and terpinolene (green) adsorption and selectivity of menthol over terpinolene (purple).

If **MENT-Hs** and **MENT-COOHs** were compared, more menthol could be adsorbed in **MENT-COOHs** than in **MENT-Hs**, even though the surface areas tended to be lower (**Figure 6.26**). This could imply that the effect of chemical interaction was stronger than the accessibility effect. On the other hand, terpinolene adsorption was higher in **MENT-H** networks than in **MENT-COOHs** (**Figure 6.27**). Absorption might rely on the higher surface areas of **MENT-Hs** than **MENT-COOHs**. As a result, the **MENT-COOHs** demonstrated a higher selectivity of menthol over terpinolene than **MENT-Hs** (**Figure 6.28**). However, a lower selectivity was found compared to the control materials.

6.3.6 Tetrahedral Monomers (T-MENT-COOHs)

We hypothesised that the networks formed above might be insufficiently shape-persistent and rigid leading to the low selectivities observed. Hence, the tetrahedral monomer, tetrakis(4-ethynylphenyl)methane, was used instead of 1,3,5-triethynylbenzene, which was expected to rigidify the networks.[58] The preparation of

the polymers followed the general procedure. As **MENT-COOHs** showed the better selectivity to menthol than **MENT-Hs**, the copolymerisation of **carboxylic acid functionalised** and **menthol functionalised monomers** with tetrakis(4-ethynylphenyl)methane was carried out in different ratios i.e. 0%, 25%, 50%, 75% and 100%, by Sonogashira-Hagihara reactions to obtain tetrahedral networks (**T-MENT-COOHs**). The networks were named as **T-MENT-COOH-x** where x referred to percentage of **menthol functionalised monomer**. (**Scheme 6.8**)

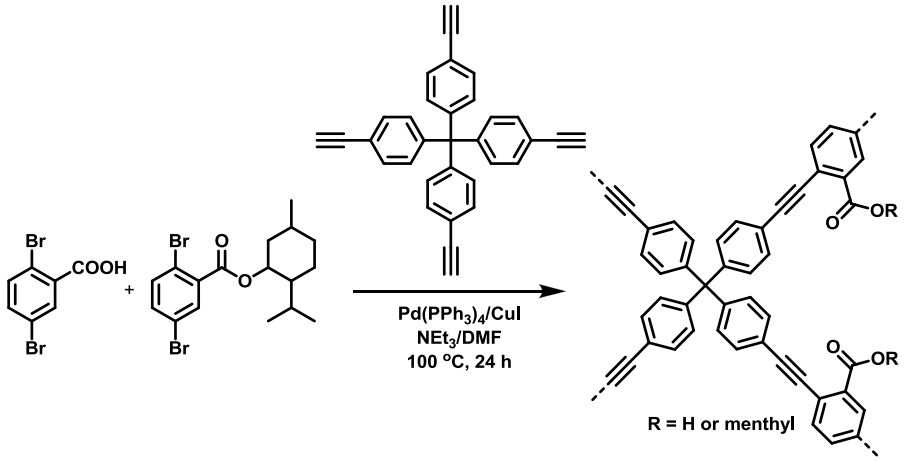

Scheme 6.8 Synthetic scheme for **T-MENT-COOHs**

The IR spectra (**Figure 6.23**) exhibited the increase of the C-H stretching intensity of menthyl group around 2900 cm^{-1} with increase ratio of **menthol fuctionalised monomers**. C=O stretching peaks were also observed in all spectra. The incorporation of tetrakis(4-ethynylphenyl)methane in the networks was indicated by alkyne peaks around 2100-2200 cm^{-1}. As expected, elemental analysis demonstrated the higher C and H contents in **T-MENT-COOH** when the percentage of **menthol functionalised monomer** was increased. The networks before hydrolysis were found to be essentially non-porous. (**Table 6.9**)

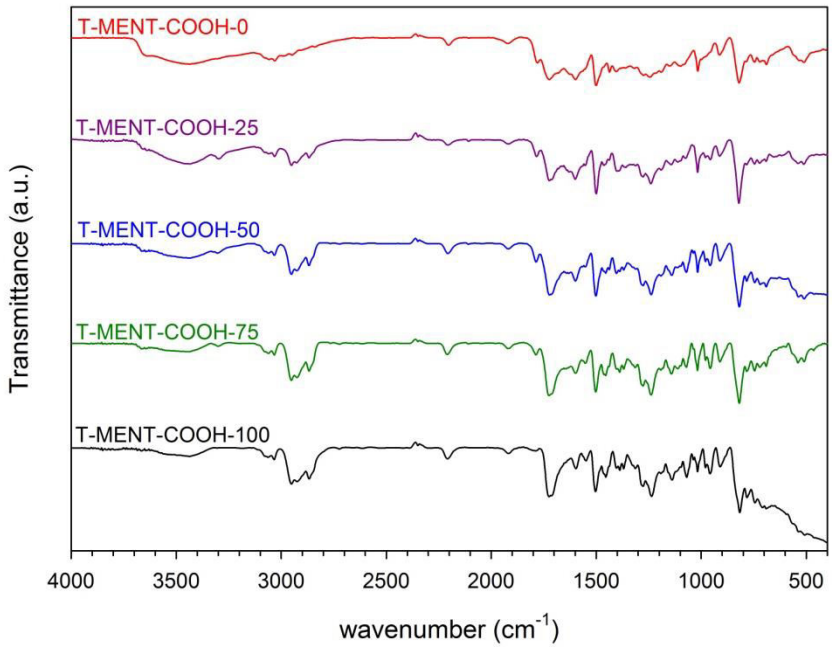

Figure 6.23 IR spectra of **T-MENT-COOHs** before hydrolysis

Table 6.9 Yields, elemental analysis and gas sorption data of **T-MENT-COOHs**

Sample	Yield (%)	Theory (%)			Analysis (%)			SA_{BET} (m^2/g)
		C	H	N	C	H	N	
T-MENT-COOH-0	109	86.49	3.71	0.00	75.09	4.22	0.44	34
T-MENT-COOH-25	115	86.53	4.61	0.00	75.30	4.88	0.50	109
T-MENT-COOH-50	108	86.56	5.35	0.00	80.05	5.36	0.08	45
T-MENT-COOH-75	109	86.58	5.98	0.00	77.94	5.63	0.00	107
T-MENT-COOH-100	102	86.60	6.51	0.00	81.54	6.10	0.00	85

Menthol templates were hydrolysed using KOH/MeOH at 35 ^{o}C. IR spectroscopy (**Figure 6.24**) was used to monitor the achievement of hydrolysis. The shift of the C=O peaks from about 1724 to 1715 cm^{-1} and the decrease of C-H stretching intensity around 2900 cm^{-1} of menthyl group were observed. Alkyne peaks around 2100-2200 cm^{-1} were still observed in the polymers.

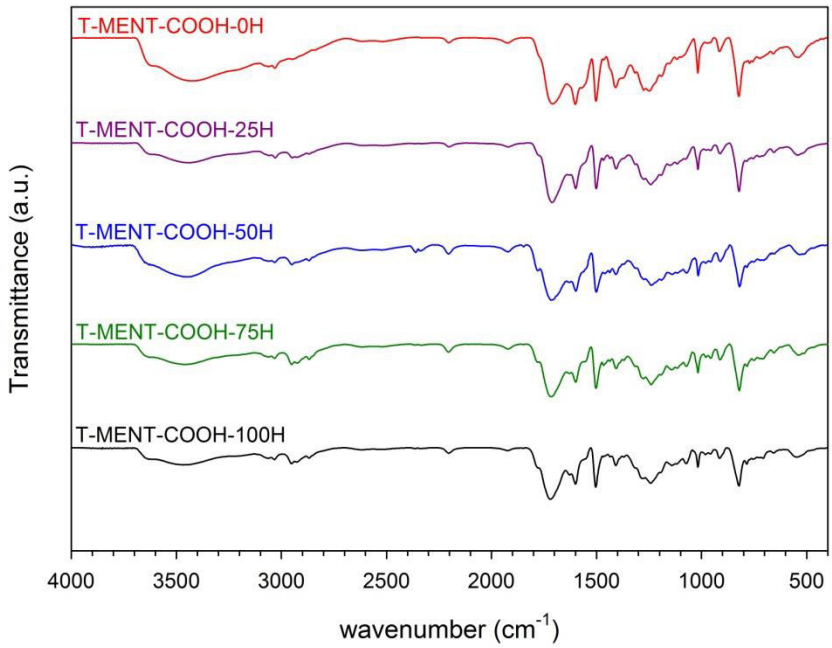

Figure 6.24 IR spectra of **T-MENT-COOHs** after hydrolysis (**T-MENT-COOH-Hs**)

After hydrolysis, **T-MENT-COOH-Hs** showed higher surface areas compared to before hydrolysis. Similar to **MENT-COOHs**, the surface areas increased with as increase in the ratio of the **menthol functionalised monomer**. (**Table 6.10**) Elemental analysis demonstrated the decrease of C and H contents indicated the success of template removals.

Table 6.10 Yields, elemental analysis and gas sorption data of **T-MENT-COOH-Hs**

Sample	Yield (%)	Theory (%)			Analysis (%)			SA_{BET} (m^2/g)
		C	H	N	C	H	N	
T-MENT-COOH-0H	68	86.49	3.71	0.00	70.70	4.20	0.00	191
T-MENT-COOH-25H	46	86.49	3.71	0.00	72.39	4.14	0.00	291
T-MENT-COOH-50H	79	86.49	3.71	0.00	75.78	4.35	0.00	138
T-MENT-COOH-75H	76	86.49	3.71	0.00	74.56	4.38	0.00	311
T-MENT-COOH-100H	92	86.49	3.71	0.00	75.26	4.10	0.00	462

The adsorption data of **T-MENT-COOHs** was summarised in **Table 6.11**. The menthol adsorptions were similar in **T-MENT-COOH-Hs**. More than 90 % of menthol could be encapsulated. The terpinolene adsorptions increased when higher percentage of **menthol functionalised monomers** were used. However, only up to 11 % could be adsorbed. Similarly to the **MENT-COOHs** and **MENT-Hs**, menthol was adsorbed more than terpinolene. Nevertheless, the amount of menthol adsorbed was similar but the amounts of terpinolene adsorbed increased with an increase of the ratio of the **menthol functionalised monomer**, and the selectivities were found to be lower than for the control polymer (**T-MENT-COOH-0H**). (**Figure 6.25**)

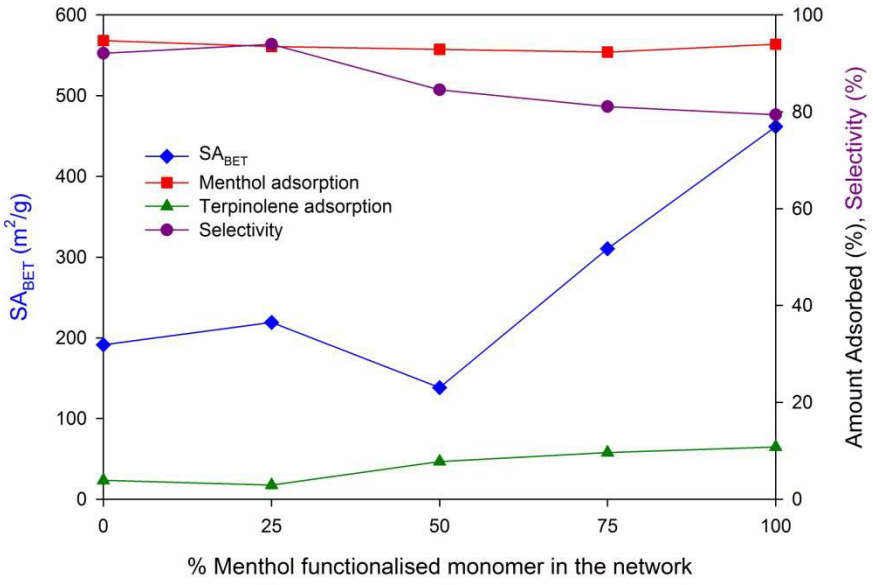

Figure 6.25 Left axis: surface areas of **T-MENT-COOH-Hs** (blue). Right axis: their menthol (red) and terpinolene (green) adsorption and selectivity of menthol over terpinolene (purple).

Comparing **MENT-Hs**, **MENT-COOHs**, and **T-MENT-COOHs**, more menthol could be adsorbed in the copolymers with carboxylic acid i.e. **MENT-COOHs** and **T-MENT-COOHs** than with non-functionalised ones, **MENT-Hs**. Changing the alkyne monomer had no significant effect on the adsorption. (**Figure 6.26**)

Terpinolene was adsorbed less than menthol. It was trapped by **MENT-Hs** better than **MENT-COOHs** and **T-MENT-COOHs**. The higher adsorption could due to the higher surface areas of these networks. Therefore, we hypothesise that the compound could diffuse and access the pore easier than in the networks with lower surface areas. The higher amount of terpinolene encapsulation when higher ratios of **menthol functionalised monomers** were used possibly resulted from the shape recognition of the pores due to the similarity in shape of terpinolene and menthol. (**Figure 6.27**)

Selectivity of copolymers with carboxylic acid functionalised monomers (**MENT-COOHs** and **T-MENT-COOHs**) demonstrated a higher selectivity to menthol compared to non-functionalised copolymers (**MENT-Hs**). This could be because of the higher number of carboxylic acids in the networks after hydrolysis, which led to the higher numbers of interactive groups for menthol adsorption. However, compared to the control polymers, the imprinted polymers showed lower selectivity. (**Figure 6.28**) As the materials did not show the promising selectivity, no repeat measurement was carried out.

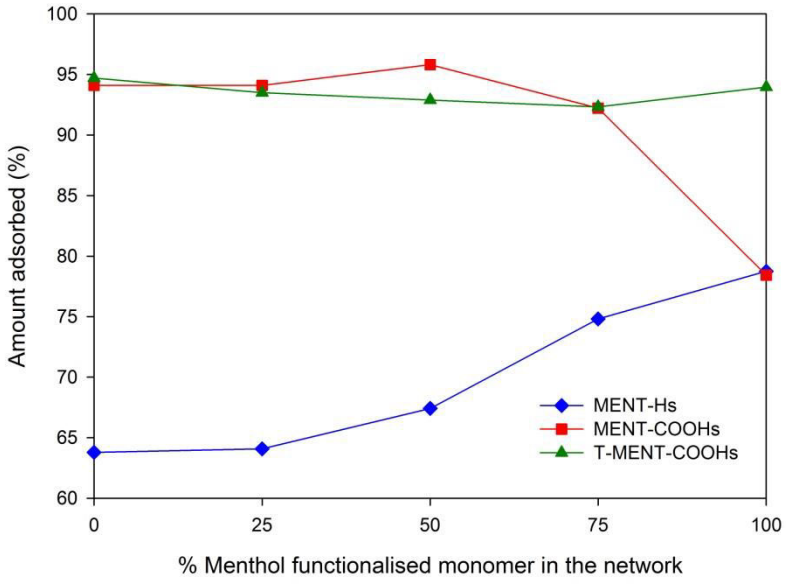

Figure 6.26 Comparison of menthol adsorption in **MENT-Hs**, **MENT-COOHs** and **T-MENT-COOHs**

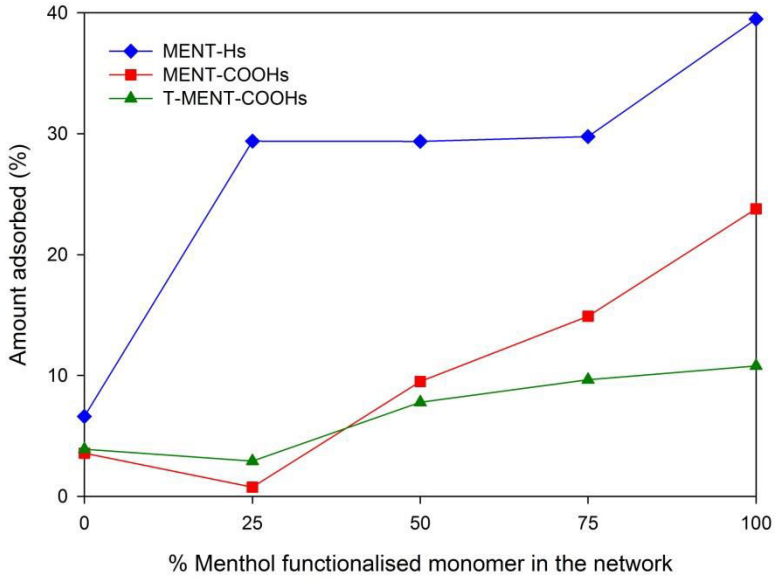

Figure 6.27 Comparison of terpinolene adsorption in **MENT-Hs, MENT-COOHs** and **T-MENT-COOHs**

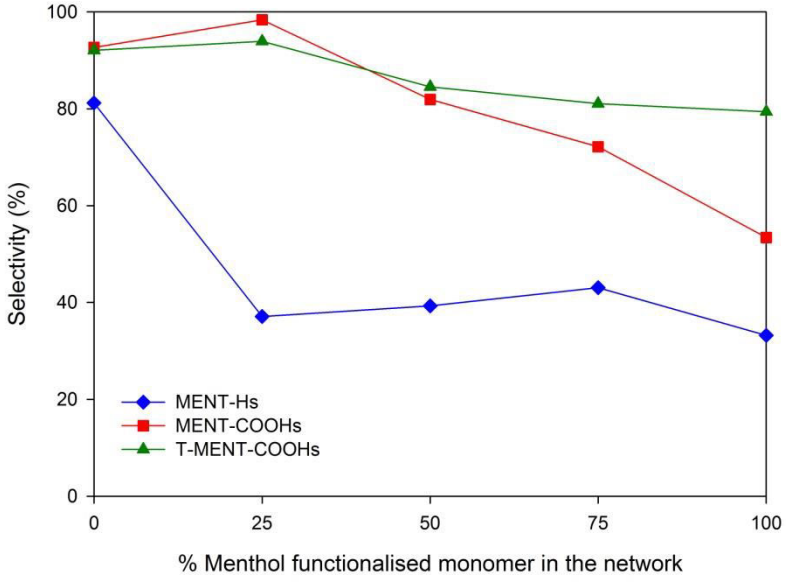

Figure 6.28 Comparison of selectivity of menthol over terpinolene in **MENT-Hs**, **MENT-COOHs** and **T-MENT-COOHs**

Table 6.11 Surface areas, adsorption and selectivity data of **MENT-CMPs**

Polymer	SA_{BET} (m^2/g)	Adsorption (%)		Selectivity (%)*
		Mentol (M)	Terpinolene (T)	
MENT-H-0H	1035	64	7	81
MENT-H-25H	832	64	29	37
MENT-H-50H	654	67	29	39
MENT-H-75H	328	75	30	43
MENT-H-100H	540	79	39	33
MENT-COOH-0H	116	95	4	93
MENT-COOH-25H	343	94	1	98
MENT-COOH-50H	443	96	10	82
MENT-COOH-75H	509	92	15	72
MENT-COOH-100H	540	78	24	53
T-MENT-COOH-0H	191	95	4	92
T-MENT-COOH-25H	291	94	3	94
T-MENT-COOH-50H	138	93	8	85
T-MENT-COOH-75H	311	92	10	81
T-MENT-COOH-100H	462	94	11	79

*Selectivity = (M-T)/(M+T) where M is menthol and T is terpinolene adsorption

The reason why the selectivity of menthol over terpinolene was low could be because of the low number of sites of binding, with only one hydroxyl group in menthol. Therefore, a compound with more functional groups, trimesic acid, was investigated.

6.4 Trimesic acid

6.4.1 O-TRIM

Trimesic acid (**Figure 6.2c**) was considered to be a good template as it contained three carboxylic acid functional groups. The high amount of functionality could potentially lead to higher interaction with the networks.

First of all, trimesic acid was functionalised with an alcohol to form the ester monomer in a similar way as previous templates. Trimesic acid was esterified with 2,4-dibromophenol in dichloromethane using DCC and DMAP as catalyst, following a literature procedure.[59] However, the conversion was low as indicated by NMR even using an increased amount of catalyst. Esterification *via* acid chloride was then applied, again following a literature procedure.[60] Trimesic acid trichloride was reacted with 2,4-dibromophenol using triethylamine as basic catalyst in toluene at 110 ^{o}C for 24 hours. After purification by precipitation in ethanol, tris(2,4-dibromophenyl) benzene-1,3,5-tricarboxylate (**trimeasate monomer**) was obtained in 18 % yield. (**Scheme 6.9**)

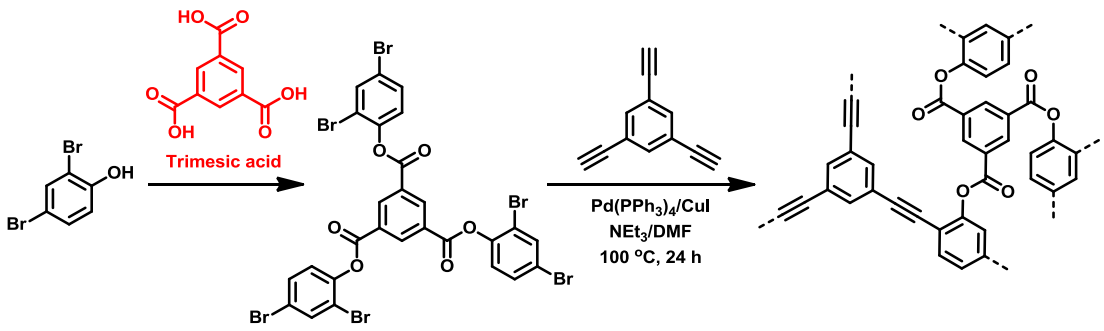

Scheme 6.9 Synthetic scheme for **O-TRIM**

The esterification was successful as shown by ^{1}H NMR, ^{13}C NMR, IR spectroscopy and elemental analysis. ^{1}H NMR spectrum illustrated the shifting of aromatic peaks of the dibromophenol as well as a peak at 9.31 ppm from the trimesic acid aromatic ring. The integration ratio was found to be 9:3 for dibromophenol to trimesic acid as expected. ^{13}C NMR spectrum also exhibited a carbonyl peak at 161 ppm. The IR spectrum (**Figure 6.29**) showed an ester C=O peak at 1747 cm^{-1} shifting from carboxylic acid peak at 1692 cm^{-1} as well as the disappearance of O-H peak around 3447 cm^{-1}. Elemental analysis agreed well with the theoretical values.

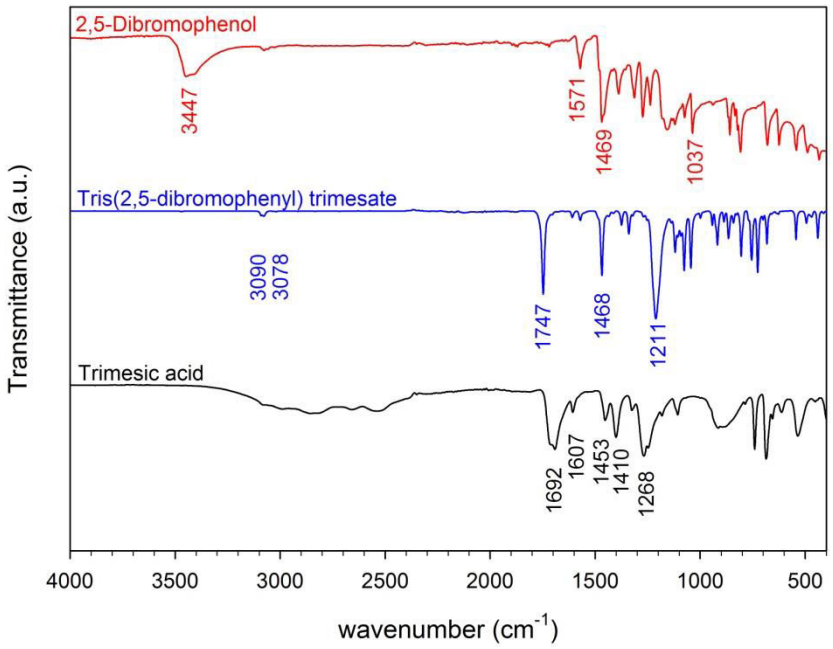

Figure 6.29 IR spectrum of tris(2,4-dibromophenyl) benzene-1,3,5-tricarboxylate (**Trimesate monomer**) (blue) compared to 2,5-dibromobenzoic acid (red) and trimesic acid (black)

Different synthetic conditions were investigated to improve the yield of the monomer. Adjusting the scale, changing concentration and longer times did not improve the yield of the reaction. Carrying out the reaction at either a smaller scale or an increase in concentration led to colour change of the product. Changing the solvent from toluene to DCM was found to provide a better yield. (**Table 6.12**)

The tris(2,4-dibromophenyl) benzene-1,3,5-tricarboxylate was then used to prepare the polymer with 1,3,5-triethynylbenzene by Sonogashira-Hagihara reaction providing **O-TRIM**. (**Scheme 6.9**)

Table 6.12 Synthetic conditions for **Trimesate monomer**

Scale (mmol)	-OH (eq.)	Solvent	Volume (mL)	Temp. (°C)	Time (h)	Product colour	Yield (%)
0.4	3.3	Toluene	30	110	24	Brown	18
2	3.3	Toluene	150	110	24	White	32
2	3.3	Toluene	100	110	24	Pale yellow	26
2	3.3	Toluene	200	110	24	White	21
2	3.3	Toluene	150	110	1	White	32
0.4	3.3	DCM	30	r.t.	24	Pale beige	71

IR spectroscopy was used to confirm the incorporate of both monomers into the polymers. The spectrum showed the C=O stretching of carboxylate group around 1728 cm^{-1}. The peaks at 1575 and 1489 cm^{-1} indicated the aromatic peaks of 1,3,5-triethynylbenzene and ester complex, respectively. Alkyne peaks were found around 2100-2200 cm^{-1}. The decreased intensity of the terminal alkyne peak at 2110 cm^{-1} and increase in intensity of the internal alkyne peak at 2206 cm^{-1} also confirmed the formation of network. (**Figure 6.30**)

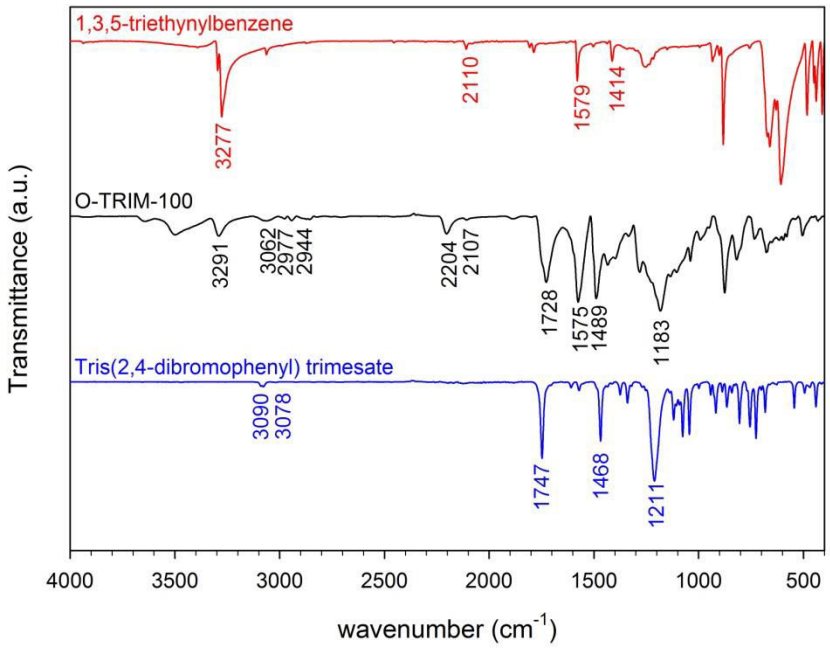

Figure 6.30 IR spectrum of **O-TRIM-100** compared to monomers

The template was then hydrolysed by using KOH/MeOH at 60 ^{o}C overnight to obtain **O-TRIM-H**. The template removal was monitored by disappearance of C=O peak around 1728 cm^{-1} in IR spectra. The aromatic and alkyne peaks were found unchanged. (**Figure 6.31**)

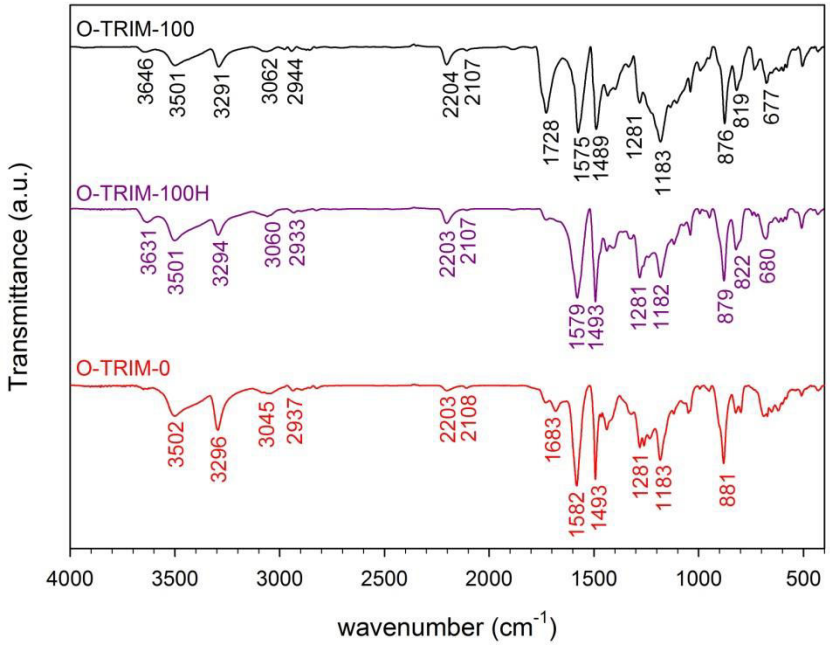

Figure 6.31 IR spectrum of **O-TRIM** before (black) and after (purple) after attempted hydrolysis compared to **O-TRIM-0** (**CMP-OH**) (red)

The 50% (**O-TRIM-50**) of **trimesate monomer** and **alcohol monomer** copolymer was synthesised. The **O-TRIM-0** or **CMP-OH**, containing only the **alcohol monomer** was also prepared as a control. (**Scheme 6.10**)

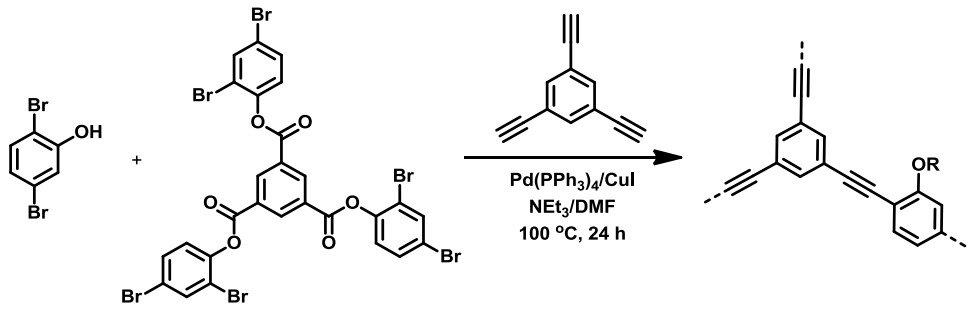

Scheme 6.10 Synthetic scheme for **O-TRIMs**

Again, the IR spectra shown in **Figure 6.32** illustrated the C=O stretching of carboxylate group around 1730 cm^{-1} in **O-TRIM-50** and **O-TRIM-100** which was not observed in **O-TRIM-0**. The peak intensity was higher as the ratio of trimesic functionalised monomer increased.

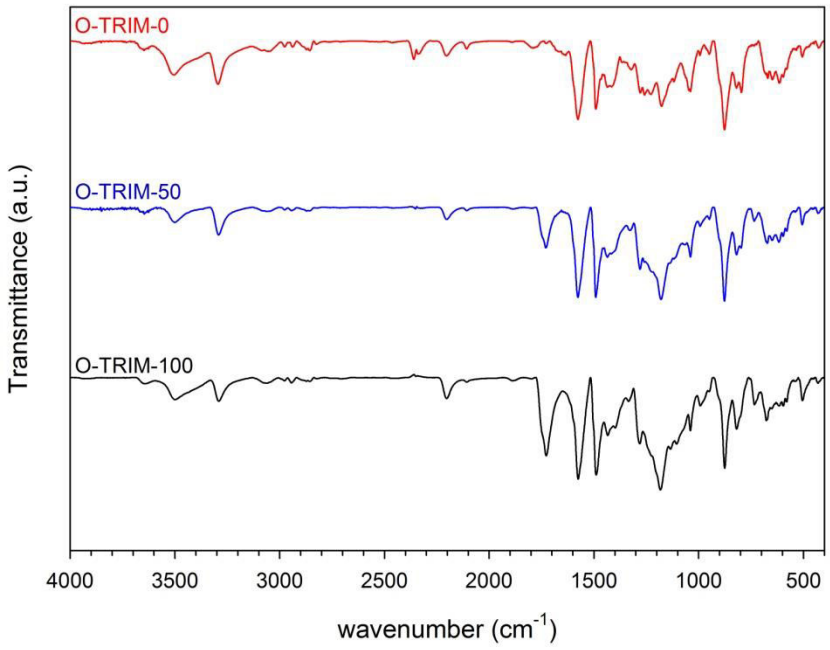

Figure 6.32 IR spectra of **O-TRIMs** before hydrolysis

Elemental analysis (**Table 6.13**) also demonstrated a decrease of the C and H content when higher ratio of **trimesate monomer** was used. The N content in the networks was possibly from a residue of solvents (DMF and NEt_3) left from the reaction or the adsorption of nitrogen from air by polymers.

Table 6.13 Yields, elemental analysis and gas sorption data of **O-TRIMs**

Sample	Yield (%)	Theory (%)			Analysis (%)			SA_{BET} (m^2/g)
		C	H	N	C	H	N	
O-TRIM-0	102	90.36	2.95	0.00	74.17	3.45	0.00	72
O-TRIM-50	103	88.29	2.66	0.00	72.72	3.36	0.27	15
O-TRIM-100	115	86.59	2.42	0.00	71.44	3.45	0.39	9

After hydrolysis using KOH/MeOH at 60 °C, the **O-TRIM-Hs** were obtained. The success of the template removal was indicated by the disappearance of the C=O peak in IR spectra as shown in **Figure 6.33**.

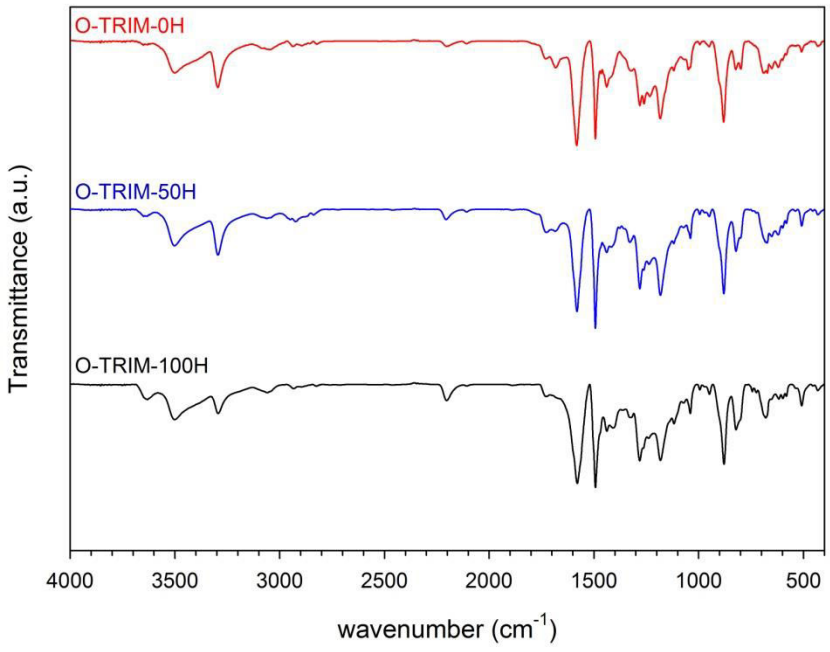

Figure 6.33 IR spectrum of **O-TRIMs** after hydrolysis

After hydrolysis, an increase in the surface areas of polymers was observed confirming the removal of trimesic acid from the networks without network collapsing. (**Table 6.14**)

Table 6.14 Yields, elemental analysis and gas sorption data of **O-TRIM-Hs**

Sample	Yield (%)	Theory (%)			Analysis (%)			SA_{BET} (m^2/g)
		C	H	N	C	H	N	
O-TRIM-0H	83	90.36	2.95	0.00	73.31	3.26	0.00	545
O-TRIM-50H	98	90.36	2.95	0.00	72.35	3.10	0.00	291
O-TRIM-100H	95	90.36	2.95	0.00	70.48	3.06	0.00	204

The adsorption of trimesic acid (TMA) was investigated using HPLC. Trimesic acid was dissolved in MeOH (1 mg/mL), then 1 mL of the solution was added to 25 mg of polymers. After leaving overnight, the solutions were analysed. **Figure 6.34** showed the chromatogram obtained from HPLC for trimesic acid solution.

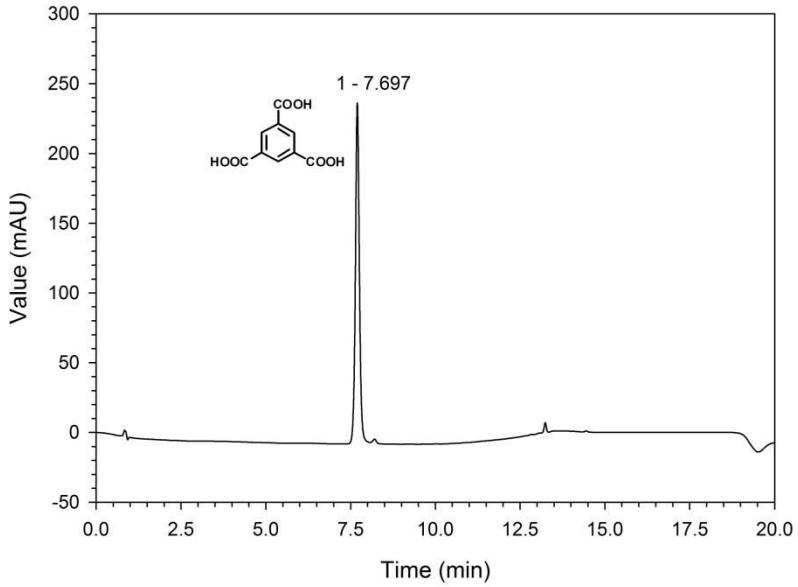

Figure 6.34 Graph shows HPLC chromatogram of trimesic acid

The absolute intensity of trimesic acid peak from HPLC was used to calculate the amount of trimesic acid left in the solution and adsorbed. A calibration curve (**Figure 6.35**) was obtained using absolute peak areas at different concentrations of the trimesic acid solutions. The amount of trimesic acid adsorbed in polymers could be calculated by the difference of initial concentration of trimesic acid solution (1 mg/mL) and the concentration of trimesic acid left in the solution after the binding experiment.

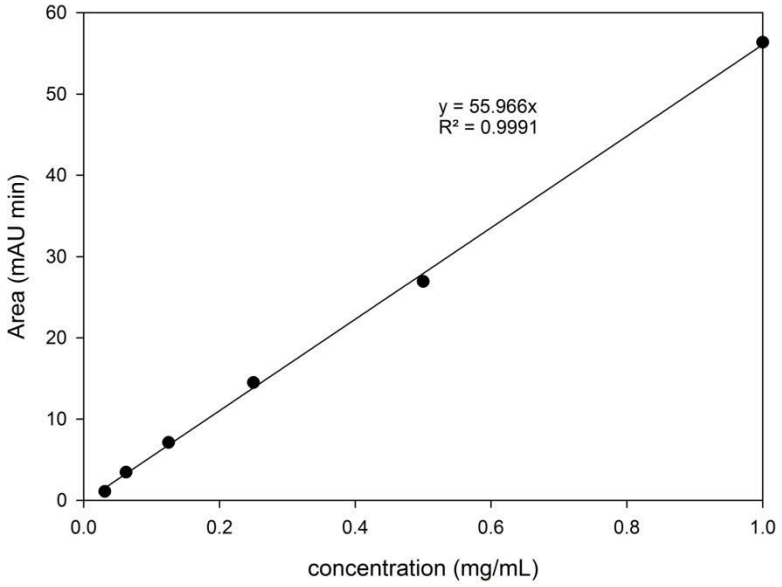

Figure 6.35 Calibration curve of trimesic acid in MeOH calculated by HPLC

Figure 6.36 illustrated the amount of trimesic acid adsorbed in the polymers. **CMP-OH** or **O-TRIM-0H** and a non-functionalised polymer (**CMP-1**) were used as controls. More trimesic acid could be adsorbed in the templated polymer (**O-TRIM-100H**) than the 50% copolymer (**O-TRIM-50H**), non-functionalised (**CMP-1**), and hydroxyl functionalised (**O-TRIM-0H**) networks respectively. The higher uptake in **O-TRIM-100H** than other polymers even the lower surface area indicated a better interaction to the template.

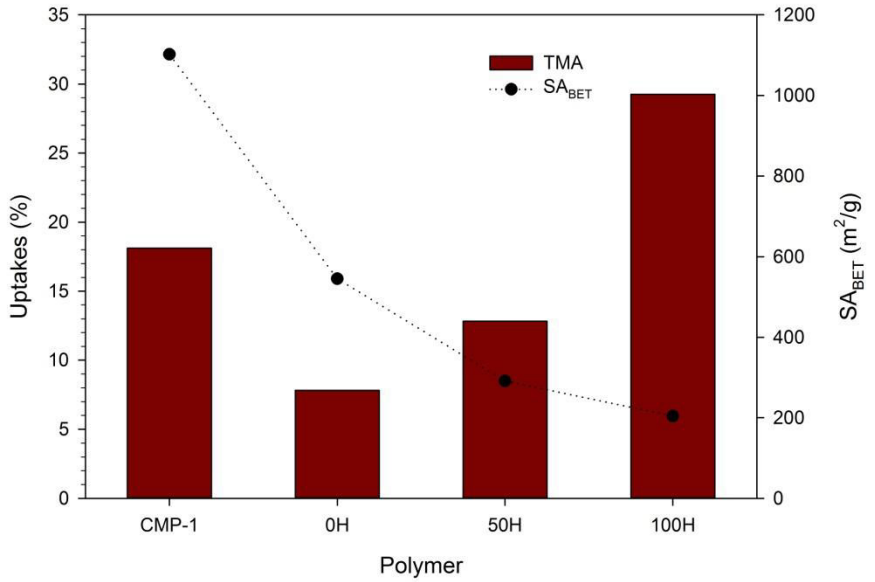

Figure 6.36 Surface areas and amount of trimesic acid adsorbed in **O-TRIM-Hs** compared to **CMP-1**

To investigate the selectivity of trimesic acid over other molecules, we examined the uptakes from a mixture of molecules i.e. benzene (BEN), 1-(tert-butyl)-3,5-dimethylbenzene (TBU), naphthalene (NAP), and 2-naphtholic acid (NTA) by networks were investigated. Benzene was chosen as its similarity in structure to trimesic acid but has no carboxylic acid group. Thus, it could be used to study the effect of interaction between a carboxylic acid group with the network. 1-(tert-butyl)-3,5-dimethylbenzene also contains a benzene ring but with a sterically bulky group instead of carboxylic acid group in trimesic acid. Larger compounds with two aromatic rings without any functional group, naphthalene, and with carboxylic acid functional group, 2-naphtholic acid, were also used to investigate the size effect on the adsorption.

A mixture of 1 mg of each compound in 1 mL of methanol (5Mix solution) was prepared. The HPLC chromatogram obtained for the solution is illustrated in **Figure 6.37**. Formic acid was used as an additive to provide better separation in the HPLC. The chromatogram showed a good separation of each compound.

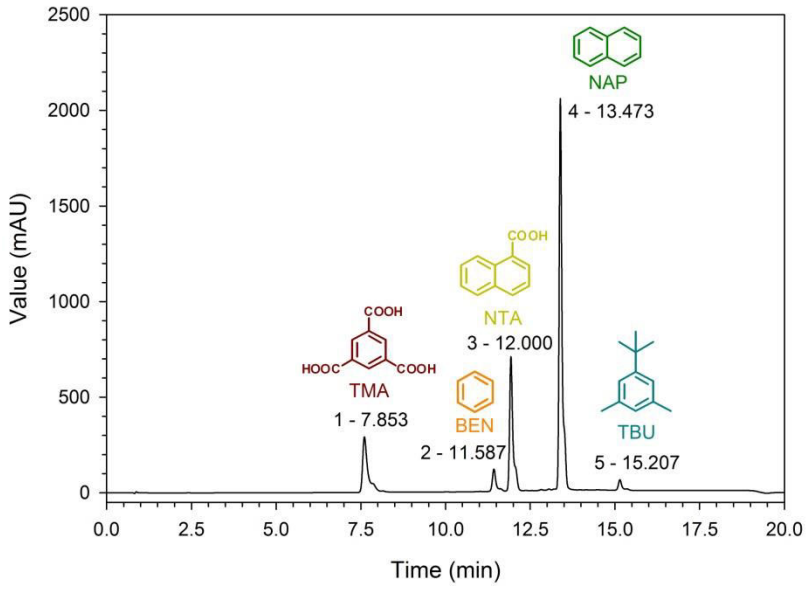

Figure 6.37 HPLC chromatogram of the 5 compound mixture

1 mL of the 5Mix solution was then added to the 25 mg polymers. After leaving overnight, the uptakes of each compound were calculated using HPLC. (**Table 6.15**)

Table 6.15 Surface areas and adsorption data of **O-TRIMs**

Polymer	SA_{BET} (m^2/g)	Adsorption (%)				
		TMA	BEN	NTA	NAP	TBU
CMP-1	1102	18.13	6.47	23.24	23.07	20.04
O-TRIM-0H	545	7.82	8.16	17.95	19.88	16.48
O-TRIM-50H	291	12.82	9.22	18.54	22.04	17.71
O-TRIM-100H	204	29.26	-6.78	15.17	12.58	9.16

CMP-1, **O-TRIM-0H** and **O-TRIM-50H** showed the similar amount of BEN, NTA, NAP and TBU uptakes with no selectivity of trimesic acid. On the other hand, the **O-TRIM-100H** exhibited higher adsorption of trimesic acid with low uptakes of other compounds indicating the selectivity. Comparing to other networks,

O-TRIM-100H showed promise for the imprinting of templates in the network. (**Figure 6.38**) Note that some of the % adsorptions of the compounds (for example BEN in **O-TRIM-100H**) showed a negative adsorption value. This could due to the adsorption of MeOH, which was used a solvent leading to the more concentration of the compound in the solution.

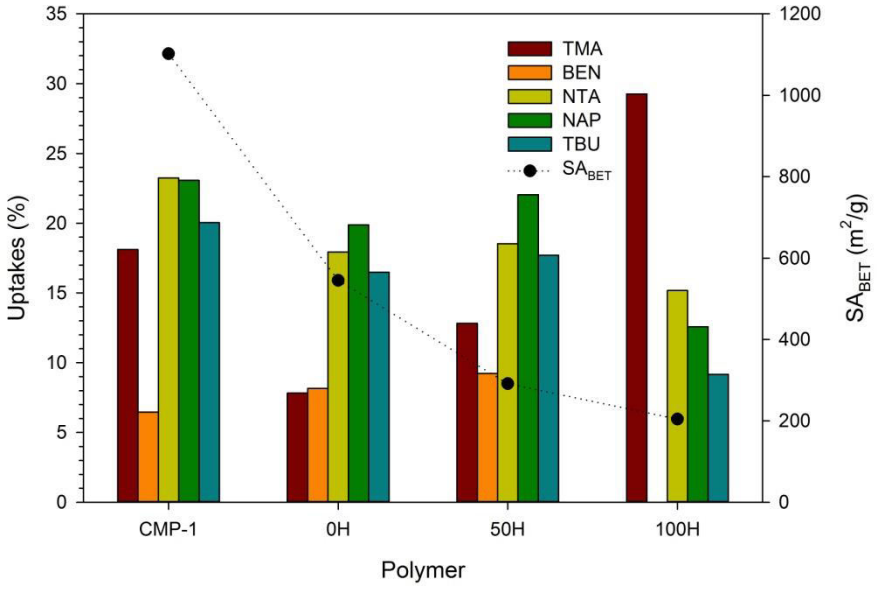

Figure 6.38 Surface areas and amount of compounds adsorbed in **O-TRIMs** compared to **CMP-1**

The repeat of experiment was then performed. The materials with the ratio of functionalised to non-functionalised monomers of 25 % and 75 % were also additionally prepared. Unfortunately, the results did not show the similar trend. The inconsistency could be because of the randomness of network formed which is expected from such amorphous networks.[56]

The IR spectra before (**Figure 6.32** and **Figure 6.39**) and after (**Figure 6.33** and **Figure 6.40**) hydrolysis of the two set of materials were similar. Before hydrolysis, the increase of C=O bands intensity of esters around 1730 cm^{-1} was observed when higher ratio of trimesic acid functionalised monomers were used. After hydrolysis, the C=O peaks disappeared. The alkyne peaks were observed at around 2100 and 2200 cm^{-1}.

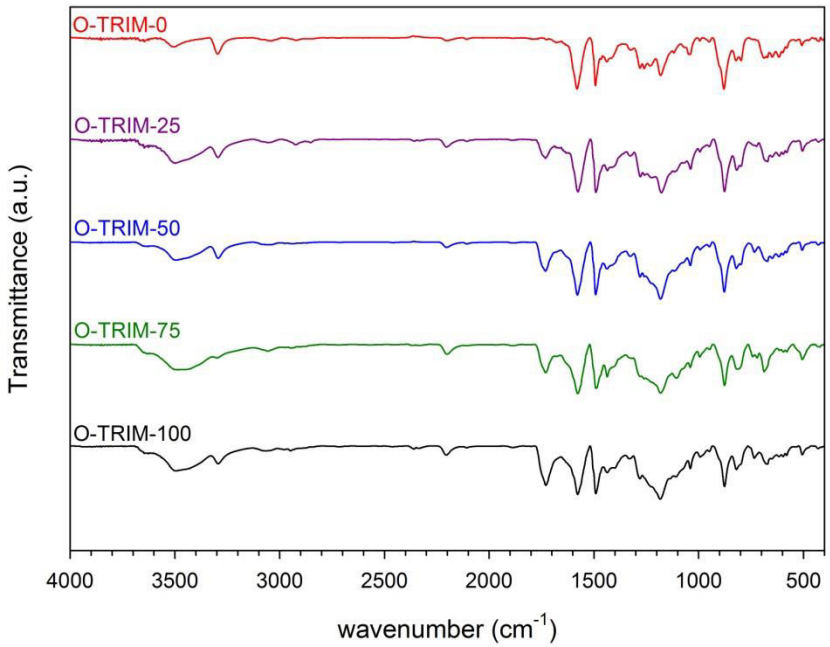

Figure 6.39 IR spectra of **O-TRIMs** before hydrolysis

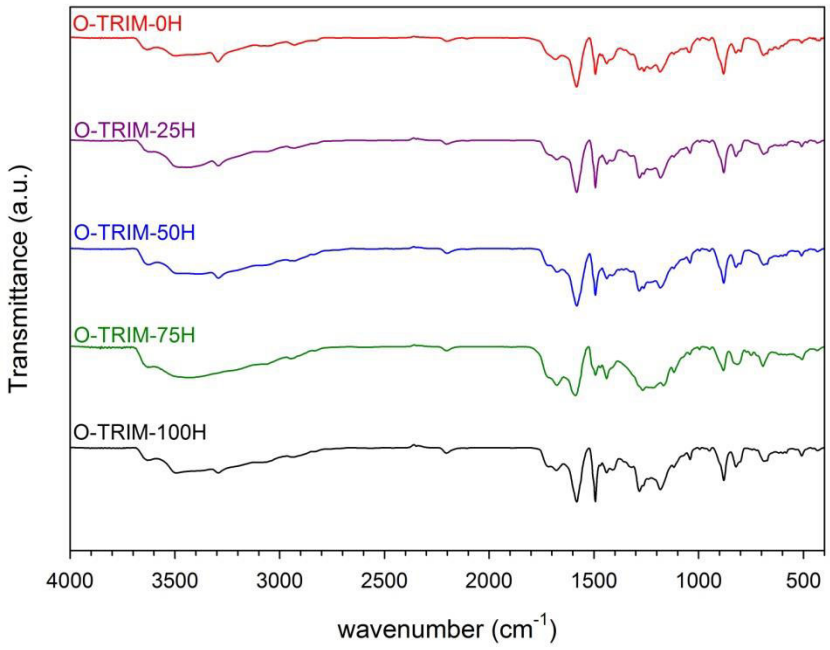

Figure 6.40 IR spectra of **O-TRIMs** after hydrolysis (**O-TRIM-Hs**)

Elemental analysis of materials before hydrolysis (**Table 6.16**) showed the similar trend that the percentage of C and H contents decrease as the ratio of trimesic acid functionalised monomers increased. However, the elemental analysis results were very similar for most of the networks. After hydrolysis, there appeared to be no consistent correlation in the elemental analysis data with the expected composition (**Table 6.17**). The materials obtained also had unsystematic surface areas. This could be because the materials synthesised each time might not be exactly the same, due to the random and amorphous natures of the synthesis process for the networks.[56]

Table 6.16 Yields, elemental analysis and gas sorption data of **O-TRIMs**

Sample	Yield (%)	Theory (%)			Analysis (%)			SA_{BET} (m^2/g)
		C	H	N	C	H	N	
O-TRIM-0	101	90.36	2.95	0.00	74.04	3.23	0.00	472
O-TRIM-25	112	89.27	2.80	0.00	70.90	3.22	0.31	13
O-TRIM-50	106	88.29	2.66	0.00	71.95	3.17	0.37	40
O-TRIM-75	122	87.40	2.54	0.00	71.28	3.28	0.32	461
O-TRIM-100	110	86.59	2.42	0.00	70.07	3.24	0.49	16

Table 6.17 Yields, elemental analysis and gas sorption data of **O-TRIM-Hs**

Sample	Yield (%)	Theory (%)			Analysis (%)			SA_{BET} (m^2/g)
		C	H	N	C	H	N	
O-TRIM-0H	72	90.36	2.95	0.00	71.55	3.50	0.00	643
O-TRIM-25H	82	90.36	2.95	0.00	63.94	3.25	0.00	321
O-TRIM-50H	105	90.36	2.95	0.00	64.98	3.27	0.00	285
O-TRIM-75H	101	90.36	2.95	0.00	60.56	3.05	0.00	394
O-TRIM-100H	89	90.36	2.95	0.00	69.24	3.18	0.00	340

We also considered that the discrepancy between batches might be due to errors from the HPLC measurements. Hence, we calculated the errors from repeat measurement of the 5Mix solution. The errors were found to be large compared to

the amount of compounds adsorbed. (**Figure 6.41**) It seems that the differences in adsorption measured might come from the error of the instrument, not only the differences in adsorption of materials. Different concentrations of 5Mix solutions and different injection volumes were attempted to reduce the error. However, the error bars were still considered to be large.

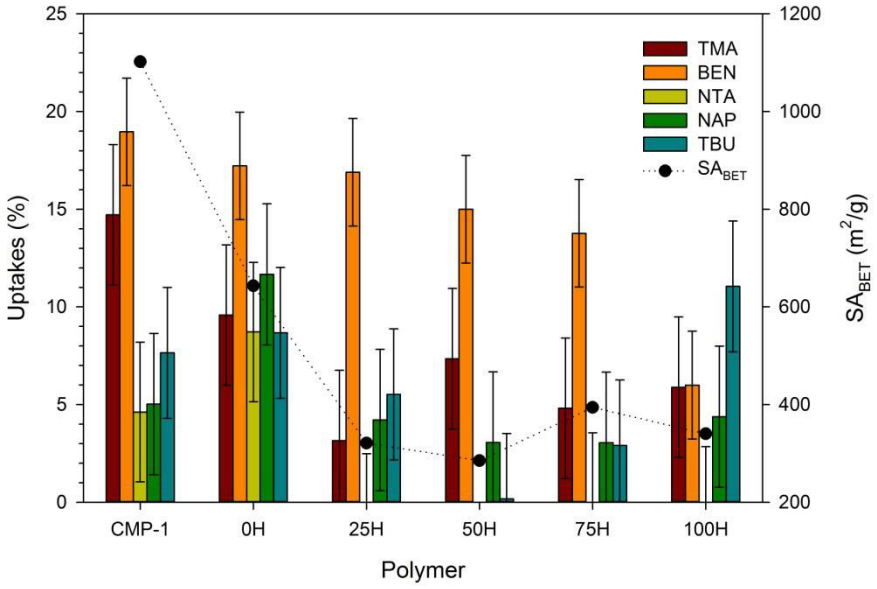

Figure 6.41 Surface areas and amount of compounds adsorbed in **O-TRIMs** compared to **CMP-1**

Table 6.18 Surface areas and adsorption data of **O-TRIMs**

Polymer	SA_{BET} (m^2/g)	Adsorption (%)				
		TMA	BEN	NTA	NAP	TBU
CMP-1	1011	14.71	18.96	4.62	5.02	7.64
O-TRIM-0H	643	9.58	17.22	8.72	11.67	8.67
O-TRIM-25H	321	3.16	16.90	-1.09	4.21	5.52
O-TRIM-50H	285	7.34	15.00	-4.08	3.06	0.17
O-TRIM-75H	394	4.81	13.77	-0.01	3.05	2.91
O-TRIM-100H	340	5.89	6.00	-0.72	4.38	11.05

6.4.2 N-TRIM

The network with **trimesic functionalised monomer** using amide instead of ester was also investigated. The amide group will be hydrolysed to an amine. Amine groups have been widely used in acid imprinting due to the basicity of amine which would be expected to interact with acid group.[61-63] The amine functionalised network would be expected to have better interaction with trimesic acid and hence higher adsorption and selectivity.

The *N*-functionalised monomer was synthesised from trimesic acid by a similar procedure as for **trimesate monomer** but coupling to the amine functionalised instead of the alcohol functionalised monomer. Toluene was initially used as a solvent, but a low yield of product was obtained.[60] Therefore, DCM was used instead, following a literature procedure.[64] The crude product was then purified by recrystallisation in DMF and water providing N^1,N^3,N^5-tris(2,4-dibromophenyl)benzene-1,3,5-tricarboxamide (**trimesamide monomer**). (**Scheme 6.11**)

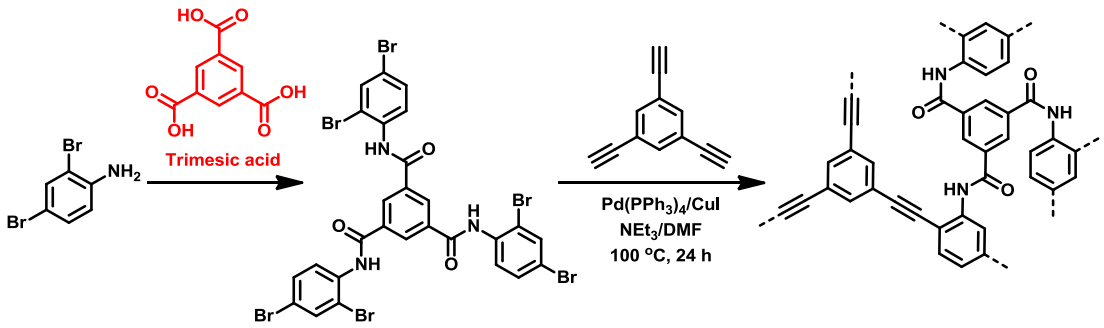

Scheme 6.11 Synthetic scheme for **N-TRIM**

Similar to the other templates, the amidation was confirmed by ^{1}H NMR, ^{13}C NMR, IR spectroscopy and elemental analysis. ^{1}H NMR illustrated the shift of aromatic peaks and the amine to amide peak from 5.50 ppm to 10.53 ppm. The peak at 8.78 ppm from the trimesic acid core was in a ratio of 3:9:3 compared to the dibromo aniline part and the amide proton was also observed. ^{13}C NMR showed the

amide C=O peak at 164 ppm. In IR spectrum (**Figure 6.42**), the shifting of the acid C=O peak at 1692 cm^{-1} to 1656 cm^{-1} of the amide as well as the appearance of N-H stretching around 3400 cm^{-1} indicated the conversion of carboxylic acid to amide. Elemental analysis agreed well with the theoretical values.

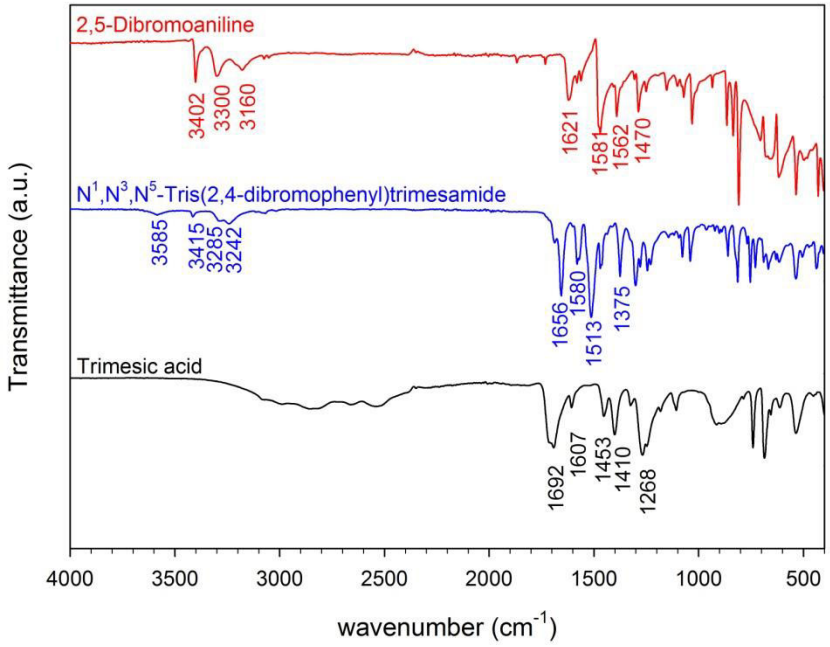

Figure 6.42 IR spectrum of N^1,N^3,N^5-tris(2,4-dibromophenyl)benzene-1,3,5-tricarboxamide (**Trimesamide monomer**) (blue) compared to 2,5-dibromoaniline (red) and trimesic acid (black)

Different conditions were investigated to improve the yield and purity of product. The purity of crude product could not be improved even when different conditions were tried. The yield of the product was found to increase by scaling up the reaction, increasing amount of amine monomer, temperature and time. The yield could be improved significantly when the amount of triethylamine used in the reaction was decreased. (**Table 6.19**)

Table 6.19 Synthetic conditions for **Trimesamide monomer**

Scale (mmol)	NH_2 (Eq)	NEt_3 (mL)	Solvent used	Solvent (mL)	Temp (^oC)	Time (h)	Yield (%)
0.4	3.3	2	Toluene	30	110	48	1
0.4	3.3	2	Toluene	30	110	24	-
0.4	5	2	Toluene	30	110	24	1
0.4	5	4	Toluene	30	110	24	1
0.4	5	2	Toluene	30	r.t.	24	4
0.4	10	4	Toluene	30	110	24	2
2	10	20	Toluene	150	110	24	19
2	10	1.5	Toluene	150	110	24	45
2	10	1.5	Toluene	150	110	1	47
0.2	10	0.15	DCM	15	r.t.	1	-
0.2	10	0.15	DCM	15	r.t.	24	11
0.2	20	0.15	DCM	15	r.t.	1	43
0.2	10	0.15	DCM	15	60	1	28
0.2	10	0.15	DCM	7.5	r.t.	1	1
0.2	10	0.5	DCM	15	r.t.	1	-
0.4	5	0.3	DCM	30	r.t.	1	36
0.4	10	0.3	DCM	30	r.t.	1	49
2	10	1.5	DCM	150	r.t.	24	46
2	5	0.8	DCM	150	r.t.	24	20
0.2	10	0.15	$CHCl_3$	15	r.t.	1	-
0.2	10	0.15	$CHCl_3$	15	60	1	-

The amide functionalised monomer (**trimesimide monomer**) was then polymerised with 1,3,5-triethynylbenzene to generate the amide functionalised polymer (**N-TRIM**). (**Scheme 6.11**)

The network formation was confirmed by IR spectroscopy. The appearance of an amide C=O stretching at 1681 cm^{-1} and the aromatic peaks around 1500 cm^{-1} showed the incorporation of **trimesimide monomer**. Alkyne peaks were observed around 2100-2200 cm^{-1} implying the incorporation of 1,3,5-triethynylbenzene in the network.[55] The intensity of terminal alkyne peak at 2110 cm^{-1} decreased and intensity of internal alkyne peak at 2203 cm^{-1} increased indicating the network formation. (**Figure 6.43**)

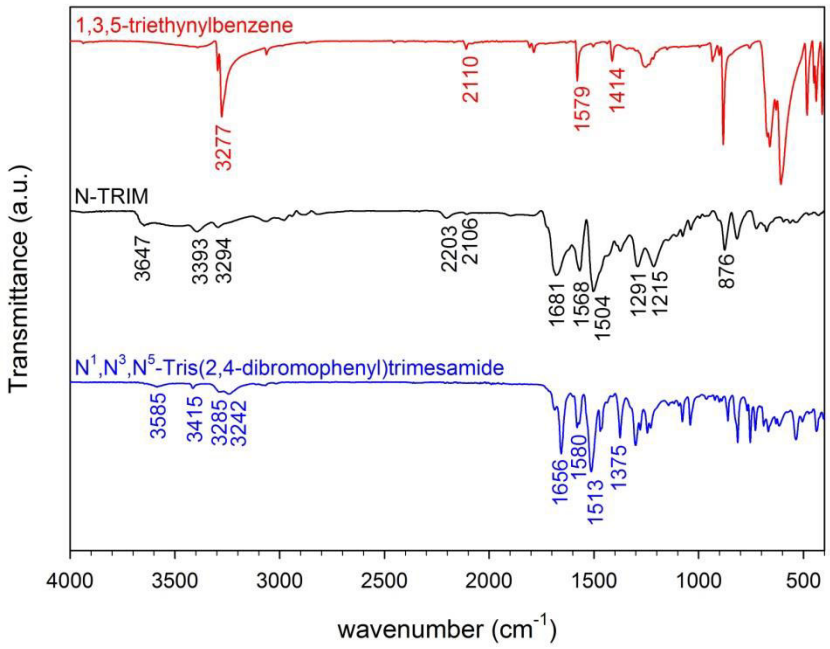

Figure 6.43 IR spectrum of **N-TRIM** compared to monomers

After hydrolysis with KOH in MeOH at 60°C overnight, disappearance of carbonyl peak at 1681 cm^{-1} in IR spectra was observed indicating the removal of trimesic acid from the networks. (**Figure 6.44**)

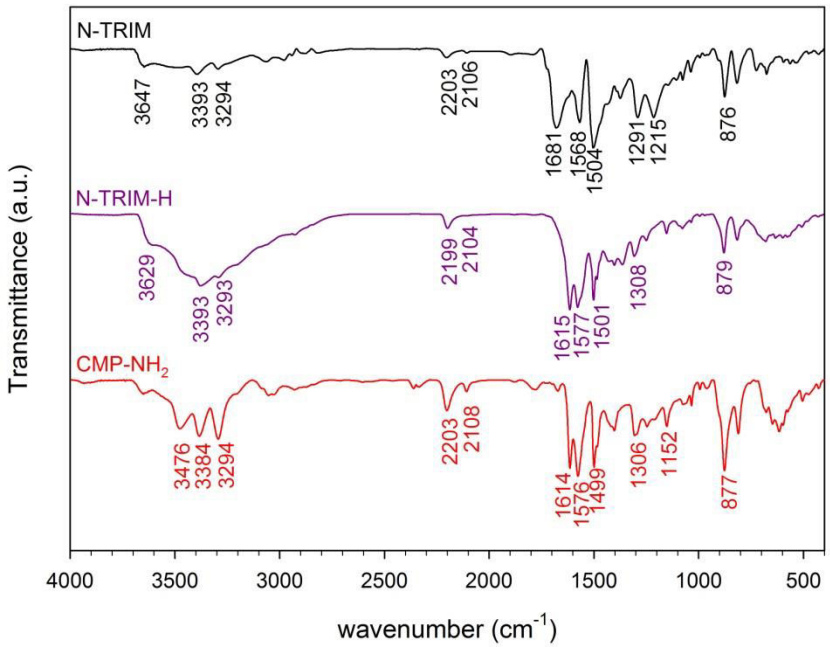

Figure 6.44 IR spectrum of **N-TRIM** before (black) and after (purple) after attempted hydrolysis compared to **N-TRIM-0** (**CMP-NH_2**) (red)

A series of amide functionalised copolymers (**N-TRIMs**) of **trimesamide monomer** and **amine monomer** with 1,3,5-triethynylbenzene were synthesised in five different ratios i.e. 0, 25, 50, 75 and 100% of the **trimesamide monomer**. (**Scheme 6.12**)

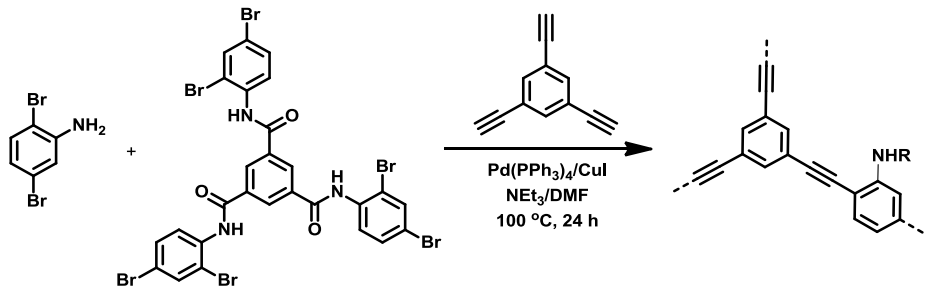

Scheme 6.12 Synthetic scheme for **N-TRIMs**

Figure 6.45 shows the IR spectra of **N-TRIMs**. As expected, the intensity of amide C=O around 1673 cm^{-1} increased and primary amine N-H stretching around 1476 cm^{-1} decreased when higher ratio of **trimesamide monomer** was used.

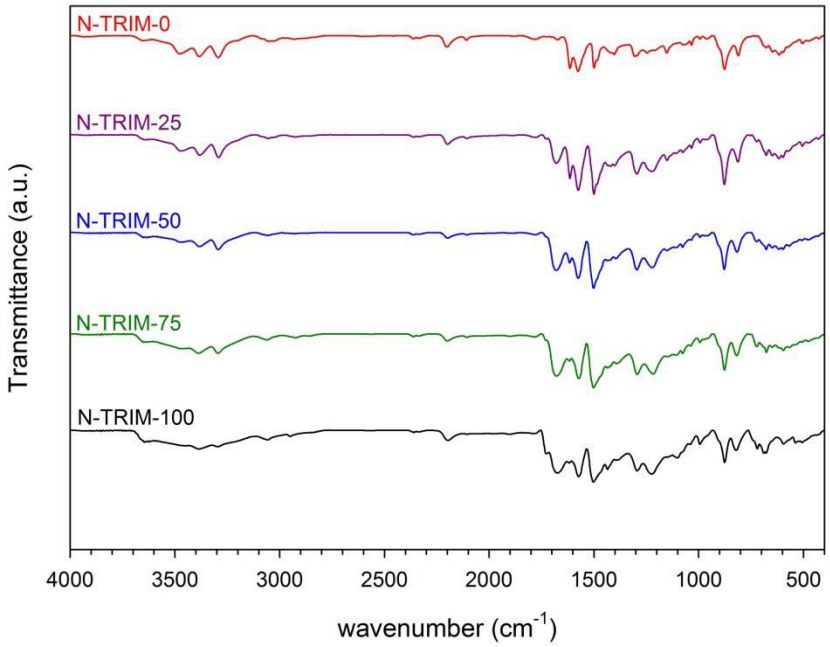

Figure 6.45 IR spectra of **N-TRIMs** before hydrolysis

With the higher ratio of **trimesamide monomer**, elemental analysis showed the decrease of the C and H contents. However, the N content increased with increasing of **trimesamide monomer**. It is possible that the reactivity of the amine monomer might be different than the amide monomer, leading to different ratio of brominated monomer to alkyne monomer formed in the networks. The total value of C, H and N content was also low implying the incorporation of other compounds in the networks. Such a compound could be water, air, solvents or catalyst residues.[52, 65, 66] Pd is possible left in the networks as the N of amines or amides were found to be able to coordinate with Pd.[67, 68] Incorporation of Pd could significantly lower the C, H and N contents. The surface areas were not found to correlate with the monomer composition. This could due to the amorphous nature of the networks leading to the different formation of porous structures. (**Table 6.20**)

Table 6.20 Yields, elemental analysis and gas sorption data of **N-TRIMs**

Sample	Yield (%)	Theory (%)			Analysis (%)			SA_{BET} (m^2/g)
		C	H	N	C	H	N	
N-TRIM-0	89	90.74	3.38	5.88	78.01	3.49	2.69	290
N-TRIM-25	95	89.62	3.21	5.57	76.70	3.39	3.04	116
N-TRIM-50	105	88.62	3.05	5.30	74.08	3.17	3.32	441
N-TRIM-75	113	87.71	2.91	5.05	72.10	3.11	3.46	108
N-TRIM-100	124	86.89	2.78	4.82	72.57	3.24	3.58	405

The template was removed by hydrolysis with KOH in MeOH at 60 °C overnight. The disappearance of amide C=O peak in IR spectrum shown in **Figure 6.46** was observed determining the successful of template extraction.

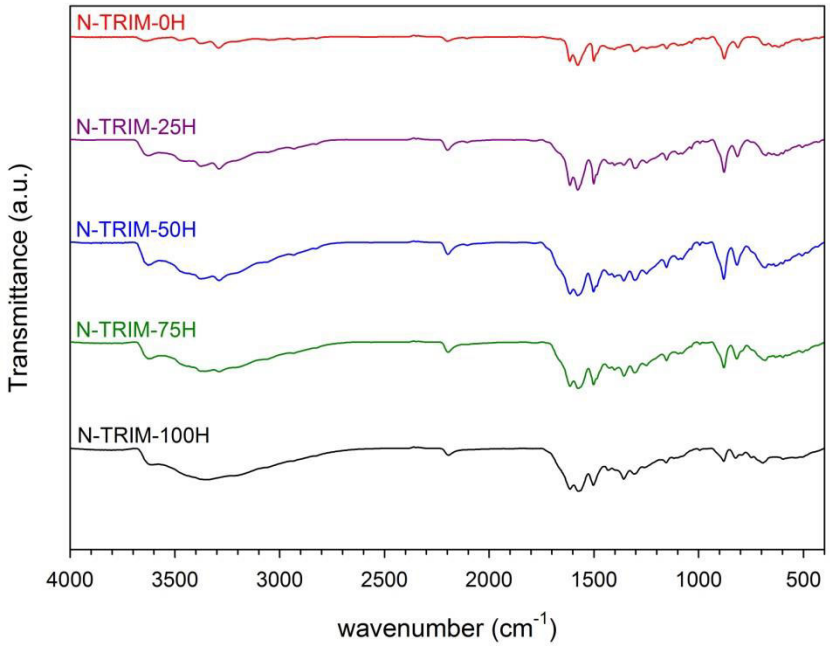

Figure 6.46 IR spectra of **N-TRIMs** after hydrolysis (**N-TRIM-Hs**)

However, from elemental analysis (**Table 6.21**), the C and N contents appear to unexpected decrease. This could be possible due to the trapped trimesate (benzene tricarboxylate) as well as KOH or K ion in the polymers. Trimesate would increase the O content in the networks. Trimesate and K then could lower the total percentage of C, H, and N contents. The surface areas of the networks after hydrolysis were found to be low implying that the networks have perhaps collapsed after template was removed.

Table 6.21 Yields, elemental analysis and gas sorption data of **N-TRIM-Hs**

Sample	Yield (%)	Theory (%)			Analysis (%)			SA_{BET} (m^2/g)
		C	H	N	C	H	N	
N-TRIM-0H	85	90.74	3.38	5.88	71.97	3.87	2.51	665
N-TRIM-25H	98	90.74	3.38	5.88	69.40	3.50	2.83	27
N-TRIM-50H	105	90.74	3.38	5.88	66.65	3.41	3.06	34
N-TRIM-75H	109	90.74	3.38	5.88	65.83	3.41	3.34	12
N-TRIM-100H	97	90.74	3.38	5.88	61.84	3.71	3.45	26

Similar to **O-TRIM-Hs**, the adsorption of trimesic acid and the selectivity over other molecules, i.e. benzene (BEN), tert-butyl benzene (TBU), naphthalene (NAP), and 2-naphthoic acid (NTA) by **N-TRIM-Hs** was investigated using HPLC. The mixture of 1 mg of each compound in 1 mL methanol was added to the 25 mg polymers. After leaving overnight, the solutions were analysed. The amine network (**N-TRIM-0H**; **CMP-NH_2**) and non-functionalised polymer (**CMP-1**) were also used as the control. The uptakes of the compounds is summarised in **Table 6.22**.

Again, the **N-TRIMs** showed apparently varying adsorption (**Figure 6.47**) and selectivity (**Figure 6.48**) of trimesic acid. The **N-TRIMs** showed the higher uptakes comparing to the **O-TRIMs**, which could result from the better interaction of amine to trimesic acid than alcohol. However, the amount of compounds adsorbed in the polymers and selectivity was also found to be low. This may be because of the different porous structures and flexibility of the polymers.

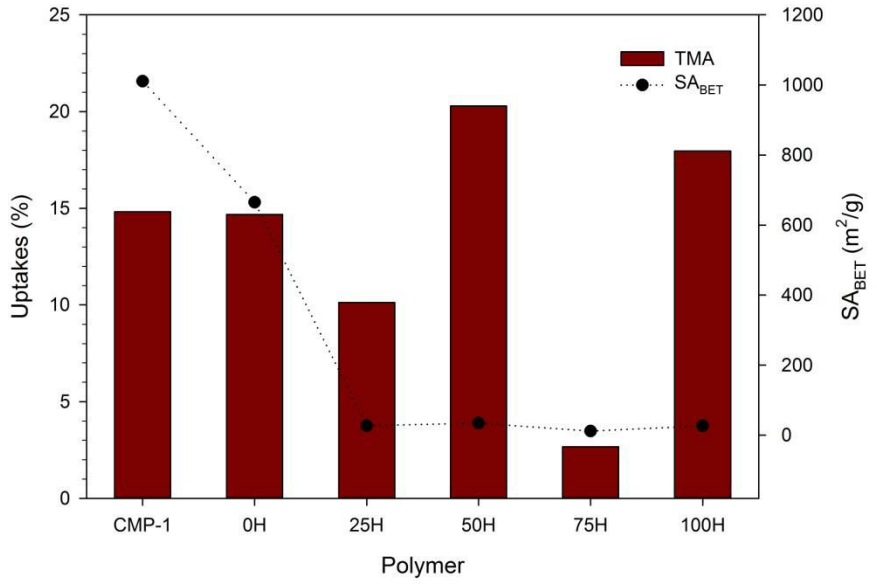

Figure 6.47 Surface areas and amount of compounds adsorbed in **N-TRIMs** compared to **CMP-1**

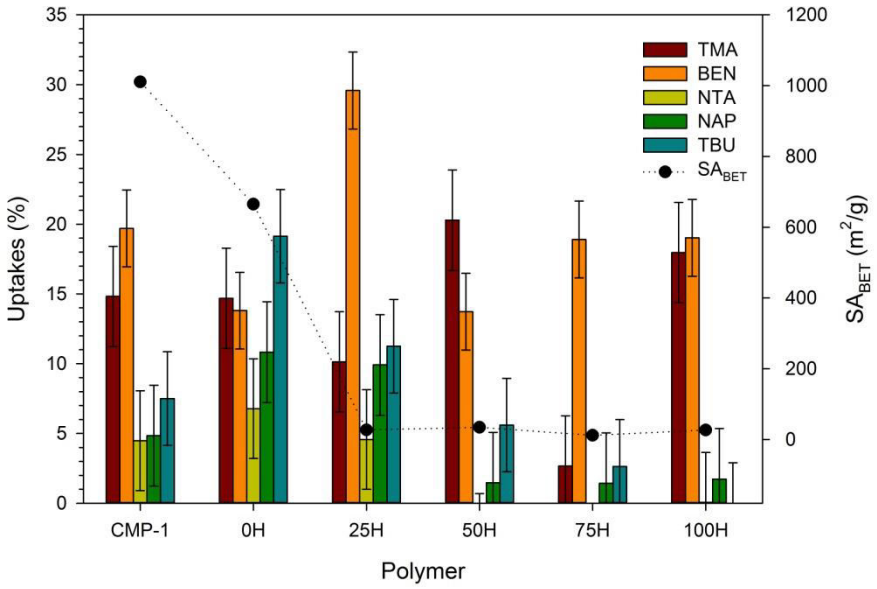

Figure 6.48 Surface areas and amount of compounds adsorbed in **N-TRIMs** compared to **CMP-1**

Table 6.22 Surface areas and adsorption data of **N-TRIMs**

Polymer	SA_{BET} (m^2/g)	Adsorption (%)				
		TMA	BEN	NTA	NAP	TBU
CMP-1	1011	14.82	19.70	4.48	4.85	7.50
N-TRIM-0H	665	14.69	13.80	6.77	10.83	19.14
N-TRIM-25H	27	10.13	29.58	4.57	9.91	11.25
N-TRIM-50H	34	20.29	13.73	-2.87	1.47	5.61
N-TRIM-75H	12	2.67	18.91	-3.67	1.43	2.64
N-TRIM-100H	26	17.97	19.03	0.07	1.74	-0.45

6.5 Conclusion

Different CMPs were attempted to be used in MIPs application. Different templates were tried. Cholesterol was difficult to remove from the materials. Menthol which is more hydrophilic and smaller was found to be easier to remove from the polymers. High amounts of menthol could be adsorbed in the polymers. However, comparing to terpinolene which has similar structure to menthol, the materials did not show a good selectivity. This could be due to the low interaction between template and polymers. Therefore, trimesic acid which contains three positions of interactions was tired. Unfortunately, the networks formed did not show the specific adsorption to the template. The networks also collapsed in case of amine functionalised networks.

There are many potential reasons for the lack of success in using CMPs as molecular imprinting polymers in this work. Accessibility of the cavities in the networks might result in low adsorption and selectivity. By using semi-covalent method, the cavity was generated by covalent bonding while non-covalent interaction was performed in the binding step. Therefore, the cavity formed in the network might not be suitable for the template i.e. might be too small. For example, it is possible that the cavity formed in the trimesic acid imprinted polymers may be too small and rigid for trimesic acid molecules as shown in **Figure 6.49**. Thus, the diffusion of template in and out from the networks would be difficult. In many cases,

spacer was used to solve such a problem.[51, 69, 70] Thus, the use of spacer might improve the adsorption of the template.

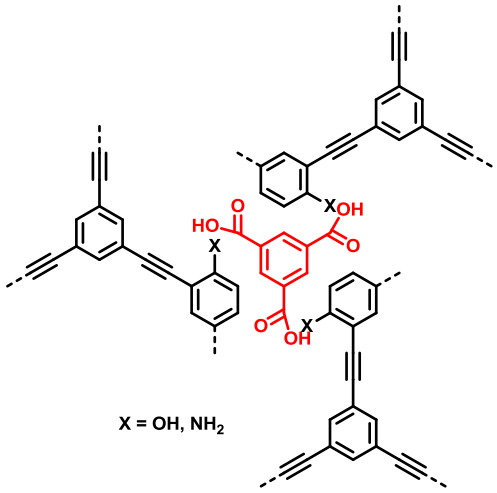

Figure 6.49 Possible model of the rigid imprinted cavity which might be too small for trimesic acid

Because of the amorphous nature of CMPs, control of their porous structures is difficult. Therefore, inconsistency was found in different batches of samples. The appropriate functionalities have to be considered to provide the networks with permanent pore after hydrolysis and removing solvents as well.

Polarity could also lead to different adsorption of compounds with different polarities as shown in the work by Dawson *et.al.* that the polar dye could be adsorbed in the polar networks better than the non-polar ones.[71] The solvent used in binding experiment was also found to affect the adsorption in some cases.[72-74] MeOH, which is also polar, used in trimesic acid adsorption might be able to competitively adsorb in the networks. Different solvents should also be attempted to improve the adsorption.

Error from both human and machine for the binding experiment was also high. A better method for this step should be further investigated.

6.6 References

1. G. Wulff, *Angewandte Chemie International Edition in English*, 1995, **34**, 1812-1832.
2. C. Alexander, H. S. Andersson, L. I. Andersson, R. J. Ansell, N. Kirsch, I. A. Nicholls, J. O'Mahony and M. J. Whitcombe, *Journal of Molecular Recognition*, 2006, **19**, 106-180.
3. P. A. G. Cormack and A. Z. Elorza, *Journal of Chromatography B*, 2004, **804**, 173-182.
4. A. G. Mayes and M. J. Whitcombe, *Advanced Drug Delivery Reviews*, 2005, **57**, 1742-1778.
5. D. R. Kryscio and N. A. Peppas, *Acta Biomaterialia*, 2012, **8**, 461-473.
6. N. W. Turner, C. W. Jeans, K. R. Brain, C. J. Allender, V. Hlady and D. W. Britt, *Biotechnology Progress*, 2006, **22**, 1474-1489.
7. K. Ren and R. N. Zare, *ACS Nano*, 2012, **6**, 4314-4318.
8. T. Wangchareansak, A. Thitithanyanont, D. Chuakheaw, M. P. Gleeson, P. A. Lieberzeit and C. Sangma, *Journal of Materials Chemistry B*, 2013, **1**, 2190-2197.
9. N. Perez, C. Alexander and E. N. Vulfson, in *Techniques and Instrumentation in Analytical Chemistry*, ed. S. Börje, Elsevier, 2001, vol. Volume 23, pp. 295-304.
10. R. Schirhagl, E. W. Hall, I. Fuereder and R. N. Zare, *Analyst*, 2012, **137**, 1495-1499.
11. W. J. Cheong, S. H. Yang and F. Ali, *Journal of Separation Science*, 2013, **36**, 609-628.
12. B. Sellergren and F. Lanza, in *Techniques and Instrumentation in Analytical Chemistry*, ed. S. Börje, Elsevier, 2001, vol. Volume 23, pp. 355-375.
13. M. Kempe, in *Techniques and Instrumentation in Analytical Chemistry*, ed. S. Börje, Elsevier, 2001, vol. Volume 23, pp. 395-415.
14. G. Mustafa and P. Lieberzeit, in *Designing Receptors for the Next Generation of Biosensors*, eds. S. A. Piletsky and M. J. Whitcombe, Springer Berlin Heidelberg, 2013, vol. 12, pp. 167-187.
15. L. I. Andersson, *Journal of Chromatography B: Biomedical Sciences and Applications*, 2000, **739**, 163-173.

16. L. I. Andersson, in *Techniques and Instrumentation in Analytical Chemistry*, ed. S. Börje, Elsevier, 2001, vol. Volume 23, pp. 341-354.

17. G. Wulff, A. Sarhan and K. Zabrocki, *Tetrahedron Letters*, 1973, **14**, 4329-4332.

18. G. Wulff, *Chemical Reviews*, 2001, **102**, 1-28.

19. G. Vlatakis, L. I. Andersson, R. Muller and K. Mosbach, *Nature*, 1993, **361**, 645-647.

20. A. L. Hillberg and M. Tabrizian, *IRBM*, 2008, **29**, 89-104.

21. M. V. Polyakov, *Zhurnal Fizieskoj Khimii*, 1931, **2**, 799-805.

22. M. V. Polyakov, P. Stadnik, M. Paryckij, I. Malkin and F. Duchina, *Zhurnal Fizieskoj Khimii*, 1933, **4**, 454-456.

23. M. V. Polyakov, L. Kuleshina and I. Neimark, *Zhurnal Fizieskoj Khimii*, 1937, **10**, 100-112.

24. P. Ehrlich, *Proceedings of the Royal Society of London*, 1899, **66**, 424-448.

25. F. Breinl and F. Haurowitz, *Hoppe-Seyler´s Zeitschrift für physiologische Chemie*, 1930, **192**, 45–57.

26. S. Mudd, *The Journal of Immunology*, 1932, **23**, 423-427.

27. L. Pauling, *Journal of the American Chemical Society*, 1940, **62**, 2643-2657.

28. F. W. Lichtenthaler, *Angewandte Chemie International Edition in English*, 1995, **33**, 2364-2374.

29. L. Pauling and D. H. Campbell, *The Journal of Experimental Medicine*, 1942, **76**, 211-220.

30. P. K. Dhal, M. G. Kulkarni and R. A. Mashelkar, in *Techniques and Instrumentation in Analytical Chemistry*, ed. S. Börje, Elsevier, 2001, vol. Volume 23, pp. 271-294.

31. F. H. Dickey, *Proceedings of the National Academy of Sciences of the United States of America*, 1949, **35**, 227-229.

32. F. H. Dickey, *The Journal of Physical Chemistry*, 1955, **59**, 695-707.

33. G. Wulff and A. Sarhan, *Angewandte Chemie International Edition in English*, 1972, **11**, 341.

34. T. Takagishi and I. M. Klotz, *Biopolymers*, 1972, **11**, 483-491.

35. R. Schwyzer, *Proceedings of the Fourth International Congress on Pharmacology*, 1970, 196-209.

36. G. Wulff and A. Biffis, in *Techniques and Instrumentation in Analytical Chemistry*, ed. S. Börje, Elsevier, 2001, vol. Volume 23, pp. 71-111.

37. B. Sellergren, in *Techniques and Instrumentation in Analytical Chemistry*, ed. S. Börje, Elsevier, 2001, vol. Volume 23, pp. 113-184.

38. G. Wulff and S. Schauhoff, *The Journal of Organic Chemistry*, 1991, **56**, 395-400.

39. G. Wulff, W. Best and A. Akelah, *Reactive Polymers, Ion Exchangers, Sorbents*, 1984, **2**, 167-174.

40. K. J. Shea, G. J. Stoddard, D. M. Shavelle, F. Wakui and R. M. Choate, *Macromolecules*, 1990, **23**, 4497-4507.

41. K. J. Shea and T. K. Dougherty, *Journal of the American Chemical Society*, 1986, **108**, 1091-1093.

42. K. J. Shea, D. Y. Sasaki and G. J. Stoddard, *Macromolecules*, 1989, **22**, 1722-1730.

43. K. J. Shea and D. Y. Sasaki, *Journal of the American Chemical Society*, 1989, **111**, 3442-3444.

44. K. J. Shea and E. Thompson, *The Journal of Organic Chemistry*, 1978, **43**, 4253-4255.

45. K. J. Shea, E. A. Thompson, S. D. Pandey and P. S. Beauchamp, *Journal of the American Chemical Society*, 1980, **102**, 3149-3155.

46. J. Damen and D. C. Neckers, *The Journal of Organic Chemistry*, 1980, **45**, 1382-1387.

47. J. Damen and D. C. Neckers, *Tetrahedron Letters*, 1980, **21**, 1913-1916.

48. J. Damen and D. C. Neckers, *Journal of the American Chemical Society*, 1980, **102**, 3265-3267.

49. L. Andersson, B. Sellergren and K. Mosbach, *Tetrahedron Letters*, 1984, **25**, 5211-5214.

50. H. Yan and K. Row, *International Journal of Molecular Sciences*, 2006, **7**, 155-178.

51. M. J. Whitcombe, M. E. Rodriguez, P. Villar and E. N. Vulfson, *Journal of the American Chemical Society*, 1995, **117**, 7105-7111.

52. T. Ratvijitvech, R. Dawson, A. Laybourn, Y. Z. Khimyak, D. J. Adams and A. I. Cooper, *Polymer*, 2014, **55**, 321-325.

53. B. Sellergren and A. J. Hall, in *Techniques and Instrumentation in Analytical Chemistry*, ed. S. Börje, Elsevier, 2001, vol. Volume 23, pp. 21-57.

54. G. Castruita, V. Garcia, E. Arias, I. Moggio, R. Ziolo, A. Ponce, V. Gonzalez, J. E. Haley, J. L. Flikkema and T. Cooper, *Journal of Materials Chemistry*, 2012, **22**, 3770-3780.

55. J.-X. Jiang, F. Su, A. Trewin, C. D. Wood, N. L. Campbell, H. Niu, C. Dickinson, A. Y. Ganin, M. J. Rosseinsky, Y. Z. Khimyak and A. I. Cooper, *Angewandte Chemie*, 2007, **119**, 8728-8732.

56. A. Laybourn, R. Dawson, R. Clowes, T. Hasell, A. I. Cooper, Y. Z. Khimyak and D. J. Adams, *Polymer Chemistry*, 2014, **5**, 6325-6333.

57. J.-X. Jiang, F. Su, A. Trewin, C. D. Wood, H. Niu, J. T. A. Jones, Y. Z. Khimyak and A. I. Cooper, *Journal of the American Chemical Society*, 2008, **130**, 7710-7720.

58. E. Stockel, X. Wu, A. Trewin, C. D. Wood, R. Clowes, N. L. Campbell, J. T. A. Jones, Y. Z. Khimyak, D. J. Adams and A. I. Cooper, *Chemical Communications*, 2009, 212-214.

59. P. J. Stackhouse, A. Wilson, D. Lacey and M. Hird, *Liquid Crystals*, 2010, **37**, 1191-1203.

60. H. Audorff, R. Walker, L. Kador and H.-W. Schmidt, *Chemistry – A European Journal*, 2011, **17**, 12722-12728.

61. D. Spivak and K. J. Shea, *The Journal of Organic Chemistry*, 1999, **64**, 4627-4634.

62. D. M. Kneeland, K. Ariga, V. M. Lynch, C. Y. Huang and E. V. Anslyn, *Journal of the American Chemical Society*, 1993, **115**, 10042-10055.

63. M. Dana, P. Luliński and D. Maciejewska, *Molecules*, 2011, **16**, 3826-3844.

64. F. D. Lewis, T. M. Long, C. L. Stern and W. Liu, *The Journal of Physical Chemistry A*, 2003, **107**, 3254-3262.

65. M. Yu, X. Wang, X. Yang, Y. Zhao and J.-X. Jiang, *Polymer Chemistry*, 2015, **6**, 3217-3223.

66. S. Ren, R. Dawson, D. J. Adams and A. I. Cooper, *Polymer Chemistry*, 2013, **4**, 5585-5590.

67. M. Albrecht, in *Palladacycles*, Wiley-VCH Verlag GmbH & Co. KGaA, 2008, pp. 13-33.

68. J. D. Hicks, A. M. Hyde, A. M. Cuezva and S. L. Buchwald, *Journal of the American Chemical Society*, 2009, **131**, 16720-16734.

69. M. J. Whitcombe and E. N. Vulfson, in *Techniques and Instrumentation in Analytical Chemistry*, ed. S. Börje, Elsevier, 2001, vol. Volume 23, pp. 203-212.

70. N. Kirsch, C. Alexander, S. Davies and M. J. Whitcombe, *Analytica Chimica Acta*, 2004, **504**, 63-71.

71. R. Dawson, A. Laybourn, R. Clowes, Y. Z. Khimyak, D. J. Adams and A. I. Cooper, *Macromolecules*, 2009, **42**, 8809-8816.

72. C. Yu and K. Mosbach, *The Journal of Organic Chemistry*, 1997, **62**, 4057-4064.

73. J. Saloni, K. Walker and G. Hill, *The Journal of Physical Chemistry A*, 2013, **117**, 1531-1534.

74. W. Dong, M. Yan, Z. Liu, G. Wu and Y. Li, *Separation and Purification Technology*, 2007, **53**, 183-188.

Chapter 7

Conclusions

7. Conclusions

7.1 Conclusions

We have demonstrated synthetic strategies to produce a series of benzene and aniline co-polymer networks using comparable inexpensive catalyst, $FeCl_3$, by Friedel-Crafts reactions. The low surface area of the aniline network could be successfully improved by incorporation of benzene into the network. Surface areas and CO_2 uptakes of the networks could be tuned by stoichiometry of benzene to aniline monomers. With increasing of aniline ratio, the surface areas of the networks dropped more significantly than CO_2 uptakes leading to enhancing of CO_2/N_2 selectivity. This may be useful for applications in CO_2 capture and separations.

As functional groups were found to be important factor to fine tune the networks for specific usage, we investigated an alternative route to incorporate carboxylic acid, which is normally difficult to introduce into the polymers prepared by the Friedel-Crafts reaction[1], into the networks. The hypercross-linked polystyrenes were synthesised by post-cross-linking of the functionalised linear polystyrene chains prepared by RAFT polymerisation[2]. The surface areas of the networks were found to depend on the degree of polymerisation (DP) of the linear polystyrenes. However, the carboxylic acid functional groups seem to be transformed to esters during the cross-linking process.

The post-synthetic modification (PSM) of conjugated microporous polymers (CMPs) was also studied. An amine functionalised CMP was post-synthetically modified by acid anhydrides to amides. By modified the network with different chain lengths of acid anhydrides, CMP functionalised with different chain lengths of amides could be obtained. The systematic drop in surface areas and pore volumes as well as the CO_2 uptakes and CO_2 heat of adsorptions with increasing of the length of amide chains was observed. This demonstrated that the new functional groups could be easily introduced into the CMPs and the properties of the networks could be tailored systematically by PSM strategy.

We also attempted to apply the PSM strategy to the preparation of molecular imprinting polymers (MIPs). Cholesterol, menthol, and trimesic acid were used as templates. The templates could be successfully removed from the networks by PSM. The MIPs could adsorb different molecules. Unfortunately, the networks did not show the specific adsorption to the templates. Further modification and optimisation should be further investigated.

All in all, we have shown in this thesis that the structures, functionalities and properties of HCPs and CMPs can be tailored by different strategies, i.e. co-polymerisation, post-cross-linking of the functionalised linear polymer chains, and post-synthetic modification. The functionalised networks could be fine tuned and utilised as sorbents for gases and small molecules. However, the further development of materials is still needed to fulfil applicable requirements both for existing and further new applications.

7.2 Future work

The synthetic strategies developed in this thesis might be further used to utilise the properties of the networks for specific applications. The strategies could be used to improve the surface areas and also introduce a wide range of functionalities into networks. The synthetic strategies might be not only limited to the HCPs and CMPs, but also useful for synthesis of other kinds of materials.

Co-polymerisation could be used to incorporate other functionalities such as thiols, ethers, and nitriles, into the networks by using different functionalised monomers. The strategy might also be used to increase complexity of the networks by using more than two precursors with different functional groups to form multi-functionalised materials.

The PSM offers the potential to extend the diversity of functionalised networks. The strategy might be further applied to other functional groups, such as carboxylic acid, which were able to be functionalised before networks formation. The PSM strategy might also be used in reversible incorporation and removal of molecules in the networks. This could lead to the possibility to use the materials in drug delivery or drug release applications.

RAFT polymerisation has an advantage on allowing modification of RAFT end groups. By varying RAFT agents to different end groups, polystyrenes and hypercross-linked polystyrenes with different functionalities could be obtained. RAFT end group in the networks could also be post-synthetic modified.[3] Further modification of RAFT end group might be done after networks formation to incorporate carboxylic acid or other functionalities into the networks. Other controlled polymerisation approaches such as atom transfer radical polymerisation (ATRP) and nitroxide-mediated polymerisation (NMP) could also be studied the effects of polymerisation methods on the properties of the networks.

In this thesis, we focused our study only on the N_2 and CO_2 adsorptions. Nevertheless, the functionalities in the networks might also have effects on the adsorption and selectivity of other gases or molecules. Thus, further investigation could be carried out. For examples, amine functionalised networks might also have a good interaction with compounds containing carboxylic acid. It is also possible to use amine functionalised materials as a catalyst for basic catalytic reactions.

The decrease of CO_2 uptakes and heat of adsorption in the **CMP-1-AMDs** could due to the decrease of the surface areas and the coverage of the active amine group by amides. The cover of the amine group could lower the interaction with CO_2 and also lower the polarity of the networks. This might not be beneficial for CO_2 capture. However, it might be useful for the adsorption and selectivity of other non-polar gases like methane. PSM of the networks with amine functional groups at the chain ends might also improve the CO_2 adsorption of the networks.

For MIPs, further studies could be carried out to optimise the materials. Many factors such as choices of templates, monomers for networks synthesis, network synthetic methods, and solvents used in binding experiments as well as the use of spacers, could affect the success of making MIPs. Templates containing more functional groups with specific shape could be used. The geometries of monomers might also be investigated. By changing the type of networks, for example, to HCPs, might also improve the rigidity of the networks and also the adsorption and selectivity to the guest molecules. Other factors like repeatability of the synthetic amorphous networks should also be considered. The appropriate methods and conditions for analysis of binding experiments should also be further explored.

7.3 References

1. M. Rueping and B. J. Nachtsheim, *Beilstein Journal of Organic Chemistry*, 2010, **6**, 6.

2. J. Chiefari, Y. K. Chong, F. Ercole, J. Krstina, J. Jeffery, T. P. T. Le, R. T. A. Mayadunne, G. F. Meijs, C. L. Moad, G. Moad, E. Rizzardo and S. H. Thang, *Macromolecules*, 1998, **31**, 5559-5562.

3. H. Willcock and R. K. O'Reilly, *Polymer Chemistry*, 2010, **1**, 149-157.